

NASA/TM-2003-211622

SIMBIOS Project 2002 Annual Report

Giulietta S. Fargion, Science Applications International Corporation, Maryland
Charles R. McClain, Goddard Space Flight Center, Greenbelt, Maryland

National Aeronautics and
Space Administration

Goddard Space Flight Center
Greenbelt, Maryland 20771

February 2003

Preface

The purpose of this technical report is to provide current documentation of the the Sensor Intercomparison and Merger for Biological and Interdisciplinary Oceanic Studies (SIMBIOS) Project activities, NASA Research Announcement (NRA) research status, satellite data processing, data product validation, and field calibration. This documentation is necessary to ensure that critical information is related to the scientific community and NASA management. This critical information includes the technical difficulties and challenges of validating and combining ocean color data from an array of independent satellite systems to form consistent and accurate global bio-optical time series products. This technical report is not meant as a substitute for scientific literature. Instead, it will provide a ready and responsive vehicle for the multitude of technical reports issued by an operational project.

The SIMBIOS Science Team Principal Investigators (PIs) original contributions to this report are in chapters four and above. The purpose of these contributions is to describe the current research status of the SIMBIOS-NRA-99 funded research. The contributions are published as submitted, with the exception of minor edits to correct obvious grammatical or clerical errors.

Table of Contents

1. AN OVERVIEW OF SIMBIOS PROJECT ACTIVITIES AND ACCOMPLISHMENTS DURING FY02..... 1

2. SIMBIOS: SCIENCE TEAM AND CONTRACTS..... 4

3. SIMBIOS PROJECT DATA PROCESSING AND ANALYSIS RESULTS..... 6

4. ADAPTATION OF A HYPERSPECTRAL ATMOSPHERIC CORRECTION ALGORITHM FOR MULTI-SPECTRAL OCEAN COLOR DATA IN COASTAL WATERS..... 33

5. BIO-OPTICAL MEASUREMENTS IN UPWELLING ECOSYSTEMS IN SUPPORT OF SIMBIOS..... 37

6. SATELLITE OCEAN-COLOR VALIDATION USING SHIPS OF OPPORTUNITY 44

7. MERGING OCEAN COLOR DATA FROM MULTIPLE MISSIONS..... 53

8. BIO-OPTICAL AND REMOTE SENSING OBSERVATIONS IN CHESAPEAKE BAY..... 59

9. REFINEMENT OF PROTOCOLS FOR MEASURING THE APPARENT OPTICAL PROPERTIES OF SEAWATER..... 68

10. OPTIMIZATION OF OCEAN COLOR ALGORITHMS: APPLICATION TO SATELLITE AND IN SITU DATA MERGING..... 74

11. THE MARINE FAST-ROTATING SHADOW-BAND NETWORK: STATUS REPORT AND ANALYSIS..... 78

12. BIO-OPTICAL MEASUREMENT AND MODELING OF THE CALIFORNIA CURRENT AND SOUTHERN OCEANS 83

13. VARIABILITY IN OCEAN COLOR ASSOCIATED WITH PHYTOPLANKTON AND TERRIGENOUS MATTER: TIME SERIES MEASUREMENTS AND ALGORITHM DEVELOPMENT AT THE FRONT SITE ON THE NEW ENGLAND CONTINENTAL SHELF..... 91

14. OCEAN OPTICS PROTOCOLS AND SIMBIOS PROTOCOL INTERCOMPARISON ROUND ROBIN EXPERIMENTS (SPIRREX)... 98

15. BERMUDA BIO OPTICS PROJECT 100

16. PLUMES AND BLOOMS: MODELING THE CASE II WATERS OF THE SANTA BARBARA CHANNEL 104

17. ALGORITHMS FOR PROCESSING AND ANALYSIS OF OCEAN COLOR SATELLITE DATA FOR COASTAL CASE 2 WATERS ... 107

18. VARIED WATERS AND HAZY SKIES: VALIDATION OF OCEAN COLOR SATELLITE DATA PRODUCTS IN UNDER-SAMPLED MARINE AREAS: II 115

19. HPLC PIGMENT MEASUREMENTS FOR ALGORITHM DEVELOPMENT AND VALIDATION IN SUPPORT OF THE SIMBIOS SCIENCE TEAM 120

20. ASSESSMENT, VALIDATION, AND REFINEMENT OF THE ATMOSPHERIC CORRECTION ALGORITHM FOR THE OCEAN COLOR SENSORS..... 122

21. ATMOSPHERIC CORRECTION ALGORITHMS FOR JAPANESE SATELLITE OCEAN PROGRAMS..... 128

22. COMPARISON OF OCEAN COLOR PRODUCTS BETWEEN OSMI AND SEAWIFS: PRELIMINARY RESULTS..... 135

23. EVALUATION AND IMPROVEMENT OF THE ATMOSPHERIC CORRECTION AND BIO-OPTICAL ALGORITHMS FOR THE BLACK AND BARENTS SEAS 142

24. SIMBADA CALIBRATION USING A LASER BASED FACILITY AND COMPARISON WITH PREVIOUS TECHNIQUES152

Chapter 1

An Overview of SIMBIOS Project Activities and Accomplishments During FY02

Charles R. McClain

NASA Goddard Space Flight Center, Greenbelt, Maryland

Giulietta S. Fargion

Science Applications International Corporation (SAIC), Beltsville, Maryland

In many respects, the past year has been one of the most eventful for the satellite ocean biogeochemistry community with the launches of the Aqua Moderate resolution Imaging Spectroradiometer (MODIS), the ENVISAT Medium Resolution Imaging Spectrometer (MERIS), the ADEOS-II Global Imager (GLI), and the ADEOS-II Polarization and Directionality of the Earth's Reflectance (POLDER-II) sensors, as well as a one-year extension of the Sea-viewing Wide Field-of-View Sensor (SeaWiFS) data buy contract. However, the past year has also been one of transition for the SIMBIOS program as NASA Headquarters decided to discontinue the program in its present form. The rationale centered on three considerations. The first was a desire by Headquarters (HQ) to integrate the various ocean color calibration and validation activities of the SIMBIOS, SeaWiFS, and the MODIS programs under a common ocean color team which would also include investigators supported under the NASA Ocean Biogeochemistry program. While the three ocean color projects have separate management and funding structures, they have been coordinated and mutually supportive with little redundancy. The second consideration stems from initial problems with MODIS ocean data quality and accessibility which has made it imperative for NASA focus its available resources on MODIS ocean calibration and validation. The third consideration is the National Polar Orbiting Environmental Satellite System (NPOESS) Preparatory Project (NPP) which is scheduled to launch in 2007. NPP includes the Visible Infrared Imaging Radiometer Suite (VIIRS) which will provide ocean color data products after MODIS. VIIRS has a design which incorporates a SeaWiFS-like rotating telescope, focal planes similar to MODIS, and a basic set of ocean color bands which does not include the MODIS fluorescence bands. HQ has asked that the VIIRS ocean color data processing build on the expertise and systems resident at Goddard Space Flight Center (GSFC). Initial NPP discipline processing data system formulation has begun and development should be well underway by 2004. As a result, much of the SIMBIOS Project's effort this past year has centered on the fourth SeaWiFS reprocessing and on assisting the MODIS ocean team. Consequently, the Project has had to assume a less proactive participation in the international missions.

Nonetheless, during FY02, the Project made substantial progress and contributions in a variety of activities including the following:

- Assisting the SeaWiFS Project with the fourth reprocessing, particularly in the area of product validation using match-up data contributed by the SIMBIOS Science Team.
- Continued development and documentation of the SeaWiFS Bio-optical Archive and Storage System (SeaBASS; Werdell and Bailey, 2002) including 310 new cruise data sets and 102 cruise updates provided by the SIMBIOS Science Team.
- Continued refinement of sun photometer calibration and data analysis procedures (Knobelspiesse et al., in press) and incorporation of the data products into SeaBASS.
- Completion of the third revision of the in-situ measurement protocols (Mueller et al., 2002).
- Documentation of the second SIMBIOS calibration round-robin (Meister et al., 2002) and completion of third which included three laboratories associated with MODIS ocean team members (NASA Wallops Flight Facility, University of Miami, and the University of South Florida).
- Development and support of a website for the diagnostic data sets which presently includes data from SeaWiFS and MODIS (Terra and Aqua).
- Evaluations of various data merger methodologies and the routine merger of global SeaWiFS and MODIS products.

- Support of MODIS processing and product evaluations including match-up analyses (bio-optical and atmospheric), and SeaWiFS-MODIS data product comparisons and diagnostic analyses (e.g., time series analyses and scan modulation effects).

More detailed descriptions of these achievements are provided in subsequent chapter by Project staff.

In 2003, the SIMBIOS Project will continue its active support of the SeaWiFS Project (the SeaWiFS program was recently extended for one year) and MODIS (Terra and Aqua) programs to help ensure that the next reprocessing of each data set provides even higher quality products. The SIMBIOS Project will also assist the MERIS, GLI, and POLDER teams by providing in situ match up data sets and by maintaining the diagnostic data sets for product comparison, but support beyond this level will be limited. The Project will participate in a CalCOFI cruise being organized in support of GLI validation. Other ongoing activities will include continued maintenance of SeaBASS, the collection and processing of sun photometer data, the completion of the calibration round robin, and the merger of SeaWiFS and MODIS data. The Project Office will continue business functions well into FY04 to properly close out the science team contracts. Finally, the Project will begin initial preparations for VIIRS calibration, validation, and data processing.

Simbios Project Publications in 2002

- Barnes, R. A., D. K. Clark, W. E. Esaias, G. S. Fargion, G. C. Feldman, and C. R. McClain, Development of a consistent multi-sensor global ocean color time series, *Int. J. Remote Sens.*, in press.
- Bailey, S, C. Pietras, K. D. Knobelspiesse, G.S. Fargion, and C.R. McClain, 2002: The SeaWifs Aerosol Product Compared to Coastal and Island In Situ Measurements, Spring 2002 American Geophysical Union Meeting, Washington, DC.
- Fargion, G., and C. R. McClain, 2002: SIMBIOS Project 2001 Annual Report, *NASA/TM-2002-210005*, NASA Goddard Space Flight Center, Greenbelt, Maryland, 184 pp.
- Gross, L, R. Frouin, C. Pietras, K.D. Knobelspiesse and G.S. Fargion, 2002: Non-supervised Classification of Ground-based Radiometer Retrievals in Order to Assess the Natural Distribution of Aerosol Volume Size Distributions and Refractive Indexes, Spring 2002 American Geophysical Union Meeting, Washington, DC.
- Kilpatrick, K., E. Kearns, E.J. Kwiatkowska-Ainsworth, and R.L. Evans, 2002: Time Series of Calibrated Ocean Products from NASA's Moderate Resolution Scanning Spectrometer (MODIS), Proceedings of the Ocean Sciences Meeting, Honolulu, Hawaii.
- Knobelspiesse, K. D., C. Pietras, and G. S. Fargion, Sun pointing error correction for sea deployment of the Microtops II sun photometer, *J. Atmos. Oceanic Tech.*, in press.
- Knobelspiesse, K.D., C. Pietras, M. Miller, M. Reynolds, R. Frouin, P. Quinn, P-Y. Deschamps, J. Werdell, and G.S. Fargion, 2002: Comparison of In Situ Aerosol Data from the ACE-Asia 2002 Experiment, Spring 2002 American Geophysical Union Meeting, Washington, DC.
- Kwiatkowska E. and G.S. Fargion, 2002: Merger of Ocean Color Data from Multiple Satellite Missions within the SIMBIOS Project, Proceedings of SPIE's Symposium on Remote Sensing of the Atmosphere, Ocean, Environment, and Space, Hangzhou, China.
- Kwiatkowska E. and G.S. Fargion, 2002: Merger of Ocean Color Information from Multiple Satellite Missions under the NASA SIMBIOS Project Office, Proceedings of the Fifth International Conference on Information Fusion, Annapolis, Maryland, 291-298.
- Kwiatkowska-Ainsworth, E. 2001: Merger of Ocean Color Information of Different Spatial Resolution: SeaWiFS and MOS, *Eos Trans. American Geophysical Union*, vol. **82**, no. 47, F675 (OS52A-0514).

- McClain, C. R., W. Esaias, G. Feldman, R. Frouin, W. Gregg, and S. Hooker, 2002: The Proposal for the NASA Sensor Intercalibration and Merger for Biological and Interdisciplinary Oceanic Studies (SIMBIOS) Program, 1995, *NASA/TM-2002-210008*, NASA Goddard Space Flight Center, Greenbelt, Maryland, 63 pp.
- Meister, G., and others, 2002: The First SIMBIOS Radiometric Intercomparison (SIMRIC-1), April-September 2001, *NASA/TM2002-210006*, NASA Goddard Space Flight Center, Greenbelt, Maryland, 60 pp.
- Meister, G., and others, Comparison of radiance calibrations at oceanographic and atmospheric research laboratories, *Metrologia*, in press.
- Meister, G., G.S. Fargion and C.R. McClain, 2002: Monitoring the Radiometric Stability of the SeaWiFS Transfer Radiometer II, Spring 2002 American Geophysical Union Meeting, Washington, DC.
- Mueller, J. L., and others, 2002: Ocean Optics Protocols for Satellite Ocean Color Sensor Validation, Revision 3, Volumes 1 and 2, J. L. Mueller and G. S. Fargion (eds.), NASA Tech. Memo. 2002-210004/Rev3-Vol1 and -Vol2, NASA Goddard Space Flight Center, Greenbelt, MD, 308 pp.
- Mueller, J. L., and others, 2002: Ocean Optics Protocols for Satellite Ocean Color Sensor Validation, Revision 3, Volume 2, J. L. Mueller and G. S. Fargion (eds.), NASA Tech. Memo. 2002-210004/Rev3-Vol2, NASA Goddard Space Flight Center, Greenbelt, MD, 171 pp.
- Pietras, C, K.D. Knobelspiesse, S. Bailey, J. Werdell, R. Frouin, M. Miller, G.S. Fargion and C.R. McClain, 2002: SeaWiFS Aerosol Product Compared to In Situ Measurements Over Open Oceans, Spring 2002 American Geophysical Union Meeting, Washington, DC.
- Van Heukelem, L., C. S. Thomas, and P. M. Glibert, 2002: Sources of Variability in Chlorophyll Analysis by Fluorometry and High-Performance Liquid Chromatography in a SIMBIOS Inter-Calibration Exercise, G. S. Fargion and C. R. McClain (eds.), *NASA/TM-2002-211606*, Goddard Space Flight Center, Greenbelt, Maryland, 50 pp.
- Werdell, P. J., and S. W. Bailey, 2002: The SeaWiFS Bio-Optical Archive and Storage System (SeaBASS): Current Architecture and Implementation, G. S. Fargion and C. R. McClain (eds.), *NASA/TM-2002-211617*, Goddard Space Flight Center, Greenbelt, Maryland, 45 pp.

Chapter 2

SIMBIOS: Science Team and Contracts

Giulietta S. Fargion

Science Applications International Corporation (SAIC), Beltsville, Maryland

2.1 SCIENCE TEAM

The Science Team is selected through a NASA Research Announcement (NRA). Presently, NASA has had two NRA's, in 1996 and 1999. NASA HQ manages the process of team selection, but the Goddard Space Flight Center (GSFC) NASA Procurement Office handles the team contracts, work statements and, if necessary, budget negotiations. The Project funds numerous US investigators and collaborates with several international investigators, space agencies (e.g., NASDA, CNES, KARI, etc.) and international organizations (e.g., IOCCG, JRC). US investigators under contract to provide *in situ* atmospheric and bio-optical data sets, and develop algorithms and methodologies for data merger schemes. NASA GSFC Procurement requires formal evaluations for all contracts at the end of each contract year. These evaluations go into a database and are shared with the PI's institution or upper management.

Chapters 4 to 20 contain the individual PI's contributions and describe the funded research topics, field study activities, and results of concluded research. Chapters 21 to 24 contain the international contributions. These chapters are reproduced as submitted with minimal editing by the Project Office.

2.2 CONTRACT OVERVIEW

The second-year of the SIMBIOS NRA-99 contracts ended on November 30, 2002. The SIMBIOS Project scheduled a telephone conference (telecon), of about 30-45 minutes, with each PI and other appropriate staff during the month of October. Prior to the telecon, the SIMBIOS Project reviewed each contract, the statement of work, and the agreed to deliveries. The Project Office followed the same procedure used in 1999 and coordinated an inside panel with key contract and project personnel to perform an across-the-board evaluation of all funded contracts (Table 2.1).

Table 2.1 Contract evaluation key personnel

Contracting Officer:	Lynne Hoppel
Contracting Assistant:	Kathy Lingerfelt
Resource/Financial Officer:	Patty Clow & S. Reising
Manager, SIMBIOS Project:	Giulietta Fargion
Manager, Office for Global Carbon Studies:	Charles McClain

The four categories to be evaluated are suggested in the "Evaluation of Performance" from the Federal Acquisition Regulation (FAR) 42.15 and NASA FAR Supplement (NSF) 1842.15 or NASA form 1680 used by GSFC. Under the "quality" category the following are considered:

- data quality and completeness;
- ancillary information provided on the data (metadata);
- the data's usefulness in relation to SIMBIOS goals, i.e., calibration, validation, and algorithm development; and
- quality of technical reports.

The “time” category is a mixed bag, but is viewed with respect to data and documentation (monthly and year-end reports, and special topic publications) and delivery times. Under the “other” category is considered:

- scientific publications and scientific achievements;
- science team collaboration and involvement; and
- other significant events occurring during the contract period evaluated.

As a result of the formal evaluation and telecon with the SIMBIOS PIs, all but two investigators were evaluated as good or very good. The GSFC Procurement Office implemented and executed 12 second-year options. Presently, the Project has in place 12 contracts, 4 interagency agreements and 2 NASA investigations. Further details on the research status and progress reports can be found on our web site at <http://simbios.gsfc.nasa.gov/status.html>.

Chapter 3

SIMBIOS Project Data Processing and Analysis Results

Giulietta Fargion, Bryan Franz, Ewa Kwiatkowska and Christophe Pietras
Science Applications International Corporation (SAIC), Beltsville, Maryland

Sean Bailey, Joel Gales and Gerhard Meister
FutureTech Corporation, Greenbelt, Maryland

Kirk Knobelspiesse and Jeremy Werdell
Science Systems and Applications Inc., Greenbelt, Maryland

Charles McClain and Gene Feldman
NASA Goddard Space Flight Center, Greenbelt, Maryland

3.1 INTRODUCTION

The SIMBIOS Project is concerned with ocean color satellite sensor data intercomparison and merger for biological and interdisciplinary studies of the global oceans. Imagery from different ocean color sensors (OCTS, POLDER, SeaWiFS, MOS, OSMI and MODIS) can now be processed by a single software package using the same algorithms, adjusted by different sensor spectral characteristics, and using the same ancillary meteorological and environmental data. This enables cross-comparison and validation of the data derived from satellite sensors and, consequently, creates continuity in ocean color information on both the temporal and spatial scale. The SIMBIOS Project Office accomplishments during 2002 year are summarized under (a) MODIS Terra & Aqua activities (SeaWiFS cross-comparison and data merger), (b) diagnostic data set, (c) SeaBASS database, (d) supporting services, (e) sun photometers and calibration activities and (f) calibration round robins. These accomplishments are described below.

3.2 MODIS ACTIVITIES

3.2.1 Level-3 Data Merger

In coordination with MODIS-Terra Collection 4 reprocessing, the SIMBIOS Project initiated an operational process to collect and merge MODIS daily global chlorophyll products with SeaWiFS daily products. The input files to this process consist of MODIS 4.6-km Level-3 binned chlorophyll from the SeaWiFS-analog OC3M algorithm (chlor_a_2 product) and the standard SeaWiFS 9-km binned chlorophyll from the OC4v4 algorithm (chlor_a product). The merging scheme is a simple weighted averaging using standard SeaWiFS time-binning software, however, several changes to the MODIS data are required to enable a bin-for-bin match-up with SeaWiFS. First, new software (modbin2seabin) was developed to convert the MODIS format to a SeaWiFS-like spacebin format. This process is simply a reorganization of the HDF fields, as the SeaWiFS and MODIS formats use the same, sinusoidal binning approach. This conversion step was limited, however, to MODIS quality zero data. The second step was to reduce the MODIS 4.6-km spacebin file to 9-km resolution, equivalent to standard SeaWiFS Level-3 format, using another new software tool (reduce_bin_resolution). This is effectively a 4-to-1 spatial averaging, weighted by the number of observations within each 4.6-km bin.

With SeaWiFS and MODIS in an equivalent, 9-km binned format, the process proceeds using standard SeaWiFS time-binning software to produce the merged SeaWiFS/MODIS-Terra daily global chlorophyll products. Recently, the provisional MODIS-Aqua data became available and the SIMBIOS Project was able to incorporate the new data stream into the merging

process within one day. The Project is now producing a complete set of daily, weekly, and monthly merged chlorophyll products, including various perturbations such as MODIS-Terra with MODIS-Aqua, MODIS-Terra with SeaWiFS, MODIS-Aqua with SeaWiFS, and MODIS-Terra/MODIS-Aqua/SeaWiFS. Merged products have been generated for the entire MODIS mission, and they are available through a browser at: <http://seawifs.gsfc.nasa.gov/cgi/level3.pl?DAY=05Mar2000&PER=&TYP=tmsea>. The merging process is fully automated and operational, with new products generated as soon as the MODIS data becomes available. The merged products can be displayed and manipulated with standard SeaWiFS software tools such as SeaDAS.

3.2.2 Time-Series Analysis

The SIMBIOS Project has collected the entire MODIS Oceans archive of global 8-day binned products for chlorophyll and several water-leaving radiance fields, covering the period from March 2000 through October 2002. This data has been used to generate long-term temporal trends for comparison with SeaWiFS, as well as seasonal trends for evaluation of MODIS product consistency from year to year.

Data Sources

The input SeaWiFS data used in this analysis were standard 9-km-resolution Level-3 timebin products from the 4th reprocessing, composited over 8-day periods. The MODIS data were standard 4.6-km-resolution Level-3 products, binned over the same 8-day periods. It should be noted that some of the MODIS data used in this study are considered provisional. Due to the extensive, on-orbit characterization required to calibrate MODIS for ocean data processing, all data collected after the MODIS Oceans Collection #4 reprocessing (after March 19, 2002) are not fully corrected. Data collected prior to November 2000 are also considered provisional, due to the instability of the spacecraft and instrument during the first year of the Terra mission. See <http://modis-ocean.gsfc.nasa.gov/processings> for more details on the MODIS data collection.

As with the Level-3 merging activity, several changes to the MODIS 8-day binned products were required to enable a bin-for-bin match-up with SeaWiFS. The first step was to convert the MODIS format to a SeaWiFS-like spacebin format. Again, this was simply a reorganization of the HDF fields, as the SeaWiFS and MODIS formats use the same, sinusoidal binning approach. At this step, specific MODIS products were associated with standard SeaWiFS products, and any necessary unit conversion was performed. Only MODIS quality zero data were retained. The MODIS products chlor_a_2, nLw_412, nLw_443, nLw_488, and nLw_551, were associated with SeaWiFS products chlor_a, nLw_412, nLw_443, nLw_490, and nLw_555, respectively. The second step was to reduce the MODIS 4.6-km spacebin file to 9-km resolution, equivalent to standard SeaWiFS Level-3 format. The final step was to reduce the MODIS and SeaWiFS 9-km bin files to common bins. For a given 8-day period, only those bins which were filled (contained one or more observations) in both the MODIS and the SeaWiFS files were retained in the final analysis.

Subset Definitions

With SeaWiFS and MODIS in an equivalent form, the data sets were further divided into several geographic subsets. Three global subsets were defined, corresponding to clear water, deep water, and coastal water. The deep water subset consists of all bins where water depth is greater than 1000 meters. Clear water was defined as deep water where the retrieved chlorophyll is less than 0.15 mg/m^3 . For the chlorophyll test, both SeaWiFS and MODIS must be below the threshold. Coastal water was defined as all bins where water depth is between 30 and 1000 meters, as defined by a shallow water mask and the deep water mask. Some caution should be exercised in analyzing the clear-water subsetted data, as anomalously high chlorophyll retrievals from either sensor can significantly alter the geographic distribution of selected bins. In contrast, the deep-water and coastal subsets are purely geographic in selection criteria. The coastal subset, however, is more likely to contain regions of significant variability in water content and atmospheric conditions, as well as case 2 water conditions, all of which can lead to greater retrieval uncertainty and larger differences between the two sensors. The deep-water subset is therefore the most stable subset for cross-sensor comparison of retrieved oceanic optical properties. The geographic extent of all three global subsets will vary, however, with the seasonal change in earth illumination and thus sensor imaging duty cycle.

Trending Analysis

For each sensor, for each 8-day product, the filled bins associated with a particular subset were identified and used to compute some basic statistics and an associated time tag. Figures 3.1, 3.2, 3.3 and 3.4 shows an example of a typical trend plot derived from this analysis. In the first panel, the common MODIS and SeaWiFS bins for the deep-water subset were spatially averaged over each 8-day binned product, and the resulting means were then plotted as a function of time. MODIS is shown as dashed lines. The gray-scales indicate different bands, where bands 1, 2, 3, and 5 correspond to 412, 443, 490, and 555 nm, respectively. The plot in the second panel shows the same data as a ratio, with MODIS means normalized by SeaWiFS means. The solid vertical lines are provided as a reference to indicate MODIS Oceans calibration epochs. These epochs are the independent periods over which MODIS calibration corrections were derived by the MODIS Oceans group at the University of Miami. In most cases, these calibration periods correspond with the calibration epochs used by the MODIS Calibration Support Team at GSFC, and they are generally associated with spacecraft safe-hold events and instrument state changes.

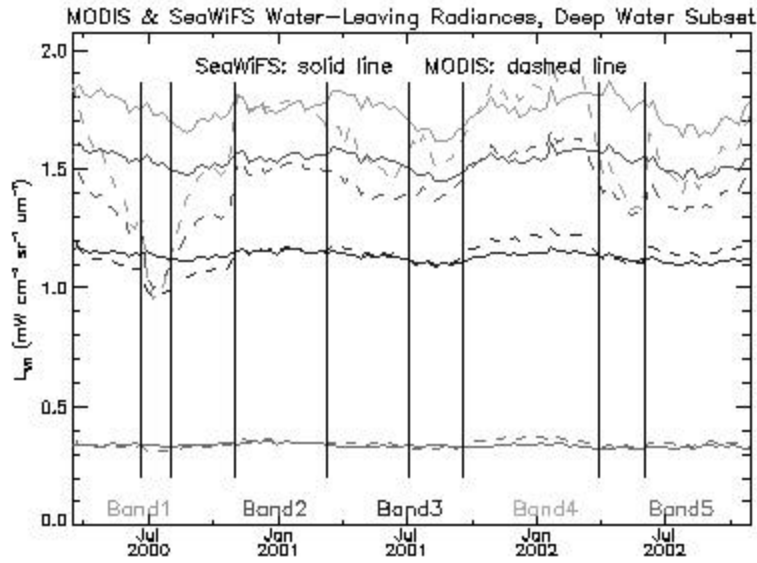


Figure 3.1: SeaWiFS and MODIS Water-Leaving Radiances

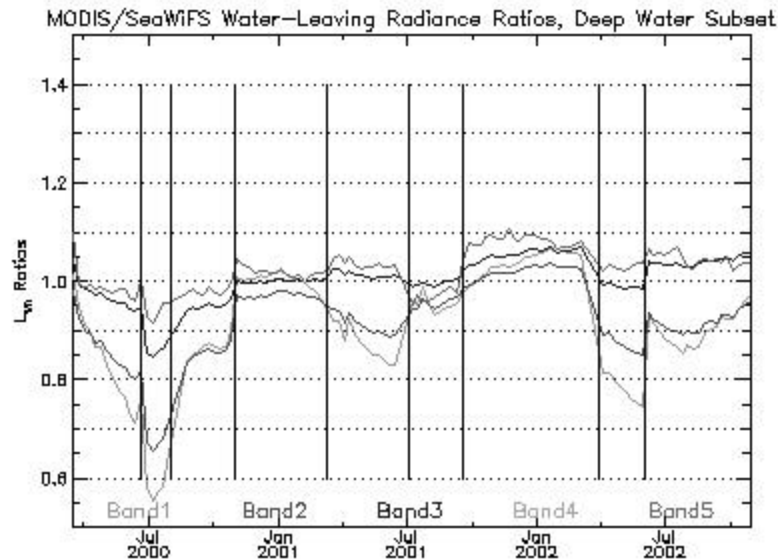


Figure 3.2: Ratio of MODIS to SeaWiFS Water-Leaving Radiances

Another set of standard plots show the radiance and chlorophyll trends for MODIS and SeaWiFS as seasonal overlays. Again, using only the data from common bins, the plots below show the annual repeatability of the two sensors for the deep-water subset over the evaluation period of nearly three years.

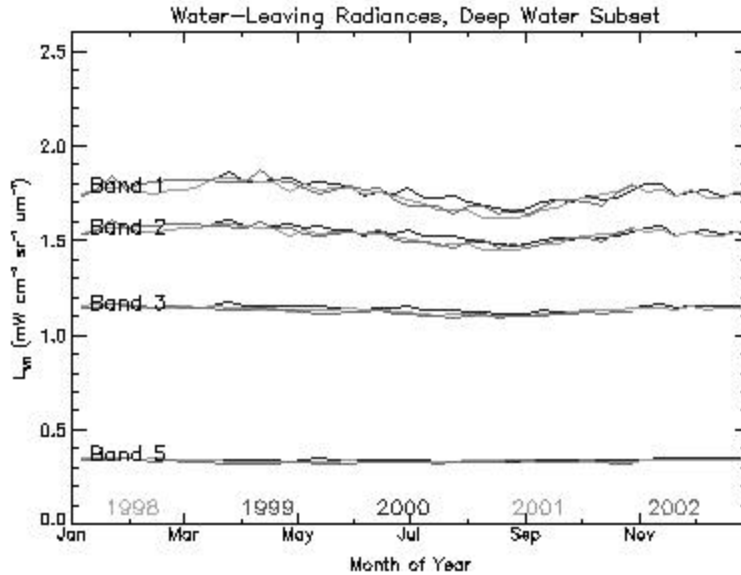


Figure 3.3: SeaWiFS Deep-Water Annual Repeatability

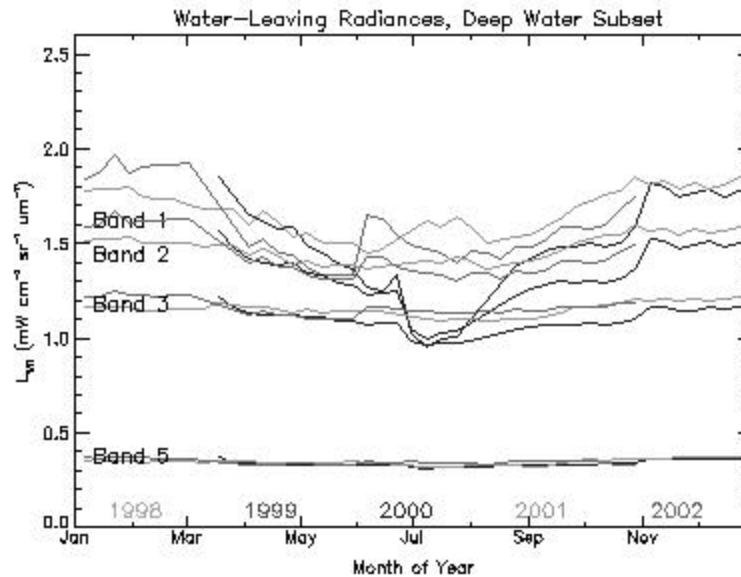


Figure 3.4: MODIS Deep-Water Annual Repeatability

A complete set of trend plots are available at http://simbios.gsfc.nasa.gov/staff/franz/13trend/modis_seawifs/, along with tabulated data and global images. Subset images show mapped chlorophyll for each 8-day period, for the common bins associated with each geographic subset. These images allow for a qualitative assessment of the agreement between the two sensors, and provide an indication of the spatial extent of the subsetted, common bins. Full product images of the chlorophyll and radiance data are also provided, allowing comparison between the two sensors prior to subsetting or reduction to common

bins. Finally, tabulated results of the mean and standard deviation for each product, for each 8-day subset are available. The tabulated means are the values plotted in the trend plots.

Discussion of Results

On average, the agreement between MODIS and SeaWiFS over the trended time-period is good. It is clear from the trend plots, however, that MODIS and SeaWiFS radiances deviate considerably at times. In general, the amount of seasonal variability measured by MODIS is two to three times larger than for SeaWiFS. The table below shows the mean and standard deviation of the 8-day, subset averages (i.e., the mean and standard deviation of the tabulated 8-day means). The table 3.1 illustrate both the good overall agreement and the higher time variability observed by MODIS..

Table 3.1: Global Means Over Common Bins, March 2000 - October 2002

		Chlor_a		nLw_412		nLw_443		nLw_490		nLw_555	
Sensor	Subset	mean	stdev								
SeaWiFS	Deep	0.186	0.0127	1.748	0.0560	1.534	0.0366	1.134	0.0193	0.336	0.0081
MODIS	Deep	0.180	0.0174	1.593	0.2071	1.415	0.1318	1.139	0.0560	0.345	0.0150
SeaWiFS	Clear	0.076	0.0030	2.255	0.0639	1.890	0.0408	1.257	0.0171	0.300	0.0058
MODIS	Clear	0.080	0.0053	2.106	0.1934	1.791	0.1136	1.283	0.0458	0.317	0.0118
SeaWiFS	Coastal	0.921	0.2013	0.831	0.0578	0.892	0.0429	0.875	0.0343	0.427	0.0228
MODIS	Coastal	0.733	0.1211	0.808	0.1243	0.823	0.0891	0.877	0.0520	0.429	0.0267

The SeaWiFS instrument has the benefit of monthly lunar calibration to track and correct for time-dependent drift in instrument response. The temporal degradation is well characterized as a simple exponential decay, and the SeaWiFS temporal stability is therefore believed to be well established. This is illustrated by the excellent annual repeatability demonstrated by SeaWiFS over the same clear, deep, and coastal-water subsets for the five years of the mission (see http://simbios.gsfc.nasa.gov/~franz/l3trend/seawifs/seawifs_8day_trends.html). While it is possible that the differences between SeaWiFS and MODIS are geophysical, due to the 90-minute difference in node crossing time, it is expected that such a physical effect would be repeatable from year to year in accordance with the seasonally changing distribution of solar and viewing angles. The instruments may differ from one another, but they should be self-consistent. The deep-water annual repeatability plots, however, show that the MODIS products are highly variable from year to year, while SeaWiFS is consistent. This suggests that the MODIS Oceans products contain significant calibration or atmospheric correction errors that significantly bias the global averages.

It should also be noted that the deviations between the MODIS and SeaWiFS trends seem to change character at intervals associated with MODIS Oceans calibration epochs. Again, these epochs are indicated by vertical lines on the trend plots. Perhaps the most clear indication of this coincidence with the MODIS calibration epochs can be seen in the ratio trends. Based on the coincidence between MODIS calibration/processing changes and MODIS product deviations relative to SeaWiFS, it seems likely that a significant portion of the temporal variability observed by MODIS is actually a calibration/instrument characterization artifact.

While the temporal stability of the MODIS products may be in question, a close inspection of the subset images indicates that MODIS may have better small-scale spatial stability than SeaWiFS (i.e., less speckling). The MODIS data is expected to have lower digitization noise, due to its 12-bit design relative to the 10-bit SeaWiFS instrument. Probably the more significant factor in this analysis, however, is that the MODIS data has a much higher sample count within each bin. This is due to the fact that the MODIS binned products are derived from 1-km-resolution data, whereas SeaWiFS binned products are derived from 1-km observations which were subsampled 4-to-1 (i.e., GAC data). All else being equal, this would give MODIS a 16-to-1 sampling advantage over SeaWiFS, significantly reducing random noise. The SeaWiFS GAC subsampling also makes it impossible to fully correct for straylight artifacts, since a complete record of bright sources is not available in the GAC dataset. A more geographically limited study could be performed in the future, using the SeaWiFS 1-km HRPT dataset as input to make the two datasets more directly comparable.

Considering the higher spatial stability of the MODIS products, it is worth noting that the standard deviations of the radiance and chlorophyll retrievals within each 8-day period are quite similar between the two instruments. This is likely due to the fact that the noise within each bin, for either sensor, is considerably lower than the large-scale, geophysical variability across the subset. In other words, the standard deviations are dominated by real, spatial structure. In addition, the speckling

noise which would tend to elevate the standard deviations in the SeaWiFS products may be offset by the residual scan-dependent artifacts observable in the MODIS products. These scan effects can be seen as near-vertical striping in the mapped radiance fields, even in some 8-day composites.

3.2.3 MODIS And SeaWiFS Cross-Comparisons

The Project closely followed subsequent versions of MODIS oceans processing leading to the collection 4 algorithm and provided the RSMAS group, University of Miami, with MODIS product matchups against SeaWiFS data to help with the evaluation of MODIS algorithm updates (<http://simbios.gsfc.nasa.gov/~ewa/SeaMODIS/seamodis-match.html>, Kilpatrick et al., 2002). When collection 4 MODIS and reprocessing 4 SeaWiFS data became available, thorough comparisons and scan angle dependence analyses were performed for data from both sensors based on 20 dates spread in time from September 2000 to July 2002.

For these comparisons, cross-calibrations, and merger, the SIMBIOS Project Office identified common MODIS and SeaWiFS data formats and products. The analyses used 4.6km daily global binned products. Although the MODIS standard bin size is 4.6km while SeaWiFS is 9.2km, existing procedures can bin SeaWiFS data to 4.6km to facilitate the comparisons with MODIS standard products. For selected analyses daily 36km bin size data were examined and for global time series studies 9km data were used which were binned over 8 days.

The SIMBIOS Project Office developed software for the combined extraction and analysis of binned MODIS and SeaWiFS files. The evaluation of data products from both sensors involved the following:

- Maps of chlorophyll differences between the two sensors for each day and for the 4 seasons.
- Matchups of product data from both sensors for daily global overlaying bin coverage and for the overlaying coverage limited to open-ocean and clear-atmosphere.
- Data product histograms.
- Time trends in matchup statistics.
- Separate matchups and histograms for different sensor view angles for daily global overlaying bin coverage and for the overlaying coverage limited to open-ocean and clear-atmosphere.
- Time trends in matchup statistics for different sensor view angles.
- Analyses of individual scan line variabilities dependent on sensor zenith angles.
- Global time series comparisons for clear waters, deep waters, and coastal waters.

Maps of global chlorophyll differences between MODIS and SeaWiFS showed spatial discontinuities in the chlorophyll difference field depending on sensor swath positions. MODIS also generally gave higher chlorophyll concentration values in the open ocean than SeaWiFS, especially in the Southern Hemisphere (<http://simbios.gsfc.nasa.gov/~ewa/SeaMODISMay/seasons/seasons.html>). Data for daily overlaying bin coverage between corresponding MODIS and SeaWiFS products were compared in the form of scatter plots. The scatter plot matchups contained accompanying statistics, including slope and intercept of the linear fit of data between MODIS and SeaWiFS, correlation, RMS error, standard deviation from the linear fit line, and standard deviation from the MODIS=SeaWiFS line. Matchups were performed on total global overlaying data sets and on the data limited to open-ocean and clear-atmosphere in order to eliminate more ambiguous coastal water and turbid atmosphere conditions. Clear atmosphere was defined as retaining AOT values below 0.2. Chlorophyll concentration and normalized water-leaving radiance (nLw) matchups in the lower visible wavelengths were in good agreement between the two sensors although some non-functional relationships, questionable data clusters, and a lot of scatter in the plots were also present. In the higher visible wavelengths, MODIS and SeaWiFS operate using different spectral bands, which prohibited direct comparisons. When considered exclusively, open ocean and clear atmosphere data showed the same statistical trends as the entire global data sets (<http://simbios.gsfc.nasa.gov/~ewa/SeaMODISMay/seamodis-match.html>). Plots of matchup statistics against time showed that there was an apparent time dependence present in the linear fit intercept (<http://simbios.gsfc.nasa.gov/~ewa/SeaMODISMay/timetrend/timetrend.html>). These time trends were later more thoroughly studied using a large time series of 8-day binned MODIS and SeaWiFS data sets (http://simbios.gsfc.nasa.gov/~franz/13trend/modis_seawifs/modis_seawifs_8day_trends.html). Dependence in data on sensor scan angle is another difficulty for the merger. SeaWiFS scan behavior has been thoroughly investigated using low chlorophyll waters around Hawaii and the Easter Islands (http://simbios.gsfc.nasa.gov/~ewa/SeaMODIS_May/scangle/scangle.html). SeaWiFS radiometric sensitivity falls off to the same degree towards both edges of the scan. Water-leaving radiances at the lower wavelengths degrade not more than

5% at the very edges of the GAC swath. In this study, an assumption was made about a relative SeaWiFS scan angle stability. This assumption was applied to investigate MODIS viewing angle dependencies. In the analysis, only data between 35° South and 35° North were used to eliminate high latitude bins which both sensors observe several times each day and the viewing directions are multiple and averaged within the bins. MODIS scans the Earth within its swath from West to East. MODIS data were divided dependent on their viewing zenith angles into four groups: from West scan edge to 25° West, from 25° West to nadir, from nadir to 25° East, from 25° East to East scan edge. Matchups with SeaWiFS were performed separately for each MODIS angle group (<http://simbios.gsfc.nasa.gov/~ewa/SeaMODISMAY/seamodis-match.html>). Statistics were calculated from these matchups and plotted through time separately for the individual MODIS scan angle ranges. Time trends turned out to be persistently different for Western and Eastern edges of the MODIS swath for nLw at bands 412nm and 443nm and chlorophyll concentration (<http://simbios.gsfc.nasa.gov/~ewa/SeaMODISMAY/timetrend/timetrend.html>). The result remained the same for data limited to open ocean and clear atmosphere bins. This showed that there were distinct view angle dependencies present in MODIS data independent of SeaWiFS viewing geometries. Figure 3.5 shows an example of MODIS data matchups against SeaWiFS performed separately for the Western and Eastern part of the MODIS scan line. The Figure also displays temporal trends in the matchup linear-fit slope for divided Western and Eastern MODIS scan data.

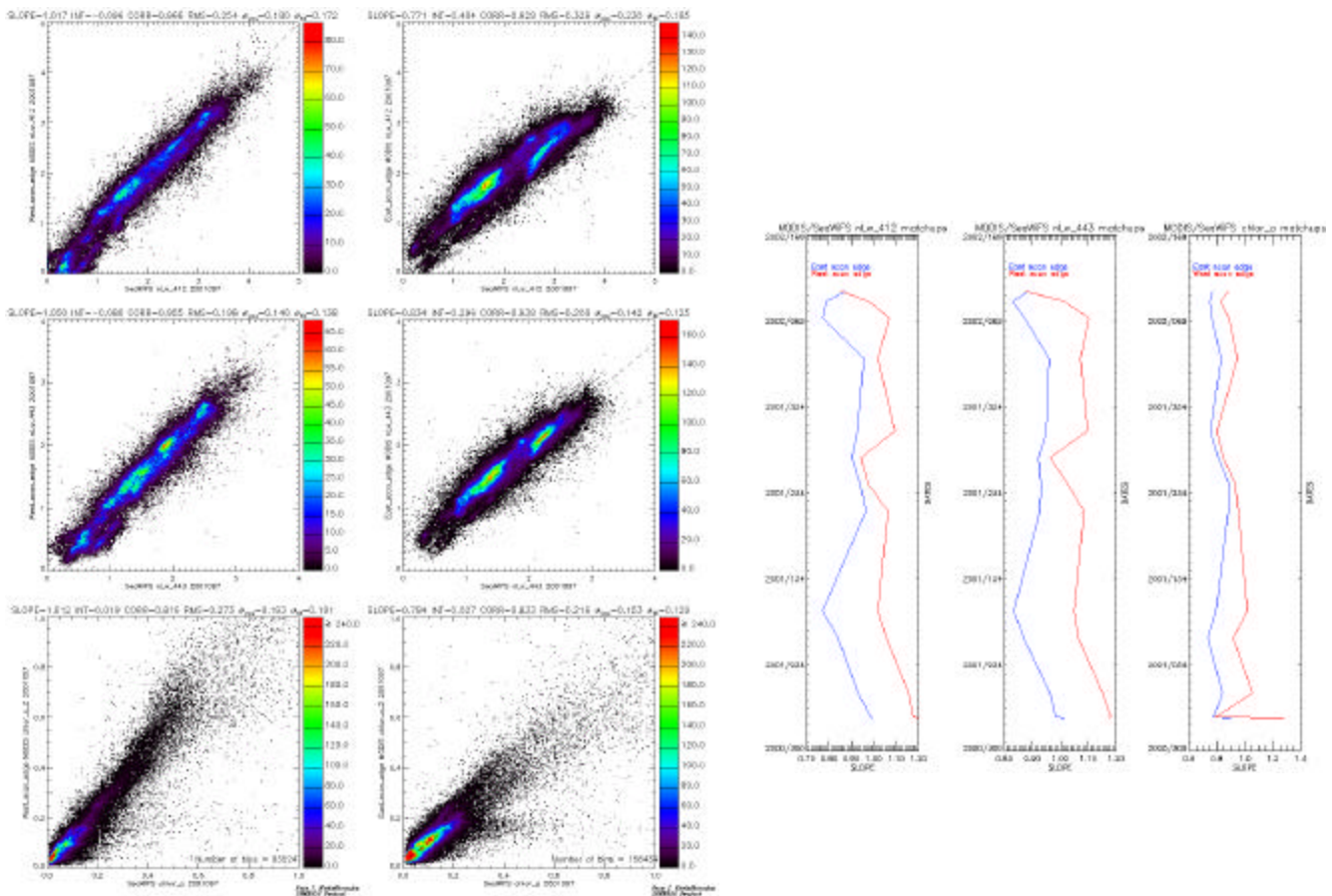


Figure 3.5: MODIS and SeaWiFS nLw (412nm), nLw(443nm), and chlorophyll matchups for 7 April 2001 for Western (left) and Eastern (right) edge of the MODIS swath. Individual time trends in matchup linear-fit slope for the Western (red) and Eastern (blue) MODIS edges.

Apparent scan angle dependencies in data forced an application of basic techniques to further investigate geometry effects for the purpose of data merger. A proof-of-concept study was pursued to cross-calibrate MODIS and SeaWiFS sensors depending on their zenith viewing angles. For this purpose, the dates were chosen for which MODIS and SeaWiFS orbits overlapped the closest, i.e. swath phase difference between the satellites was zero (<http://simbios.gsfc.nasa.gov/~ewa/SeaMODISMAY/seamodis-match.html>). There were very few such days since both satellites had been on orbit. To limit cross-

comparison ambiguities, only open ocean, clear atmosphere ($AOT < 0.2$), and low chlorophyll (chlorophyll concentration $< 0.1\text{mg}/\text{m}^3$) regions were chosen located within ocean gyres from 15° to 30° latitude in the Northern and Southern Hemisphere. Within these zones, 4.6km bins were searched for scan lines with large amounts of overlapping data available from both sensors. Resulting scan lines were studied depending on sensor zenith viewing geometries. Statistics derived from a line fit of data across the sensor zenith angle were recorded and averaged over all extracted scan lines for MODIS and SeaWiFS nLw and chlorophyll concentrations. Figure 3.6 shows an example of an individual MODIS and SeaWiFS overlapping scan line for the date 9 January 2002. There is a significant amount of noise present in the scan data, especially apparent for SeaWiFS. This is because the magnitude of nLw and chlorophyll values is very low. Also, SeaWiFS original spatial resolution of GAC data, which went into 4.6-km bins, is already at 4km while MODIS data are averaged over 1km pixels. It can be seen from the Figure 3.6 that even in these clear-water idealized conditions there is a visible drift in MODIS chlorophyll values across the MODIS zenith angle, possibly coming from a slight slope present at the yellow wavelengths. The average MODIS chlorophyll slope line was calculated as $y = -0.000078x + 0.065$ while the SeaWiFS slope was significantly more leveled, considering the low magnitude of chlorophyll values, $y = -0.000013x + 0.047$.

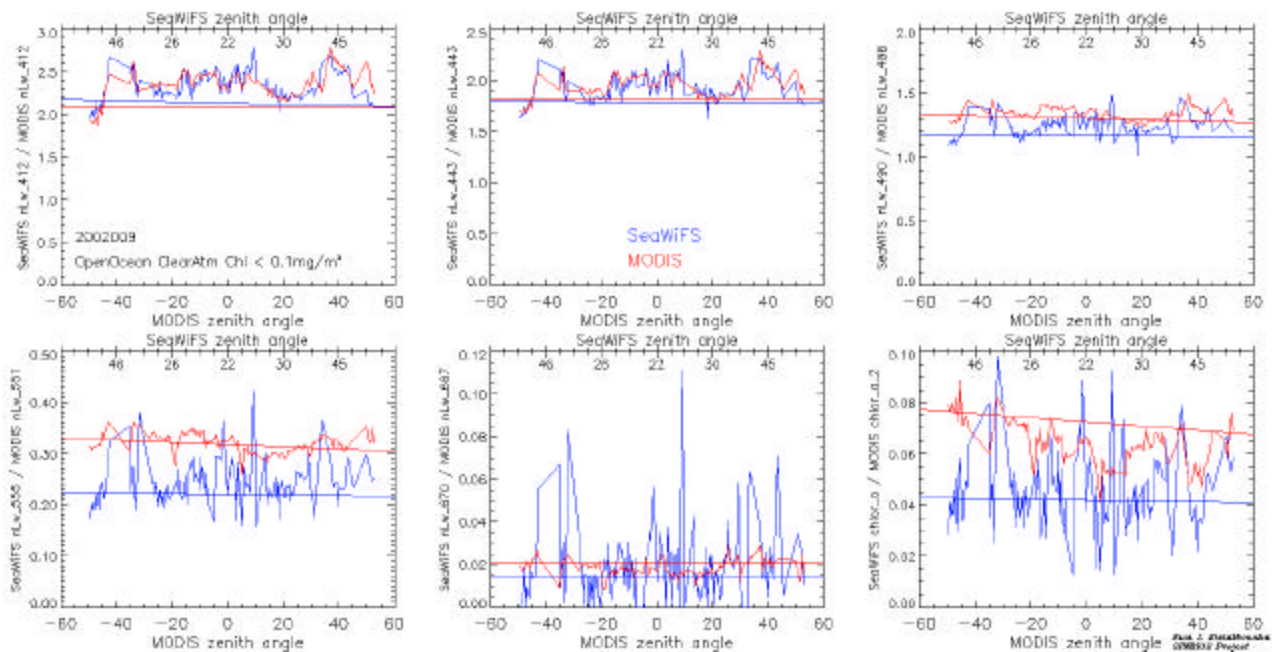


Figure 3.6: Dependence on sensor viewing angle in an individual MODIS and SeaWiFS overlapping scan line, on January 9, 2002.

Using statistics derived from MODIS and SeaWiFS scan line cross-calibration, MODIS data were corrected for that day depending on their zenith-viewing angles. The correction improved sensor chlorophyll concentration matchups based on the slope of 0.934 in the linear fit between the two data sets to the slope of 0.984.

Concluding, the cross-comparisons of multi-sensor data products have a critical importance for the merger activity. Experience gained in the process is helpful in establishing suitable merger approaches. The histograms enable the examination of data distributions. The product inter-comparisons give information on the transfer functions for product data between the two sensors. The matchups between MODIS and SeaWiFS products resulted in the extraction of

- temporal trends,
- and scan-angle dependencies

in MODIS data. These conditions should be eliminated before the merger using additional calibrations and sensor cross-calibrations or should be resolved by the merger algorithm itself in order to obtain a stable series of merged MODIS and SeaWiFS data sets.

3.2.4 Neural-Network And Support-Vector-Machine Regression Mapping

The purpose of the regression mapping is to bring multi-instrument, multi-platform, and multi-year ocean color observations to a common baseline, where the baseline is an ocean color data template consistently calibrated through time and space and well validated against *in situ* measurements. In other words, the goal is to cross-calibrate multi-sensor data to a single “benchmark” representation, regardless of the calibration and other problems of individual sensors. Regression mapping reproduces or emulates the response from the baseline given data from different sensors. This is done through mapping of individual sensor data points given a variety of information describing the sensor, geometry, in-water and atmospheric conditions, and other properties which univocally characterize the given sensor’s data point. In the proof-of-concept analyses performed at the Project, SeaWiFS data were treated as the baseline, thoroughly calibrated and well validated global ocean color benchmark, and MODIS data were mapped to SeaWiFS-like chlorophyll concentration values.

Although the mapping between sensors can be performed using linear or non-linear regression, the use of artificial neural networks or support vector machines is preferred because any complex mapping functions can be approximated using these methodologies (Atkinson and Tatnall, 1997). Neural networks and support vector machines can best be understood as data transformers where the objective is to associate the elements in one set of data with the elements in the second set. They perform more accurately than other techniques, like statistical, particularly when the feature space is complex and the source data have different statistical distributions (Pao, 1989) which is true for ocean color data including these from MODIS and SeaWiFS. The most time-consuming stages of the regression approach are the determination of an optimal set of input features, choice of the model architecture, and training on representative global and temporal data sets so as to cover the widest range of ocean color, atmospheric, sensor geometry, and other ancillary conditions. The algorithm learns by itself through the regression it does between data and, at the same time, fortuitously discovers the differences in sensor data originating from sensor designs, characteristics, calibration peculiarities, and data processing. This training is highly automatic and, when once accomplished, the stored weights and system parameters can always produce new regression output.

Before applying the neural networks or support vector machines regression, input data needed to be prepared to simplify the training process. One important task was elimination of trends in data because the algorithm might have ignored important subtle information present in the data in favor of a large variation exhibited by a trend. This was partially accomplished by sensor cross-calibration or inclusion of input feature elements which characterized the location of data within the temporal and spatial sequence. The other consideration was scaling. MODIS and SeaWiFS chlorophyll data were passed through a logarithm scaling function because they inherently possessed a lognormal distribution (Campbell et al., 1995). All input feature data, including the chlorophyll logarithm, were then scaled and translated so that they were 0 mean and 90% of their values were within a domain range of 6. One of the most important concerns in defining the regression model was choosing the most effective input features for the algorithm. To map MODIS data to SeaWiFS chlorophyll concentration values, dependencies between MODIS data products and SeaWiFS chlorophyll were studied using a genetic algorithm. The algorithm evaluated and propagated the fitness of various combinations of MODIS inputs through generations of neural networks trained on MODIS and SeaWiFS data sets scaled down for fast processing. The training data sets came from overlapping bins between the two sensors which were used in the matchups. MODIS input vectors were composed of nLw at all spectral bands, chlorophyll concentrations, K-490, atmospheric parameters (AOT, ϵ), viewing geometries (sensor and sun zenith and azimuth angles), geographic locations (latitude and longitude), and other ancillary parameters, like ozone, atmospheric pressure, humidity, wind, and date. The genetic algorithm estimated that the following MODIS input features gave the best regression results in mapping to SeaWiFS chlorophyll values: nLw at bands 412nm, 488nm, 551nm, and 678nm, AOT-865, ϵ , chlor_a_2, satellite zenith angle, sun zenith angle, ozone, latitude, longitude, and date. Chlorophyll dependence on the viewing geometry and atmospheric and ancillary parameters meant that not all of these dependencies were eliminated in data processing. To improve the mapping, other input features such as spatial-texture and temporal chlorophyll parameters could also be considered.

Both multilayer feedforward neural networks and support vector machines were used to perform the regression from MODIS data to SeaWiFS chlorophyll. MODIS mapping to SeaWiFS chlorophyll running across 2 years of concurrent sensor coverage was investigated on a Cray supercomputer at the GSFC NASA Center for Computational Sciences. This cross-seasonal mapping will still need to be refined, thus the results presented here are based on the regression performed on a single-day data set. Half of the overlapping MODIS and SeaWiFS bins for this day were used as a training set and the other half as a testing set. Figure 3.7 shows the result of support vector machine mapping of MODIS unique-coverage data from 9 January 2002 to SeaWiFS chlorophyll values. Consequently, the result illustrates joint MODIS and SeaWiFS coverage for this day represented entirely through SeaWiFS chlorophyll values. The radial basis function was used as a kernel to perform the regression (Schölkopf et al., 1996). The accuracy of the mapping was estimated on the testing set and its mean absolute error was equal to 0.09mg/m^3 of chlorophyll concentration.

Support vector machine regression is a promising tool for data merger, especially that it helps to overcome sensor disparity problems. On the other hand, ocean color data pose a very complex regression problem, highly nonlinear and high multidimensional, and more studies are needed to make the regression mapping more general and accurate. Both neural networks and support vector machines provide intrinsic means for the evaluation of the accuracy of their learning. They are trained to converge to a stable solution and a given allowable error on the training set. Their knowledge is stored in system weights and can be tested anytime against data for which the result is known in advance. Once trained, the regression mapping has minimal computational requirements.

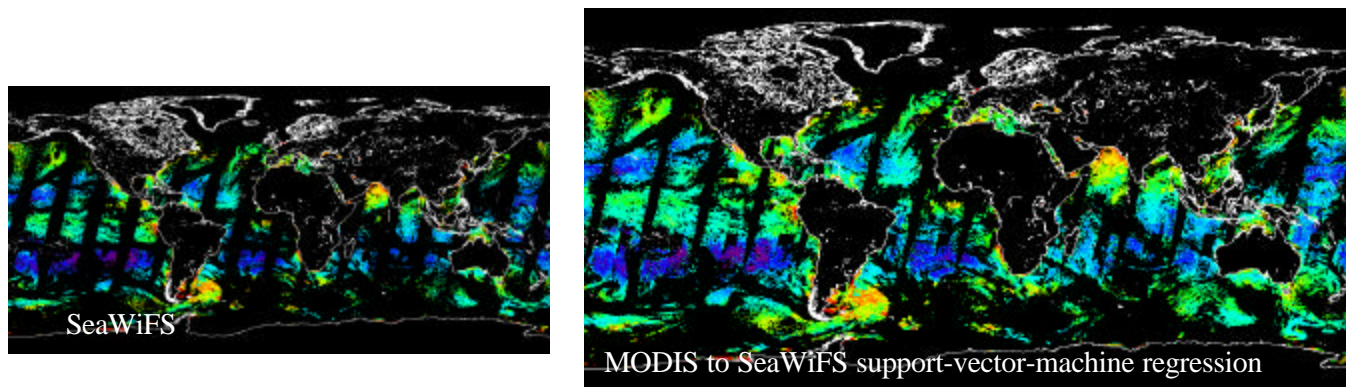


Figure 3.7: Original MODIS and SeaWiFS 36km binned chlorophyll concentration data sets for 9 January 2002 and the result of support-vector-machine regression: SeaWiFS coverage supplemented by MODIS coverage mapped to SeaWiFS-like chlorophyll.

3.3 DIAGNOSTIC DATA SETS

The diagnostic data set is a set of pre-defined geographic regions for which ocean color data products are routinely extracted. The purpose of this activity is to simplify and standardize the intercomparison of ocean color sensors from multiple space missions, and to allow rapid reprocessing of selected areas for calibration and algorithm evaluation. Participants include SeaWiFS and MODIS (Terra & Aqua), as well as MERIS and GLI. The SIMBIOS Project is collecting and distributing the MODIS Level-2 diagnostic data set at http://seawifs.gsfc.nasa.gov/cgi/seawifs_region_extracts.pl?TYP=ocean, and developing procedures for comparative analysis against SeaWiFS and other instruments. Significant effort was made to coordinate the multiple MODIS granules associated with each region, and to compile the related MODIS products into a single daily file per region, thus making the data more accessible to the ocean color community. The Project has recently started to receive the MODIS Level-1B diagnostic data sets. At the present time, there is no software capable of processing these Level-1B extracts to Level-2, but the SIMBIOS Project is working on a modification of the SeaWiFS processing software, MSL12, to provide that capability.

3.4 SeaBASS INTERFACE

The SeaWiFS Bio-optical Archive and Storage System (SeaBASS) serves as a local repository for *in situ* data used in a variety of scientific analyses, for example, satellite data product validation, bio-optical algorithm development, and data merger studies. Archived data include measurements of apparent and inherent optical properties, phytoplankton pigment concentrations, aerosol optical thickness, and other related oceanographic and atmospheric data collected on ships, moorings, and drifters. Additional information on SeaBASS is provided in Werdell and Bailey (2002) and via the World Wide Web at: <http://seabass.gsfc.nasa.gov>. As of November 2002, SeaBASS contains data from over 1000 cruises, encompassing more than 31,000 data files. The volume of archived data is rapidly increasing, as SIMBIOS US Science Team members are contractually obligated to provide data (McClain and Fargion 1999, Fargion and McClain 2002).

SeaBASS data files are flat text, in the American Standard Code for Information Interchange (ASCII) format, with data presented as a matrix, much like a spreadsheet. Each file includes a series of predefined metadata headers, which provide descriptive information about the data, such as the names of the contributors and experiment, the date and location data were

collected, and other ancillary metadata. All data files and related documents are stored in a directory tree organized by contributor affiliation, experiment, and specific cruise. Data are further archived using a relational database management system (RDBMS). The RDBMS is used to catalog and archive metadata and data information from each data file, and to locate and retrieve specific metadata and geophysical data information from the full bio-optical data set. The standard file format and the storage protocols did not change significantly during the past year of the SIMBIOS effort.

The SIMBIOS Project maintains software, named FCHECK, to validate the format of SeaBASS data files. Contributors are required to use FCHECK to verify the format of their files prior to data submission. Once the files meet SeaBASS format requirements, the contributor may submit their data and related documentation, such as cruise reports and instrument calibration files, to the SeaBASS Administrator via File Transfer Protocol. Additional information regarding FCHECK and data submission protocols is available online at: http://seabass.gsfc.nasa.gov/seabass_submit.html.

Protocols for format validation and data submission have not been altered over the past year. The full bio-optical data set is available online via the SeaBASS Web site. Data are located and retrieved using a series of online search engines, listed and described in detail at: <http://seabass.gsfc.nasa.gov/dataordering.html>.

Each search engine allows users to limit queries to particular experiment, contributors, dates, locations, and data types. A new, unique utility, the SeaBASS Validation Cruise Search Engine, was put online this past year. This utility was designed specifically to assist researchers in need of validation data for their satellite calibration and validation activities, and as such, queries may be limited only by ocean color mission (e.g., SeaWiFS, MODIS Terra and Aqua, and MERIS). Queries return a table of potential validation cruises, including metadata for each cruise, such as start and end date and center latitude and longitude. To supplement this utility, mission-specific maps of pigment, radiometer, and sun photometer data points are posted online daily. To protect the publication rights of contributors' data, full access to SeaBASS is limited to members of the SIMBIOS Science Team and other NASA-funded researchers. A password is required to access the full bio-optical data set. All data collected prior to 31 December 1999, however, are available to the public and are additionally available through the National Oceanic and Atmospheric Administration National Oceanographic Data Center. The development of a CD-ROM version of the full public bio-optical data set is planned for Spring 2003. The procedures for the water-leaving radiance, chlorophyll *a*, and aerosol optical thickness satellite-to-*in situ* match-up analyses changed little during the past year of the SIMBIOS effort. Information on these analyses may be found in the SeaWiFS Postlaunch Technical Report Series Volume 10 (Bailey et al. 2000).

3.5 SUPPORT SERVICES

In an effort to improve the quality and quantity of calibration and validation data sets, the SIMBIOS Project offers several support services to field investigators. These services include; scheduling of on-board LAC recording for SeaWiFS; overflight predictions for operational sensors (currently SeaWiFS, OCTS, MOS-B, MODIS-PM, MODIS AM, OCI, OCM, OSMI and MERIS); near real time SeaWiFS imagery for cruise locations; and sunphotometer instrumentation from a pool of project-owned instruments. These services may be requested via the World Wide Web at <http://simbios.gsfc.nasa.gov>. In return for these services, the SIMBIOS Project requests that the field investigators provide *in situ* validation data to the Project's bio-optical archive, SeaBASS. Since January of 2002, the SIMBIOS Project has supported 76 cruises (Table 3.2).

Scheduling SeaWiFS On-board LAC Recording

Since much of the world's oceans are not covered by a SeaWiFS HRPT station, high-resolution data may be recorded onboard the SeaWiFS sensor. As a service to the scientific community, the SIMBIOS Project in conjunction with the SeaWiFS Project can schedule SeaWiFS onboard LAC for cruises that occur outside HRPT coverage. SeaWiFS has the ability to record a maximum of 10 minutes of high-resolution data per downlink. Typically, a 30-second interval is allotted for LAC target, which corresponds to 180 scan lines or approximately 200 km along track at nadir. Detailed information on LAC scheduling is available on the SIMBIOS web site.

Overflight Predictions for Operational Sensors

For calibration and validation purposes, *in situ* measurements should be made as close to the sensor overflight time as is possible. To aid investigators in determining when sampling should occur, the SIMBIOS Project offers overflight predictions

for all operational ocean color remote sensors. Currently, the sensors supported are SeaWiFS, MOS-B, OCI, MODIS, OSMI, OCM and MERIS. Detailed information on overflight predictions is available on the SIMBIOS web site.

Near Real Time SeaWiFS Imagery

In addition to providing predictions for satellite overflight times, the SIMBIOS Project offers near real time imagery of the operational SeaWiFS products in JPEG or GIF format to cruises at sea. 'True color' images are in JPEG format, all other products are in GIF format. These images provide field investigators with additional information with which they may maximize *in situ* sampling of transient oceanographic features. The default specifications for the images provided include:

- available LAC, HRPT, and GAC;
- chlorophyll-a and pseudo-true color images;
- 2-degree box about a designated location or the entire designated region;
- image width of 600 pixels;
- minimum percent valid chlorophyll pixels: 5%;
- images may be customized to best accommodate individual investigator needs.
- Detailed information on near real-time imagery is available on the SIMBIOS web site.

Table 3.2: SIMBIOS supported cruises with services provided.

Experiment Name	Investigator	Period		Services
NC-01-02	Varis Ransi	Jan 4 2002	Feb 28 2002	overflight
SOFeX	Francisco Chavez	Jan 5 2002	Mar 31 2002	image, overflight
CoOP WEST W02	Raphael Kudela	Jan 8 2002	Jan 31 2002	image
DIAPALIS 3	Cecile Dupouy	Jan 9 2002	Jan 22 2002	LAC, image
POS283	Thomas Martin	Feb 1 2002	Feb 26 2002	image
SECRET	Doug Pirhalla	Mar 1 2002	Mar 31 2002	overflight
NOAA NC 03 2002	Doug Pirhalla	Mar 1 2002	Apr 30 2002	overflight
POS284	Thomas Martin	Mar 3 2002	Mar 26 2002	image
Visayas Color	Kathleen Silvano	Mar 7 2002	Mar 18 2002	LAC, overflight
TAG A GIANT 02	Andreas Walli	Mar 10 2002	May 11 2002	image
EPSCOR Cruise	Richard Miller	Mar 11 2002	Mar 30 2002	image
MAR02BR	Ajit Subramaniam	Mar 28 2002	Apr 18 2002	LAC, overflight
DIAPALIS04	Cecile Dupouy	Apr 2 2002	Apr 21 2002	LAC, image, overflight
CYCLOPS 2002	Steve Groom	Apr 15 2002	Jun 5 2002	image
MOMAP North Sea	Marcel Wernand	Apr 15 2002	May 5 2002	image, overflight
Arc02 1	Glenn Cota	May 6 2002	Jun 15 2002	image, overflight
MERIS2002	Thomas Ohde	May 13 2002	May 18 2002	overflight
SCIPIO	Peter Miller	May 15 2002	Jul 12 2002	image
TN147	Ricardo Letelier	May 20 2002	Jul 1 2002	image
DIAPALIS 5	Cecile Dupouy	May 20 2002	May 30 2002	LAC, image
Swedish Lakes	Anu Reinart	May 21 2002	Jun 1 2002	overflight
MP5	Ajit Subramaniam	Jun 1 2002	Jul 21 2002	image
CoOP W 200206	Raphael Kudela	Jun 1 2002	Jul 1 2002	image
CICESE	Mati Kahru	Jun 7 2002	Jun 14 2002	overflight
Bongo VPR	John E. O'Reilly	Jun 9 2002	Jun 23 2002	image
EN372	Ru Morrison	Jun 14 2002	Jul 17 2002	image, overflight
VARIAS Aqua	Maria Paola Bog	Jun 29 2002	Jul 4 2002	overflight
Turkey HAB	Raphael Kudela	Jul 1 2002	Jul 21 2002	image
JUL02PAC	Ajit Subramaniam	Jul 2 2002	Jul 12 2002	overflight
T MAST02	Will Aicken	Jul 4 2002	Jul 27 2002	image
MELEE VII Erie	Steven Wilhelm	Jul 8 2002	Jul 30 2002	image

Arc02 2	Glenn Cota	Jul 15 2002	Aug 31 2002	image, overflight
RESE 5	Susanne Kratzer	Jul 17 2002	Aug 29 2002	image
RR0208	Ricardo M Letelier	Jul 28 2002	Aug 28 2002	image
S2087	Will T Aicken	Jul 29 2002	Aug 17 2002	image
Bering Cocco	Peter Miller	Jul 30 2002	Aug 18 2002	image
DIAPALIS 6	Cécile Dupouy	Aug 2 2002	Aug 16 2002	LAC, image
TowCrom0206	Jeffrey Polovina	Aug 4 2002	Aug 15 2002	image
Argentina 2002	Ajit Subramaniam	Aug 19 2002	Dec 31 2002	image
COVE 2002	Bill Smith	Aug 20 2002	Oct 16 2002	image
Bloom Chaser	Ajit Subramaniam	Aug 23 2002	Oct 18 2002	image
Pamlico Fall02	Doug Pirhalla	Sep 1 2002	Oct 31 2002	overflight
Oc381	Larry Madin	Sep 5 2002	Sep 30 2002	image
Benguela cruise	Stan Hooker	Sep 15 2002	Nov 1 2002	image
Project Lake Water	Janet Campbell	Sep 17 2002	Dec 1 2002	overflight
TIR02	Kirk Knobelspiese	Sep 20 2002	Oct 11 2002	image, overflight
CT020927	Ru Morrison	Sep 25 2002	Oct 13 2002	image, overflight
IRONFROMABOVE	Marcel Wernand	Sep 26 2002	Nov 2 2002	image
GP6-02-KA	Victor Kuwahara	Oct 2 2002	Oct 30 2002	LAC
METEOR 55	Thomas Martin	Oct 10 2002	Nov 17 2002	image
DIAPALIS 7	Cecile Dupouy	Nov 11 2002	Dec 6 2002	LAC, image
MLML Beatman	Luke Beatman	Nov 20 2002	Mar 20 2003	overflight
Korb JR82	Peter Miller	Dec 4 2002	Feb 28 2003	image

3.6 SIMBIOS SUNPHOTOMETERS AND CALIBRATION

Twelve Microtops II, two SIMBAD and two PREDE Mark II sun photometers were deployed in fifty-one cruises in 2002. Two SIMBADA radiometers were added to the pool this year and were deployed in several cruises. A characterization of these new sun photometers was performed at NIST (see chapter 24). Two Microtops II sun photometers were sent to the manufacturer to replace the filters, the photodiodes and the front windows. The SIMBIOS instrument pool now includes fourteen Microtops II sun photometers.

Sun Photometer Calibration

The calibration of the sun photometers is described in McClain and Fargion (1999). Details on the operation, calibration and theoretical principles of sun photometry are posted on the internet (<http://simbios.gsfc.nasa.gov/Sunphotometers/calibration.html>).

The Sun Photometer Instrument Pool web site was extensively updated this year, and now includes information about the deployment and data processing status of each instrument (<http://simbios.gsfc.nasa.gov/Sunphotometers>). The cross calibration time series is reported in Table 3.3 for the Microtops #3768, the SIMBAD #972306, the SIMBAD #972309 and the SIMBADA #07 and #09.

Complete and updated calibration coefficients can be found on the internet at <http://simbios.gsfc.nasa.gov/cgi-bin/cal.cgi>. The calibration processing code was standardized for all sun photometers and upgraded to account for the new SIMBADAs. This code allows the cross calibration with a master Cimel instrument based on the time to time voltage ratios (V_0). Only clear days that show a variation $\Delta V_0/V_0$ less than 1% were retained as calibration days. Cross calibration was performed for each sun photometer roughly every three months, but varied with particular instrument deployment, maintenance, and the availability of appropriate weather for calibration (which is much less common in the summer).

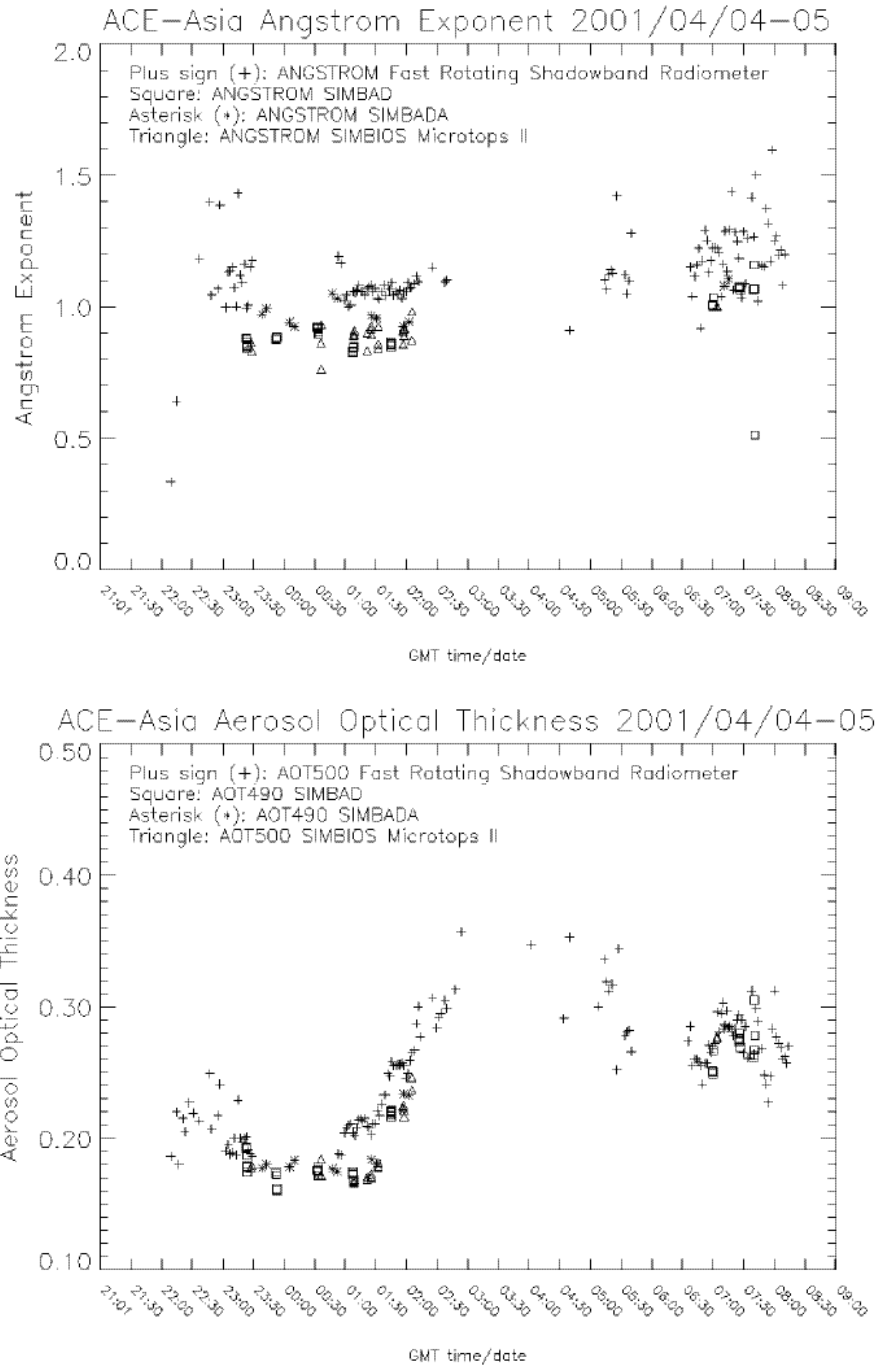


Figure 3.8: ACE-Asia 2001 AOT and Angstrom Exponent time series plots for 2002/04/04

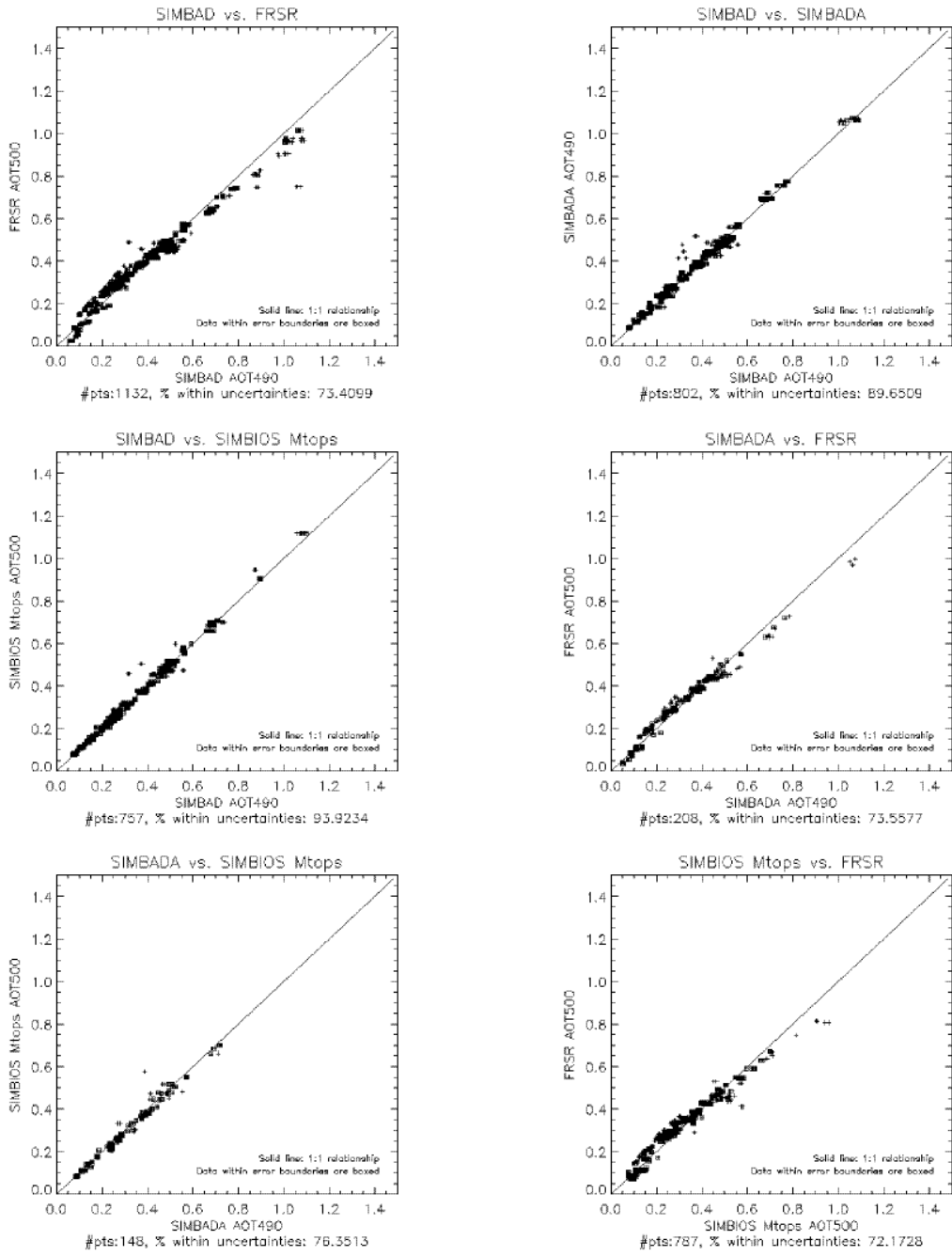


Figure 3.9: Multiple instrument scatter plots of ACE-Asia 2001 AOT's measured within 15 minutes of each other.

Above Water Radiometer Calibration

The SIMBAD and SIMBADA radiometers are also designed to do above water measurements (in addition to being a sun photometer). The optics and filters are the same but the electronic gain is different. The calibration is generally performed at GSFC using a 6' or a 42" integrated sphere at GSFC. Table 3.4 shows the reflectances per count obtained for various calibrations performed since 1999 with two SIMBAD and two SIMBADA sun photometers. The analysis code that process the sphere calibration is ready and is able to account for the new channels of SIMBADA, various levels of lamps or various spheres. Uncertainties of the calibration coefficient determination, based on the standard deviation obtained from the measurements and the accuracy of the integrated sphere calibration, are computed by the code. The values are not shown in table 3.4. The recent characterization at NIST of the two SIMBADA radiometers using the SIRCUS facility (see chapter 24) was able to provide realistic spectral response of each radiometer. Spectral responses provided by preliminary analysis of the SIRCUS experiment were used to replace the spectral responses provided by the manufacturer of the SIMBADAs. A second round of analysis was conducted at NIST in December 2002. The calibration coefficients reported for the SIMBADA radiometers in table 3.4 will be revisited when final analysis is available. New techniques implemented last year to monitor the behavior of the radiometers over time and between two absolute calibration methods were still used for both SIMBAD and SIMBADA radiometers. The SeaWiFS Quality Monitor (SQM) and the Spectralon plaque were still used in 2002. Data are being processed and are not shown here.

Validation And Comparison During ACE-Asia 2001

The Asian Pacific Regional Aerosol Characterization Experiment (ACE-Asia) cruise of the R/V Ron Brown was an ideal platform to validate the consistency of the variety of sun photometer instrument types, calibration techniques and deployment personnel. The R/V Ron Brown, which departed from Hawaii on March 15, 2001 and arrived in Yokosuka, Japan on April 19, 2001, encountered a variety of aerosol types, from maritime low optical thickness conditions to extremely high optical thickness due to Asian dust. Table 3.5 lists the five sun photometers from which valid data were gathered. Four of the sun photometers were handheld, while the Fast Rotating Shadowband Radiometer (FRSR) is an automated instrument. The SIMBAD, SIMBADA and SIMBIOS Microtops II are owned, calibrated and deployed by the SIMBIOS Project. The Fast Rotating Shadowband Radiometer is owned, calibrated and deployed by the SIMBIOS Project funded Shipboard Oceanographic and Atmospheric Radiation (SOAR) Project, at the Brookhaven National Laboratory. The NOAA-PMEL Microtops II is owned, calibrated and deployed by the National Oceanic and Atmospheric Administration's (NOAA) Pacific Marine Environmental Laboratory (PMEL). Unfortunately, the measurement protocol set for the NOAA-PMEL Microtops II was not appropriate for measurements at sea, so a large amount of data had to be removed to account for sun pointing errors. Therefore, comparisons between the NOAA-PMEL Microtops II and other instruments were very limited in number.

Visual inspections of data time series suggest that despite differences in instrument design, calibration and deployment, AOT and Angstrom Exponent typically agree within uncertainties. Figure 3.8a shows the aerosol optical thickness (AOT) for the filter band with a central wavelength of 490nm (for the SIMBAD and SIMBADA) or 500nm (for the FRSR and Microtops II). This band was chosen for comparison because it is common to all instruments and exhibits a higher signal in most conditions than bands common to longer wavelengths (such as 870nm). The Angstrom Exponent, which expresses the spectral character of the AOT and is calculated as shown above is compared for the same day in figure 3.8b. Figures 3.9 and 3.10, and table 3.6 present a more rigorous comparison, where temporally similar data from different instruments are compared on scatter plots. Data from instruments whose bands have similar (within 10nm) center wavelengths, and have calculated uncertainty values were analyzed to find measurements taken within fifteen minutes of each other. These temporally similar measurements were plotted to assess trends or biases between the data. Figure 3.9 shows these scatter plots for AOT at 490nm or 500nm. Nearly all data fall within one uncertainty unit of the 1:1 line. Figure 3.10 shows the same for the Angstrom Exponent. While a higher percentage of the Angstrom Exponent values fall within one uncertainty unit of the 1:1 line, it is important to note that the Angstrom Exponent uncertainties are often up to 50% of the total Angstrom Exponent value. Initially, this analysis revealed an underestimation of high AOT values measured by the FRSR when compared to the other sun photometers. This lead to a refinement of the AOT retrieval algorithm for that instrument (see chapter 11). Despite these changes, the FRSR tends to overestimate the Angstrom Exponent with respect to other sun photometers. Figures 3.9 & 3.10 represent data calculated with the new retrieval algorithm. Finally, it is important to note that some bands were omitted for a lack of comparable bands in other instruments or uncertainty values for those bands. Table 3.6 describes the relationship between different instrument products by showing the percentage of concurrent measurements that fall within one uncertainty unit of each other. The weighted (by number of concurrent data points) averages presented in the last column highlight the

strengths and weaknesses of each instrument. Generally speaking, at least 80% of all AOT data compare within one uncertainty unit of the value from another instrument. With its high uncertainty values, the Angstrom Exponent comparisons are even better, at 90% or more. Finally, the weighted average percentages for the NOAA-PMEL Microtops II are lower than for most other instruments, which is most likely due to the improperly set measurement protocol of that instrument during ACE-Asia 2001.

Table 3.3: Top of Atmosphere (TOA) signals (digital counts) and standard deviations for the sun photometers determined by transfer calibration from a calibrated Cimel at GSFC between August 1998 and December 2002.

MicroTops 03768	Cimel #	440 nm		500 nm		675 nm		870 nm				
12/14/1998	94	1017		987		1203		802				
03/30/1999	37	972		982		1201		800				
06/09/1999	101	894		980		1204		807				
09/23/1999	94	826		982		1206		784				
11/11/2000	Replacement of 440nm filter and front window and calibration											
11/11/2000	-	1263		1024		1193		813				
90/20/2000	37	1247		981		1205		802				
03/19/2001	94	1231		958		1105		675				
05/22/2001	Replacement of front window											
07/06/2001	101	1246		979		1207		807				
06/09/2001	94	1243		974		1188		790				
06/12/2001	89	1247		977		1201		802				
01/04/2002	37/89	1235		940		1172		783				
02/28/2002	89/94	1245		979		1197		792				
06/25/2002	89	1251		975		1201		802				
08/07/2002	101/89	1250		979		1188		794				
08/11/2002	101/89	1245		971		1178		783				
03/12/2002	101/89	1244		974		1193		793				
SIMBAD 932706		440 nm		490 nm		560 nm		675 nm		870nm		
8/21/1998	37	388591		479121		406870		421086		304820		
12/14/1998	94	388269		473101		394874		410455		311944		
9/23/1999	94	376205		464224		391526		416182		300000		
10/28/1999	101	376820		462637		387034		410887		302475		
3/6/2000	37	382815		465574		382168		408538		301005		
SIMBAD 932709												
01/14/2000	94	271780		385589		331527		402221		315555		
03/06/2000	37	290782		417612		345272		412919		294661		
06/09/2001	94	297265		419856		343879		422271		266048		
02/28/2002	89/94	307323		425318		333614		414814		252585		
03/12/2002	89	303348		419680		315668		409029		224736		
SIMBADA 07 - $V_0 * 10^3$		350 nm	380 nm	410 nm	440nm	490 nm	510 nm	560 nm	620 nm	670 nm	750 nm	870 nm
06/09/2001	94	937	1,821	1,351	2,229	3,119	2,575	2,320	3,266	3,145	3,169	2,528
01/04/2002	37/89	935	1,650	1,378	2,303	2,888	2,585	2,321	3,206	3,140	3,224	2,681
06/25/2002	89	1,034	1,600	1,381	2,281	2,925	2,580	2,335	3,277	3,177	3,218	2,599
07/08/2002	89/101	908	1,495	1,353	2,200	2,840	2,535	2,263	3,182	3,187	3,223	2,492
SIMBADA 09 - $V_0 * 10^3$		350 nm	380 nm	410 nm	440nm	490 nm	510 nm	560 nm	620 nm	670 nm	750 nm	870 nm
06/09/2001	94	853	1,714	1,350	2,288	2,935	2,647	2,381	3,004	3,171	3,249	2,246
01/04/2002	89/37	858	1,555	1,410	2,385	2,999	2,683	2,366	2,993	3,170	3,301	2,377
07/08/002	89/101	836	1,383	1,395	2,303	2,940	2,657	2,324	2,990	3,211	3,310	2,213

Table 3.4: Calibration coefficients (relectance/counts) for SIMBAD # 06 and 09 between 1999 and 2002 and for SIMBADA 07 and 09 in 2002.

<i>SIMBAD</i> #972306	443nm	490nm	560nm	675nm	870nm			
08-12-1999	3.8181	2.1922	2.4319	4.2292	8.0289			
01-14-2000	3.7650	2.1339	2.3894	4.1096	7.6506			
03-06-2000	3.6442	2.1186	2.4042	4.1324	7.7366			
08-18-2000	3.7942	2.2376	2.5963	4.3958	8.2380			
<i>SIMBAD</i> #972309								
08-12-1999	4.931	2.425	2.695	4.312	8.277			
01-14-2000	5.0134	2.3451	2.6511	4.2599	7.9370			
03-06-2000	4.7363	2.2771	2.6234	4.2219	8.0104			
03-28-2001	4.6895	2.2732	2.6727	4.2406	8.5264			
01-23-2002*	4.7769	2.3225	2.7864	4.2340	9.3258			
01-23-2002	4.7603	2.3178	2.7769	4.2277	9.3403			
12-13-2002	5.0143	2.4103	2.9708	4.3152	10.8240			
<i>SIMBADA</i> #07	443nm	490nm	510nm	560nm	630nm	675nm	750nm	870nm
05-20-2002	2.3609	1.9225	1.8932	2.0918	1.4884	1.5571	1.4506	1.7713
10-31-2002	2.4289	1.9669	1.9223	2.0992	1.4993	1.5664	1.4609	1.8560
12-13-2002	2.4489	1.9943	1.9500	2.1356	1.5170	1.5742	1.4589	1.8768
<i>SIMBADA</i> #09								
05-20-2002	1.5399	2.0929	2.0615	2.4935	1.2154	1.3325	1.6864	1.8725
10-31-2002	2.2459	1.9547	1.9119	2.3122	1.6076	1.6098	1.5845	2.4717

Table 3.5: Sun photometers deployed on the ACE-Asia 2001 cruise of the R/V Ron Brown

Instrument	Type	Calibrate	Center wavelengths, per band (nm)											
						443	490		560		670		870	
SIMBAD	Direct Solar	Cross*				443	490		560		670		870	
SIMBADA	Direct Solar	Langley	350	380	412	443	490	510	560	620	670	750	870	
SIMBIOS Microtops II	Direct Solar	Cross*				440	500				675		870	936
NOAA-PMEL Microtops II	Direct Solar	Langley		380		440	500				675		870	
Fast Rotating Shadowband Radiometer	Shadow band	Langley			410		500			615	680		870	940

*SIMBIOS Project sun photometers are calibrated on land by a cross calibration to CIMEL sun photometers maintained by the AERONET Project. The CIMEL sun photometers are calibrated with the Langley method at Mauna Loa

Table 3.6: Percentage of ACE-Asia concurrent measurements that fall within calculated uncertainties

	SIMBAD	SIMBADA	SIMBIOS Microtops II	NOAA-PMEL Microtops II	FRSR	Weighted Averages
SIMBAD 443		90.6	87.3	83.3	-	88.8
“” 490		89.7	93.9	70.0	73.4	83.9
“” 560		90.1	-	-	-	90.1
“” 670		77.3	89.7	66.7	75.8	79.9
“” 870		81.7	88.6	46.7	87.1	85.0
“” Angstrom		95.1	98.3	86.7	98.8	97.3
SIMBADA 412			-	-	98.8	98.8
“” 443	90.6		77.0	47.1	-	87.8
“” 490	89.7		76.4	41.2	73.6	84.6
“” 560	90.1		-	-	-	90.1
“” 620	-		-	-	73.6	73.6
“” 670	77.3		79.1	35.3	65.7	75.0
“” 870	81.7		73.0	35.3	84.2	80.3
“” Angstrom	95.1		83.8	53.0	89.2	92.1
SIMBIOS Microtops II 440	87.3	77.0		70.0	-	85.4
“” 500	93.9	76.4		100.	72.2	82.5
“” 675	89.7	79.1		100.	85.1	86.7
“” 870	88.6	73.0		90.0	94.2	89.8
“” Angstrom	98.3	83.8		100.	99.5	97.6
NOAA-PMEL Microtops II 440	83.3	47.1	70.0		-	74.7
“” 500	70.0	41.2	100.		87.5	70.9
“” 675	66.7	35.3	100.		93.8	69.0
“” 870	46.7	35.3	90.0		100.	57.3
“” Angstrom	86.7	53.0	100.		100.	84.5
FRSR 410	-	98.8	-	-		98.8
“” 500	73.4	73.6	72.2	87.5		73.1
“” 615	-	73.6	-	-		73.6
“” 680	75.8	65.7	85.1	93.8		78.4
“” 870	87.1	84.2	94.2	100.		89.6
“” Angstrom	98.8	89.2	99.5	100.		98.2

Pointing Error Screening

Porter, et al., (2001) and members of the SIMBIOS Project realized that the default measurement protocol for the Microtops II were insufficient to remove erroneous data collected when the instrument was not pointed accurately at the sun. The 2001 SIMBIOS Annual Report, and Knobelspiesse, Pietras and Fargion, (2002), describes the changes to the Microtops II measurement protocol and processing to account for these errors. In 2002, the new protocols were implemented in both the instrument deployment and post deployment processing. Figure 3.11 shows a flowchart of the default measurement protocol and the new protocol adopted by the SIMBIOS Project. In addition, the entire Microtops II data set archived in SeaBASS was reprocessed to remove data with erroneous sun pointing. Since these data were collected with the default (manufacturer supplied) protocol, a separate routine was built for this purpose. This routine analyzes the standard deviation of the data

averaged into each measurement (see figure 3.10), and rejects data whose standard deviation is above a threshold. As a result, a large amount of erroneous data were removed from SeaBASS.

Uncertainty Analysis

Separate uncertainty analyses were performed for the Microtops II, SIMBAD and FRSR sun photometers. While some of the components of the uncertainty calculation have yet to be determined, as is the case for the SIMBAD and less so for the Microtops II, these values are a starting point which should be very close to the actual value.

The Microtops II uncertainty analysis was performed using the work of Russel, et al. (1993) and Dubovik, et al. (2000) as models. Dubovik et al. (2000) was also used as the source of cross-calibration uncertainties, as it presents the uncertainty for the CIMEL sun photometers used to calibrate the Microtops II. Equation 3.1 presents the governing equation for Microtops II error:

$$dt_a = \left[\left(\tau \frac{dm}{m} \right)^2 + \left(\frac{1}{m} \frac{dV_o}{V_o} \right)^2 + \left(\frac{1}{m} \frac{dV}{V} \right)^2 + \left(\frac{d\tau_r}{\tau_r} \right)^2 + \left(\frac{d\tau_{oz}}{\tau_{oz}} \right)^2 + \right]^{\frac{1}{2}} \quad (3.1)$$

where $\delta\tau_a$ is the AOT uncertainty, τ is the total optical thickness, m is the airmass, $\delta m/m$ is the airmass uncertainty, given as 0.001, $\delta V_o/V_o$ is the uncertainty in the calibration coefficient, V_o , expressed as 0.015 when cross calibration has been performed with respect to an AERONET CIMEL, $\delta V/V$ is the uncertainty in the instrument voltage, with a value of 0.01, $\delta\tau_r/\tau_r$ is the uncertainty of the Rayleigh optical thickness, 0.005, and $\delta\tau_{oz}/\tau_{oz}$ is the uncertainty of the ozone optical thickness. Utilizing the individual values of τ and m , these values are calculated for each data point independently in the SIMBIOS Microtops processing code. As can be seen in equation 3.1, the Microtops uncertainty has a very slight (due to the low airmass error) dependency on the value of τ , and a stronger inverse relationship with airmass. Details about the calculation of uncertainties for the SIMBAD and FRSR are written elsewhere (Deschamps et al., 2002 and Miller et al. 2002). Table 3.7 (from Deschamps et al. 2002) presents the quadratic uncertainty for each band of the SIMBAD.

Table 3.7: Uncertainty of the SIMBAD AOT (m=1)

Wavelength	443	490	560	670	870
$\delta\tau_a$	± 0.021	± 0.020	± 0.018	± 0.011	± 0.010

FRSR uncertainties are expressed in terms of airmass, m , as expressed in equation 3.2, where c is a constant defined as 0.036 for the band at 400nm, and 0.028 for all other bands.

$$dt_a = \left(\frac{c}{m} \right)^2 \quad (3.2)$$

Standard Calculation of the Angstrom Exponent

As there are a number of ways, operationally, to calculate the Angstrom exponent (by varying the number and combinations of AOT bands used), the SIMBIOS Project decided to standardize the computation of Angstrom exponent for archival of data in SeaBASS. The chosen method uses multiple bands and a linear fitting routine to paired wavelength and natural logarithm of AOT values. The Angstrom Exponent is the negative slope of this fit. Equation 3.3 is an expression of this computation:

$$a = -LINFITslope \{ \ln(\tau_{a0}), \ln(\tau_{a1}), \ln(\tau_{a2}) \dots \ln(\tau_{aN}), \} \quad (3.3)$$

where α is the Angstrom Exponent and $\tau_a(\lambda)$ is the AOT for each band whose center wavelength is between 440 and 870nm. LINFIT is a linear fitting routine in IDL that minimizes the Chi-square error statistic to fit X (wavelengths, in nm) and Y (natural logarithm of AOT) to the model $Y=A+BX$. The Angstrom Exponent, α , is equal to $-B$, and the Chi-square error statistic is recorded as the deviation of the data from a perfect linear fit.

This Angstrom Exponent calculation method uses a recursive routine that makes an analytical computation of uncertainty impossible. To account for this, an Angstrom Exponent calculation method was devised that incorporates the individual AOT uncertainties and the Chi-square error to determine an Angstrom Exponent uncertainty. This is expressed in equation 3.4:

$$\mathbf{a} = -LINFITslope \left\{ \begin{array}{l} \ln(t_{a_0} + dt_{a_0}), \ln(t_{a_1} + dt_{a_1}), \ln(t_{a_2} + dt_{a_2}) \dots \ln(t_{a_N} + dt_{a_N}), \\ \ln(t_{a_0} - dt_{a_0}), \ln(t_{a_1} - dt_{a_1}), \ln(t_{a_2} - dt_{a_2}) \dots \ln(t_{a_N} - dt_{a_N}) \end{array} \right\} \quad (3.4)$$

Essentially, the linear fitting is not performed upon the AOT values themselves, but to pairs of AOT plus or minus uncertainty. When compared to analytical computations of uncertainty (in two band situations where this is possible), the uncertainty values are nearly identical if the AOT values follow the Junge Law and do not deviate from a linear relationship. This fitting approach to computation of Angstrom Exponent has several advantages over the standard two-band approach. The primary advantage is that it utilizes the entire spectral data set to calculate a parameter intended to represent the spectral nature of AOT values. This allows greater freedom from possible single band calibration problems, and helps reduce the overall uncertainty. Furthermore, the uncertainty metric includes not just a propagation of uncertainties from individual AOT values, but also includes uncertainty for failures of the data to fit the Junge Law.

Matchup Analysis

In 2002, match-ups analysis between AOT data obtained from *in situ* observations and satellite-derived AOT levels were again conducted. This was conducted with data collected by SIMBIOS PI's using the SIMBIOS pool of sun photometers. Over than 300 cruises were supported by SIMBIOS Program since 1997 and more than 4000 Microtops records and 5000 SIMBAD records were gathered. The data that have been used are available on the SeaBASS database (<http://seabass.gsfc.nasa.gov>). Figure 3.12 shows the match-up results at 865nm obtained with SeaWiFS and MODIS Oceans products. Match-up analysis were also conducted again using some AERONET ground stations. Table 3.8 provides the AERONET station name, location (latitude and longitude), and the corresponding responsible AERONET PIs. These sites are located at either coastal or island stations and were operational for a reasonable length of time after SeaWiFS and MODIS Terra became operational. Match-ups have been obtained for the SeaWiFS-derived aerosol properties or the MODIS Oceans-derived aerosol properties and AOT levels calculated from AERONET and SIMBIOS sun and sky radiometer data. The results are presented for AOT 865 in Figure 3.13. Efforts have been made to refine the measurement protocols and the cloud-screening algorithms. Strong efforts have also been made to associate uncertainties with aerosol optical thickness measured by various sun photometers that compose the SIMBIOS pool of sun photometers. Match-up results obtained using data collected in the open ocean (SeaBASS database) and collected by stations in coastal or island sites (AERONET) agree very well. The AOT measured from space is overestimated at 865nm compared to *in situ* sun photometer measurements. MODIS Oceans and SeaWiFS AOT products are derived using similar atmospheric correction algorithms. The comparison of SeaWiFS and MODIS AOT products with *in situ* measurements agree reasonably well. The slight overestimation at 865nm is probably due the tendency of the algorithm to overestimate the AOT in order to derive adequate water leaving radiances.

Table 3.8: AERONET sites used for aerosol matchups analyses (* SIMBIOS Project Office).

Station	Latitude	Longitude	AERONET PI
Arica	-18.47	-70.31	B. Holben
Ascension Island	-7.98	-14.41	C. McClain*
Azores	38.53	-28.63	C. McClain*
Bahrain	26.32	50.50	C. McClain*
Bermuda	32.37	-64.70	B. Holben
Anmyon Island	36.52	126.32	C. McClain* & B. Holben
Coconut Island	21.433	-157.79	C. McClain*
Dry Tortugas	24.60	-82.80	K. Voss & H. Gordon
Kaashidhoo	4.97	73.47	B. Holben
Lanai	20.83	-156.99	C. McClain*
Venise	45.31	12.50	G. Zibordi
Capo Verde	16.73	-22.93	D. Tanre
Nauru	-0.52	166.92	M. Miller
Puerto Madryn	-42.79	-65.01	C. McClain*
Rottneest Island	-32.00	115.30	C. McClain*
SanNicolas	33.26	-119.49	R. Frouin
Tahiti	-17.58	-149.61	C. McClain*
Erdemli	36.56	34.25	C. McClain*
Wallops	37.94	-75.47	C. McClain* & B. Holben
Dahkla	23.72	-15.95	C. McClain*

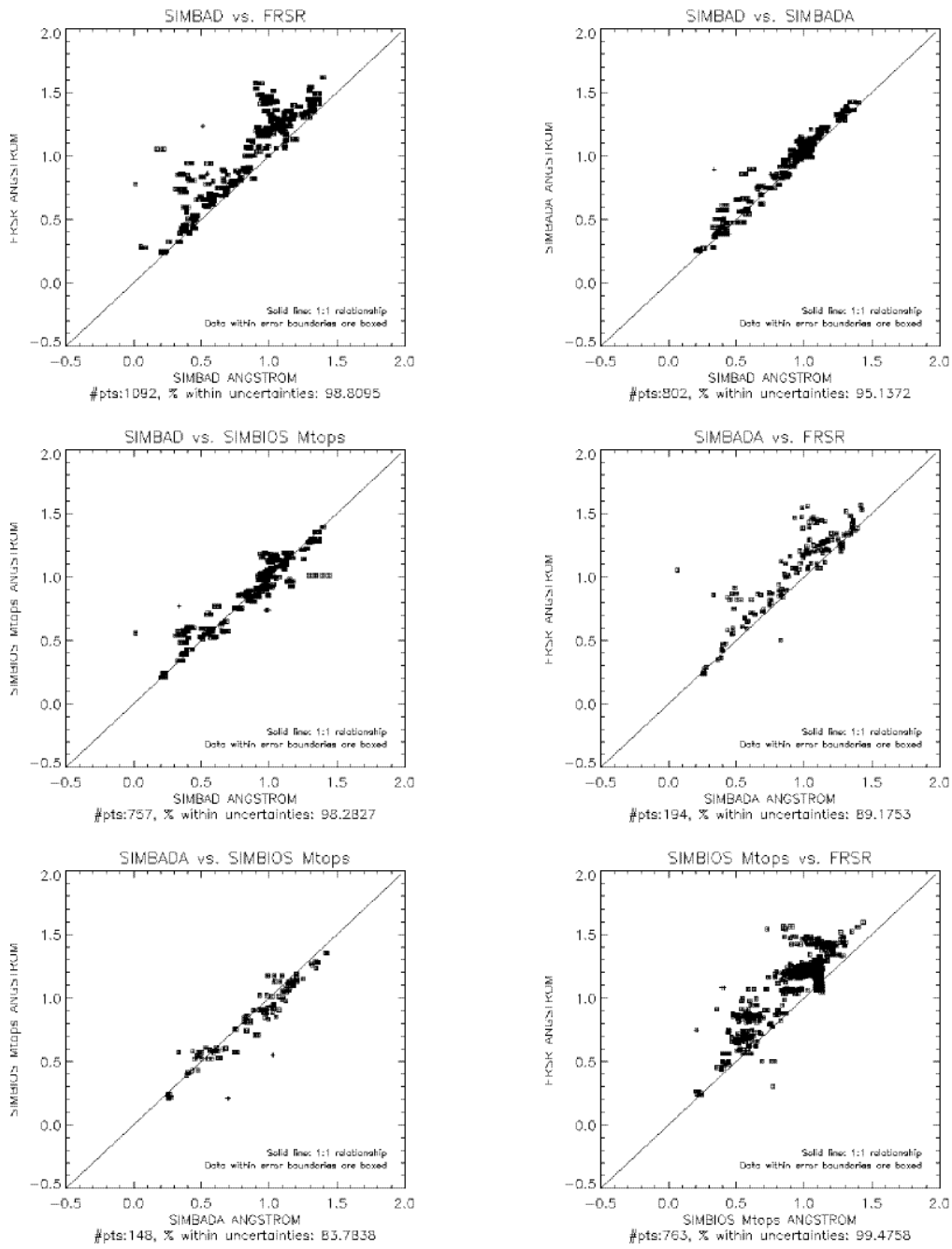


Figure 3.10: Multiple instrument scatter plots of ACE-Asia Angstrom Exponents measured within 15 minutes of each other.

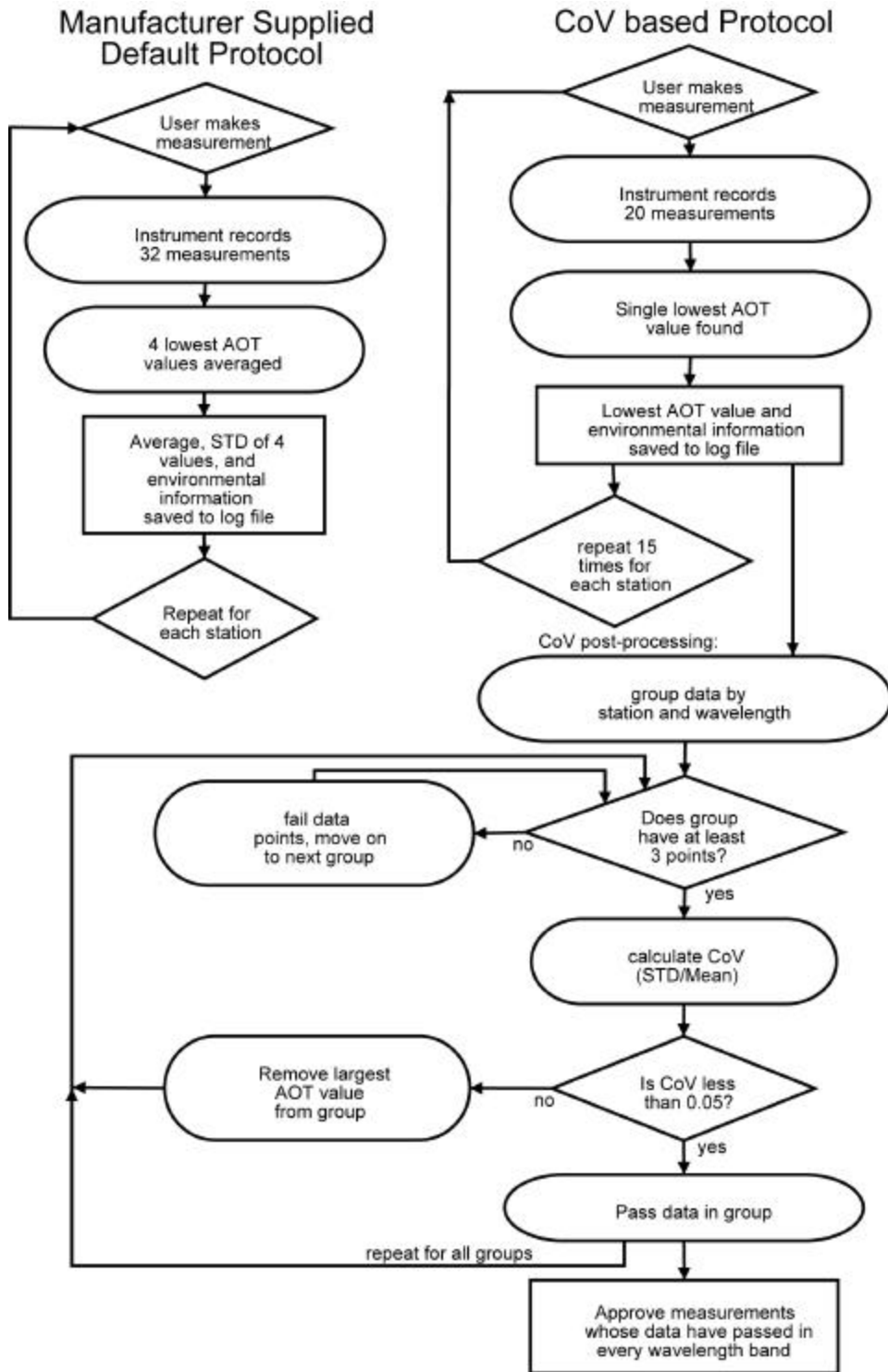


Figure 3.11: Microtops II measurement protocols

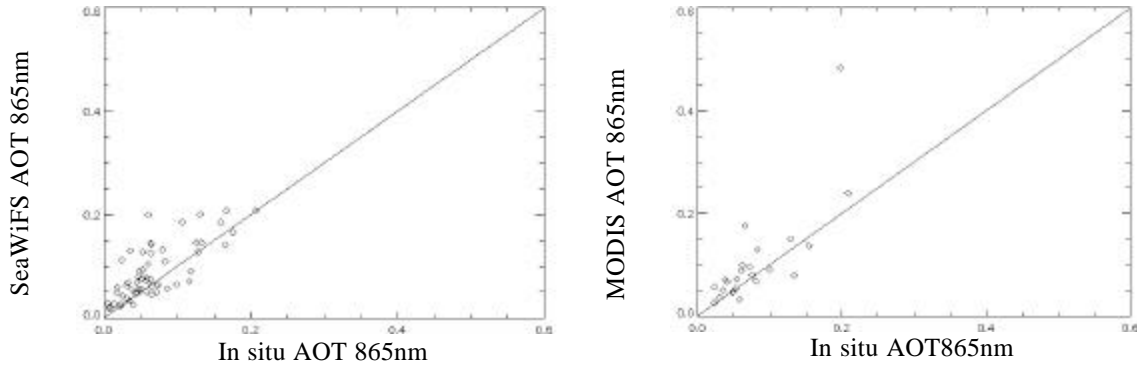


Figure 3.12: SeaWiFS/MODIS – In situ matchups for AOT at 865nm using data collected by the SIMBIOS PI’s since 1997 using the MicroTops and SIMBAD sun photometers in the Open Ocean.

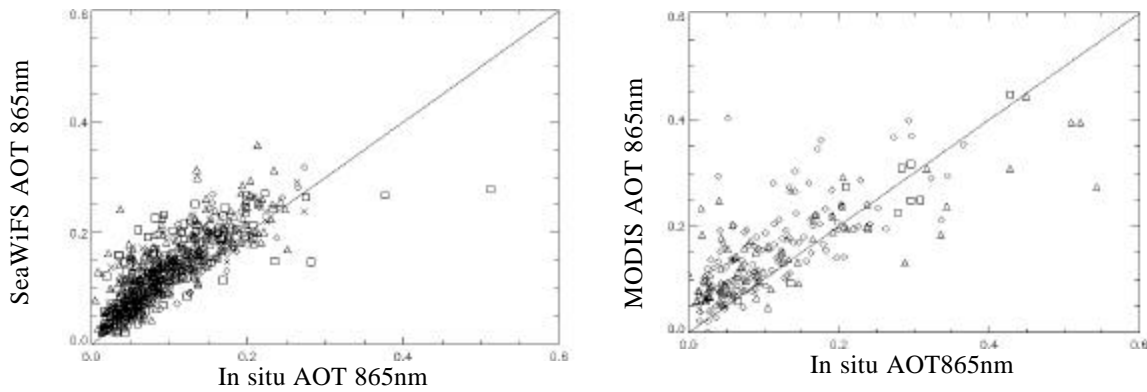


Figure 3.13: SeaWiFS/MODIS – In situ matchups for AOT at 865nm using data collected by the CIMEL sun photometers provided by the SIMBIOS Project and maintained by the AERONET group.

3.7 CALIBRATION ROUND ROBIN

Calibration round-robin intercomparison experiments are conducted by the SIMBIOS Project. The specific goals are to:

- verify that all laboratories are on the same radiometric scale
- detect and correct problems at any individual laboratory in a timely fashion
- enforce the common use of calibration protocols
- identify areas where the calibration protocols need to be improved
- document the calibration procedures specific to each laboratory.

The participating laboratories include academic institutions, government agencies and instrument manufacturers that either directly or indirectly contribute to SeaBASS (see section 3.4). In the year 2002, the participating laboratories of the second SIMBIOS Radiometric Intercomparison SIMRIC-2 include:

- Naval Research Laboratory (NRL), Optical Sensing Section, Code 7212, Washington, DC

- NASA Code 920.1 Calibration Facility, Greenbelt, MD
- Wallops Flight Facility, NASA Code 972.0, Wallops Island, VA
- Marine Optical Buoy (MOBY), Honolulu, HI
- Scripps Institution of Oceanography, University of California, San Diego, CA
- Biospherical Instruments Inc., San Diego, CA
- The Institute for Computational Earth System Science (ICESS), University of California at Santa Barbara, CA
- Marine Science Laboratory at the University of South Florida, FL
- Atmospheric and Ocean Optics Laboratory at the University of Miami, FL
- Satlantic Inc., Halifax, Canada
- Stennis Space Center, MS

The above laboratories were visited by SIMBIOS staff with a NIST designed and calibrated radiometer, the SeaWiFS Transfer Radiometer II (SXR-II), described in Johnson et al., 1998a. The light sources of MOBY were measured during a NIST calibration in Gaithersburg, Maryland. The radiances produced by the laboratories for calibration were measured in six channels from 411 nm to 777 nm and compared to the radiances expected by the laboratories. A NASA-TM (Meister et al., 2003) documents the various calibration procedures in these laboratories, evaluates the comparison results, and discusses areas where the calibration protocols should be improved. Furthermore, several characteristics of the SXR-II (e.g. its radiometric stability and its field of view) are described.

The major result of the SIMRIC-2 is that typically the SXR-II measured radiances agree within the combined uncertainties with the expected radiances, see Figure 3.14. This level of agreement is satisfactory. Relatively high differences were found at 777 nm for several laboratories, which may indicate a problem with the baffling material. Several issues identified during the preceding round-robin SIMRIC-1 (e.g. reflectance calibration of the reference plaques, NIST 2000 irradiance scale, effective distance correction) still need to be addressed by several laboratories. For those participants who also took part in the SIMRIC-1, preliminary results indicate that their calibration radiances were stable. At Wallops Flight Facility, a protocol error in the positioning of the calibration lamp was detected. At the University of Miami, differences between 2 % (441 nm) and 6 % (777 nm) were found, the reason for these discrepancies is still under investigation. Preliminary results from the University of South Florida indicate that their calibration sphere provides the required linearity.

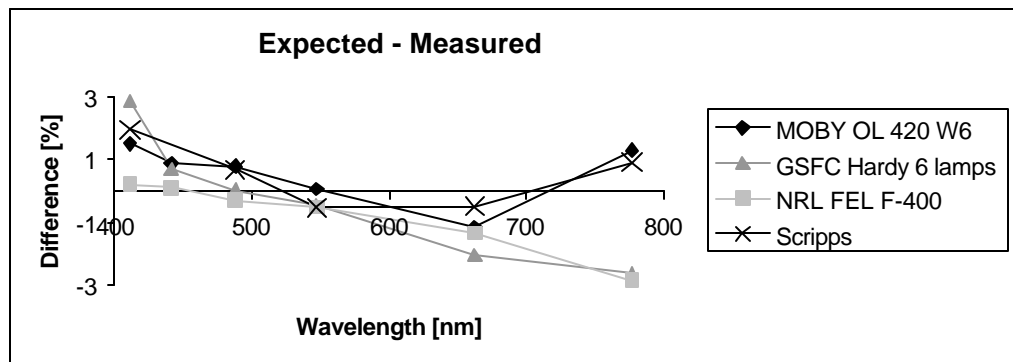


Figure 3.14: Comparison of the radiances measured by the SXR-II at some of the laboratories participating in the SIMRIC-2 and the radiances expected by these laboratories. The differences (expected radiance minus measured radiance) are plotted in % as a function of wavelength. Note that the SXR-II values in channel 1 at 411 nm are about 2 % too low for the MOBY and Scripps data sets and will be corrected after the new NIST calibration for the SXR-II is available (presumably in the beginning of 2003).

The SXR-II was calibrated by NIST in December 2000 and December 2001 on SIRCUS (Spectral Irradiance and Radiance Calibrations with Uniform Sources), which is a calibration facility that combines the use of tunable lasers and integrating spheres. The two calibrations revealed that the sensitivity of the 441 nm channel of the SXR-II increased during 2001 by about 1.6 %, whereas the other channels changed by less than 1 %. A third calibration is scheduled for January 2003. The radiometric stability of the SXR-II from November 2001 to November 2002 was monitored by two SeaWiFS Quality Monitors, whose basic design is described in Johnson et al., 1998b. The SIMBIOS Project uses an SQM from YES, Inc. (OCS-5002) and an

SQM from Satlantic, Inc. (SQM-II). The stability of both SQMs was comparable during 2002, with long term variations of less than 1 %. Both SQMs indicate a 2 % drop of the 411 nm channel of the SXR-II in September 2002, similar to the behavior measured in the summer of 2001. The time series of the SQM/SXR-II measurements for 2002 were acquired in the SIMBIOS Optical Laboratory, which was taken in operation in the beginning of 2002. The SIMBIOS Project is preparing to enhance its radiometric measurement capabilities with an irradiance radiometer that will participate in the calibration round-robin in the following year, and with the operation of FEL lamps in the SIMBIOS Optical Laboratory for improved long term stability measurements.

REFERENCES

- Atkinson P.M. and A.R.L. Tatnall, 1997: Neural Networks in Remote Sensing, *Int. J. Remote Sens.*, vol. **18**, no. 4,699-709.
- Bailey, S.W., C.R. McClain, P.J. Werdell, and B.D. Schieber, 2000: Normalized water-leaving radiance and chlorophyll *a* match-up analyses, in SeaWiFS Postlaunch Calibration and Validation Analyses, Part 2, *NASA Tech. Memo. 2000-206892*, S.B. Hooker and E.R. Firestone, Eds. NASA Goddard Space Flight Center, Greenbelt, Maryland, 45-52.
- Campbell, J.W., J.M. Blaisdell, and M. Darzi, 1995: Level-3 SeaWiFS Data Products: Spatial and Temporal Binning Algorithms, *NASA Technical Memorandum 104566*, vol. **32**.
- Deschamps, P-Y, B. Fougnie, R. Frouin, P. Lecomte and C. Verwaerde, 2002: SIMBAD: A field radiometer for satellite ocean-color validation, *Applied Optisc* (submitted).
- Dubovik, O., A. Smirnov, B.N. Holben, M.D. King, Y.J. Kaufman, T.F. Eck, and I. Slutsker, 2000: Accuracy assessments of aerosol optical properties retrieved from Aerosol Robotic Network (AERONET) Sun and sky radiance measurements, *J. Geophys. Res.*, **105**, D8, 9791-9806.
- Fargion, G.S., and C.R. McClain, 2002: SIMBIOS Project 2001 Annual Report, *NASA Tech. Memo. 2002-210005*, NASA Goddard Space Flight Center, Greenbelt, Maryland, 184 pp.
- Kilpatrick, K., E. Kearns, E.J. Kwiatkowska-Ainsworth, and R.L. Evans, 2002: Time Series of Calibrated Ocean Products from NASA's Moderate Resolution Scanning Spectrometer (MODIS), *Proceedings of the Ocean Sciences Meeting*, Honolulu, Hawaii.
- Knobelspiesse, K.D., C. Pietras and G.S. Fargion, 2002: Sun pointing error correction for sea deployment of the Microtops II hand held sun photometer, *J. Atmos. Ocean. Tech.* (accepted).
- McClain, C.R., and G.S. Fargion, 1999: SIMBIOS Project 1998 Annual Report, *NASA Tech. Memo. 1999-208645*, NASA Goddard Space Flight Center, Greenbelt, Maryland, 105 pp.
- Miller, M.A., M.J. Bartholomew, and R.M. Reynolds, 2002: The Accuracy of Marine Shadow-band Sun Photometer Measurements of Aerosol Optical Thickness and Angstrom Exponent, *J. Atmos. Ocean Tech.* (submitted).
- Pao, Y.P., 1989: Adaptive Pattern Recognition and Neural Networks, Reading, MA, Addison-Wesley.
- Porter, J.N., M. Miller, C. Pietras, and G. Motell, 2001: Ship-based sun photometer measurements using Microtops sun photometers, *J. Atmos. Ocean. Tech.*, **18**, 765-774.
- Russell, P.B., J.M. Livingston, E.G. Dutton, R.F. Pueschel, J.A. Reagan, T.E. DeFoor, M.A. Box, D. Allen, P. Pilewskie, B.M. Herman, S.A. Kinne, and D.J. Hofmann, 1993: Pinatubo and Pre-Pinatubo Optical-Depth Spectra: Mauna Loa Measurements, Comparisons, Inferred Particle Size Distributions, Radiative Effects, and Relationships to Lidar Data, *J. Geophys. Res.*, **98**, D12, 22,969-22,985.

Schölkopf, B., K. Sung, C. Burges, F. Girosi, P. Niyogi, T. Poggio, V. Vapnik, 1996: Comparing Support Vector Machines with Gaussian Kernels to Radial Basis Function Classifiers, *Massachusetts Institute of Technology Artificial Intelligence Laboratory Memorandum*, no. **1599**, 142 pp.

Werdell, P.J., and S.W. Bailey, 2002: The SeaWiFS Bio-optical Archive and Storage System (SeaBASS): Current architecture and implementation, *NASA Tech. Memo. 2002-211617*, G.S. Fargion and C.R. McClain, Eds. NASA Goddard Space Flight Center, Greenbelt, Maryland, 45 pp.

Chapter 4

Adaptation of a Hyperspectral Atmospheric Correction Algorithm for Multi-spectral Ocean Color Data in Coastal Waters

Bo-Cai Gao, Marcos J. Montes, and Curtiss O. Davis

Remote Sensing Division, Naval Research Laboratory, Washington, D.C.

4.1 INTRODUCTION

This SIMBIOS contract supports several activities over its three-year time-span. These include certain computational aspects of atmospheric correction, including the modification of our hyperspectral atmospheric correction algorithm for various multi-spectral instruments, such as SeaWiFS, MODIS, and GLI. Additionally, since absorbing aerosols are becoming common in many coastal areas, we are incorporating the calculation and incorporation of various absorbing aerosol models into tables used by our atmospheric correction algorithm. Finally, we will use MODIS data to characterize thin cirrus effects on aerosol retrieval.

4.2 RESEARCH ACTIVITIES

Our main accomplishment this year was to complete modifications of our hyperspectral atmospheric correction algorithm (Gao et al. 2000; Montes et al. 2001) to make versions compatible with MODIS and SeaWiFS, and to apply the derived algorithm to various scenes. We have successfully compiled and run a pixel-to-pixel version of this algorithm (previously we averaged scene geometry in boxes) on several platforms.

The pixel-to-pixel version runs reasonably fast, about 9 minutes for a MODIS pass on a 195MHz SGI Octane. A key feature of the new code is that is a generic Fortran 90 code that can be modified for other multispectral sensors, such as GLI and MERIS. This modular source code also allows enhancements, such as the Asian dust model, to be easily propagated to the versions for all multispectral sensors.

Each version was compiled on both SGI and Linux workstations. The Linux version is at the SeaWiFS project office for further testing. The source code has also been shared with Arnone et al. at NRL Stennis so that they can help with the testing.

We are actively planning to participate in field observations of Asian Dust events over the Monterey Bay area in April, 2003. This is a cooperative experiment with a variety of in-water and airborne measurements by researchers from Moss Landing and NRL-Monterey; additionally, we are planning to mount our PHILLS hyperspectral imager on the CIRPAS aircraft that will carry a suite of instruments to characterize the Asian dust aerosols, given the repeat of dust events seen in April for the last several years. We will fly the aircraft above, through, and below the dust layer. We will time the flight to obtain coincident data from SeaWiFS, MODIS (both Terra and Aqua), and MERIS. The aerosol measurements will allow us to create an Asian dust model for our lookup tables. These new lookup tables will be used to correct images acquired from the various hyperspectral and multispectral sensors. The in-water measurements will provide data for closure experiments.

4.3 RESEARCH RESULTS

The modification of the algorithms has proceeded to a purely pixel-to-pixel version, where we calculate the geometric effects for each pixel. This requires us to interpolate across the geometric dimensions of the lookup table for each pixel. There was a substantial modification from the original box-averaged version, especially in getting it to run reasonably fast.

We have processed several scenes of MODIS and SeaWiFS data with the pixel-to-pixel versions of the atmospheric correction code. Our algorithm and Gordon's algorithm return very similar results over areas of the open ocean. Our algorithm makes use of both the ocean channels of MODIS, as well as the land channels. Use of the land channels allows us to perform atmospheric corrections in certain turbid areas where the normal algorithms fail – for example, in areas with enough sediment

so that there is measurable signal at 0.75 micron. Our results for a sediment rich area are shown Figure 4.1; Gordon's algorithm does not provide a result for this area. The land channels also provide some much-needed redundancy in cases when the ocean channels saturate, as over some coccolithophore blooms, and in some areas with high concentrations of sediments. Some results from an area of a coccolithophore bloom are presented in Figures 4.2 and 4.3.

Our analysis has pointed to several modifications we hope to have in place by the end of calendar year 2002. First, while the use of MODIS land channels gives us the ability to perform retrievals over brighter areas, they are probably not sensitive enough to use over the more typically dark areas of the ocean. This implies that we will need to automatically be able to switch methods depending on the radiance in certain land and ocean channels. Second, we will add the ability to correct for ozone on a pixel-by-pixel basis, instead of using a single value for a whole scene. Third, we need to investigate the possibility of using wind speed data on a pixel-by-pixel basis. Wind speed controls both specular reflection of the ocean, and the amount of foam on the surface of the ocean.

Other areas of research include Gao's collaborations to study methods of discriminating the effects of cirrus clouds and aerosols at longer wavelengths (Gao et al., 2002) and algorithms for masking sediment laden waters where it is necessary to use longer wavelengths to achieve any atmospheric correction (Li et al., 2002).

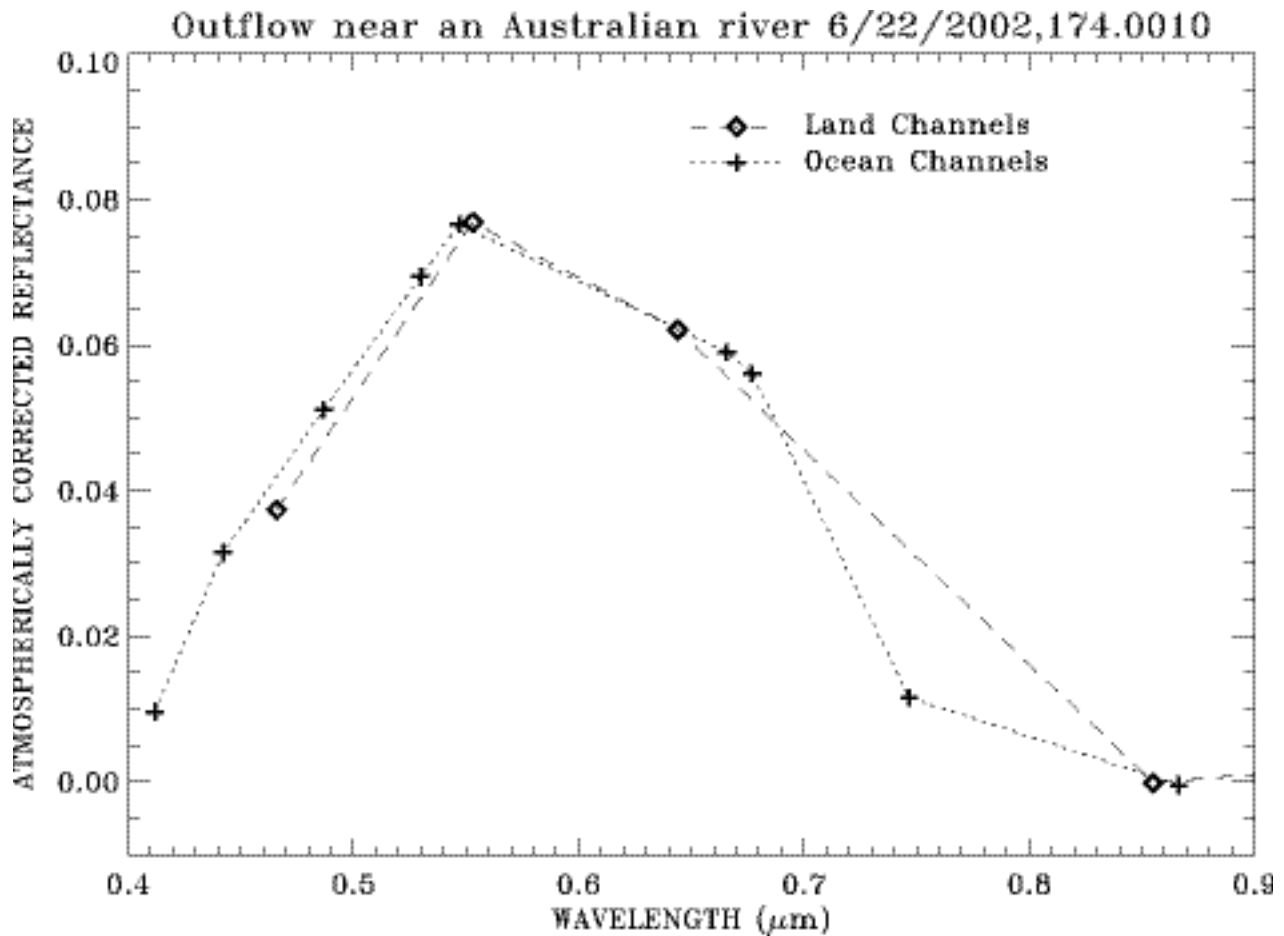


Figure 4.1: Atmospherically corrected reflectance from a MODIS image off the coast of Eastern Australia. The long dashes connect the sets of land channels (open diamonds), and the short dashes connect sets of ocean channels (plusses). These results were derived using some of the land channels and the pixel-to-pixel version of Tafkaa to determine an atmospheric correction. Note, in particular, that our results yield significant water leaving radiance at 0.75 micron. Water leaving reflectance cannot be retrieved for pixels like this one using Gordon's algorithm.

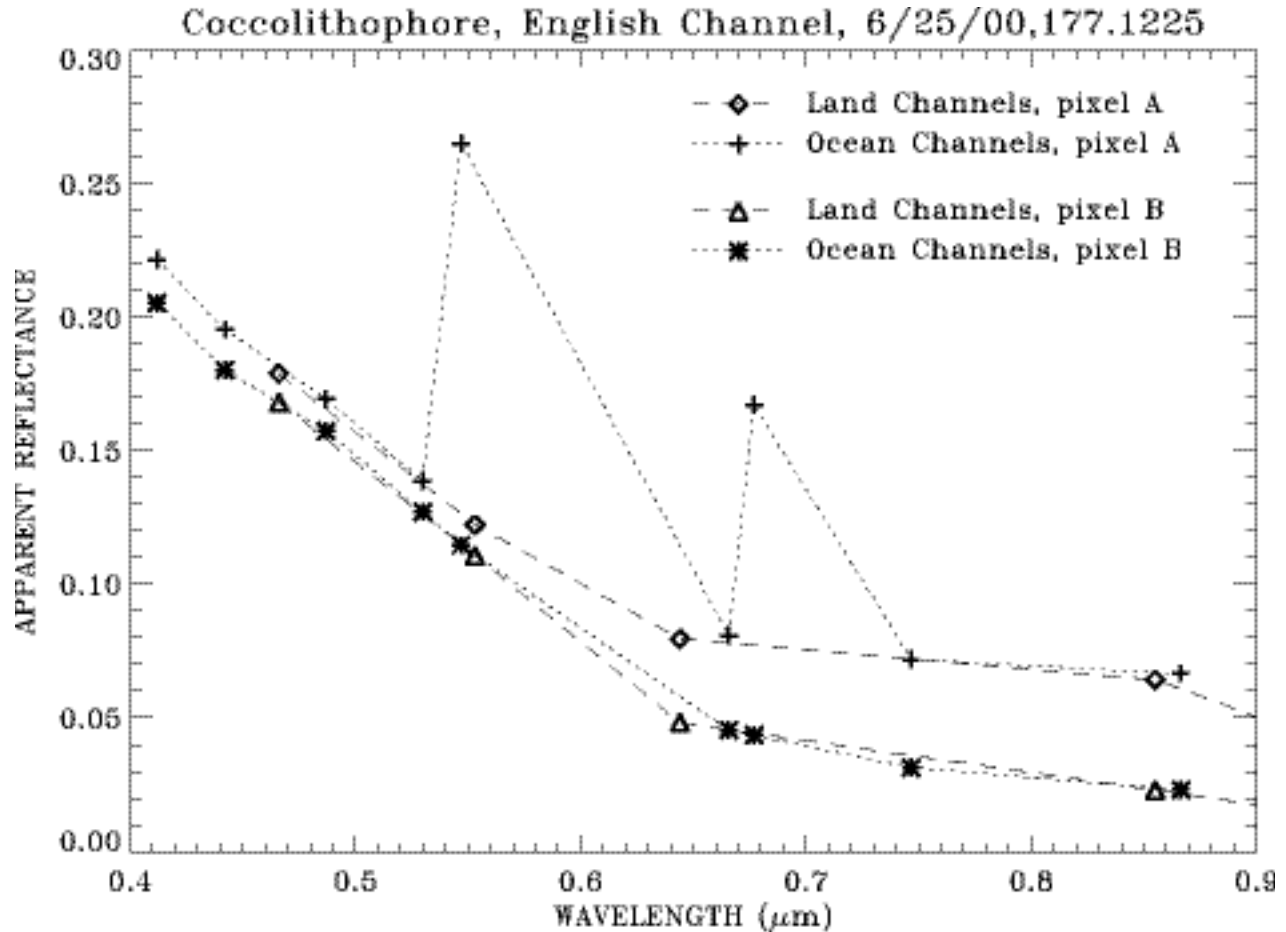


Figure 4.2: The at-sensor apparent reflectance from a MODIS image of the English Channel, 2000 June 25, comparing results from land and ocean channels from two different pixels in a coccolithophore bloom. The long dashes connect the land channels, and the short dashes connect ocean channels. The open diamonds (land channels) and pluses (ocean channels) are from pixel A, which is clearly saturated in the fifth and seventh ocean channels from the left. Spectra from nearby unsaturated pixel B are shown with open triangles (land channels) and asterisks (ocean channels).

4.4 FUTURE WORK

We have made progress in modifying our atmospheric correction algorithm to be used with multi-spectral data from MODIS and SeaWiFS. Our algorithm takes advantage of MODIS' long wavelength and land bands to provide atmospheric correction over brighter ocean scenes including sediments and coccolithophore blooms. These algorithms now use the complete geometry of each pixel. Our results are promising, especially over turbid areas. We are in the process of refining our algorithms and are involved in testing with both groups working with the SIMBIOS program at GSFC and NRL-Stennis.

REFERENCES

- Gao, B. C., M.J. Montes, Z. Ahmad, and C.O. Davis, 2000: Atmospheric correction algorithm for hyperspectral remote sensing of ocean color from space, *Appl Opt.*, **39**(6), 887-896.
- Montes, M.J., B. C. Gao, and C.O. Davis, 2001: A new algorithm for atmospheric correction of hyperspectral remote sensing data, *SPIE*, **4383**, 23-30.

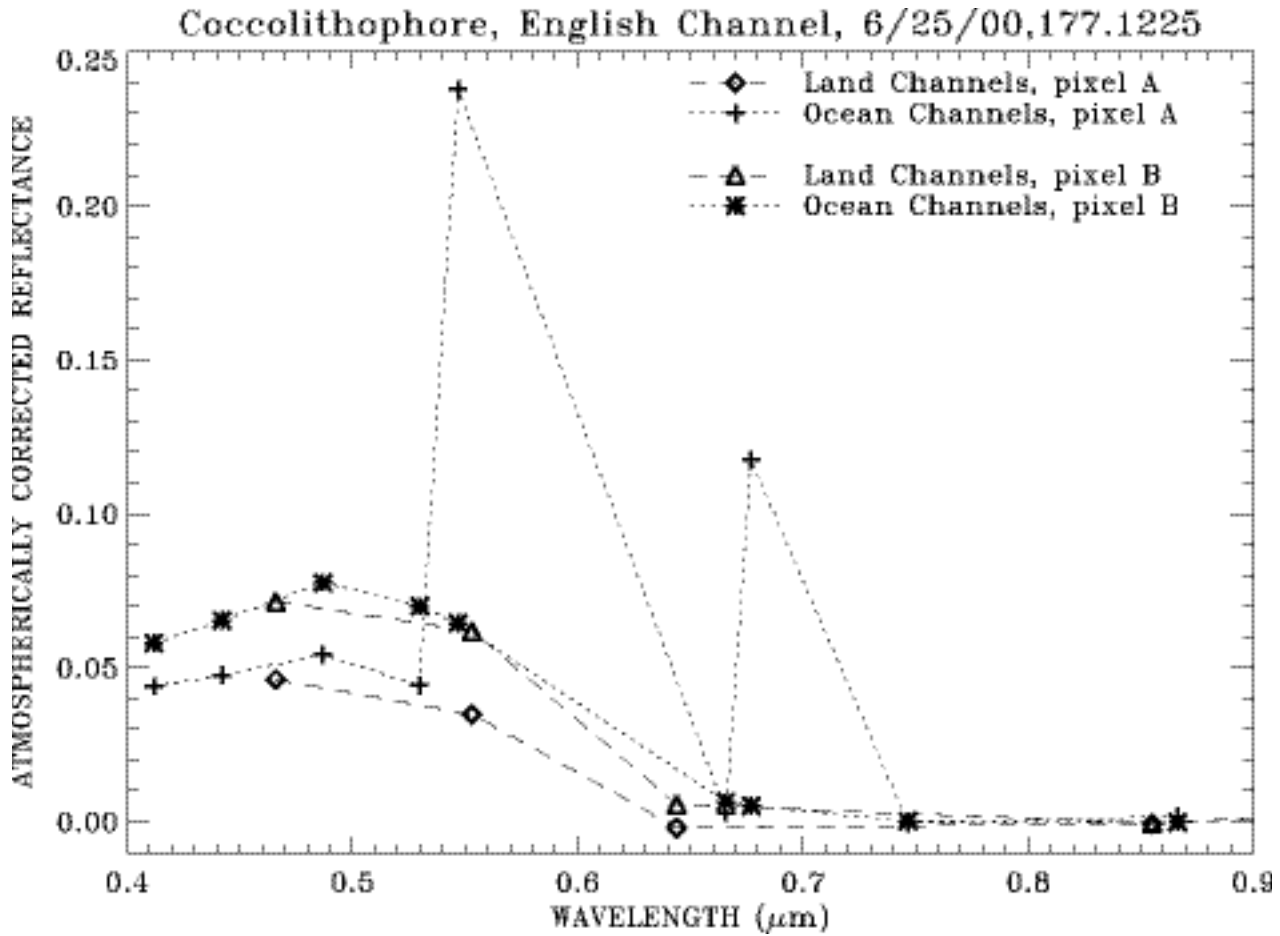


Figure 4.3: Atmospherically corrected reflectance from the same locations as in Figure 4.2. The symbols are the same as in Figure 4.2. Note the quite reasonable agreement between the atmospherically corrected land channels and ocean channels except for the two saturated channels

Chapter 5

Bio-Optical Measurements in Upwelling Ecosystems in Support of SIMBIOS

Francisco P. Chavez, Peter G. Strutton, Victor S. Kuwahara and Eric Drake
Monterey Bay Aquarium Research Institute, Moss Landing, California

5.1 INTRODUCTION

The equatorial Pacific is a key component of global biogeochemistry. This upwelling system, which spans one quarter of the Earth's circumference, has significant implications for global CO₂ fluxes (Tans et al., 1990; Takahashi et al., 1997; Feely et al., 1999), as well as primary and secondary production (Chavez and Barber, 1987; Chavez and Toggweiler, 1995; Chavez et al., 1996; Dugdale and Wilkerson, 1998; Chavez et al., 1999; Strutton and Chavez, 2000). The region also represents a large oceanic (case 1) region over which validation data for SeaWiFS are necessary. This project consists of an optical mooring program and cruise-based measurements aimed at quantifying the spectrum of biological and chemical variability in the equatorial Pacific and obtaining validation data for SeaWiFS. Since 1997, the MBARI equatorial Pacific program has demonstrated ability to:

- obtain high quality, near real time measurements of ocean color from moored platforms in the equatorial Pacific;
- process these data into files of the required format for routine ftp to the SeaBASS database;
- obtain robust ship-based optical profiles and pigment concentration measurements, also for submission to SeaBASS; and
- process and interpret the time series, satellite and ship-based data in order to quantify the biogeochemical processes occurring in the equatorial Pacific on time scales of days to years (Chavez et al., 1998; Chavez et al., 1999; Strutton & Chavez, 2000; Strutton et al., 2001; Strutton & Chavez, submitted).

5.2 RESEARCH ACTIVITIES

Moorings

Chavez et al. (1998; 1999) and McClain and Fargion (1999) describe the configuration of the MBARI bio-optical and chemical instruments deployed at 0°, 155°W and 2°S, 170°W; two of the 70 moorings which form the Tropical Atmosphere Ocean (TAO) array. From these locations, daily bio-optical and chemical data collected at local 10 am and noon (approximate time of MODIS and SeaWiFS overpasses, respectively) are transmitted via service ARGOS to MBARI, and then displayed on the web at: <http://bog.shore.mbari.org/~bog/oasis.html>.

Higher frequency, publication-quality data (15-minute intervals) are also recovered at approximately six month intervals, and sent to the SeaBASS database after rigorous quality control. Derived products, such as water leaving radiance (L_w), and remote sensing reflectance (R_{rs}) are included in these data files for validation efforts. In the past, L_w has been calculated via three different methods (McLain and Fargion, 1999b), but is currently calculated only as follows. The diffuse attenuation coefficient ($K\lambda$) over the upper 20m of the water column is calculated using Ed_{3m+} and Ed_{20m-} , then using this $K\lambda$, Lu_{20m} is extrapolated back to just below the surface. This parameter (Lu_{0m-}) is multiplied by 0.544, to account for transmission across the air-water interface, to obtain Lu_{0m+} . Of the three methods previously used, this has been shown to be the most reliable, because the 3m+ and 20m- instruments are less susceptible to fouling. With the addition of a 10 m hyperspectral radiometer, the efficacy of this method can now be assessed. During 2002 our data processing, quality control and data provision capabilities have improved. The following quality control procedures are currently applied to our data:

- Measured surface-incident irradiance (E_s) must be less than 1.15 times modeled, clear-sky E_s (Frouin, 1989).
- $K\lambda$ must be greater than that of pure water (Morel, 1988).
- OC4V4 chlorophyll is calculated for the Rrs ratios of 412/555, 443/555, 490/555, and 510/555 and the coefficient of variance is calculated for each sample. Coefficients of variance less than 0.4 are acceptable.
- Time series of all parameters at all wavelengths for all individual instrument deployments are plotted together as one long time series to identify discontinuities between deployments, due to problems such as vandalism and calibration issues. Normalizing specific wavelengths against others, and investigating between-deployment differences in the ratio can improve this technique.
- In the coming year we hope to finalize improvements of these criteria and use the results to perhaps modify mooring and instrument configurations.

With the buoy design and data acquisition protocols now proven in the field, we are making significant advancements to the quantity and quality of optical data collected during this funding period. In October 2001 HOBILabs hyperspectral HR3s were deployed at a depth of 10 m at both equatorial Pacific moorings - 0° 155°W and 2°S 170°W - to augment the discrete wavelengths collected at 20 m. These configuration changes produced data of significantly higher quality for almost the same cost as the existing discrete-wavelength instruments. These instruments were recovered in June 2002 (new HR3 units were subsequently deployed after recovery) providing hyperspectral data consisting of :

- downwelling irradiance above the surface (3m)
- downwelling irradiance and upwelling radiance at 10m depth.

The Hydrorad data are available in programmable bin sizes (highest resolution 0.37nm), over the range ~300 to 850nm, but for deployment in the equatorial Pacific, data have been binned to ~2nm resolution. We also successfully recovered and deployed HOBILabs Hydroscat 2 (HS2) instruments fitted with new copper anti-fouling shutters. The HS2 measures backscatter and fluorescence at two wavelengths. With the deployment of these new instruments, in particular the hyperspectral radiometers, we have been able to submit optical data beyond our initial deliverables as stated in the SIMBIOS grant, and can better support new and forthcoming ocean color missions such as MODIS, and the development of ocean color algorithms that will go beyond chlorophyll to other pigments.

Optical Profiling Measurements

On mooring maintenance cruises, optical profiles of the upper 100 m of the water column are performed, daily when possible, close to local noon. The instrument used is the Satlantic SeaWiFS Profiling Multispectral Radiometer (SPMR). Profile data are processed using Satlantic's ProSoft software, and a suite of derived products, including diffuse attenuation coefficients ($K\lambda$), normalized water leaving radiances (L_{wn}) and light penetration depths are obtained. Parameters of interest (mostly L_{wn}) are provided to NASA post-cruise, and the profile data are archived at MBARI along with existing optical profiles from almost every oceanic province.

In Situ Measurements

Table 5.1 summarizes the cruises undertaken by MBARI this fiscal year in support of SIMBIOS. Essentially, the cruise-based measurements consist of chlorophyll (using the fluorometric method described by Chavez et al. (1995) and nutrient profiles (8 depths, 0-200m) obtained at CTD stations between 8°N and 8°S across the Pacific from 95°W to 165°E. A comprehensive collection of the shipboard data can now be viewed at: <http://www.mbari.org/~ryjo/tropac/sections>.

An example is shown in Figure 5.1. On selected cruises (the 155°W and 170°W meridional transects), HPLC samples are collected and productivity (^{14}C , ^{15}N) measurements are also performed. These data are archived at MBARI and the pigment data provided to the SeaBASS database for algorithm development. Figure 5.2 shows good agreement between fluorometric and HPLC (CHORS; Center for Hydro-Optics & Remote Sensing/SDSU) chlorophyll a concentrations.

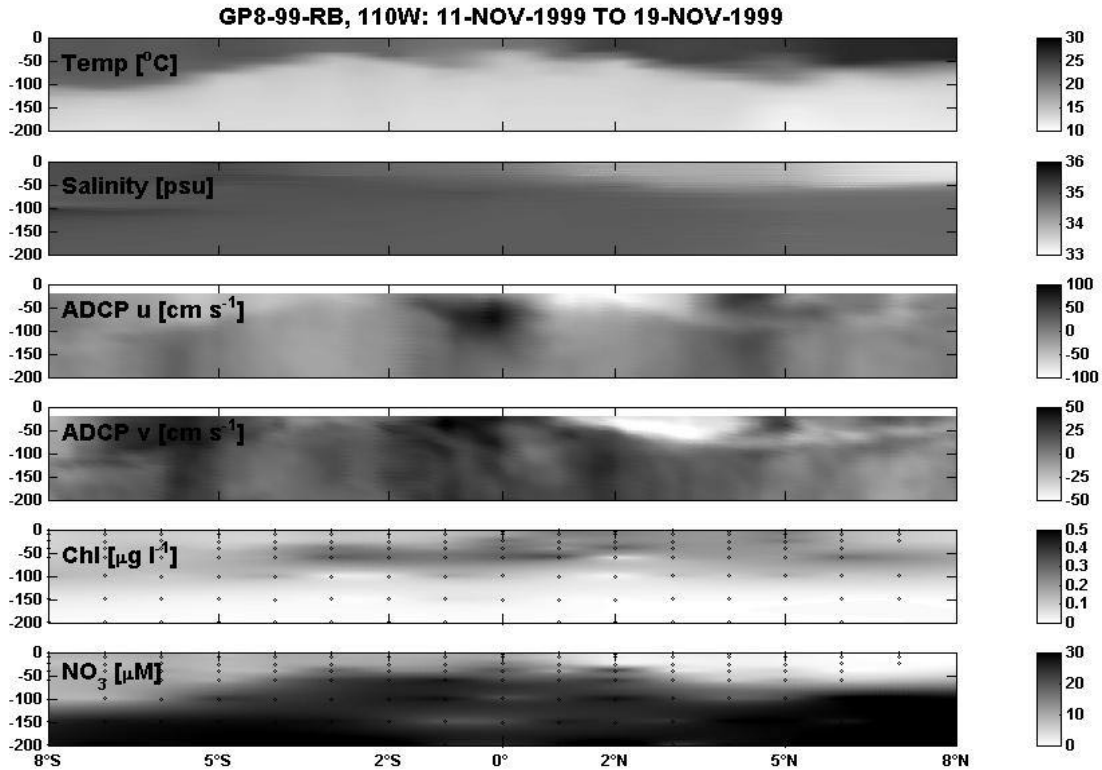


Figure 5.1: An example of the data that are collected along each north-south transect of the TAO array during mooring deployment cruises (see also <http://www.mbari.org/~ryjo/tropac/sections>). The data sections span 8°N to 8°S along 110°W from the surface to 200m, 11-Nov-1999 to 19-Nov-1999 – a period of moderate tropical instability wave activity. Significant zonal and meridional velocity anomalies are visible, and chlorophyll maximum, usually centered at the equator, is clearly shifted to the north. CTD temperature and salinity data are courtesy of Greg Johnson and Kristy McTaggart at NOAA/PMEL; ADCP data are courtesy of Eric Firing’s group at the University of Hawaii. Only NO₃ data are plotted, but corresponding sections of NO₂, PO₄ and SiO₄ exist.

5.3 RESEARCH RESULTS

Biogeochemical Cycles

Several publications describing ecosystem variability in the equatorial Pacific have been produced under MBARI’s SIMBIOS funding. Chavez et al. (1998) used mooring data from 0°, 155°W to describe the biological-physical coupling observed in the central equatorial Pacific during the onset of the 1997-98 El Niño. Chavez et al. (1999) combined the physical, biological and chemical data from moorings, ships and SeaWiFS to provide a comprehensive view of the ecosystem’s response to the extreme physical forcings experienced during the 1997-98 El Niño. Strutton and Chavez (2000) summarized the *in situ* cruise measurements spanning the period from November 1996 to December 1998, and used these data to describe the perturbations to chlorophyll, nutrients and productivity during the same time period. Strutton et al. (2001) used time series from smaller Atlantic bio-optical packages and SeaWiFS imagery, to quantify the extreme anomalies in chlorophyll associated with the passage of tropical instability waves (TIWs) during the second half of 1998 and 1999. These data not only quantified the magnitude of the chlorophyll anomalies observed, but also helped to elucidate the mechanisms potentially responsible for the concentration of chlorophyll in association with TIWs.

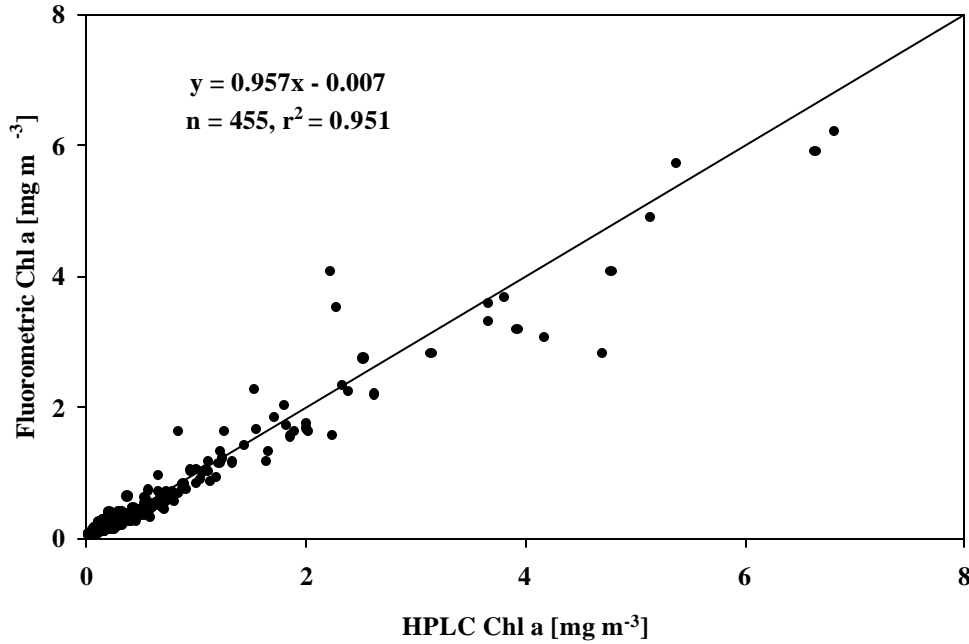


Figure 5.2: Regression model comparing *in situ* Chlorophyll *a* determined by a Turner fluorometer at sea versus HPLC-derived Chlorophyll *a* (CHORS). Samples were collected from both the equatorial Pacific and Monterey Bay. The one-to-one line is plotted

In addition to the manuscripts just described, Chavez et al. (2000) documented the design, and demonstrated the efficacy of the shutter mechanism which protects the 20 m radiometer on the moorings from fouling. Further, we have been actively working on the mooring chapter for the 4th revision of the Mueller protocols TM. Other manuscripts currently in preparation include a book chapter for submission to a CRC Press publication (Strutton et al. In prep), a paper describing the evolution of the 1998 La Niña blooms (Ryan et al, in press), a manuscript describing the biological component of the equatorial Pacific heat budget (Strutton and Chavez, in revision), and a paper that analyzes the time series of optical data collected at the mooring location (Kuwahara et al., in preparation)

SeaWiFS Calibration/Validation

Currently, we are focusing on improving our data analysis and quality control methods of the full mooring records (1996-2002) for both moorings in conjunction with the recently reprocessed SeaWiFS data. Analysis and improvements to quality control methods continue on the reprocessed data. These data have been uploaded to SeaBass. Figures 5.3 shows our most recent update of the time series of Lwn. Note: Lwn collected from the upwelling region is more variable than data collected from EP2 which is less susceptible to upwelling.

McClain and Fargion (1999b) showed matchup data derived from optical profiles of the SPMR in the equatorial Pacific. The mooring data collected at EP1 (excluding the anomalous El Nino year) indicated good agreement between the satellite- and profile-derived water-leaving radiance values (Figure 5.4)

5.4 FUTURE WORK

Despite unavoidable setbacks related to vandalism, the two major mooring installations at 0°, 155°W and 2°S, 170°W are operating relatively well. The results from the deployment of hyperspectral and backscatter instruments at both moorings are promising, and will better support validation efforts for ocean color missions.

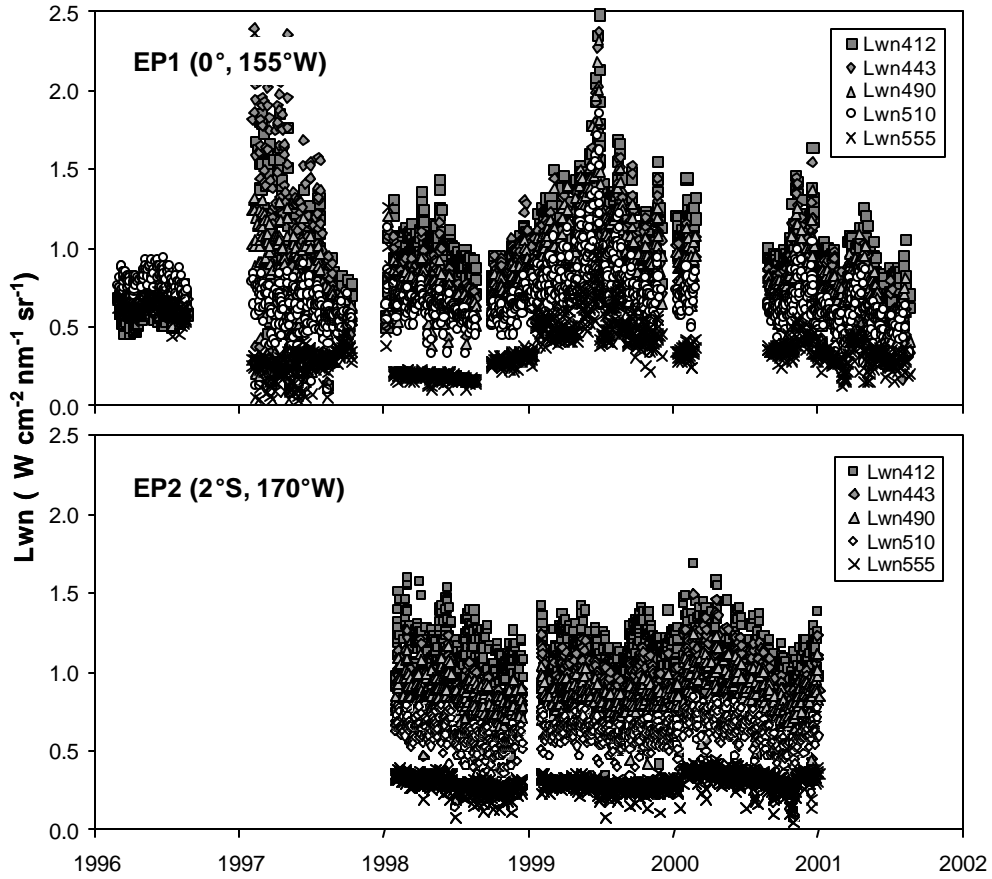


Figure 5.3: The time series of normalized water-leaving radiance, L_{wn} [$\mu\text{W cm}^{-2} \text{nm}^{-1} \text{sr}^{-1}$], derived from the L_n and K_d data obtained from MBARI optical instruments on the TAO moorings at 0° 155°W (EP1) and 2°S 170°W (EP2). The data have been subject to quality control as described in methods.

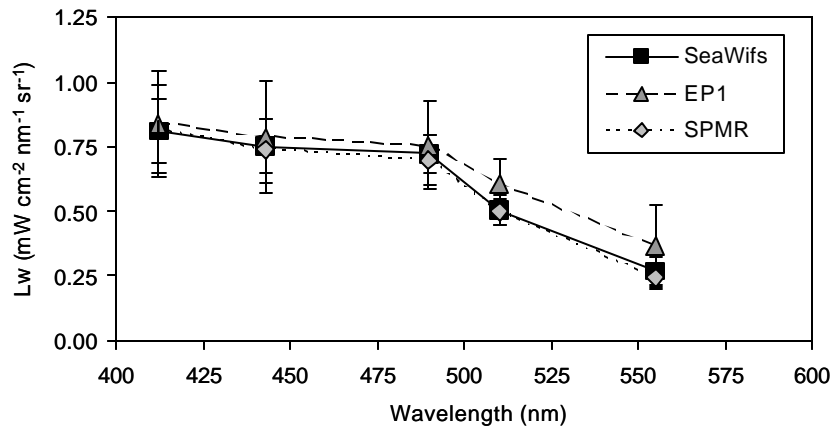


Figure 5.4: Water leaving radiance matchups between SeaWiFS, EP1 (0° , 155°W) optical mooring, and SPMR profiles (where applicable) from June 1998 to Oct 2001. Anomalous data collected during the 1997 – 1998 El Nino period were not included. The number of matching points between SeaWiFS and the optical mooring at 412, 443, 490, 510, and 555 nm were, $n = 245$, 238, 236, 208 and 210, respectively. For SPMR profiles, $n = 10$.

This year alone we have conducted over 50 SPMR profile casts, analyzed more than 2500 shipboard chlorophyll measurements, processed over 500 nutrient samples, processed 200 a* samples and collected close to 500 HPLC samples. Currently, we are analyzing over 400 HPLC samples in conjunction with optical profile data. The program of cruise-based measurements as described above will continue on eight equatorial Pacific cruises during 2003-2004, with scheduled SeaWiFS LAC where applicable.

REFERENCES

- Chavez, F.P., and R.T. Barber, 1987: An estimate of new production in the equatorial Pacific, *Deep-Sea Research*, **34**, 1229-1243.
- Chavez, F.P., K.R. Buck, R.R. Bidigare, D.M. Karl, D. Hebel, M. Latasa, L. Campbell and J. Newton, 1995: On the chlorophyll a retention properties of glass-fiber GF/F filters, *Limnology and Oceanography*, **40**, 428-433.
- Chavez, F.P. and J. R. Toggweiler, 1995: Modern Processes and Ancient Records, in *Upwelling in the Ocean*. Summerhayes, et al. Eds., Wiley & Sons, Chichester Publisher, 313-320.
- Chavez, F.P., K.R. Buck, S.K. Service, J. Newton and R.T. Barber, 1996: Phytoplankton variability in the central and eastern tropical Pacific, *Deep-Sea Research*, **43** (4-6), 835-870.
- Chavez, F.P., P.G. Strutton, and M.J. McPhaden, 1998: Biological-physical coupling in the central equatorial Pacific during the onset of the 1997-98 El Niño, *Geophysical Research Letters*, **25** (19), 3543-3546.
- Chavez, F.P., P.G. Strutton, G.E. Friederich, R.A. Feely, G. Feldman, D. Foley and McPhaden, 1999: Biological and chemical response of the equatorial Pacific Ocean to the 1997-98 El Niño, *Science*, **286**, 2126-2131.
- Chavez, F.P., D. Wright, R. Herlien, M. Kelley, F., Shane, P.G. and Strutton, 2000: A device for protecting moored spectroradiometers from bio-fouling, *Journal of Oceanic and Atmospheric Technology*, **17**, 215-219.
- Dugdale, R.C. and F.P. Wilkerson, 1998: Silicate regulation of new production in the equatorial Pacific upwelling, *Nature*, **391**, 270-273.
- Feely, R.A., R. Wanninkhof, T. Takahashi and P. Tans, 1999: Influence of El Niño on the equatorial Pacific contribution to atmospheric CO₂ accumulation, *Nature*, **398**, 597-601.
- Frouin, R., D.W. Ligner, and C. Gautier, 1989: A simple analytical formula to compute clear sky total and photosynthetically available solar irradiance at the ocean surface, *Journal of Geophysical Research*, **94**, 9731-9742.
- McClain C.R. and G.S. Fargion, 1999a: SIMBIOS Project 1998 Annual Report, *NASA Tech. Memo. 1999-208645*, Eds., NASA Goddard Space Flight Center, Goddard, Maryland, 105pp.
- McClain C.R. and G.S. Fargion, 1999b: SIMBIOS Project 1999 Annual Report, *NASA Tech. Memo. 1999-209486*, Eds., NASA Goddard Space Flight Center, Goddard, Maryland, 137pp.
- Morel, A. 1988: Optical modeling of the upper ocean in relation to its biogenous matter content (Case I waters), *Journal of Geophysical Research*, **93**, 10749-10768.
- Strutton, P.G and F.P. Chavez: Radiant heating in the equatorial Pacific: Spatial and Temporal variability, *Deep-Sea Research I*, in revision.
- Ryan, J.P., P.S. Polito, P.G. Strutton and F.P. Chavez, Anomalous phytoplankton blooms in the equatorial Pacific, *Progress in Oceanography*, in revision.

- Strutton, P.G., J.P. Ryan and F.P. Chavez, 2001: Enhanced chlorophyll associated with tropical instability waves in the equatorial Pacific, *Geophysical Research Letters*, **28**(10), 2005-2008.
- Strutton, P.G. and F.P. Chavez, 2000: Primary productivity in the equatorial Pacific during the 1997-98 El Niño, *Journal of Geophysical Research*, **105**(C11), 26,089-26,101.
- Strutton, P.G., F.P. Chavez, J.P. Ryan, and G.E. Friederich: Merging data from ships, satellites, moorings and drifters to understand biological-physical coupling in the oceans. In preparation for 'Handbook of scaling methods in aquatic CRC Press.
- Strutton, P.G and F.P. Chavez: Radiant heating in the equatorial Pacific: Spatial and Temporal variability, *Deep-Sea Research I*, submitted.
- Tans, P.P., I. Y. Fung, T. Takahashi 1990: Observational constraints on the global atmospheric CO₂ budget, *Science*, **247**, 1431-1438.
- Takahashi, T, R.A. Feely, R.F. Weiss, R. Wanninkhof, D.W. Chipman, S.C. Sutherland and T.T. Takahashi 1997: Carbon dioxide and climate change, *Proceedings of the National Academy of Sciences*, **94**, 8314-8319.

Table 5.1: Summary of cruises during which *in situ* data have been obtained by MBARI in support of SIMBIOS. All cruises are undertaken aboard the NOAA ship *Ka'imimoana*, with the exception of GP6-02-RB aboard the *Ronald H. Brown*. Meridional transects indicate the lines occupied by the ship. Along each line, CTD stations were performed approximately every degree of latitude from 8°N to 8°S, and every 0.5° between 3°N and 3°S. Measurements consisted of chlorophyll (Chl) plus nitrate, phosphate and silicate (Nutrients) at 8 depths between 0 and 200m. On selected cruises, primary production (PP) and new production (NP) measurements were also made using ¹⁴C and ¹⁵N incubation techniques, respectively. Daily optical profiles were obtained using the Satlantic SeaWiFS Profiling Multispectral Radiometer (SPMR) where indicated.

Cruise ID	Dates	Meridional transects	Measurements
GP7-01-KA	27-Sep-01 to 25-Oct-01	155W and 170W	Chl, NP, PP, Nutrients, SPMR, a*, HPLC
GP8-01-RB	14-Oct-01 to 14-Nov-01	95W and 110W	Chl, Nutrients, a*
GP9-01-KA	30-Oct-01 to 25-Nov-01	165W and 180W	Chl, Nutrients, a*
GP1-02-KA	04-Mar-02 to 5-Apr-02	95W and 110W	Chl, Nutrients, a*
GP2-02-KA	08-Apr-02 to 13-May-02	125W and 140W	Chl, Nutrients, a*
GP3-02-KA	29-May-02 to 30-Jun-02	155W and 170W	Chl, NP, PP, Nutrients, SPMR, a*, HPLC
GP4-02-KA	04-Jul-02 to 29-Jul-02	165W and 180W	Chl, Nutrients, a*
GP5-02-KA	16-Aug-02 to 16-Sep-02	140W	Chl, Nutrients, a*
GP7-02-KA	02-Oct-02 to 01-Nov-02	155W and 170W	Chl, NP, PP, Nutrients, SPMR, a*, HPLC
GP6-02-RB	07-Oct-02 to 08-Nov-02	95W and 110W	Chl, Nutrients, a*
GP8-02-KA	04-Nov-02 to 07-Dec-02	165E and 180	Chl, Nutrients, a*

Chapter 6

Satellite Ocean-Color Validation Using Ships of Opportunity

Robert Frouin, David L. Cutchin, Lydwine Gross-Colzy and Antoine Poteau
Scripps Institution of Oceanography, University of California San Diego, La Jolla

Pierre-Yves Deschamps
Laboratoire d'Optique Atmosphérique, Université des Sciences et Technologie de Lille, France

6.1 INTRODUCTION

Our investigation's objective is to collect from platforms of opportunity (merchant ships, research vessels) concomitant normalized water-leaving radiance and aerosol optical thickness data over the world's oceans. A global, long-term data set of these variables is needed to verify whether satellite retrievals of normalized water-leaving radiance are within acceptable error limits and, eventually, to adjust atmospheric correction schemes. To achieve the objective, the volunteer officers, technicians, and scientists onboard the selected ships use portable SIMBAD radiometers. These instruments are specifically designed for evaluation of satellite-derived ocean color; they measure radiance in spectral bands typical of ocean-color sensors, i.e., at 443, 490, 560, 670, and 870 nm. Aerosol optical thickness is obtained by viewing the sun disk like a classic sun photometer. Normalized water-leaving radiance, or marine reflectance, is obtained by viewing the ocean surface through a vertical polarizer in a specific geometry to minimize direct sun glint and reflected sky radiation, i.e., near the Brewster angle at a relative azimuth angle of 135 degrees with respect to the sun. The SIMBAD data collected, after proper quality control and processing, are delivered to the SIMBIOS project office for inclusion in the SeaBASS archive. They complement SIMBAD data collected similarly by the University of Lille, France.

The SIMBAD data are used to check the radiometric calibration of satellite ocean-color sensors after launch and to evaluate derived ocean-color variables (i.e., normalized water-leaving radiance, aerosol optical thickness, and aerosol type). Analysis of the SIMBAD data provides information on the accuracy of satellite retrievals of normalized water-leaving radiance, an understanding of the discrepancies between satellite and *in situ* data, and algorithms that reduce the discrepancies, contributing to more accurate and consistent global ocean color data sets.

6.2 RESEARCH ACTIVITIES

During the period from 01 October 2001 to 31 October 2002, SIMBAD measurements were made during 10 research cruises of opportunity, bringing to 62 the number of campaigns with SIMBAD measurements realized during the period October 1996-October 2002. The 10 cruises are listed in Table 6.1 with name of cruise, SIMBAD instrument(s) used, region of measurements, name of operator, and dates of measurements. The location of the measurements is displayed in Figure 6.1. The data were collected mostly off the West Coast of the United States and Baja California, Mexico (CalCOFI and IMECOCAL cruises) and in the Atlantic Ocean between Kiel, Germany and the Antarctic Peninsula (IOFFE0 0102 cruise). The advantage of the IMECOCAL cruises, compared with the CalCOFI cruises, is that they take place in a less cloudy region, offering the possibility of more match-ups with satellite observations. The measurement program during the IOFFE0102 cruise included not only SIMBAD measurements, but also collection of water samples for pigment and absorption analysis. The AMLR2002 cruise was accomplished under mostly cloudy conditions, and the SIMBAD instrument malfunctioned during the CalCOFI 0201 cruise (no data at 870 nm). A total of 1210 complete SIMBAD data sets were processed and transferred to the SeaBASS archive.

The history of SIMBAD calibration coefficients and the accuracy of the view angles measured by the radiometers were analyzed. This effort started during the first year of the investigation, but was continued the second year with additional data. Trends in the calibration coefficients and biases in the view angles were removed, and all the SIMBAD data acquired since October 1996 are being re-processed. A similar effort is conducted at the University of Lille with complementary SIMBAD

data. Processing of the two data sets is made separately, yet in a consistent manner for a statistical evaluation of satellite-derived ocean color.

Several aspects of satellite ocean-color remote sensing were examined. They include aerosol models for atmospheric correction, SeaWiFS performance during ACE-Asia, biological variability in the retrieval of chlorophyll-a concentration, modeling of phytoplankton absorption, ocean color remote sensing using MISR data, estimation of PAR from POLDER and GLI data, and retrieval of chlorophyll-a concentration without explicit atmospheric correction. The main results and findings are summarized in the next section (see also, below, the list of publications).

Table 6.1. SIMBAD cruises during 01 October 2001 – 31 October 2002

- CalCOFI 0201, Southern California Bight, Antoine Poteau, Simbad02 and Simbada12, 24 Jan 02 - 11 Feb 02
- IMECOCAL 0201/02, Ensenada-San Carlos, Simbad06, Elsa Alguirre, 17 Jan 02 - 07 Feb 02
- AMLR2002, Southern ocean, R/V Yuzhmoregeologiya, Simbad04, John Wieland, 19 Jan 02 - 09 Feb 02
- CalCOFI 0207, Southern California Bight, Simbad06, Haili Wang, 02 Jul 02 – 18 Jul 02
- IOFFE 0102, Kiel-Recife-Ushuaia-Antarctica-Montevideo-Kiel, Simbad03 and Simbad07, Anatoly Grigoriev and Alexander Khrapko, 05 Oct 01 - 29 Apr 02
- CalCOFI 0204, Southern California Bight, Simbad06, Haili Wang, 24 Mar 02 - 25 Apr 02
- IMECOCAL 0204/05, Ensenada-San Carlos, Simbad04, Elsa Alguirre, 18 Apr 02 - 09 May 02
- HILLARYS TRANSECT, Eastern Australia, Simbad08, Leon Majewski, 06 Jun 02 – 11 Jun 02
- IMECOCAL 0207/08, Ensenada-San Carlos, Simbad04, Jushiro Cepeda-Morales, 12 Jul 02 - 02 Aug 02
- IMECOCAL 0207/08, Ensenada-San Carlos, Simbad08, Elsa Aguirre, 16 Oct 02 - 06 Nov 02

6.3 RESEARCH RESULTS

A non-supervised classification of CIMEL-derived aerosol optical properties, i.e., volume size distribution and refractive index, was performed, leading to 23 clusters (Figure 6.2). These clusters may be used as new aerosol mixtures in atmospheric correction algorithms. The classification was accomplished using a probabilistic self-organizing map to approximate the distribution of the data. The resulting referent vectors then were subjected to hierarchical clustering to identify the geophysical conditions most encountered in the database. Figure 6.3 displays the phase function and single scattering albedo of the SeaWiFS aerosol models (left) and the statistical mixtures (right). The statistical phase functions exhibit less variability than the SeaWiFS ones, but the statistical single scattering albedos vary within a larger range (0.86-0.99 instead of 0.96-1). The statistical models, which take into account the entire atmospheric column, appear as a suitable alternative to the SeaWiFS models. Their use with SeaWiFS data, however, would require re-adjusting the calibration coefficients of the satellite instrument.

A maritime aerosol model was derived from CIMEL sky radiometer data collected at three AERONET island locations, Bermuda, Lanai, and Kaashidhoo. It is characterized by a bimodal distribution, with fine and coarse modes of effective radius 0.11-0.14 and 1.8-2.1 μm , respectively, and a refractive index of 1.37 - 0.001i. In terms of Angstrom coefficient in the red and near infrared, this model corresponds to the SeaWiFS coastal aerosol model with 80% humidity. Phase functions of the two models, however, differ substantially in both the visible and near infrared, with implications on the accuracy of SeaWiFS retrievals. The aerosol model selected for the vicarious calibration of SeaWiFS is not dominant at the MOBY location, suggesting that the relative calibration of bands 7 and 8 should be revisited and determined using more representative models obtained from the CIMEL data at nearby Lanai.

SeaWiFS imagery of the East Asian seas acquired during ACE-Asia (March-April 2001) revealed large areas of underestimated, even negative water-leaving radiance in the blue. To investigate the cause of the problem, concomitant satellite and ship observations at three locations around Japan were analyzed. Using an optimization method, information on aerosol composition was obtained from sky radiance data collected onboard the ship. An iterative radiation-transfer simulation was carried out to reproduce the satellite radiance. The agreement between simulated and measured values was good when the effect of sub-micron absorbing particles was considered in the radiation-transfer simulation. These particles, e.g., soot from diesel fuel and coal consumption, not only Asian dust, contribute to negative water-leaving radiance estimates in East Asian seas.

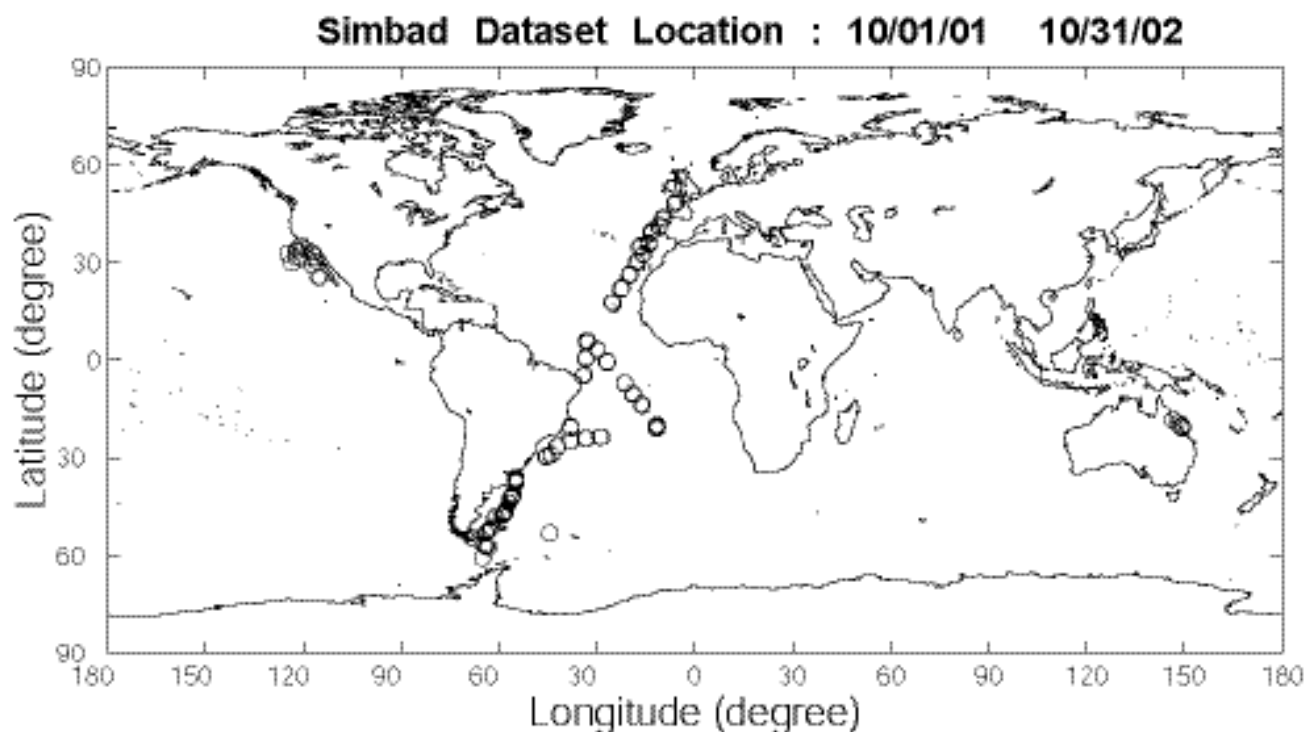


Figure 6.1: Geographic location of the SIMBAD data sets acquired during the period from 01 October 2001 to 31 October 2002.

The POLDER atmospheric correction scheme was adapted to MISR and tested with MISR data acquired during ACE-Asia on 13 April 2001 (Orbit 7015, Path 111, Block 62). The multi-angle capability of MISR (9 cameras and view zenith angles from 0 to 70.5 degrees) is expected to improve atmospheric correction in the presence of absorbing aerosols. The first results show some inconsistency between retrievals in the 9 directions, suggesting that the radiometric calibration of the MISR cameras should be adjusted for quantitative interpretation of the data in terms of water-leaving radiance. Other MISR images over clear areas (i.e., with few aerosols) are being processed to help with the radiometric calibration.

The SeaWiFS Photo-synthetically Available Radiation (PAR) code was adapted to POLDER and applied to 8 days (December 11-18, 1996) of POLDER data over the global ocean. Processing of the entire POLDER data set (November 1996-June 1997) is envisaged by the POLDER ocean color team at the University of Lille, France, as well as producing operationally PAR from the next POLDER on ADEOS-2. One advantage of POLDER is its bi-directional capability, allowing a more accurate transformation of reflectance in albedo. The SeaWiFS PAR code was also adapted to GLI data and tested on GLI synthetic data created from actual MODIS data. A regional (2.5 degree x 2.5 degree resolution), diurnal (hourly) albedo climatology based on 5 years of narrow field-of-view data from the Earth radiation Budget Satellite was obtained to improve the daily PAR estimates.

During the IOFFE 0102 campaign, the characteristics of the ocean and atmosphere required for evaluating satellite ocean-color algorithms were measured, without stopping the ship, along two Atlantic Ocean transects from Kiel to Ushuaia (October-November 2001) and Ushuaia to Kiel (March-April 2002) and off the Antarctic Peninsula (November 2001-March 2002). A total of 337 stations were made. Comparison of data acquired by different means allowed a check of the results and estimation of uncertainties. An evaluation of bio-optical characteristics (water-leaving radiance, chlorophyll-a concentration, and back-scattering coefficient) retrieved from SeaWiFS data was performed, and reasonable agreement was obtained between field data and satellite-based estimates. Seven bio-optical provinces in the Atlantic and three in the Antarctic study area were selected based on SeaWiFS data, and the features and seasonal variability of their optical properties, as measured *in situ*, were contrasted (important to develop regional bio-optical algorithms). A neural network was constructed to retrieve chlorophyll-a concentration from marine reflectance in the SeaWiFS spectral bands in the visible. The network was calibrated using a synthetic data set accounting for variability due to atmospheric content, light, and secondary pigments. Pigment variability was simulated empirically from *in situ* observations in the western Pacific Ocean.

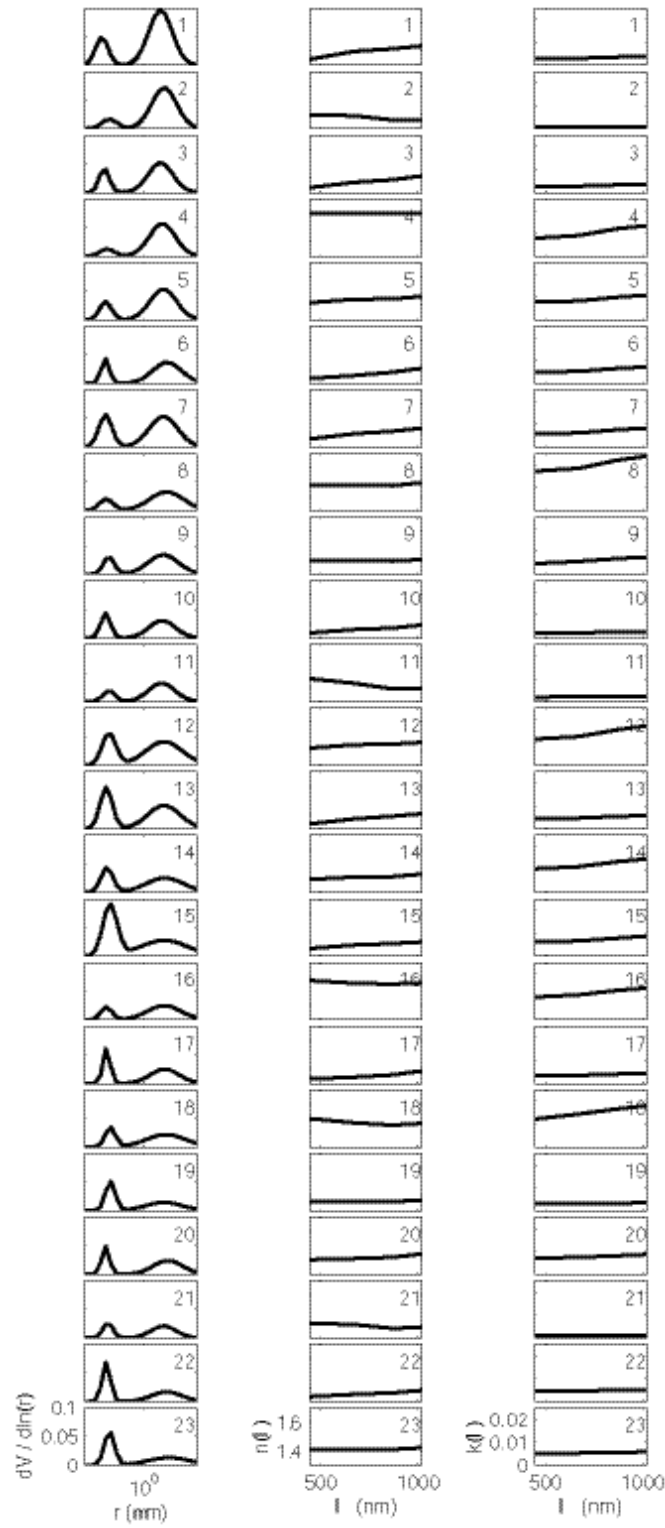


Figure 6.2: Gravity centers of the 23 clusters obtained by the non-supervised classification of CIMEL aerosol size distributions and refractive indices at island and coastal sites. First column is size distribution $dV/d\ln r$, second column is real part n of the refractive index, and third column is imaginary part k of the refractive index.

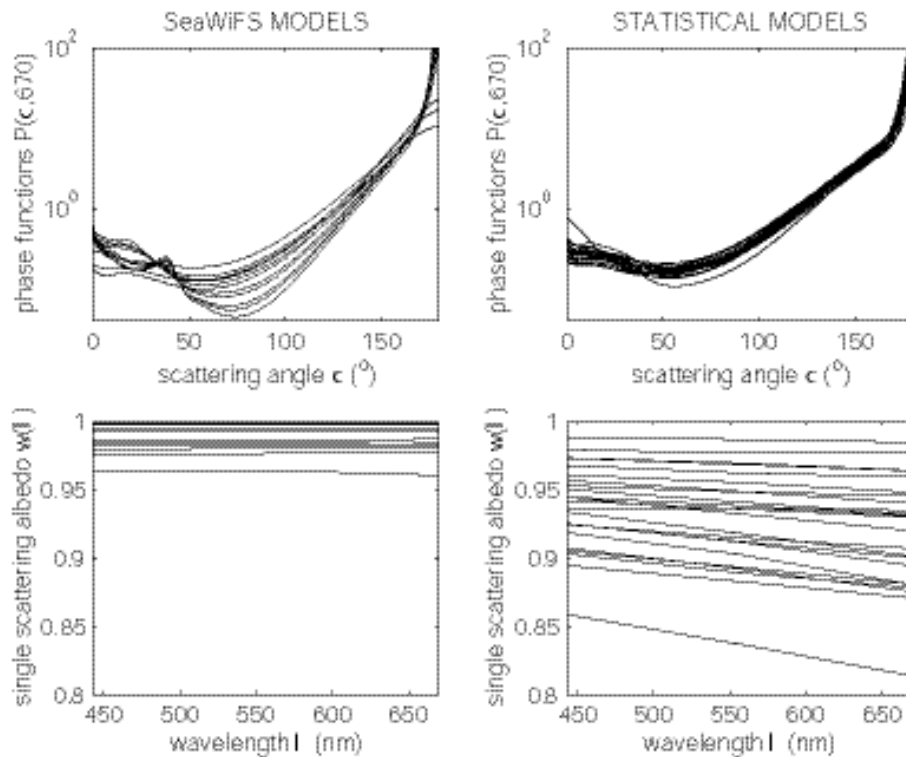


Figure 6.3: Phase function at 670 nm and spectral single scattering albedo of the 12 SeaWiFS aerosol models and the 23 statistical aerosol models. The Angström exponent at 670 nm varies between -0.08 and 1.49 for the SeaWiFS models and between 0.72 and 1.98 for the statistical models.

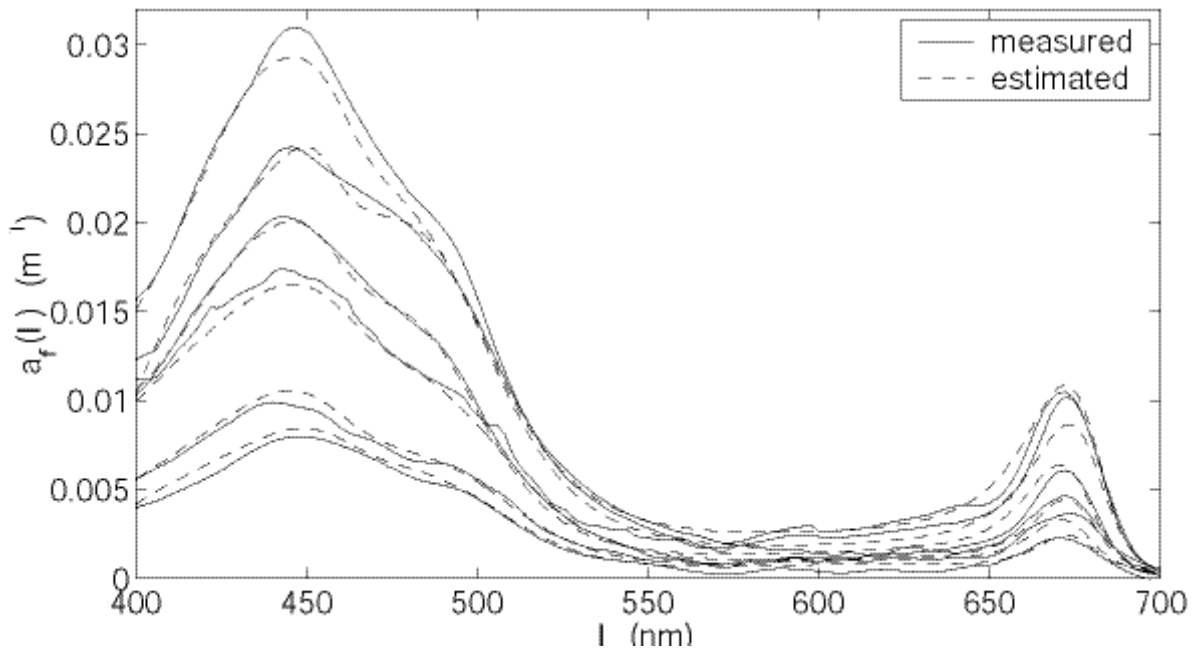


Figure 64: Examples of simulated phytoplankton absorption spectra compared with *in situ* measurements. Simulated spectra are obtained via neural network modeling as a function of chlorophyll-a, -b, and -c, and photosynthetic and photoprotectant carotenoids

The methodology included the forward modeling, also via neural network, of phytoplankton absorption as a function of chlorophyll-a, -b, and -c, photosynthetic and photoprotectant carotenoids. This modeling reproduced accurately the effect of secondary pigments on the absorption spectrum, at any wavelength in the visible domain (Figure 6.4). The retrieval of chlorophyll-a concentration was improved by 33% using the neural approach instead of a classic algorithm based on reflectance ratio, demonstrating the ability of the neural network methodology to reduce the effect of secondary pigments on the reflectance/chlorophyll-a relationship.

A new algorithm was developed to estimate chlorophyll-a concentration from space without explicit aerosol correction. In the algorithm, the satellite reflectance in the visible and near infrared is linearly combined after correction of direct sun glint and molecular scattering. The coefficients of the linear combination minimize the perturbing effects, which are modeled by a polynomial, and do not depend on geometry. The algorithm utilizes spectral bands centered at 443, 565, 667, and 866 nm, but is applicable to other sets of spectral bands. Using a polynomial with exponents -2, -1, and 0 to determine the coefficients, the residual influence of the atmosphere on the linear combination is small compared with the corrected satellite reflectance, generally within ± 0.001 , except at large view and sun zenith angles, for which it may reach 0.005 in magnitude. The resulting rms error on chlorophyll-a concentration is 8.4%. Application of the method to GLI simulated imagery shows that estimated and actual chlorophyll-a concentrations are in agreement, with an rms difference of 32.1% and an average bias of -2.2% (Figs. 6.5 and 6.6). The advantage of the algorithm resides in its simplicity and rapidity of execution. Knowledge of aerosol amount and type is avoided. There is no need for look-up tables of aerosol optical properties. However, accuracy depends on the bio-optical model selected to relate the linear combination to chlorophyll abundance.

6.4 FUTURE WORK

During the third year of the investigation (01 December 2002-30 November 2003), collection of SIMBAD data will continue during the quarterly CalCOFI and IMECOCAL cruises. Data will also be acquired during the R/V Ioffe return voyage from Ushuaia to Kiel in March-April 2003. This measurement activity is especially important for the ADEOS-2 mission, since the satellite will be launched during 10-15 December 2002 with the POLDER instrument and GLI. The SIMBAD data acquired after the 3-month commission phase will be used for vicarious calibration and various initialization tasks. The spring 2003 CalCOFI cruise will include complementary measurements by other investigators of aerosol extinction profiles and columnar size distribution, and the full set of bio-optical variables that influence water-leaving radiance.

The construction of five advanced SIMBAD (SIMBADA) radiometers, started during the second year of the investigation, will be completed. The optical and mechanical assemblies have been built, but the electronic cards remain to be made. The advanced instruments are lighter and more compact than the regular instruments, and they measure in 11 spectral bands instead of 5, from 350 to 870 nm. They also operate without cables (integrated GPS), have improved electronics, reduced noise, a larger internal memory, better batteries, an internal charger, and a numerical display of the viewing angles. The software to process the SIMBADA data, including correction of residual polarization by the water body, will be tested and adjusted on data acquired with instruments belonging to the University of Lille.

The performance of various SeaWiFS atmospheric correction algorithms in the presence of absorbing aerosols (i.e., pollution particles, dust) will be evaluated. Data acquired in the Sea of Japan, the East China Sea, and the Philippine Sea during ACE-Asia (March-April 2001) will be used. Eight suitable days with contrasted aerosol conditions have been identified for the comparison. The SeaWiFS data have been extracted, the standard SeaDAS algorithm applied, and the *in situ* data (water-leaving radiance, chlorophyll-a concentration, and aerosol properties) processed. Even though the number of satellite/ship match-ups is small, the *in situ* data set is comprehensive, allowing a detailed and complete analysis of each case. Prof. Howard Gordon and Drs. David Antoine, Hajime Fukushima, and Pierre-Yves Deschamps will run specific algorithms, designed to handle absorbing aerosols more adequately than the operational algorithm.

The SeaWiFS and field data acquired during the IOFFE 0102 campaign will be analyzed to describe spatial variability of atmospheric and oceanic characteristics (aerosol optical thickness, ocean color, pigment concentration) in the Atlantic Ocean between 50N and 55S in two different seasons. Changes during November to March in the poorly sampled region south of 55S, including eutrophic waters near South America, mesotrophic-oligotrophic waters in the central part of the Drake Passage, and eutrophic waters East of the Antarctic Peninsula, will be examined. Absorption spectra and pigment composition of various bio-optical provinces will be contrasted, and the impact on accuracy of bio-optical algorithms will be evaluated. The relation between aerosol optical thickness and hydrosol back-scattering coefficient, also estimated from SeaWiFS data, will be investigated in an attempt to get information on the relative importance of biogenous and terrigenous material in the back-scattering coefficient.

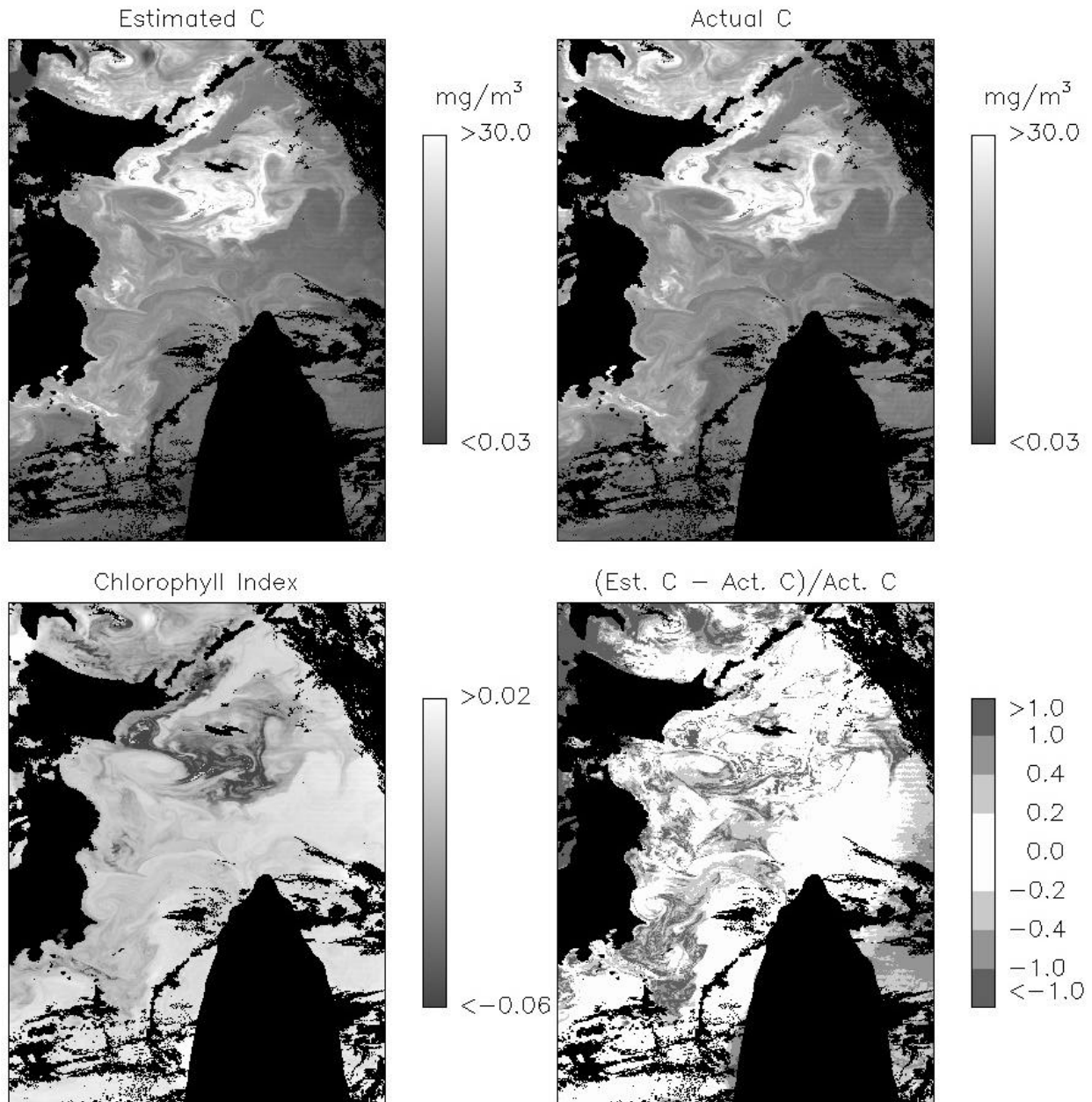


Figure 6.5: Linear combination of GLI simulated top-of-atmosphere reflectance at 443, 565, 670 and 866 nm after correction of molecular scattering and direct sun glint (lower left), estimated chlorophyll-a concentration C (upper left), actual C (upper right), and fractional C error (lower right).

The SIMBAD data set acquired since September 1997 will be used in a statistical evaluation of the SeaWiFS radiometric calibration, atmospheric correction, and derived ocean color. The history of the SIMBAD calibration coefficients will be taken into account in the data processing. A comparison of SIMBAD and other instruments (MER and PRR for water-leaving radiance, Microtops, fast-rotating shadow-band radiometer for aerosol optical thickness) will be made to estimate accuracy of the SIMBAD values. More stringent criteria will be used to select match-up situations for sensor calibration than for product evaluation. The significant differences between *in situ* measurements and satellite estimates will be quantified as a function of environmental and geometric variables, such as aerosol amount and type, water type, wind speed, and view and sun angles.

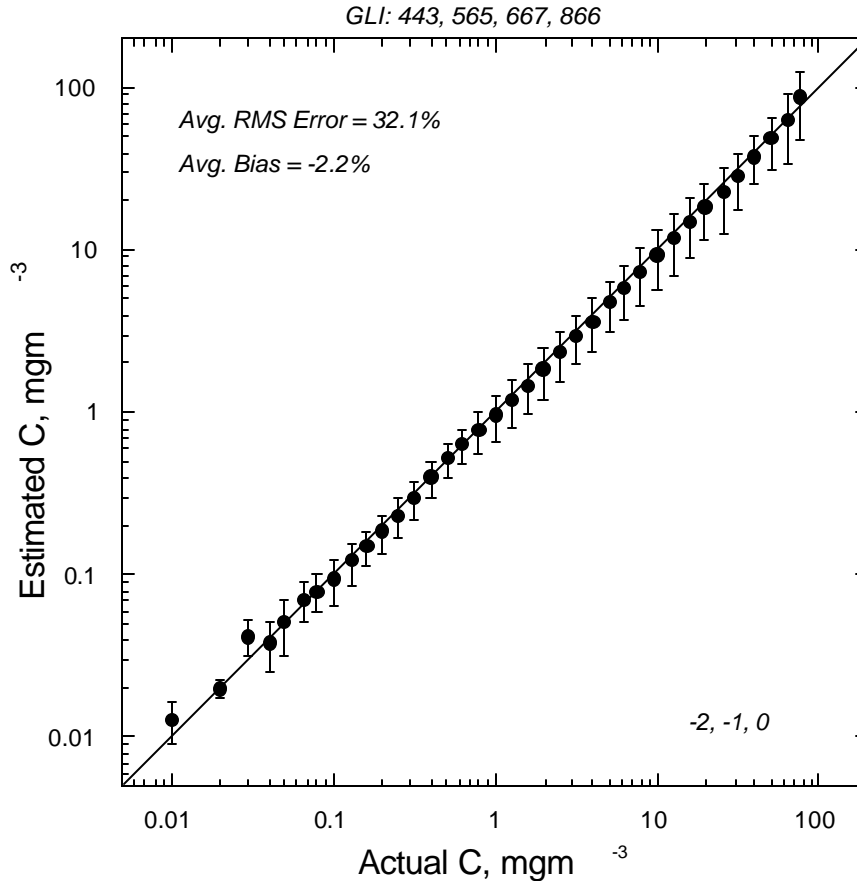


Figure 6.6: Estimated versus actual chlorophyll concentration C for the GLI simulated imagery. Estimated C is obtained from a linear combination of top-of-atmosphere reflectance at 443, 565, 670, and 866 nm after correction of molecular scattering and direct sun glint.

The new algorithm to estimate chlorophyll-a concentration without explicit aerosol correction will be optimized and adapted to SeaWiFS and MODIS. A principal component analysis of the perturbing effects, simulated for a wide range of conditions, will be performed, leading to a linear, accurate expression of the perturbing effects as a function of the principal components' coordinates in the base of selected wavelengths (instead of a polynomial decomposition). Keeping all the principal components will reproduce the entire variability of the perturbing effects. Neglecting the less significant components will allow introduction of constraints to ensure that the linear combination is sufficiently sensitive to chlorophyll-a concentration and minimally influenced by noise in the satellite signal and phytoplankton type.

The aerosol mixtures obtained by non-supervised classification of CIMEL size distributions and refractive indices (self-organized mapping, hierarchical clustering) will be used in the atmospheric correction of SeaWiFS data. The resulting water-leaving radiance and chlorophyll-a concentration estimates will be compared with those from the standard atmospheric correction scheme. For this purpose, look-up tables of aerosol optical properties will be created for the statistical models. The comparison will be made using simulated and actual SeaWiFS data. Application to actual SeaWiFS data will require modifying the relative calibration of bands 7 and 8 using CIMEL measurements at Lanai (to specify the aerosol model) and then propagating the changes to the other bands. Kohonen mapping will also be used to classify top-of-atmosphere imagery into aerosol and water classes that will be labeled (e.g., type of aerosol, range of pigment concentration, type of water).

ACKNOWLEDGMENTS

We wish to thank the officers, technicians, and scientists that have voluntarily collected SIMBAD data and contributed to data analysis, namely Elsa Aguirre, Guislain Becu, Peter Fearn, Bertrand Fougnie, Jushiro Cepeda-Morales, Jean-Marc Nicolas, Leon Majewski, Ajit Subramaniam, Haili Wang, and John Wieland. We also gratefully acknowledge Oleg Kopelevich for organizing the R/V Ioffe campaign, John McPherson for programming support, Hiroshi Murakami for providing the GLI simulated imagery, and the SeaWiFS and SIMBIOS project staff for helping with match-up data and for stimulating discussions. This work is supported by the National Aeronautics and Space Administration under contract NAS5-00194, the Scripps Institution of Oceanography, the California Space Institute, the Centre National d'Etudes Spatiales, and the Centre National de la Recherche Scientifique.

Chapter 7

Merging Ocean Color Data From Multiple Missions

Watson W. Gregg

NASA Goddard Space Flight Center, Greenbelt, Maryland

7.1 INTRODUCTION

Oceanic phytoplankton may play an important role in the cycling of carbon on the Earth, through the uptake of carbon dioxide in the process of photosynthesis. Although they are ubiquitous in the global oceans, their abundances and dynamics are difficult to estimate, primarily due to the vast spatial extent of the oceans and the short time scales over which their abundances can change. Consequently, the effects of oceanic phytoplankton on biogeochemical cycling, climate change, and fisheries are not well known.

In response to the potential importance of phytoplankton in the global carbon cycle and the lack of comprehensive data, NASA and the international community have established high priority satellite missions designed to acquire and produce high quality ocean color data (Table 7.1). Ten of the missions are routine global observational missions: the Ocean Color and Temperature Sensor (OCTS), the Polarization and Directionality of the Earth's Reflectances sensor (POLDER), Sea-viewing Wide Field-of-view Sensor (SeaWiFS), Moderate Resolution Imaging Spectrometer-AM (MODIS-AM), Medium Resolution Imaging Spectrometer (MERIS), Global Imager (GLI), MODIS-PM, Super-GLI (S-GLI), and the Visible/Infrared Imager and Radiometer Suite (VIIRS) on the NPOESS Preparatory Project (NPP) and the National Polar-orbiting Operational Environmental Satellite System (NPOESS). In addition, there are several other missions capable of providing ocean color data on smaller scales. Most of these missions contain the spectral band complement considered necessary to derive oceanic chlorophyll concentrations and other related parameters. Many contain additional bands that can provide important ancillary information about the optical and biological state of the oceans.

In previous efforts, we have established that better ocean coverage can be obtained in less time if the data from several missions are combined (Gregg et al., 1998; Gregg and Woodward, 1998). In addition to improved, and faster coverage, data can be taken from different local times of day if the missions are placed in different orbits, which they are. This can potentially lead to information on diel variability of phytoplankton abundances. Since phytoplankton populations can increase their biomasses by more than double in a single day under favorable circumstances (Eppley, 1972; Doney et al., 1995), observations of their abundances at different times within a single day would be useful.

7.2 RESEARCH RESULTS

We propose to investigate, develop, and test algorithms for merging ocean color data from multiple missions. We seek general algorithms that are applicable to any retrieved Level-3 (derived geophysical products mapped to an Earth grid) ocean color data products, and that maximize the amount of information available in the combination of data from multiple missions. Most importantly, we will investigate merging methods that produce the most complete coverage in the smallest amount of time, nominally, global daily coverage. We will emphasize 5 primary methods: 1) averaging, 2) subjective analysis, 3) spatial analysis, 4) blending, and 5) statistical interpolation. We will evaluate the effects of the different algorithms on the representation of the derived Level-3 fields, emphasizing not only daily products, but also larger time increments, such as 2-day, 4-day, 8-day (weekly), monthly, and seasonal.

Candidate Merger Methods

We intend to investigate a set of 5 merging algorithms utilizing Level-3 data products. None of the candidate algorithms are limited to any Level-3 grid size or temporal frequency. The choice of grid size and frequency issue depends on how sparse the final fields are and the acceptance level for data gaps. We will leave this choice to the SIMBIOS Project. For our analyses,

however, we will use the grid and frequency specifications of the SeaWiFS Project, which are 9-km equiangular spatial, and daily, 8-day, monthly, and seasonal time fields. We will also investigate the usefulness of 2- and 4-day fields as potential new products. Candidate merger algorithms under investigation in this proposed effort are: averaging, subjective analysis, spatial analysis, blending, and statistical (optimal) interpolation.

- *Averaging*: This method is a simple, straightforward application of weighting data from each sensor equally. At grid points where only data from one satellite are available, it enters the merged field unadjusted.

$$C_{ij} = \frac{\sum_s C_{ijs}}{\sum_s n_{ijs}} \quad (1)$$

where C indicates chlorophyll from sensor s, n is the number of observations from sensor s, ij represents the Level-3 grid point in question, and the summations are over the sensors. Although we use chlorophyll to represent the equation, any Level-3 data product can be used. This method has the advantage of simplicity and total objectivity, i.e., no sensor data are preferred over others. It can potentially suffer from this same objectivity in the case of relatively poorer performance. If Level-3 grid locations are common among the different sensor products, the application of the method is straightforward. If they are not, then interpolation may be required.

- *Subjective Analysis*: In the subjective analysis, quantitative information about the quality of the sensors is used to develop a system of weighting functions W, that enable the production of an enhanced merged data set, at least in principle

$$C_{ij} = \frac{\sum_s W_s C_{ijs}}{\sum_s W_s} \quad (2)$$

where

$$W_s = W_s(\mathbf{q}, \mathbf{q}_o, s, L_g)$$

and $\mathbf{q}, \mathbf{q}_o, s, L_g$ represent satellite zenith angle, solar zenith angle, sensor behavior, and sun glint, respectively, and are intended to be a small subset of the possible variables that may determine superior performance of one sensor over the others. This quality information can vary from sensor to sensor over the Level-3 grid. For example, sun glint will impact different sensors in different locations on the Earth depending upon the orbit and observation characteristics. If no quality information is available, this method can default to equal weighting, and is thus identical to the averaging method. A comprehensive quantitative weighting system is a difficult task that exceeds the abilities of a single investigator. Thus its successful application requires detailed information about different missions from the mission representatives, the SIMBIOS Project, and the scientific community at large. It is probably unlikely that complete definitions can be made for all missions. However, it is widely used in missions now, at least in some form. For example, a mask is a condition in which $W = 0$. A flag is a qualitative data quality indicator. The advantage of this method is that it relies entirely on scientific and engineering information to produce the highest quality merged data product. Conceptually it is superior to all of the other methods because fundamental information about sensor performance is explicitly incorporated into the final product. It suffers from the informational demands required. Not only must one know the reasons for relative performance and the errors resulting from the influences, but also how to quantitatively represent them. It is most likely that this method can be used most effectively in combination with other methods.

- *Spatial analysis*: This method has the same form as Eq. 2, but the weights W are defined as a function of the spatial separation distance between sensor data from different sensors at Level-3 grid point, subject to an error correlation length scale (Chen and Wang, 1999). This de-correlation length scale essentially represents the distance that data may have influence on the final merged product

$$W_{ik} = \exp \left[- \left(\frac{R_{ij-kn}}{R_e} \right)^2 \right] \quad (3)$$

where R_{ij-km} is the distance between the Level-3 grid point ij and a sensor observation km , and Re is the error correlation length scale. Determination of Re relies on the behavior and uncertainty of the data. Thus each Level-3 grid point depends on the distribution of sensor data around it. This method has the advantage of simplicity, objectivity, and physical realism if the error correlation scale can be estimated. It also explicitly accounts for different Level-3 grids. As written, sensor data observations replace the Level-3 merged grid if the separation distance is 0, in a sequential fashion. However, additional weighting (perhaps based on subjective analysis) can easily be incorporated.

- *Blended analysis:* The blended analysis has traditionally been applied to merging satellite and *in situ* data (Reynolds, 1988). Also known as the Conditional Relaxation Analysis Method (CRAM; Oort, 1983), this analysis assumes that *in situ* data are valid and uses these data directly in the final product. The satellite chlorophyll data are inserted into the final field using Poisson's equation

$$\nabla^2 C^b = \mathbf{y} \quad (4)$$

where C^b is the final blended field of chlorophyll, and \mathbf{y} is a forcing term, which is defined to be the Laplacian of the gridded satellite chlorophyll data ($\nabla^2 S$). *In situ* data serve as internal boundary conditions, and are inserted directly into the solution field C^b

$$C_{ibc} = I \quad (5)$$

where the subscript ibc indicates internal boundary condition (IBC) and I is the *in situ* value of chlorophyll. Thus *in situ* data appear un-adjusted in the final blended product. In its application to multiple ocean color data sets, *in situ* data would be replaced by a determination of superior performance by one of the sensors data, and utilized as the IBC. This could occur across the domain for an individual sensor, if its calibration was considered superior, for example. Or it could occur by location as the environmental conditions provide for better performance of one sensor over the others (e.g., location of sun glint, individual scan problems, etc.). Where one sensor data could be established as superior, it would serve as the IBC. If no distinction could be provided, the data could simply be merged using one or more of the other methods. Then the final merged product would be blended, so that the internal boundary conditions are upheld, and the rest of the Level-3 field is adjusted according to the spatial variability of the other sensors. This can provide a bias correction to the non-IBC points, while retaining their spatial structure, and potentially produce an overall enhanced data set. The requirement of superior data field insertion unaltered into the merged field can be relaxed. For example, the IBC weight could be 0.25 for sensor 2 and 0.75 for sensor 3 at grid point ij . This can be a useful modification of several sensor data sets are superior to others but not necessarily from one another, or if clear superiority is difficult to quantify. This method has the disadvantage of reducing the grid resolution.

- *Statistical Interpolation:* This method is often referred to as optimal interpolation (e.g., Reynolds and Smith, 1994), but is technically only optimal when all of the error correlations are known (Daley, 1991), which is rare. In this method the weights W are chosen to minimize the expected error variance of the analyzed field (Daley, 1991). It differs from the spatial analysis method by allowing error correlations to determine the effective separation distance, and from the blended analysis by use of a statistical approach for defining the weights. A weight matrix W represents the error correlations, and is referred to as the error covariance matrix.

$$C_{ij} = C_{sij} + \sum W_{ijkm} (C_{s+1,km} - C_{skm}) \quad (6)$$

This method has the advantage of widespread use in data assimilation problems, and objectivity in selection of the weights. It also preserves the original grid resolution. The disadvantage is the statistical interpretation of the merged data set, as opposed to a scientific evaluation. It is possible that the best merging method will be one that utilizes combinations of these algorithms. For example, some level of subjective analysis will be used in data masking, and then averaged. Reynolds and Smith (1994) combine the use of blending for bias correction followed by statistical interpolation to recover the grid resolution. We may easily envision a combination of approaches.

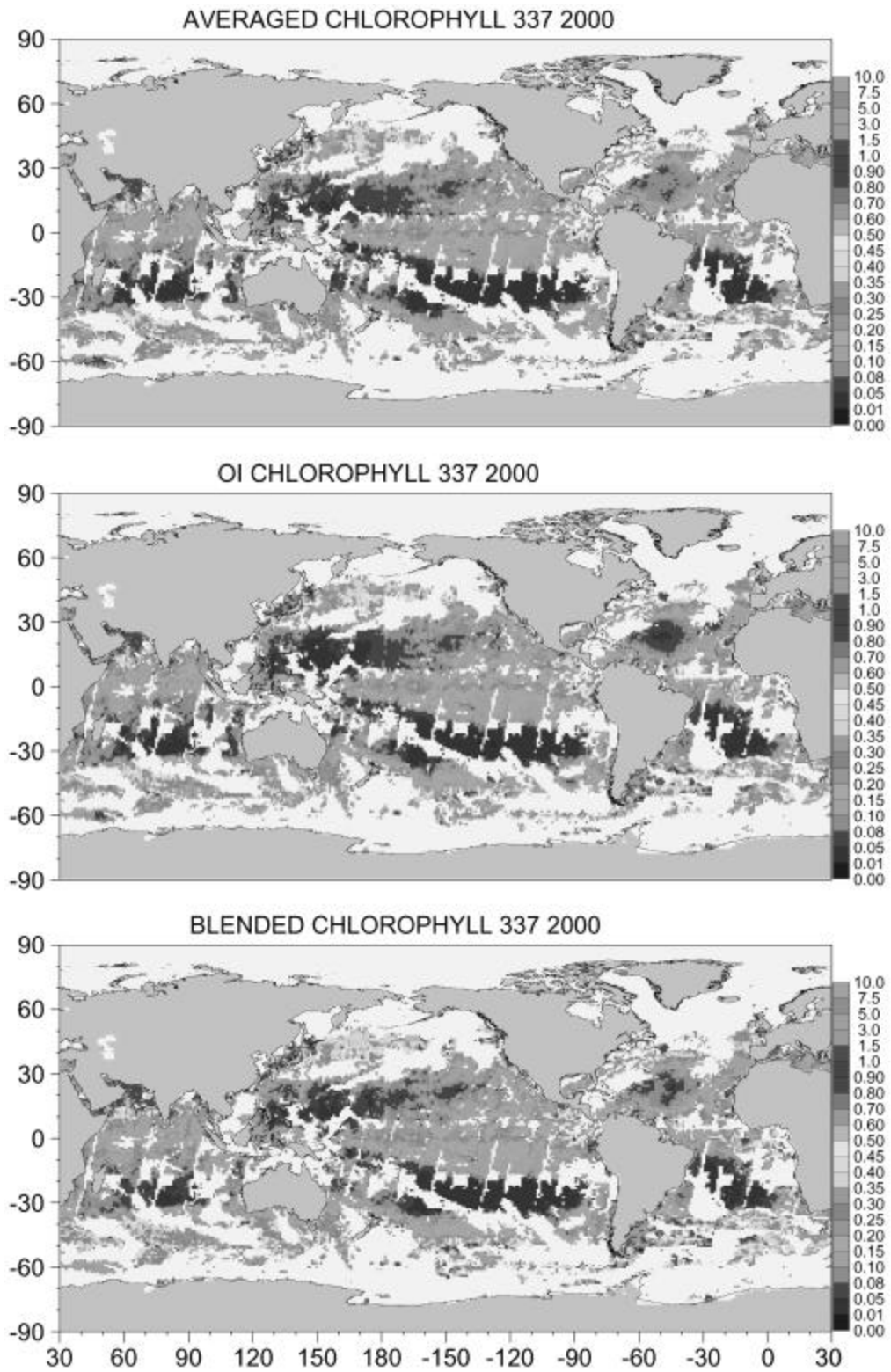


Figure 7.1: Comparison of 3 different methodologies for SeaWiFS and MODIS on December 2, 2000.

7.3 FUTURE WORK

Three of the four candidate merger algorithms have been tested using SeaWiFS and MODIS data. The SeaWiFS data is Version 3 and the MODIS is Collection 3. Newer versions of each data set are now available but not included in our analyses yet. Results indicate promising behavior from all three candidate algorithms (Figure 7.1). However, there are some problems remaining, most associated with data quality of the sensors and our ability to understand and correct for them prior to application of the algorithms. These problems will be different in the newer versions so it is not advisable to dwell on them in this analysis.

Overall the averaging method is best for data with no biases, because it is simple, objective, and computationally fast. If there are biases in either or both data sets that are uncorrected or unrecognized, this method will propagate these errors into the merged field, and produce a poor quality data set. Knowledge of biases in the new versions of each sensor is presently lacking, and requires substantial effort. The blended method is effective at eliminating biases if a "truth field" can be identified. In the analyses done so far, we assumed SeaWiFS to be a truth field unilaterally, and MODIS was the data blended to produce the final merged product. The effectiveness of the bias-correction capability of the blended analysis is quite well known in *in situ*-satellite data merging, but not in satellite-satellite merging. Our results indicate that significant differences in satellite data quality coupled with the very large coverage of both sensors, results in over-correction by the blended method.

The statistical (optimal) interpolation (OI) method has many of the advantages of the blended method in bias-correction. However, the over-correction behavior of the blended method is reduced to the point that it is not readily apparent in the resulting merged field. The method suffers from computational complexity and is very slow.

It is clear that proper selection of merging algorithms depends critically upon knowledge of the error characteristics of the data sets being merged. Consequently, we invested significant effort into analyzing the SeaWiFS data behavior as compared against the SeaBASS data archive. We investigated and intercompared the previously available SeaWiFS archive (Version 3, called R3, available from May 2000-Aug 2002) against the new version (Version 4, called R4, available beginning Aug 2002). Our analysis led to the following conclusions:

- 1) In a global match-up analysis of chlorophyll (the primary geophysical product of SeaWiFS) with SeaBASS, R4 did not improve the fit (r^2 was equal), but the slope was closer to 1.0 and the y-intercept was lower. R3 underestimated high chlorophyll and overestimated low chlorophyll. R4 does but not as much.
- 2) Regionally the improvements are sometimes very good. The Equatorial Pacific represents a region of high reliability because of the absence of contaminating environmental features (absorbing aerosols, variable CDOM, and representative phytoplankton species), and showed major improvement in the area-weighted means.

	SeaBASS	R3	R4
Chlorophyll (mg m^{-3})	0.178	0.196	0.170

Of the 12 major oceanographic basins where data were coincident, only the Antarctic indicated a reduction in performance from R3 to R4 while all others showed improvement.

- 3) Most of the improvement occurred in the open ocean (where depth > 200m). RMS decreased when compared to SeaBASS from 319% in R3 to 232% in R4 (untransformed data). The global mean over the SeaBASS points improved also, from 0.51 to 0.48 mg m^{-3} (SeaBASS was 0.46). The coastal regions unfortunately showed some deterioration. RMS increased from 291% in R3 to 316% in R4. R3 overestimated chlorophyll on the coasts. This trend is worse in R4.
- 4) Excessive numbers and magnitudes of high outliers were observed in the monthly R4 L3 data sets, especially occurring near the southern termination of data collection. It was most noticeable here but actually occurred elsewhere. This was causing global means and variances to be higher than R3. A new masking/filtering procedure was introduced by the project, and a May 1999 evaluation showed major improvement. Low and high outliers were brought into line, the global mean decreased by 10% and variance decreased significantly. Unfortunately this last fix to R4 did not correct some extreme outliers (factor of 10 or more larger than background). They are low in number but large in magnitude and their presence is worse than what was observed in R3. They are clearly visible as spikes in the imagery and most likely result from inadequate cloud masking. Cloud masking is not a science at this time. These results are being summarized for publication in a NASA Technical Memorandum. A similar analysis of MODIS Collection 4 data is forthcoming.

Table 7.1: Mission characteristics of proposed and present global ocean color sensors. For node , D indicates descending, A indicates ascending. Incl. Indicates inclination (degrees). ETC mean local equator crossing time on the node. GIFOV means ground instantaneous field of view at nadir.

Sensor	Launch	Spacecraft	Altitude	Incl.	ECT	Node	Swath	Tilt	GIFOV
SeaWiFS	1997	OrbView-2	705 km	98.2	noon	D	45°	+20°	1 km
MODIS-AM	1999	EOS-Terra	705 km	98.2	10:30 AM	D	55°	none	1 km
MERIS	2002	Envisat	780 km	98.5	10:00 AM	D	41o	none	1 km
GLI	2002	ADEOS-II	803 km	98.6	10:30 AM	D	45°	+20°	1 km
POLDER-II	2000	ADEOS-II	803 km	98.6	10:30 AM	D	51o	+20°	7 km
MODIS-PM	2002	EOS-Aqua	705 km	98.2	1:30 PM A	55°	none	1 km	
S-GLI	2003	ADEOS-III	803 km	98.6	10:30 AM	D	45°	+20°	1 km
VIIRS	2006	NPP	TBD	TBD	TBD	TBD	TBD	TBD	1 km
VIIRS	2009	NPOESS	TBD	TBD	TBD	TBD	TBD	TBD	1 km

ADEOS=Advanced Earth Observing Satellite EOS= Earth Observing System Envisat= Environmental Satellite
NPP= NPOESS Preparatory Project NPOESS= National Polar Orbiting operational Environmental Satellite System

REFERENCES

- Chen, C.-S. and D. P. Wang, 1999: Data assimilation study of the Santa Barbara channel circulation, *J. Geophys. Res.*, **104**, 15727-15741.
- Daley, R., 1999: Atmospheric data analysis, Cambridge Univ. Press, Cambridge, 457 pp.
- Doney, S.C., R.M. Najjar, and S.E. Stewart, 1995: Photochemistry, mixing, and diurnal cycles in the upper ocean, *J. Mar. Res.*, **53**, 341-369.
- Eppley, R.W., 1972: Temperature and phytoplankton growth in the sea, *Fish. Bull.*, **70**, 1063-1085.
- Oort, A.H., 1983: Global atmospheric circulation statistics, 1958-1973, *NOAA Prof. Paper 14*, 180 pp.
- Reynolds, R.W., 1988: A real-time global sea surface temperature analysis *J. Clim.*, **1**, 75-86.
- Reynolds, R.W. and T.M. Smith, 1994: Improved global sea surface temperature analyses using optimum interpolation, *J. Clim.*, **7**, 75-86.

Chapter 8

Bio-Optical and Remote Sensing Observations in Chesapeake Bay

Lawrence W. Harding Jr. and Andrea Magnuson

University of Maryland Center for Environmental Science, Cambridge, Maryland

8.1 INTRODUCTION

The SIMBIOS project supports our collection in-situ bio-optical measurements for validation of SeaWiFS observations and analysis of algorithm performance for the Case 2 waters of Chesapeake Bay. We have amassed a multi-year times series of observations resolving seasonal and inter-annual variability of bio-optical properties in the Bay. During this year of support, we have continued to provide in-situ data to SIMBIOS/SeaBASS on a regular basis, and have also focused on several other areas, including: (1) evaluation of potential uncertainties in our radiometric measurements; (2) evaluation of the performance of the Garver-Siegel (GSM01) semi-analytical model for the waters of Chesapeake Bay; (3) utilization of the information we have acquired on spatial and temporal variability of bio-optical properties in the Bay to customize a semi-analytical algorithm for the Chesapeake Bay region; (4) participation in an inter-laboratory comparison of high-performance liquid chromatography (HPLC) pigment analyses with the CHORS laboratory in San Diego, using split samples from several sources to elucidate some differences in chlorophyllous pigment concentrations.

8.2 RESEARCH ACTIVITIES

In the past year, we completed three cruises on Chesapeake Bay that continued a multi-year time series of bio-optical measurements on a seasonal (spring, summer and fall) basis. The cruises covered the main stem of the Bay over a period of 4-5 days, and collected radiometric, inherent optical property (IOP), pigment and physical data. Radiometric profiles were conducted at ~ 10 stations on each cruise. Measurements of downwelling irradiance (Ed) and upwelling radiance (Lu) were made with a MER-2040 with bands at 412, 443, 455, 490, 510, 535, 550, 560, 589, 625, 671, 683, 700 nm. Simultaneous measurements of surface irradiance (Es) were obtained with a MER-2041 deck cell at the same bands. Discrete surface samples were collected at each station to determine spectral absorption coefficients for dissolved and particulate (pigmented and non-pigmented) fractions, and for a suite of algal pigments analyzed by HPLC. Discrete samples were also collected ~ 50 stations on each cruise to determine chl-a concentrations fluorometrically.

We made some additions to our sampling protocol in 2002. Two new radiometric instruments were acquired that we now deploy on cruises, and one was provided by SIMBIOS for our use. These include a Satlantic MicroPro free-falling radiometer, a Satlantic Hyperspectral Tethered Spectral Radiometer Buoy, and a MicroTops Sun Photometer. The MicroPro measures Ed and Lu at 14 bands (400, 412, 443, 455, 490, 510, 535, 555, 565, 589, 625, 671, 683, and 700 nm). The MicroPro has a smaller diameter than the MER-2040 and is thereby less subject to instrument self-shading, and it is also small enough to be deployed from small boats. Radiometric profiles were made on each cruise with the MER-2040 (typically one cast) and the MicroPro (2 to 5 casts). All casts were completed within ~5 to 8 minutes, depending on the number of MicroPro casts that were made. The Hyper TSRB measures surface Ed and Lu with a 120-channel detector from 400 to 800 nm. We deployed the Hyper TSRB at each bio-optical station and ran it continuously during the radiometric profiles. The MicroTops was used to measure aerosol optical thickness on the cruises.

We have been participating in an inter-laboratory comparison of HPLC pigment determinations from Horn Point Laboratory's Analytical Services and CHORS in San Diego. The goal is to resolve differences in our respective recoveries of a couple of the chlorophyllous pigments. We met in summer at Goddard Space Flight Center and identified steps in this process, some of which have not been completed as of this writing. We plan a conference call for later in November to discuss progress on the comparisons. Both laboratories will participate in a broader inter-laboratory comparison that will begin in the near future.

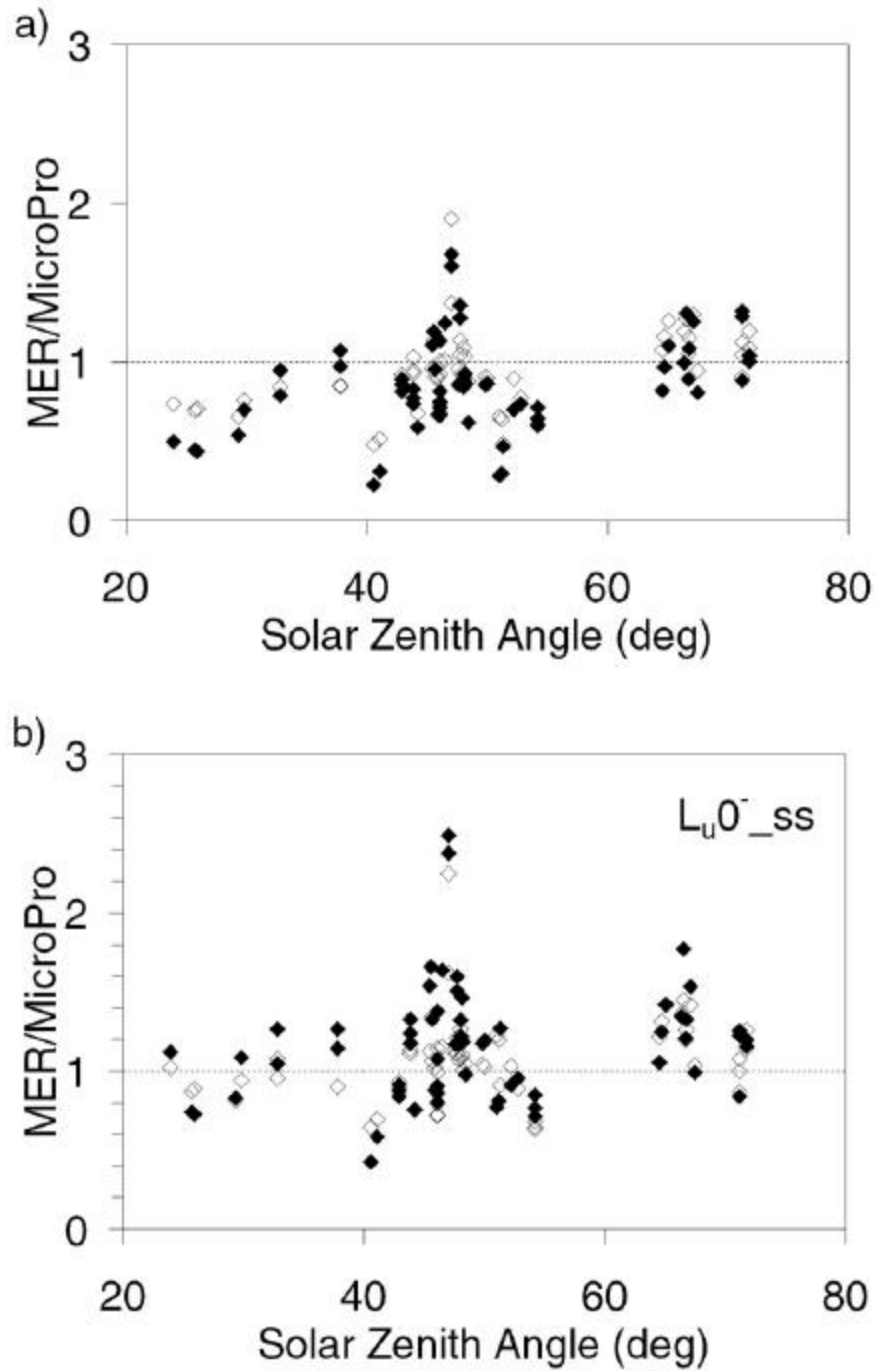


Figure 8.1: Comparison of $Lu0^-$ measurements from the MER-2040 and Satlantic MicroPro at 412 nm (filled diamonds) and 490 nm (open diamonds) before (a) and after (b) corrections for instrument self-shading. Data collected on three cruises in Chesapeake Bay in July 2001, October 2001, and April 2002.

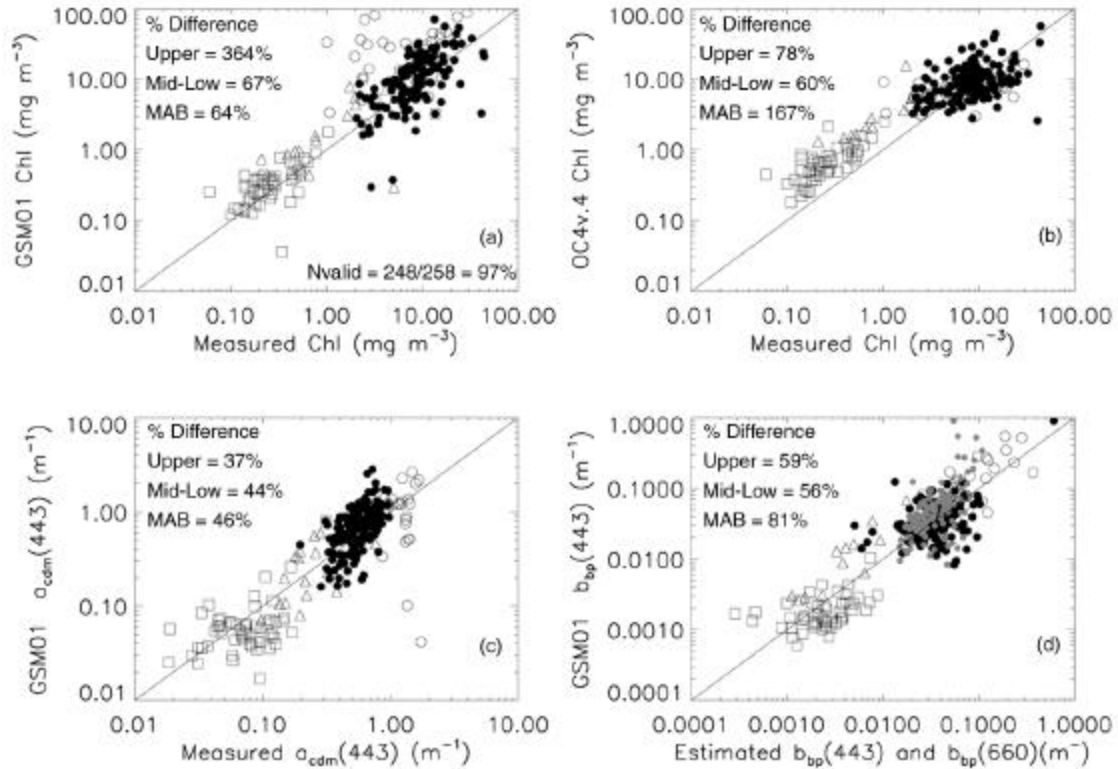


Figure 8.2: Results from the globally optimized GSM01 model using RRS data from the MER-2040 collected from Chesapeake Bay and adjacent MAB waters as inputs. (a) chl-a, (b) chl-a from OC4v.4, (c) aCDM443, (d) $b_{\text{bp}}443$. Each panel provides mean percent differences for modeled and measured values for each region. Regions are indicated by symbols: open circles represent upper Bay, filled circles represent mid- and lower Bay, open triangles represent inshore MAB and open squares represent offshore MAB. Grey circles in (d) represent alternate estimates of $b_{\text{bp}}(660)$ for the Bay calculated from measurements of beam attenuation. Panel (a) also provides the percentage of valid estimates returned by the GSM01 model.

8.3 RESEARCH RESULTS

Radiometric Comparisons

The stated goal of the SeaWiFS Project is to produce LWN with an uncertainty of 5% or less and chl-a to within 35% (Hooker and Esaias, 1993). It is essential to obtain accurate measurements of apparent optical properties to have a valid data set for “ground truth” and to develop algorithms that can be used with satellite-measured radiances. Estuarine and coastal waters such as Chesapeake Bay are commonly turbid with high diffuse attenuation coefficients for PAR (KPAR 0.3 - > 1.5 m^{-1}). This constrains the data that are available from in-situ radiometric profiles that are used to extrapolate to the surface and recover properties of interest, such as LWNs. Another consideration that is potentially important in estuarine and coastal waters is instrument self-shading that can be strongly expressed when attenuation and absorption coefficients are high (Gordon and Ding, 1992; Zibordi and Ferrari, 1995). On all cruises since July 2001, we have conducted radiometric profiles using both the MER-2040 and the MicroPro to compare the performance of the two instruments. The MicroPro has advantages over the MER-2040 for work in Case 2 waters due to its smaller diameter (MicroPro 4.8 cm relative to the MER-2040 21 cm) that reduces instrument self-shading, and higher sampling frequency that gives greater depth resolution in waters where KPAR is high and slight changes in depth of the sensor have a larger effect on the measurement.

We analyzed radiometric data from the two profiling instruments and identified advantages of the MicroPro in the turbid waters of Chesapeake Bay. Measurements of Ed_0^+ with the MER-2040 were often difficult to reconcile with Es. Larger

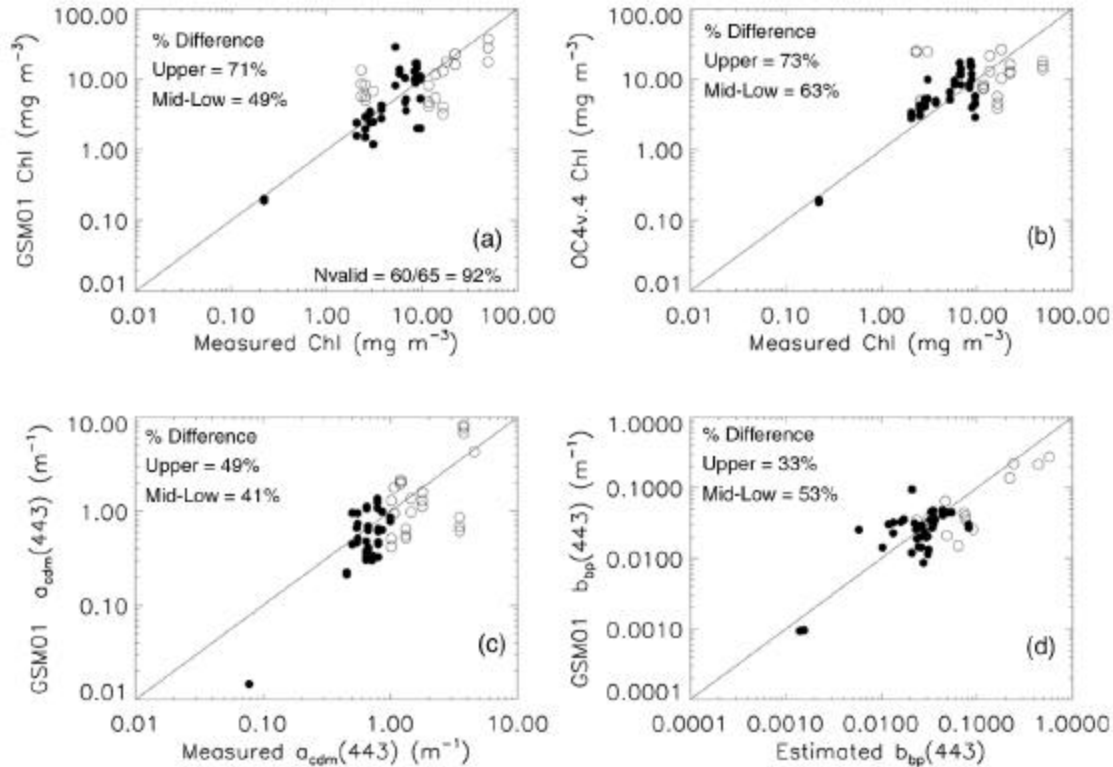


Figure 8.3: Results from the globally optimized GSM01 model using RRS data from the MicroPro collected from Chesapeake Bay as input. Each panel provides mean percent differences between modeled and measured values for each region. Regions are indicated by symbols: open circles represent upper Bay, filled circles represent mid- and lower Bay. Panel (a) also provides the percentage of valid estimates returned by the GSM01 model.

discrepancies occurred spectrally at blue wavelengths (Table 8.1), and regionally in the upper Bay, showing a strong correlation with water column absorption/attenuation. The bias of Ed_0+ for the MicroPro was much smaller in magnitude, positive, and also exhibited a spectral trend with higher values at wavelengths for waters of higher absorption/attenuation (Table 8.2). The improved depth resolution of the MicroPro (~25 measurements per meter) compared to the MER-2040 (~10 measurements per meter) partially compensated for the shallow optical depths in Chesapeake Bay, and likely accounted for the smaller RMS errors for radiometric data from the MicroPro. These results underscore the importance of making simultaneous measurements of E_s during in-water profiles if these measurements are to be used to calculate RRS or LWN for ocean color applications.

Comparisons of Lu_0^- measurements indicated that the MER-2040 often returned lower values than the MicroPro in conditions when instrument self-shading was expected to be high, including: (1) small solar zenith angles that cause instrument shadows to reach deeper in the water column and have a greater effect on measured Lu (Fig. 8.1); and (2) wavelengths with high attenuation/absorption (typically blue wavelengths in these waters) (Table 8.3). At small solar zenith angles, Lu_0^- from the MER-2040 were always less than Lu_0^- from the MicroPro, and application of the Gordon and Ding instrument self-shading correction improved the agreement between sensors. At larger solar zenith angles (40-60°), Lu_0^- from the MER-2040 often were lower than the Lu_0^- from the MicroPro, but occasionally values from the MER-2040 were higher. When the MER-2040 values were higher, the instrument self-shading correction increased the discrepancy between the two instruments. The increased discrepancies between radiometers after corrections for instrument self-shading may result from scattering in the waters column.

The Gordon and Ding model was developed primarily for Case 1 waters, and assumes that scattering is small relative to absorption ($b_T \ll a_T$). As scattering becomes increasingly important in the water column, it serves to fill in the region shadowed by the instrument and reduce the impact of instrument shading. Zibordi and Ferrari (1995) compared the theoretical predictions of instrument self-shading of the Gordon and Ding model to field measurements obtained in a lake under a range of environmental conditions, and found the model predictions of instrument self-shading exceeded experimental measurements at two stations with total suspended solid (TSS) concentrations of 3.2 and 3.5 mg l⁻¹. The reduction in instrument self-shading demonstrated by the field measurements, relative to model predictions, was attributed to scattering by particles. Typical TSS concentrations in the Bay range from ~2 to 15 mg l⁻¹, with high values of up to 50 mg l⁻¹. Therefore, particle scattering in Chesapeake Bay may be expected to result in reductions in instrument self-shading relative to model predictions. An evaluation of the magnitude of the reduction in instrument self-shading due to particle scattering would require a further study.

At very large solar zenith angles (> 60°), the Lu0⁻ values from the MER-2040 were always higher than those from the MicroPro. Shadows cast by the instrument at large solar zenith angles are relatively shallow and the in-water light field is more diffuse. Instrument self-shading would be minimized under these conditions, and the discrepancy between the two instruments at large solar zenith angles may indicate a difference in the collection optics of each instrument in highly diffuse light fields.

Lastly, we investigated the effects of small changes in the depth interval used for extrapolation to the surface on the calculated Kd, Ku, Ed0⁻ and Lu0⁻. In Chesapeake Bay, rapid attenuation of light with depth often limited the depth range over which to select the extrapolation interval to the upper four meters or less. We reprocessed radiometric profiles from two cruises in 2001 selecting a depth interval that was shifted down by 0.2 m, and calculated the differences between the derived products for both the MER-2040 and MicroPro (Table 8.4). We found that the change in depth intervals had a larger effect on data from the MER-2040 than on those from the MicroPro. The magnitude of the differences was greatest at low wavelengths (up to ~15%), while at the higher wavelengths the results were the same for both the MER-2040 and MicroPro. The change in depth interval affected Ed0⁻ and Lu0⁻ to a greater extent than Kd and Ku.

The comparisons discussed above summarize the results for the Bay as a whole, while recognizing that many of the potential errors increase as a function of water column absorption /attenuation. Therefore, uncertainties generally are greater in the upper Bay where absorption/attenuation is typically higher than in the lower Bay, and spectrally at low wavelengths where absorption due to dissolved and particulates materials is highest. Radiometric profiles with each instrument were conducted as close in time (within 5-8 minutes) and space (within ~ 50 feet) as possible in coordination with the other research objectives of the cruise, but did not represent a controlled experiment focused directly on comparisons of instrumentation performance. The importance of temporal and spatial variability on these scales is unknown. As mentioned in the previous section, we also deployed the Hyper-TSRB on our cruises. These data, when processed, will provide a third source of data with which to evaluate and verify radiometer performance, as well as examine temporal variability.

Algorithm Evaluation

Products from the Garver-Siegel-Maritorena model (GSM01) (Maritorena et al., 2002) are now available for SeaWiFS data. The GSM01 model can be expressed as:

$$L_{wN}(\lambda) = \frac{tF_0(\lambda)}{n_w^2} \sum_{i=1}^2 g_i \left(\frac{b_{bw}(\lambda) + b_{bp}}{b_{bw}(\lambda) + b_{bp} + a_w(\lambda) + a_{ph}(\lambda) + a_{cdm}(\lambda)} \right) \quad (1)$$

where t is the sea-air transmission factor, $F_0(\lambda)$ is the extraterrestrial solar irradiance, n_w is the index of refraction of water, and the g_i terms are modeled coefficients derived from Monte Carlo simulations describing the effects of sun elevation and atmospheric conditions on the upwelling light field. The absorption and backscattering terms are expressed as the linear sum of the absorption by seawater [$a_w(\lambda)$], phytoplankton [a_{ph}], combined [a_{CDM}], and particles [b_{bp}].

$$a_{ph}(\lambda) = chla_{ph}^*(\lambda) \quad (2)$$

$$a_{cdm}(\lambda) = a_{cdm}(\lambda_0) \exp[-S_{CDM}(\lambda - \lambda_0)] \quad (3)$$

$$b_{bp}(\lambda) = b_{bp}(\lambda_0) \quad (4)$$

where $a_{ph}^*(\lambda)$ is the chl-a specific absorption coefficient, S is the spectral slope for CDM absorption, ζ is the power law λ_0 is the wavelength of normalization. The GSM01 model parameters were selected using an optimization technique designed to provide the best performance in the global applications (Maritorena et al., 2002). We evaluated the performance of this model for the Case 2 waters of Chesapeake Bay.

We used in-situ RRS data from Chesapeake Bay and the adjacent waters of the middle Atlantic bight (MAB) as inputs to the GSM01 model that was provided to us in IDL code by Stephane Maritorena. The model was run with both MER-2040 and MicroPro data. The MER-2040 data were limited to stations at which measured $Ed_0^{+412}/Es_0^{412} > 0.5$. By using this criterion, the original *in-situ* data set was reduced from 358 to 256 observations. No stations were excluded from the MicroPro data set. All RRS data were corrected for instrument self-shading when solar zenith angles were $< 60^\circ$. IOP data were also examined in an attempt to customize the model for conditions encountered in Chesapeake Bay the MAB. Regional and seasonal mean values for the spectral shape parameters of the model (i.e., $a_{ph}^*(\lambda)$, S_{CDM}), and the initial guess values were selected based on evaluation of field data collected on cruises covering 1996-2001 (see Table 8.5 for spectral shape parameters). We assumed scattering in turbid waters of the Bay was relatively wavelength independent. The value of ζ was set at zero for the Bay and inshore MAB and one for the offshore MAB. Results from the globally optimized GSM01 model and the regionally tuned GSM01 model are shown in Figs. 8.2 and 8.3. Estimates from the GSM01 model are plotted against measured chl-a, measured $a_{CDM}(443)$ and estimates of $b_{bp}(443)$ derived from field measurements of diffuse attenuation and total absorption, according to the model of Kirk (1981, 1984, 1994). In addition, estimates of $b_p(660)$ were calculated from measurements of beam attenuation at 660 nm to provide an estimate of backscattering that was independent of our radiometric measurements. Literature values of backscattering ratios (b_b/b) were used to convert estimates of b_p to b_{bp} . We selected b_b/b values of 0.014, 0.010, 0.006 for the upper Bay, mid-and lower Bay, and MAB, respectively, in this work.

The comparisons showed that the performance of the model usually varied by region. Chl-a estimates from globally optimized GSM01 were superior to those from the operational SeaWiFS chl-a algorithm, OC4v.4 (Fig. 8.2). OC4v.4 chl-a exhibited a bias for MAB waters that was improved in the GSM01 chl-a estimates. Estimates of chl-a from GSM01 and OC4v.4 for the mid- and lower Bay were comparable. The greater dispersion of points in the upper Bay may be due to the greater uncertainties in the radiometric data collected in these very turbid waters. The GSM01 model utilizes all of the SeaWiFS wavebands, while estimates of chl-a from OC4v.4 in the Bay primarily use only the 510 and 555 nm wavebands. As discussed previously, the 490 and 555 nm wavebands had much lower uncertainties than did the 412, 443 and 671 nm wavebands. It is notable that the results for the MicroPro exhibited much less scatter in the upper Bay. Estimates of $a_{CDM}(443)$ showed fairly good agreement with in-situ values from the Bay, and increased scatter in the MAB. Estimates of $b_{bp}(443)$ also showed fairly good agreement. The most significant difference between the globally optimized GSM01 model and the regionally tuned version is that the globally optimized model returns a much higher percentage of valid estimates, despite the fact that the spectral shape parameters [a_{ph}^* , S_{CDM}]

model are significantly different from those that were found in the Bay/MAB waters. An estimate was considered valid if all products returned by the model (chl-a, $a_{CDM}443$ and $b_{bp}443$) were non-negative and with a reasonable range of values (chl-a - 0-100 $mg\ m^{-3}$; $a_{CDM}443$ - 0-10 m^{-1} ; $b_{bp}443$ - 0-1 m^{-1}). Clearly, the parameter optimization technique developed by Maritorena et al. (2001) greatly enhances the performance of the model. We continue to examine ways to improve the parameterization of the regionally tuned model, especially for parameters that are especially variable in time and space. In the case of Chesapeake Bay, the most variable parameter is a_{ph}^* , while in the MAB it appears to be S_{CDM} .

SeaWiFS Products

We are in the process of examining the effects that the 4th re-processing has on SeaWiFS products for Chesapeake Bay and the MAB. The quality of the SeaWiFS radiances will determine the performance of the GSM01 products. We are optimistic the current version of the model will provide valuable information on the spatial distribution and short-term variability of chl-a, a_{CDM} , and b_{bp} that are not resolved in our in-situ data.

8.4 FUTURE WORK

We have continued to improve our capabilities for collecting in-situ radiometric data with the addition of the Atlantic MicroPro and Hyper TSRB radiometers. Comparisons of data from the two profiling radiometers, the MER 2040 and the

MicroPro, have helped us quantify uncertainties in derived apparent optical properties. This type of information is important for evaluating the impact that these radiometric uncertainties have on algorithm performance. The initial performance of the GSM01 model in Chesapeake Bay is encouraging. Despite the global optimization of parameters, chl-a values from GSM01 were within ~ a factor of 2 of *in-situ* values, and a_{CDM443} values from GSM01 were within 50% of in-situ values, on average. b_{bp443} estimates from GSM01 were also reasonable, although the lack of b_{bp} measurements in the Bay limits the value of these comparisons. Our initial attempts to regionally tune the parameters of the GSM01 model for local conditions did not improve overall performance. However, we will continue our modeling efforts and to fill in gaps in our current in-situ data by obtaining b_{bp} data from Gallegos' group at the nearby Smithsonian Environmental Research Center with whom we are collaborating on optical measurements in the Bay and tributaries.

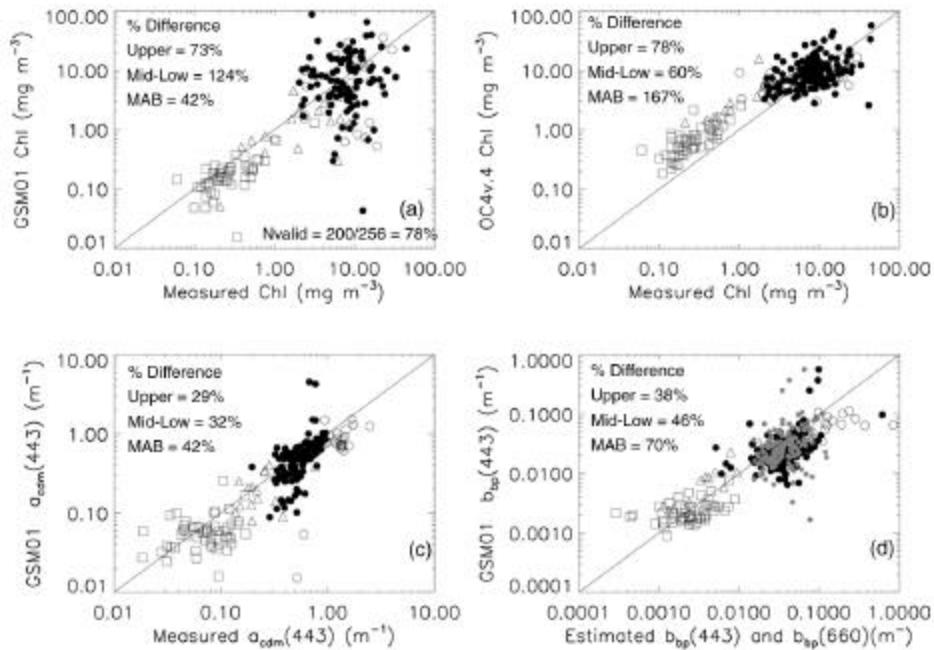


Figure 8.4: Results from the regionally tuned version of the GSM01 model using RRS data from the MER-2040 collected from Chesapeake Bay and adjacent MAB waters as input. See Fig. 2 legend for panel descriptions.

REFERENCES

- Gordon, H. R. and K. Ding, K. 1992: Self-shading of in-water optical instruments, *Limnol. Oceanogr.*, **37**, 491-500.
- Hooker, S. B. and Esaias, W. E. 1993: An overview of the SeaWiFS project, *Eos. Trans. AGU*, **74**, 241-246.
- Kirk, J. T. O. 1981: Monte Carlo study of the nature of the underwater light field in, and the relationships between optical properties of turbid yellow waters, *Aust. J. Mar. Freshwater Res.*, **32**, 517-532.
- Kirk, J. T. O. 1984: Dependence of relationship between inherent and apparent optical properties of water on solar altitude, *Limnol. Oceanogr.*, **29**(2), 350-356.
- Kirk, J. T. O. 1994: Characteristics of the light field in highly turbid waters: A Monte Carlo study, *Limnol. Oceanogr.*, **39** (3), 702-706.

Maritorena, S., Siegel, D.A., and Peterson, A.R. 2002: Optimization of a semianalytical ocean color model for global scale applications, *Appl. Opt.*, **41**(15), 2,705-2,714.

Zibordi, G. and Ferrari, G. M. 1995: Instrument self-shading in underwater optical measurements: Experimental data, *Appl. Opt.*, **34**, 2,750-2,754.

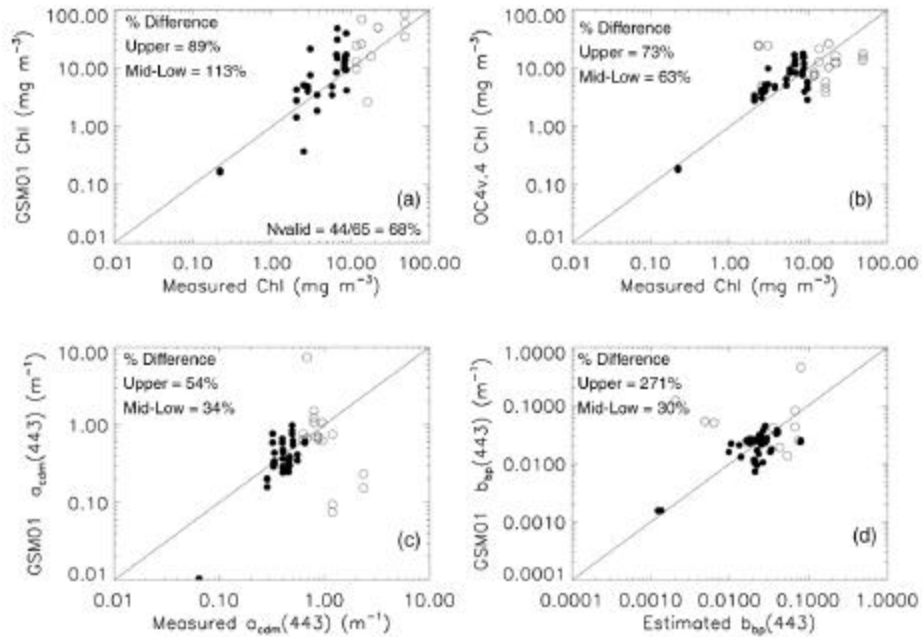


Figure 8.5: Results from the regionally tuned version of the GSM01 model using RRS data from the MicroPro collected from Chesapeake as input. See Fig. 3 legend for panel descriptions.

Table 8.1: Comparison of $E_d 0^+$ and E_s from the MER-2040 at selected wavebands. Data from cruises in July 2001, October 2001 and April 2002. n = 65.

Chesapeake Bay	412	443	490	555	671
MNB(%) [*]	-36.9	-30.4	-15.2	-3.9	-17.03
RMS(%) ^{**}	46.1	45.8	31.8	25.0	27.5
Slope	0.66	0.61	0.76	0.91	0.77
R ²	0.64	0.51	0.67	0.76	0.83

^{*}Mean normalized bias (MNB) = mean[($E_d 0^+$ - E_s)/ E_s] x 100

^{**}Normalized RMS error (RMS) = [(sum($E_d 0^+$ - E_s)²/(n-1))^{0.5}/(mean(E_s))x100

Table 8.2: Comparison of $E_d 0^+$ and E_s from the MicroPro at selected wavebands. Data from cruises in July 2001, October 2001 and April 2002. n = 65.

Chesapeake Bay	412	443	490	555	671
MNB(%) [*]	8.49	-1.1	-0.53	0.76	5.13
RMS(%) ^{**}	18.4	21.1	13.6	10.0	14.2
Slope	1.12	1.00	1.02	1.06	1.08
R ²	0.93	0.83	0.92	0.96	0.93

Table 8.3: Comparison of L_u0^+ and $L_u0^-_{ss}$ from the MER-2040 and MicroPro at selected wavebands. n = 65.

	412	443	490	555	671
L_u0^-					
MNB(%)*	-12.63	-4.75	-6.02	4.20	1.97
RMS(%)	32.20	25.08	25.70	29.22	24.97
Slope	0.88	0.89	0.83	0.85	0.80
R ²	0.94	0.93	0.89	0.79	0.75
$L_u0^-_{ss}$					
MNB(%)*	16.6	19.5	8.1	4.7	22.3
RMS(%)	33.9	30.8	26.2	31.6	45.8
Slope	0.94	0.98	0.90	0.90	0.99
R ²	0.90	0.90	0.88	0.78	0.77

*Mean normalized bias (MNB) = mean[(MER-MicroPro)/MicroPro] x 100

**Normalized rms error (RMS) = [(sum(MER-MicroPro)²/(n-1))^{0.5}/(mean(MicroPro))]x100

Table 8.4. Mean percent change in variables calculated from radiometric profiles using the MER-2040 (n = 19) and MicroPro (n = 44) when the depth interval used for extrapolation to the surface is shifted by 0.2 m. Profiles from Chesapeake Bay cruises in July and October 2001.

		412		443		490		555		671	
	Instrument	Mean	(SD)								
KE_d	MER-2040	4.82	(5.71)	5.05	(5.18)	2.28	(3.20)	2.13	(2.33)	2.89	(1.95)
	MicroPro	2.74	(2.85)	2.68	(2.67)	2.55	(3.32)	2.49	(2.85)	2.21	(2.31)
E_d0^-	MER-2040	14.6	(14.6)	13.1	(13.3)	5.93	(5.20)	2.29	(3.96)	7.32	(6.51)
	MicroPro	8.34	(7.30)	7.15	(6.04)	6.33	(4.96)	5.60	(3.37)	6.16	(4.45)
KL_u	MER-2040	3.24	(4.22)	3.17	(4.52)	2.13	(2.83)	1.74	(1.63)	2.28	(2.73)
	MicroPro	2.78	(3.03)	4.07	(4.10)	1.98	(1.53)	2.06	(2.00)	2.62	(3.36)
L_u0^-	MER-2040	10.4	(15.0)	9.67	(13.5)	5.04	(6.69)	2.84	(2.99)	4.35	(4.94)
	MicroPro	9.33	(9.95)	4.64	(5.90)	2.91	(2.39)	2.20	(2.06)	3.86	(4.68)

Table 8.5. Values for a_{ph}^* , S_{CDM} and ζ used in the globally optimized GSM01 and the regionally tuned version of GSM01 for Chesapeake Bay/MAB.

		a_{ph}^* 412	a_{ph}^* 443	a_{ph}^* 490	a_{ph}^* 510	a_{ph}^* 555	a_{ph}^* 671	S_{CDM}	ζ
GSM01		0.0066	0.05582	0.02055	0.01910	0.01015	.01424	.0206	1.0337
Chesapeake Bay/MAB									
Upper Bay	spring	0.05967	0.04817	0.02845	0.02278	0.01222	0.01985	.012	0
	summer	0.02486	0.02614	0.01429	0.01052	0.00424	0.01754	.012	0
	fall	0.04425	0.04090	0.02410	0.01944	0.00964	0.02023	.012	0
Mid-Bay	spring	0.01660	0.01801	0.01047	0.00800	0.00373	0.01262	.014	0
	summer	0.02846	0.03300	0.01960	0.01412	0.00522	0.01935	.014	0
	fall	0.02454	0.02705	0.01610	0.01276	0.00635	0.01815	.014	0
Inshore		0.06319	0.0763	0.05154	0.03489	0.01532	0.03273	.014	0
Offshore		0.09631	0.12476	0.08357	0.05141	0.01632	0.03696	.017	1

Chapter 9

Refinement of Protocols for Measuring the Apparent Optical Properties of Seawater

Stanford B. Hooker

NASA/GSFC Greenbelt, Maryland

Giuseppe Zibordi and Jean-François Berthon

JRC/IES/Inland and Marine Waters, Ispra, Italy

André Morel and David Antoine

CNRS/UPMC/Laboratoire d'Océanographie de Villefranche, Villefranche-sur-Mer, France

9.1 INTRODUCTION

Ocean color satellite missions, like the Sea-viewing Wide Field-of-view Sensor (SeaWiFS), the Moderate Resolution Imaging Spectroradiometer (MODIS), or the Medium Resolution Imaging Spectrometer (MERIS) projects, are tasked with acquiring a global ocean color data set, validating and monitoring the accuracy and quality of the data, processing the radiometric data into geophysical units using a set of atmospheric and bio-optical algorithms, and distributing the final products to the scientific community. The long-standing objective of the SeaWiFS Project, for example, is to produce water-leaving radiances to within 5% absolute (Hooker and Esaias 1993). The accurate determination of upper ocean apparent optical properties (AOPs) is essential for the vicarious calibration of ocean color data and the validation of the derived data products, because the sea-truth measurements are the reference data to which the satellite observations are compared (Hooker and McClain 2000).

Water-leaving radiances can be derived by extrapolating in-water measurements taken close to the sea surface, or they can be obtained directly from above-water measurements. Although it has not been as extensively validated as the in-water approach, above-water methods for vicarious calibration remain nevertheless attractive, because a) the data can presumably be collected more rapidly and from a ship underway, and b) the frequently turbid and strongly absorbing waters in shallow coastal (Case-2) environments impose severe limitations on in-water measurements, particularly because of the instrument self-shading effect. One of the difficulties with above-water measurements, however, is the instruments involved cannot be floated away to prevent any reflection or shading perturbations associated with the measurement platform, which is easily accomplished with an in-water system.

Another problem within the general perspective of ocean color calibration and validation activities is the paucity of data at high chlorophyll *a* concentrations, particularly in Case-1 waters—the peak in the distribution of the data being archived is in a chlorophyll *a* range of 0.1–1.0 mg m³ (O'Reilly et al. 2000), i.e., the so-called mesotrophic regime. This deficiency influences not only the higher order products, because the algorithms being used are not as robustly determined at high concentrations, but also much of the lower order understanding of uncertainty budgets, because the various experiments used to determine uncertainties also do not include high productivity waters.

Whether for biogeochemical studies or ocean color validation activities, high performance liquid chromatography (HPLC) is an established reference technique for the analysis of chlorophyll *a* and associated phytoplankton pigments. For example, the SeaWiFS Project requires agreement between the *in situ* and remotely sensed observations of chlorophyll *a* concentration to within 35% over the range of 0.05–50.0 mg m³ (Hooker and Esaias 1993). This value is based on inverting the optical measurements to derive pigment concentrations using a bio-optical algorithm, so the *in situ* pigment observations will always be one of two axes to derive or validate the pigment relationships. Given the already established emphasis on understanding the

uncertainties associated with the AOP measurements, it seems appropriate to also investigate the uncertainties in determining pigment concentrations using HPLC methods, so an understanding of the total uncertainty budget can be produced. The latter was the rationale behind the first SeaWiFS HPLC Analysis Round-Robin Experiment (SeaHARRE-1)

SeaHARRE-1 was based solely on natural samples with a range in chlorophyll *a* concentration of about 0.05–2.2 mg m⁻³ (Hooker et al. 2000a) and involved four international laboratories: the European Joint Research Centre (JRC), the American Horn Point Laboratory (HPL), the French *Laboratoire d'Océanographie de Villefranche* (LOV), and the South African Marine and Coastal Management (MCM). Despite the diversity in trophic conditions and HPLC methods, the agreement between the participating laboratories in SeaHARRE-1 was approximately 7.0% for total chlorophyll *a*, (Tchl_a), which is well within the accuracy objective for remote sensing validation purposes. For other pigments (mainly chemotaxonomic carotenoids), the agreement between methods was 21% on average (ranging from 11.5% for fucoxanthin to 32.5% for peridinin), and inversely depended on pigment concentration (with large disagreements for pigments close to the detection limits).

SeaHARRE-1 also showed that better agreement between methods can be achieved if some simple procedures are employed: a) disregarding results less than the effective limit of quantitation (an alternative to the method detection limit), b) standardizing the manner in which the concentration of pigment standards are determined, and c) accurately accounting for divinyl chlorophyll *a* when computing (Tchl_a) for those methods which do not chromatographically separate it from chlorophyll *a*. The use of these quality assurance procedures improved the agreement between methods, with average APD values dropping from 7.0% to 5.5% for (Tchl_a) and from 21.5% to 13.9% for the principal carotenoids (Claustre et al. 2002). Additionally, it was shown that subsequent grouping of individual pigment concentrations into sums and ratios significantly reduced the variance and, thus, improved the agreement between laboratories. This grouping, therefore, provides a simple mechanism for decreasing the variance within databases composed of merged data from different origins and future submissions to a database should include the relevant information related to the limit of detection for the HPLC method.

9.2 RESEARCH ACTIVITIES

The three primary research activities were to a) complete the field experiments to quantify the effect of platform perturbations on above-water measurements made in proximity of an oceanographic tower, b) organize and execute a field campaign to collect (in-water) calibration and validation optical data in the high productivity waters of the Benguela Current, and c) use the latter to collect field samples for a second SeaWiFS HPLC Analysis Round-Robin Experiment (SeaHARRE-2).

The tower perturbation experiments were a collaboration between the JRC and the SeaWiFS Project. In preparation for the first series of experiments, the JRC built and deployed an horizontal deployment system on the *Aqua Alta* Oceanographic Tower (AAOT). The deployment system was composed of a tubular box frame that was connected together with prefabricated sections. The box frame was approximately 25m long and could be extended 11m away from the tower and still remain rigid (at a 10m extension, the frame sagged approximately 1°). The SeaWiFS micro Surface Acquisition System (microSAS), a gimballed above-water instrument, was mounted at the end of the frame, and was positioned with respect to the sun before the frame was extended the desired distance away from the tower. The gimbal ensured the sensors achieved a horizontal reference (to within 0.5°) after the frame was positioned. The frame was moved in and out by hand, guided by rollers mounted within a series of square supports. The basic experimental plan for the first campaign in 2001 was to make a series of above-water measurements in 1m increments with respect to the tower (usually 10 incremental measurements were made), all the while maintaining the pointing requirements with respect to the solar plane (90° with respect to the sun). The latter ensured that a variety of viewing distances with respect to the tower base were collected. Although a large number of experiments were executed during the first campaign, they did not capture all the various geometrical viewing considerations, so the horizontal deployment system was left on the AAOT to allow for a second campaign in 2002.

The BENCAL cruise was organized and sponsored by five international partners: the South African MCM group with support from the University of Cape Town (UCT), the SeaWiFS Project, the British Plymouth Marine Laboratory (PML), LOV, and the European Space Agency (ESA). The primary objective of the cruise was to collect a high-quality optical data set, based on measurements of the inherent and apparent optical properties of seawater, in high productivity waters. The day-to-day sampling was scheduled to ensure a maximum amount of the observations could be used for calibration and validation (ground truth) activities. The sampling strategies employed involved a daily evaluation of three criteria: a) the overpass times for the remote sensors, b) the availability of clear-sky regions in the area of operations, and c) the need to adequately sample a large range in chlorophyll concentrations. The secondary objectives were to execute specialized optical experiments (discussed below) and to collect the field samples for SeaHARRE-2.

The planning for SeaHARRE-2 emphasized a) collecting field samples in a region of high productivity, so the dynamic range in chlorophyll *a* could be extended beyond the oligotrophic and mesotrophic regimes of the first round robin; b) adding a set of laboratory samples whose concentration and composition are known, so an absolute truth—and not just a consensus truth—can be used in the analysis of the results; c) including an intercomparison of the HPLC extracts using spectrophotometric techniques; and d) expanding the number of participants. The participating groups included three of the original institutes (HPL, LOV, and MCM) plus five new ones: the Canadian Bedford Institute of Oceanography (BIO), the Australian Commonwealth Scientific and Industrial Research Organization (CSIRO), the Danish DHI Water and Environment Institute, PML, and the Center for Hydro-Optics and Remote Sensing (CHORS). The addition of DHI and CHORS are particularly important, because much of the ocean color community relies on DHI for pigment standards, and CHORS is doing all of the HPLC analyses for the SIMBIOS program.

9.3 RESEARCH RESULTS

The second tower perturbation campaign took place from 18–28 June 2002 and 30 experiments were conducted (composed of 314 individual above-water measurement sequences). The difficulty with these types of experiments is the orientation of the tower and the horizontal deployment system with respect to the sun are fixed, so certain viewing geometries are only possible during certain parts of the day. Given the normal variance in environmental conditions (cloud coverage, sea state, water type, etc.), a large number of experimental opportunities (days in the field) are needed to collect a comprehensive (statistically robust) data set. A preliminary assessment of the data matrix showed the addition of the second campaign fills in almost all of the needed viewing geometries.

Although the 2002 field campaign provided the necessary data, there were repeated difficulties in collecting the data because of instrument performance problems. The most troubling problem was the microSAS solar irradiance and the sky- and sea-viewing radiance sensors would overheat and provide corrupted measurements when the wind speed dropped to zero during clear-sky conditions. The solution to this problem was to wrap the sensors with white cloth and to keep the cloths damp (Fig. 9.1). This was a time consuming and difficult requirement, because the water had to be added without wetting the sensor apertures (which would also have corrupted the measurements).

Table 9.1 presents a summary of the daily environmental parameters for the optical data collection during the BENCAL cruise. Also shown is the estimated chlorophyll *a* concentration, which was determined at sea following the spectrophotometric method of Jeffrey and Humphrey (1975). These near-real time results were used to verify the greatest range in chlorophyll concentration was sampled, and that the sampling was as evenly distributed as possible. The majority of the data were acquired in excellent conditions: wind speeds less than 10 m s⁻¹ (79%), wave heights less than 1 m (60%), and cloud coverage less than 3/8 (74%). Although environmental uncertainty is minimized in excellent conditions, there are other sources of uncertainty that need to be addressed. One of the most important of these is the stability of the light sensors. To make sure this uncertainty could be accurately determined, two or three in-water instruments were deployed simultaneously under a wide range of illumination conditions, solar zenith angles, and chlorophyll concentrations.

Table 9.1 also lists some of the specialized experiments that were executed during the BENCAL cruise: a) measurements of the *Q*-factor as the sun went down during clear-sky conditions, and b) intercomparisons of vertical profile measurements with a hyperspectral (surface) buoy. The respective purpose of these experiments was to compare theoretical and *in situ* values of the *Q*-factor as a function of a large change in the solar zenith angle, and to evaluate the capabilities of near-surface monitoring techniques in a variety of concentration regimes. The *Q*-factor investigation is a recurring objective of SeaWiFS Field Team deployments, and the inquiry into surface buoy methods and protocols is a recent addition to the generalized problem of coastal monitoring. The latter was first addressed with the joint production and testing of the SeaWiFS Photometer Revision for Incident Surface Measurements (SeaPRISM) with the JRC (Hooker et al. 2000b and Zibordi et al. 2002).

Before the BENCAL cruise, the liquid nitrogen dry shippers that would be used to transport the field samples from Cape Town to the participating laboratories, were filled with liquid nitrogen and then repeatedly refilled to make sure they were “charged” to the maximum. During this initial phase, one of the dewars was found to have an excessive evaporation rate and was eliminated as a possible shipping container. The remaining dewars were weighed and stored for the duration of the cruise. After the cruise, the dewars were weighed to determine their evaporation rates, and all were found to be within nominal storage capabilities. Unfortunately, and despite the careful planning, three of the dewars arrived at their final destinations completely defrosted, even though the total shipping time was much less than the anticipated usage time based on the measured evaporation rates.



Figure 9.1: Cooling down the microSAS radiometers during the 2002 campaign to investigate platform perturbations on above-water methods

An analysis of samples from two of the defrosted dewars showed the (Tchla) values were on average more than 15% lower than a set of duplicates from one of the dewars that arrived properly charged. This has potentially serious consequences as to how best to proceed with the original work plan, and this is being evaluated. A series of tests were also initiated with the shipping dewars to see if an explanation for the anomalously high evaporation rates could be found. The dewars were refilled, monitored, and found to have evaporation rates in keeping with the values measured in the field. The dewars were then refilled, turned upside down, and remonitored. In the upside down configuration, the two dewars that arrived defrosted were found to have significantly higher evaporation rates that could easily have caused defrosting if they had been stored inverted for a few days; the other dewars had higher evaporation rates, but they were not so high as to cause defrosting over the time period of the shipment.

9.3 FUTURE WORK

The emphasis for the coming year is a) completing the documentation (Doyle et al. 2002 and Zibordi et al. 2002) and analysis associated with the tower perturbation campaigns already conducted, b) analyzing the data acquired during the BENCAL cruise, c) completing and documenting the analyses for the SeaHARRE-2 activity, and d) initiating an inquiry into the uncertainties associated with plaque calibrations.

Table 9.1: BENCAL optics master log for FRS *Africana* (SDY 278 is 5 October 2002).

SDY	Sta.	Wind	Wave	Cloud	Tchla	Sky Conditions	Experiment	Notes
278	1		0.5	1	5.1	Clear with haze		
278	2		0.5	1	1.8	Clear with haze		
279	3	1.4	3.5	1	3.6	Clear with some haze		
279	4	9.7	3.5	0	2.3	Clear with some haze		
279	5	10.5	3.5	0	1.8	Clear with some haze		
280	6	3.1	0.5	0	8.1	Clear with some haze		
280	7	3.3	0.5	1	4.3	Clear with some haze		2 buoy experiments
280	8	3.5	1.0	0	5.0	Clear with some haze		
280	9	8.2	1.0	0		Clear with some haze		Q-factor experiment

281	10	3.3	0.5	0	6.2	Clear with some haze	
281	11	2.2	0.5	0	2.5	Clear with some haze	Buoy experiment
281	12	6.7	1.0	0	4.3	Clear with some haze	Buoy experiment
281	13	8.9	0.5	0		Clear with some haze	Q-factor experiment
282	14	10.1	2.0	8	4.4	Overcast	
282	15	10.8	2.0	4		Clear with some haze	
282	16	6.7	2.5	8	3.2	Overcast	Buoy experiment
283	18	5.0	0.5	2	22.0	Clear with some haze	Buoy experiment
283	19	4.8	1.0	1	9.5	Clear with some haze	Buoy experiment
283	20	5.2	0.5	2	22.8	Clear with some haze	Buoy experiment
283	21	3.6	0.5	1	0.2	Clear with some haze	Q-factor experiment
284	22	0.5	0.5	1		Clear with some haze	Buoy experiment
284	23	0.0	0.5	2		Clear with some haze	
284	24	1.0	0.5	7	0.4	Clear with some clouds	
285	25	3.9	0.5	4		Clear with some haze	
286	26	2.4	0.5	3	0.2	Clear with little haze	Buoy experiment
286	27	2.4	0.5	3	0.2	Clear with little haze	
287	28	6.5	0.5	3		Clear with some haze	
287	29	8.6	0.5	3	0.9	Clear with little haze	
287	30	13.2	2.0	2	0.9	Clear with little haze	
287	31	13.4	2.0	2	0.9	Clear with little haze	Q-factor experiment
288	32	4.6	0.5	0	2.9	Clear with little haze	
288	33	2.4	1.5	0	7.0	Clear with little haze	Buoy experiment
288	34	2.8	0.5	0	15.3	Clear with little haze	Buoy experiment
288	35	2.8	0.5	0		Clear with little haze	Q-factor experiment
289	36	2.8	0.5	2	10.6	Clear with little haze	
289	37	2.6	0.5	1	1.8	Clear with little haze	Buoy experiment
289	38	2.0	0.5	0		Clear with little haze	Buoy experiment
290	39	4.7	2.0	8	3.2	Overcast	Buoy experiment
290	40	5.1	0.5	4	3.2	Clear with little haze	
290	41	5.2	2.0	2	5.7	Clear with little haze	Buoy experiment
295	42		1.5	1		Clear with little haze	
295	43		1.5	2		Clear with little haze	

REFERENCES

- Claustre, H., S.B. Hooker, L. Van Heukelem, J-F. Berthon, R. Barlow, J. Ras, H. Sessions, C. Targa, C. Thomas, D. van der Linde, and J-C. Marty. 2002: An intercomparison of HPLC phytoplankton pigment methods using *in situ* samples: Application to remote sensing and database activities, *Marine Chem.*, (submitted).
- Doyle, J., G. Zibrodi, J-F. Berthon, D. van der Linde, and S.B. Hooker, 2002: Validation of an In-Water, Tower-Shading Correction Scheme, *NASA Tech. Memo. 2002-206892, Vol. 23*, S.B. Hooker and E.R. Firestone, Eds., NASA Goddard Space Flight Center, Greenbelt, Maryland, (in prep.).
- Hooker, S.B., and W.E. Esaias, 1993: An overview of the SeaWiFS project, *Eos, Trans. Amer. Geophys. Union*, **74**, 241-246.
- Hooker, S.B., and C.R. McClain, 2000: The calibration and validation of SeaWiFS data, *Prog. Oceanogr.*, **45**, 427-465.
- Hooker, S.B., H. Claustre, J. Ras, L. Van Heukelem, J-F. Berthon, C. Targa, D. van der Linde, R. Barlow, and H. Sessions, 2000a: The First SeaWiFS HPLC Analysis Round-Robin Experiment (SeaHARRE-1), *NASA Tech. Memo. 2000-206892, Vol. 14*, S.B. Hooker and E.R. Firestone, Eds., NASA Goddard Space Flight Center, Greenbelt, Maryland, 42pp.

- Hooker, S.B., G. Zibordi, J-F. Berthon, S.W. Bailey, and C.M. Pietras. 2000b. The SeaWiFS Photometer Revision for Incident Surface Measurement (SeaPRISM) Field Commissioning. *NASA Tech. Memo. 2000-206892, Vol. 13*, S.B. Hooker and E.R. Firestone, Eds., NASA Goddard Space Flight Center, Greenbelt, Maryland, 24pp.
- Hooker, S.B., G. Zibordi, J-F. Berthon, D. D'Alimonte, D. van der Linde, and J.W. Brown, 2002: Tower Perturbation Measurements in Above-Water Radiometry, *NASA Tech. Memo. 2002-206892, Vol. 22*, S.B. Hooker and E.R. Firestone, Eds., NASA Goddard Space Flight Center, Greenbelt, Maryland, (in prep.).
- Jeffrey, S.W., and G.F. Humphrey, 1975: New spectrophotometric equations for determining chlorophylls *a*, *b*, *c*₁, and *c*₂ in higher plants, algae and natural phytoplankton, *Biochem Physiol. Pflanzen*, **167**, 191–194.
- O'Reilly, J.E., and 24 Coauthors, 2000: SeaWiFS Postlaunch Calibration and Validation Analyses, Part 3, *NASA Tech. Memo. 2000-206892, Vol. 11*, S.B. Hooker and E.R. Firestone, Eds., NASA Goddard Space Flight Center, 49pp.
- Zibordi, G., S.B. Hooker, J-F. Berthon, and D. D'Alimonte, 2002: Autonomous above-water radiance measurements from an offshore platform: A field assessment experiment, *J. Atmos. Ocean. Tech.*, **19**, 808–819.

Chapter 10

Optimization Of Ocean Color Algorithms: Application To Satellite And In Situ Data Merging.

Stéphane Maritorena and David A. Siegel

Institute for Computational Earth System Science, UCSB, Santa Barbara, CA 93106-3060, USA

André Morel

Laboratoire de Physique et Chimie Marines, Villefranche Sur Mer, France

10.1 INTRODUCTION

Since the launch of MODIS-Terra and over the next decade, several global ocean color missions will be operational simultaneously and great potential benefits are expected from the unification of these ocean color data sets. Beside improved spatial and temporal coverage of the global ocean (Gregg et al., 1998; Gregg and Woodward, 1998) ocean color data merging should also result in new, more diverse and better data products with lower uncertainties. The development of a unified ocean color time series and a better temporal coverage of ocean processes are other major aspects of such a merging activity. The NASA SIMBIOS program supports the development of methodologies for ocean color data merging. Our SIMBIOS contribution aims at developing an ocean color data merging procedure that works at the level of normalized water-leaving radiances (L_{wN}). Our SIMBIOS effort has three major components: 1) the assemblage of a large, global *in situ* data set for algorithm development, 2) the development of our semi-analytical ocean color model for data merging and, 3) the use of the model for the merging of ocean color data.

10.2 RESEARCH ACTIVITIES AND RESULTS

Inherent And Apparent In Situ Optical Properties Data Set

Although the current version of our merging model performs well (Maritorena et al., 2002a), we are working on improving its overall performance and design. To that end, we are assembling a comprehensive *in situ* ocean color data set that contains inherent (IOP) and apparent (AOP) optical properties required for ocean color semi-analytical algorithm development and testing. Most of the data included in the data set come from the NASA SIMBIOS SeaBASS archive but several investigators have provided data sets or subsets directly to us. Various quality control (QC) procedures have been developed (Fargion & McClain, 2002) and several analyses have been conducted on the data. In particular, the component absorption has been studied using the data collected in the AOP/IOP data set and this study shows that the absorption of the soluble fraction of seawater is a major contributor to the absorption budget over most of the chlorophyll a (Chl) range of oceanic waters. Backscattering data are sparse and show important dispersion. The status of the IOP/AOP data set is described in Table 10.1.

Algorithm Development

We are developing a semi-analytical model, called GSM, (Maritorena et al., 2002a) for ocean color data merging that mingles the normalized water-leaving radiances and retrieves several biogeochemical variables simultaneously (namely the chlorophyll concentration, the combined dissolved and detrital absorption coefficient at 443 nm, $a_{dm}(443)$, and the particulate backscattering at 443 nm, $b_{p}(443)$). This approach has the advantage of using a consistent algorithm to generate the several data products simultaneously and the model can handle single or multiple data sources with similar or different bands. The model is also designed to deal with the uncertainties associated with each source of input data and to allow the calculation of uncertainty estimates of the retrieved products. We are working on a “spectrally independent” (or “bandless”) version of the

model that would allow the model to work with data sources having virtually any kind of bands (the current version of the model has some spectral constraints). We are also working on some alternative parameterizations for several components of the model. A preliminary version of the bandless model has been developed and it shows good results for the 3 retrieved variables and clear improvement in the $a_{dm}(443)$ and $b_{p}(443)$ retrievals. However, in some extreme conditions (either in very clear or very rich waters) the accuracy of some of the retrievals is not always good. Additional modifications of our model are currently underway which should result in a fully operational version of the “bandless” model.

Satellite Ocean Color Data Merging

We have successfully tested (Maritorena et al., 2002b) our merging approach with SeaWiFS (reprocessing #4, 9 km) and MODIS (collection #4, 4.5 km) daily level-3 data for 6 different dates. Only MODIS “good” data (i.e. quality 0) were used during these tests. These preliminary results show very good consistency in all data products generated by the merging model with no apparent discontinuities when the model switches from an area with a single data source to an area where SeaWiFS and MODIS $L_{wN}(\lambda)$ data are both used. The merged products also show reduced uncertainties compared to those generated from a single data source. Various analyses including the comparison of operational products of each individual satellite and of our merged products are currently under way. These analyses can be seen at: http://www.icess.ucsb.edu/~dcourt/request_gsm_results.html

GSM-01 Chlorophyll Results (2000339)

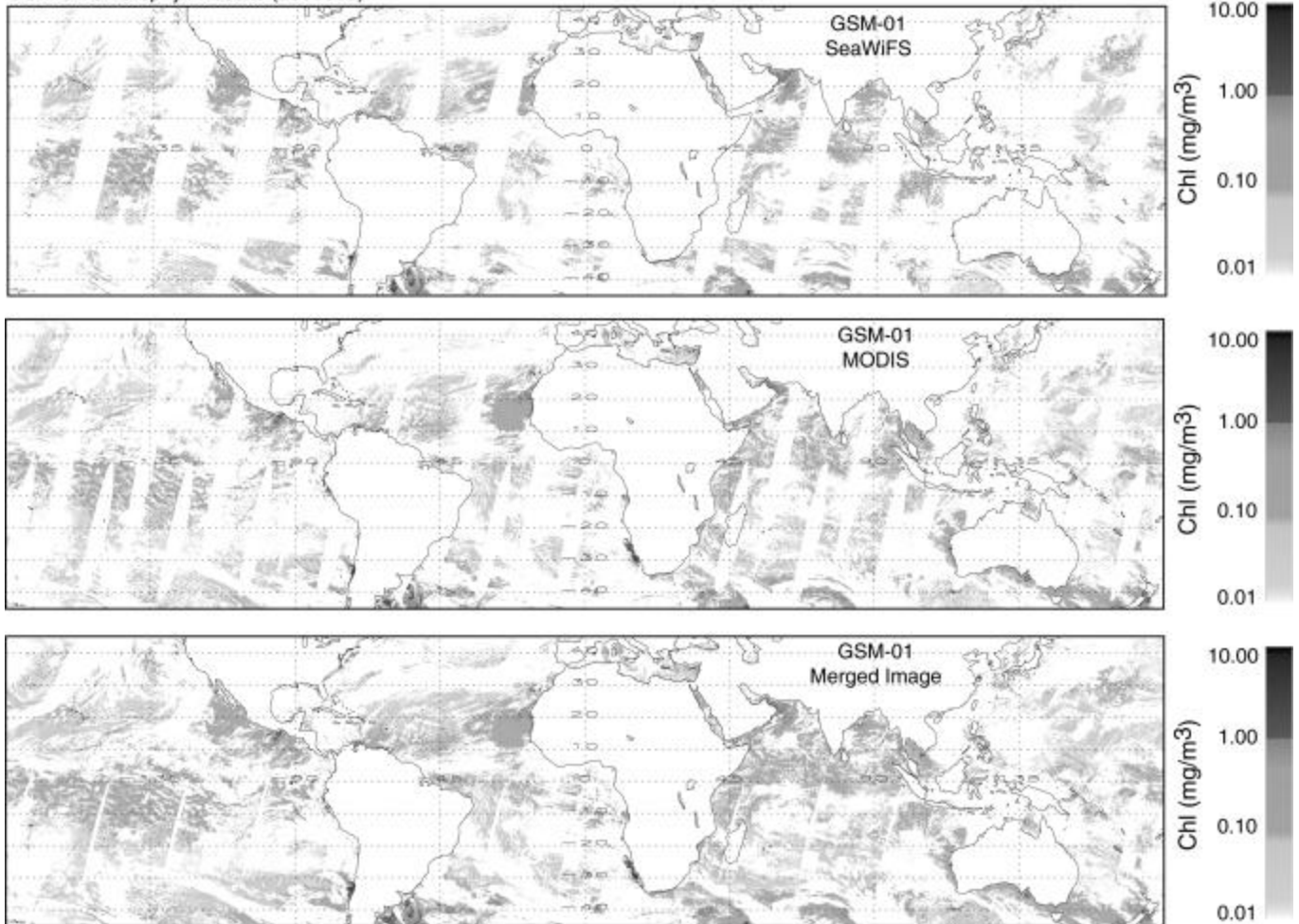


Figure 10.1: Global daily (December 4, 2000) chlorophyll maps using the GSM01 model with SeaWiFS data alone (upper panel), MODIS data alone (mid panel, quality 0 data) and with the merged $L_{wN}(\lambda)$ data (lower panel).

Global daily chlorophyll maps using the GSM model with SeaWiFS data alone, MODIS data alone and with the merged L_{wN} s are presented in figure 10.1. At this point, the ability of our merging model to use L_{wN} data weighed by their uncertainty level has not been used mostly because the uncertainties associated with the MODIS bands cannot be assessed yet. This requires matchup analyses from a large and diverse set of *in situ* and satellite data. These analyses are available for SeaWiFS but more matchup points are needed to complete the analysis for the MODIS data. Some regional data merging tests were also conducted using SeaWiFS and MOS data. These results were presented on January 2002 at the SIMBIOS Science Team Meeting in Baltimore.

10.3 FUTURE WORK

We will continue to develop, QC and perform analyses on the AOP/IOP data set. Provided that the AOP/IOP data set contains complete sets of data from a variety of different oceanic regimes, we will test the data for regional differences and analyze the possible differences in terms of algorithms parameterization and performance.

The bandless version of the merging model will be finalized and tested with both *in situ* and satellite data. More data merging and refined analyses on the merged products will be conducted and we will work on implementing a BRDF correction scheme. Should the matchup data set for MODIS continue to grow, we will test and analyze the $L_{wN}(\lambda)$ uncertainty weighting feature of our merging model.

Table 10.1: Status of the AOP/IOP data set. The first number in each cell indicates the number of stations for which data are available. The numbers in parentheses indicate the number of available wavelengths. na indicates missing data or data that are not yet included in the data set.

EXPERIMENT	Chl	K_d	L_{wN}	b_b	a_d	a_g	a_p
Aerosols Indoex	53	35 (12)	35 (6)	na	53 (225)	49 (200)	53 (225)
Ace-Asia	116	43 (18)	40 (18)	38 (6)	48 (225)	50 (200)	48 (225)
AMLR	60	62 (18)	62 (18)	na	58 (225)	50 (200)	58 (225)
Bermuda Bio-Optics Project	147	226 (16)	240 (12)	na	77 (520)	77 (520)	77 (520)
BIOCOMPLEXITY	20	na	24 (13)	na	11 (500)	11 (315)	11 (500)
CALCOFI	430	232 (12)	115 (12)	na	159 (225)	130 (200)	143 (225)
ECOFRONT	16	30 (6)	38 (7)	na	16 (225)	16 (200)	16 (225)
Ecology of Harmful Algal Blooms	422	na	303 (6)	na	422 (200)	398 (200)	422 (200)
Globec Biomapper	45	na		na	43 (200)	43 (200)	43 (200)
GOCAL	NA	na	29 (5)	28 (6)	na	na	na
Gulf of Maine	148	na	8 (6)	na	150 (200)	137 (200)	150 (200)
JGOFS	56	65 (12)	62 (12)	na	23 (225)	23 (225)	23 (225)
LAB96/97/2000	125	na	113 (12)	na	122 (500)	74 (500)	122 (500)
LMER-TIES	86	na	52 (7)	na	85 (250)	85 (200)	85 (250)
Ocean Research Consortium	17	na	18 (10)	14 (6)	16 (470)	16 (470)	16 (470)
Plumes and Blooms	492	369 (7)	362 (9)	196 (7)	369 (13)	309 (13)	306 (13)
Sea of Japan	42	37 (12)	37 (6)	32 (6)	32 (225)	32 (200)	32 (225)
Scotia Prince Ferry	3606	na	1380 (6)	3377 (3)	na	na	na
Tongue of the Ocean	77	na	167 (6)	16 (6)	95 (200)	95 (225)	95 (200)
Total	5958	1099	3085	3701	1779	1595	1700

REFERENCE

- Fargion G.S. and C.R. McClain. 2002: SIMBIOS Project 2001 Annual Report, *NASA TM-2002-21005*, NASA GSFC, 184pp.
- Gregg, W.W., W.E. Esaias, G.C. Feldman, R. Frouin, S.B. Hooker, C.R. McClain and, R.H. Woodward. 1998: Coverage opportunities for global ocean color in a multimission era, *IEEE Transactions On Geoscience And Remote Sensing*, **36**, 1620-1627.
- Gregg, W.W. and R.H. Woodward. 1998: Improvements in coverage frequency of ocean color: Combining data from SeaWiFS and MODIS, *IEEE Transactions On Geoscience And Remote Sensing*, **36**, 1350-1353.
- Maritorena S., D. A. Siegel and A. Peterson. 2002a: Optimization of a Semi-Analytical Ocean Color Model for Global Scale Applications, *Applied Optics*, **41**(15): 2705-2714.
- Maritorena S., D.A. Siegel, and D.B. Court. 2002b: Ocean Color Data Merging Using A Semi-Analytical Model, *Ocean Optics XVI*, Santa Fe.

Chapter 11

The Marine Fast-Rotating Shadow-band Network: Status Report and Analysis

Mark A. Miller, R.M Reynolds, and M.J. Bartholomew

The Brookhaven National Laboratory, Earth Systems Science Division, New York

11.1 INTRODUCTION

A network of ship-mounted marine shadow-band radiometers (FRSRs) and broadband radiometers have been deployed over the past four years on several backbone ships, along with periodic ships of opportunity, as part of the atmospheric correction exercises conducted by SIMBIOS (Reynolds et al., 2002). These radiometers operate continuously and automatically during daylight hours. This report provides a summary of the current status of the network, an analysis of a large amount of data that has been collected, and a summary of “lessons learned” during the four year period of operation.

There fundamental measurements made by the FRSRs in the network are the direct-normal irradiance and diffuse irradiance in six 10-nm wide channels that span the visible and near-infrared wavelengths (440 nm, 500 nm, 610 nm, 660 nm, 870 nm, and 936 nm) and a broadband channel. These measurements are complemented by broadband solar and infrared irradiance using standard Eppley pyranometers and pyrgeometers. A key enabling technology is the ability to compensate for ship motion without using a stabilized platform. This is accomplished by monitoring the platform motion and heading using advanced sensors, carefully understanding all aspects of the radiometer calibration, particularly the directional characteristics, and applying an appropriate averaging window (two minutes) to the four-second samples. Using this information, software compensation for ship motion can be made.

To date, there are over 100 independent cruises in the FRSR database, ranging in duration from a week to over four months. Data have been collected from all three oceans, as well as during important field campaigns such as Aerosols99, INDOEX, Nauru99, ACE-Asia, and the Northeast Aerosol Characterization Experiment (Voss et al. 2001; Quinn et al., 2001). The database consists of over 120,000 individual measurements of the radiation budget over the world’s oceans, including approximately 40,000 measurements of aerosol optical thickness in clear and partly cloudy skies. An important and, currently, untapped resource within the database are measurements of the impacts of clouds on the surface radiation budget in many different marine cloud systems.

11.2 RESEARCH ACTIVITIES

Four years of operation have enabled us to develop a mature system. We have advanced our understanding of the caveats of the FRSR technique at sea, as well as the intricacies of maintaining a well-calibrated system.

Over the past two years we performed a thorough uncertainty analysis on the FRSR and understand the uncertainty in the measurements quite well (Miller et al., 2002; Porter et al., 2001). We were able to demonstrate analytically and through Monte-Carlo simulations that the uncertainty in the individual measurements depended strongly on the accuracy of the sensors used to characterize ship motion. The current motion sensors allow us to achieve an accuracy of approximately 0.03 when measuring the aerosol optical thickness, and more accurate motion sensors are now becoming affordable, which may improve this uncertainty in future versions of the instrument. We demonstrated that the Langley technique could not be used to calibrate the FRSR at sea because the uncertainty introduced by imperfect information about radiometer position offset the “lever arm” effect, which improves estimates of aerosol optical thickness at high solar zenith angle. Thus, it is necessary to calibrate FRSRs on land.

Because the spectral head used on the FRSR has a diffuser that is composed of Spectralon, which is a semi-porous material, it is subject to changing characteristics when continuously exposed to the elements. Its Lambertian response and absorption can drift with time. In addition, the interference filters that lie in front of the optical detectors have a long history of

drift for various reasons. Therefore, it was necessary to develop a technique to track calibration drift through the duration of a cruise. Because broadband Eppley pyranometers are less subject to drift because they don't use interference filters or a diffuser material, they can be used as a baseline for tracking drift in the FRSR head assembly. We can track the drift in individual channels by first comparing the Eppley broadband signal with the broadband signal from the FRSR, and subsequently, comparing the scaled signals from the narrow-band channels with the Eppley broadband signal. These comparisons are performed at noon during the brightest (clearest) days in the cruise time series. They provide a time series of the calibration drift of the FRSR from which a correction coefficient can be obtained and applied to the FRSR time series, thereby bringing it back into calibration. We have discovered that the radiometers drift differently and some don't drift at all. The network radiometer that drifts the least is the one mounted on the Explorer of the Seas, a large cruise ship constantly traversing the Caribbean.

Another operating caveat was uncovered during the ACE-Asia experiment through comparison of FRSR data with Microtops, SIMBAD, and SIMBAD-A data. We discovered that the algorithm used on the FRSR did not appear to work properly when the aerosol optical thickness exceeded unity, a characteristic found in highly polluted air masses. Detailed analysis of these data revealed that the FRSR algorithm's chosen values of the edge and shadow irradiances were inappropriate in these conditions due to enlargement of the solar aureole. The land-based shadow-band community, when observing ultra-thin cirrus, has noted similar discrepancies when comparing with observations collected with collimated sun photometers. As a consequence, we developed a new algorithm that compensates for this effect. This new algorithm is applicable to both land-based and marine shadow-band radiometers, so it represents an advance in the field as a whole.

11.3 RESEARCH RESULTS

One key element of checking current atmospheric correction algorithms and devising new ones is to understand the relationship between the aerosol optical thickness in the near IR and the Angstrom exponent, which relates this single measurements to the aerosol optical properties in the visible wavelengths. It is, therefore, of fundamental importance to define the actual phase space that relates these two fundamental measures of aerosol radiative characteristics, as opposed to the phase space used in current models. A composite of this phase space constructed from a subset of the total FRSR database is shown in Figure 11.1. The figure shows data from Aerosols99, INDOEX, ACE-Asia, Nauru99, and several other high-profile experiments. This mix of data provides a relatively comprehensive assay of marine aerosol conditions across the planet. The plot shows a clear disposition for the upper and lower bounds of the Angstrom Exponent to asymptotically approach a value just above zero as the aerosol optical thickness at 870 nm increases. Further, the upper bound suggests an increasing contribution in the near IR when the atmosphere becomes increasingly polluted, perhaps through absorption in the near IR. The lower boundary shows an increasing trend away from negative Angstrom Exponent as the atmosphere becomes increasingly polluted. The reasons for this characteristic are not well understood. The behavior of the lower bound is less smooth than its upper counterpart, perhaps suggesting that local processes play a more important role. Few negative Angstrom Exponents are observed when the aerosol optical thickness in the near IR is greater than 0.1. Clearly, the observed negative Angstrom Exponents are associated with relatively clean air masses. In addition, recent analyses suggest a link between the negative Angstrom Exponents and precipitation in the area, but more work is required to understand the physics involved. This suggestion is tractable because relatively large amounts of liquid and/or ice in an otherwise clear atmosphere may provide differential absorption across the spectrum, with almost no absorption in the blue-green part of the spectrum and relatively large absorption in the near IR. It should be reinforced that relatively large amounts of liquid or ice must be available in comparison to the amount of liquid present on the surface of activated aerosols. Moreover, scattering physics suggests that the particles containing this liquid and/or ice must be large so as to have a minor impact on scattering in the visible, but a major impact on absorption in the near IR.

Another interesting characteristic of this phase-space analysis is the predisposition of the Angstrom Exponent to approach zero as the aerosol optical thickness in the near IR increases. This suggests that as the marine boundary layer becomes increasingly polluted that it begins to replicate the behavior of a cloudy atmosphere. Clouds provide a multiple scattering environment, thereby removing the spectral response in the visible and near IR typically observed in a single scattering situation. Such a situation is likely to present an untenable situation for ocean color retrievals, which rely on spectral fidelity for determination of water-leaving radiance. Another interesting characteristic of the parallel between clouds and these highly polluted marine boundary layers is the increasing IR emission by the aerosol particles. In the tropics, this may not represent a major factor in the IR budget because the atmosphere contains a large quantity of water vapor, thereby blocking the IR

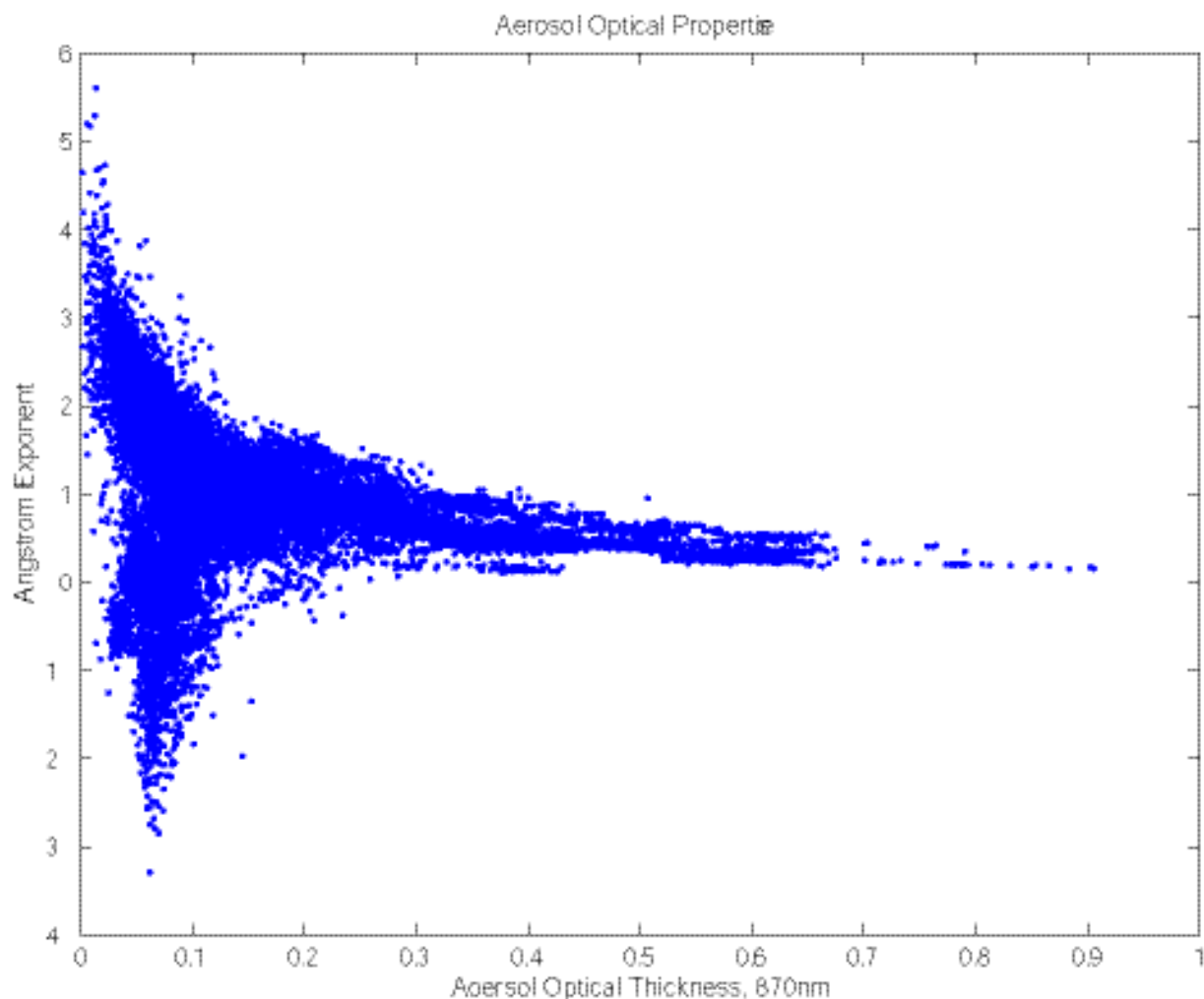


Figure 11.1: Composite plot of FRSR-measured aerosol optical thickness at 870 nm versus Angstrom Exponent (line fit across all wavelengths) at from several cruises, including ACE-Asia, INDOEX, Aerosols99, Nauru99, PolarStar, Ioffe, and Ewing. The uncertainty in each plotted data point is 0.03 and there are 36,000 individual measurements plotted. Data from all three oceans are included.

window. Potential IR impacts of these highly polluted marine boundary layers may be more important in the mid-latitudes and the arctic. Shadow-band radiometers provide a unique capability for testing the aerosol models used in atmospheric correction schemes. The aerosol models can be introduced into a radiation transfer model and the diffuse and direct-normal radiation components computed. These calculations can be compared with the FRSR-measured diffuse and direct components in a given situation. If the calculations for a particular model agree with the observations, it can be assumed that the aerosol model being tested faithfully represents the aerosol radiation transfer characteristics that existed at the time of the FRSR observations. This technique provides a clear pathway for determining whether the correct aerosol model has been chosen in a given circumstance. We collaborated with Menghua Wang, another SIMBIOS PI, to test the viability of this technique. Some preliminary results for the ACE-Asia Experiment are shown in Figure 11.2. Several different aerosol models were tested for 7 April 2001 by computing the difference between the modeled and measured diffuse irradiances. When the difference is zero, the aerosol model is faithfully representing the aerosol conditions that were present. As the figure shows, excellent agreement between the measured and modeled data are found for the urban aerosol model with 90% relative humidity. This is a powerful validation technique that can be used to determine if the aerosol model being used in the atmospheric correction scheme is appropriate for the circumstances. Unlike a simple measure of aerosol optical thickness, this technique is able to identify the specific model that was most correct in the observed circumstances.

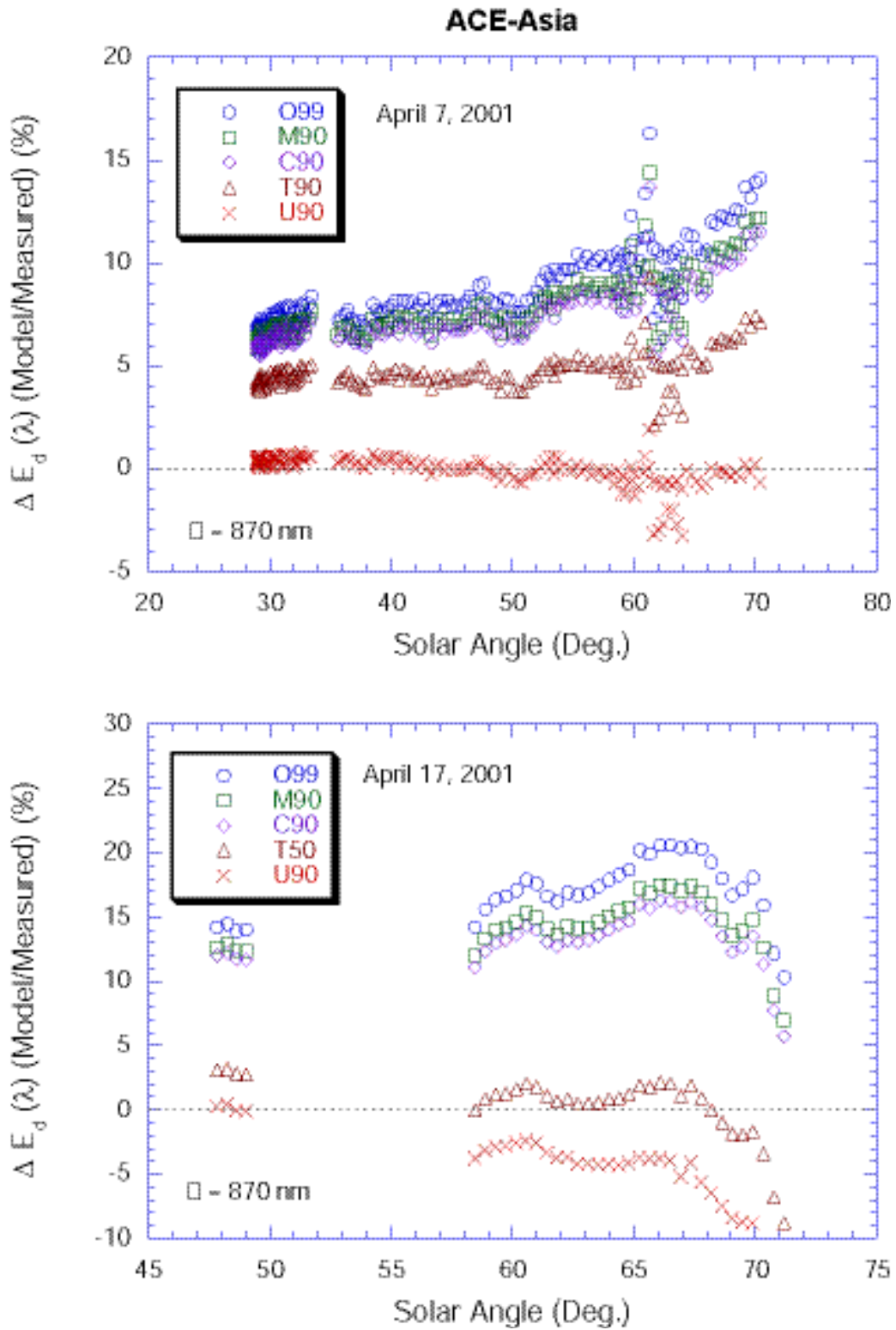


Figure 11.2: The ratio between the modeled and FRSR-measured diffuse irradiance for five different aerosol models. Proximity to unity represents the relative agreement.

REFERENCES

- Miller, M.A., M.J. Bartholomew, and R.M. Reynolds, 2002: The accuracy of marine shadow-band measurements of aerosol optical thickness and Angstrom exponent, *J. Atmos. Ocean. Tech.* (accepted).
- Porter, J.N., M.A. Miller, C. Motell, and C. Pietras, 2001: Use of hand-held sun photometers for measurements of aerosol optical thickness at sea, *J. Atmos. Ocean. Tech.*, Vol. **18**, 765-774.
- P.K. Quinn, D.J. Coffman, T.S. Bates, T.L. Miller, J.E. Johnson, E.J. Welton, C. Neusüss, M.A. Miller, and P. Sheridan: Aerosol Optical Properties during INDOEX 1999, 2001: Means, Variability, and Controlling Factors, *J. Geophys. Research*, (in press).
- Reynolds, M.R., M.A. Miller, and M.J. Bartholomew, 2001: A fast-rotating, spectral shadowband radiometer for marine applications, *J. Atmos. Ocean. Tech.*, Vol. **18**, No. 2, pp. 200–214.
- Voss, K.J., E.J. Welton, P.K. Quinn, R. Frouin, M.A. Miller, and R.M. Reynolds, 2001: Aerosol optical depth measurements during the Aerosols99 experiment, *J. Geophys. Research*, **106**, 20811-20820.

Chapter 12

Bio-Optical Measurement and Modeling of the California Current and Southern Oceans

B. Greg Mitchell

Scripps Institution of Oceanography, University of California San Diego, La Jolla, California

12.1 INTRODUCTION

This SIMBIOS project contract has supported *in situ* ocean optical observations in the California Current, and in the north Pacific, Southern and Indian Oceans. Our principal goals are to validate standard or experimental ocean color products through detailed bio-optical and biogeochemical measurements, and to combine ocean optical observations with modeling to contribute to satellite vicarious radiometric calibration and algorithm development. In collaboration with major oceanographic ship-based observation programs (CalCOFI, JGOFS, AMLR, INDOEX, and ACE Asia) our SIMBIOS effort has resulted in data from diverse bio-optical provinces. For these global deployments we generate a methodologically consistent data set encompassing a wide-range of oceanic conditions. We have initiated several collaborations with scientists in East Asian countries to study the complex Case-2 waters of their marginal seas. Global data collected in recent years are routinely evaluated relative to our CalCOFI time-series. The combined database we have assembled now comprises more than 1000 stations and includes observations for the clearest oligotrophic waters, highly eutrophic blooms, red-tides and coastal Case-2 conditions. The data has been used to validate water-leaving radiance estimated with SeaWiFS as well as bio-optical algorithms for chlorophyll pigments. The comprehensive data is utilized for development of standard and experimental algorithms.

12.2 RESEARCH ACTIVITIES

We continue to participate on CalCOFI cruises to the California Current System (CCS) for which we have an 8-year time-series. This region experiences a large dynamic range of coastal and open ocean trophic structure and has experienced strong interannual forcing associated with the El Niño – La Niña cycle from 1997-2000 (Kahru and Mitchell, 2000; Kahru and Mitchell, 2002). CalCOFI data provides an excellent reference for evaluating our other global data sets (O’Reilly et al. 1998; Mitchell et al. 2002b, 2002c).

During the second year of our contract, we participated in 3 CalCOFI cruises, two collaborative cruises to the Southern Ocean (AMLR and SOFEX), and received data from colleagues in Korea and Hong Kong for 3 East Asian coastal cruises. The global distribution of our present data set is shown in Figure 12.1. On most cruises, an integrated underwater profiling system was used to collect optical data and to characterize the water column. The system included an underwater radiometer (Biospherical Instruments MER-2040 or MER-2048) measuring depth, downwelling spectral irradiance (E_d) and upwelling radiance (L_u) in 13 spectral bands. A MER-2041 deck-mounted reference radiometer (Biospherical Instruments) provided simultaneous measurements of above-surface downwelling irradiance. Details of the profiling procedures, characterization and calibration of the radiometers, data processing and quality control are described in Mitchell and Kahru (1998). The underwater radiometer was also interfaced with 25 cm transmissometers (SeaTech or WetLabs), a fluorometer, and SeaBird conductivity and temperature probes. When available, additional instrumentation integrated onto the profiling package included AC9 absorption and attenuation meters (WetLabs Inc.), and a Hydrosat-6 backscattering meter (HobiLabs). For two AMLR, ACE Asia and recent CalCOFI cruises we deployed our new Biospherical Instruments PRR-800 freefall radiometer that included 19 channels of surface irradiance (312-865 nm) and three geometries of underwater radiometry (L_u , E_u , E_d) from 312 to 700 nm. We have shown that measuring these three radiometric geometries with our MER 2048 allowed us to retrieve backscatter and

absorption coefficients (Stramska et al., 2000). Our colleagues in Hong Kong and Korea use PRR-800 profilers and collect samples for chlorophyll and absorption with methods consistent with ours.

At *in situ* optical stations discrete water samples were collected from a CTD-Rosette immediately before or after each profile for additional optical and biogeochemical analyses. Pigment concentrations were determined fluorometrically and with HPLC. All HPLC samples acquired in the past year have been submitted to San Diego State University for analysis under a separate SIMBIOS contract. Spectral absorption coefficients (300-800 nm) of particulate material were estimated by scanning particles concentrated onto Whatman GF/F filters (Mitchell, 1990) in a dual-beam spectrophotometer (Varian Cary 1). Absorption of soluble material was measured in 10 cm cuvettes after filtering seawater samples through 0.2 μm pore size polycarbonate filters. Absorption methods are described in more detail in Mitchell et al. (2002a). For some cruises we collected measurements of other optical and phytoplankton properties including photosynthesis, particulate organic matter (carbon and nitrogen), phycoerythrin pigment, and size distribution using flow cytometry and a Coulter Multi-sizer.

For most of our field work in association with CalCOFI and AMLR we submit all data directly to NASA SIMBIOS including supporting CTD and water bottle information. For the collaborations with Asian colleagues, we process their optical data and with their permission we will submit some of the Asian data to SIMBIOS in 2003. On the SOFEX cruise to the Southern Ocean we did not deploy a profiling radiometer, but we collected data for particle absorption; other SOFEX PIs collected samples for fluorometric chlorophyll and HPLC pigments. Our absorption data from SOFEX will be submitted to SIMBIOS and we will request approval to submit the pigment data.

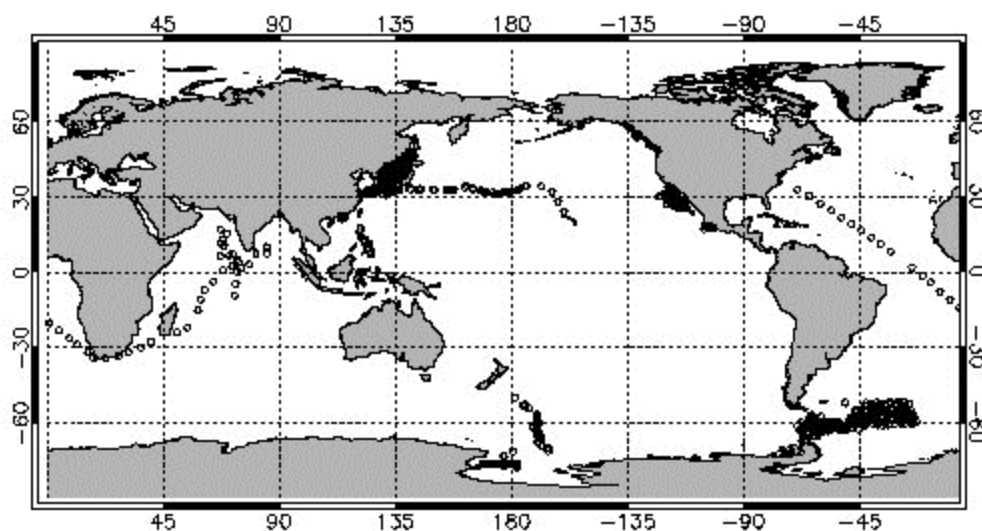


Figure 12.1: Global distribution of bio-optical stations accomplished in the past 5 years by the Scripps Photobiology Group (SPG). All stations include spectral reflectance and fluorometric chlorophyll. Most include particle and soluble absorption and HPLC pigments. For many cruises since 1997 we have deployed Hydrosat backscatter and AC9 absorption and attenuation meters to better understand the variables that govern remote sensing reflectance.

12.3 RESEARCH RESULTS

Remote sensing reflectance (R_{rs}) derived from the in-water measurements, defined as the ratio of upwelling radiance (L_u) and downwelling irradiance (E_d), is closely related to the normalized water-leaving radiance (L_{wn}) product of satellite ocean color data. $R_{rs}(\lambda)$ in Case-1 waters is well correlated to chl-*a*. As chl-*a* increases, R_{rs} generally decreases for SeaWiFS wavelengths 412, 443, 490, 510 nm due to increased absorption, but increases at SeaWiFS wavelength 555 and 665 nm due to increased backscatter (Mitchell and Kahru, 1998; O'Reilly et al., 1998). To explore issues with Case-2 waters we have

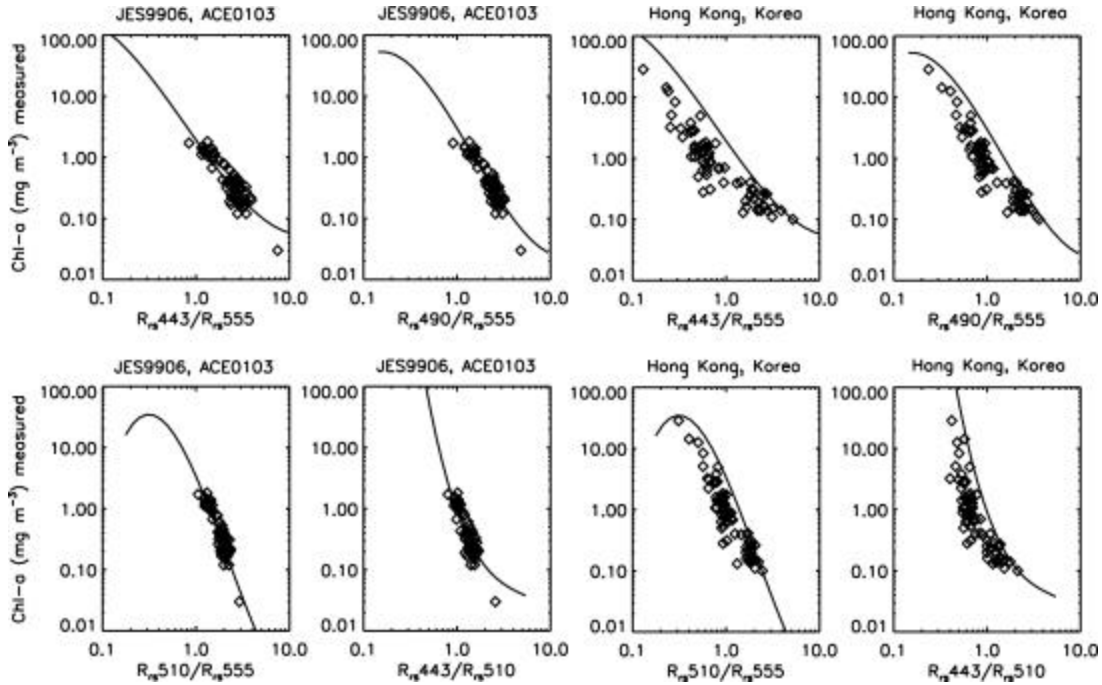


Figure 12.2: Surface reflectance ratios of SeaWiFS bands for *in situ* data. The line is an average fit from our CalCOFI reference dataset representing Case-1 waters, the diamond symbols are from cruises to East Asian waters summarized in Figure 1. The set of ratios from our Japan/East Sea (JES9906) and ACE-Asia (ACE0103) cruises (left panels) show good agreement with Case-1 relationships. The set of ratios from Hong Kong and Korean cruises in the East China and South China Seas (right panels) show strong diversion from Case-1 relationships.

collaborated with colleagues in Korea (NFRDI), and Hong Kong (HKUST) to assemble a large regional data set from the East China Sea, South China Sea and coastal waters of Eastern Asia. Relationships between Rrs and chl-a for HKUST and NFRDI data can be both lower and higher than the Case-1 (CalCOFI) relationships, depending on whether absorption or scattering is the dominant process (data not shown).

Typical ocean color algorithms take ratios of reflectance for different spectral bands. The standard SeaWiFS chl-a algorithm is currently OC4v4 (O'Reilly et al., 1998; O'Reilly et al., 2000). In Figure 12.2 we show 2-band Rrs ratios from our *in situ* data for combinations of SeaWiFS channels plotted versus surface chl-a for our Asian and CalCOFI data sets. CalCOFI data are a good reference data set since it covers a large range of chl-a, was acquired with very consistent methodology, and comprises approximately 25% of the data used for development of the SeaWiFS OC4v4 algorithm (O'Reilly et al., 2000). Kahru and Mitchell (1999; 2001) have shown that the chl-a retrieved by satellite in the CalCOFI region is in good agreement with our ship data when computed with our regional algorithm or NASA's OC4v4. A large portion of the variability attributed to backscatter cancels when taking ratios of different bands but the Case-2 data from the HKUST and NFRDI data tend to fall below the reference CalCOFI data due to enhanced absorption while the ACE Asia and Japan/East Sea data sets are very similar to CalCOFI (Figure 12.2).

Application of the standard NASA OC4 Case-1 algorithm, and our similar California Current algorithm for HKUST *in situ* data, produces significant scatter and bias (Figure 12.3). Both the standard SeaWiFS chl-a algorithm (OC4v4) and our similar Case-1 algorithm (OC4-SPG) switch to the maximum band ratio (the maximum of either Rrs or Lwn at 443, 490 or 510 nm divided by Rrs or Lwn at 555 nm) to calculate chl-a. In Case-1 waters most bio-optical variables including absorption are well correlated with chl-a which is why simple empirical band ratio algorithms work well for Case-1 waters. In the Hong Kong waters (Figure 12.4A) the lower range of the particulate absorption (a_p) data approaches the Case-1 CalCOFI relationship of a_p versus chl-a but the majority of the samples have significantly higher absorption at the respective chl-a level. This "excess" particulate absorption, attributed to suspended organic sediments, is especially dominant at low chl-a and causes a_p to be up to two orders of magnitude higher than would be predicted from chl-a concentration using typical Case-1 models.

(OC4-SPG). For most of the HKUST data, standard algorithms overestimate chl-a by 3-10x.

In Case-1 waters most bio-optical variables including absorption are well correlated with chl-a which is why simple empirical band ratio algorithms work well for Case-1 waters. In the Hong Kong waters (Figure 12.4A) the lower range of the particulate absorption (a_p) data approaches the Case-1 CalCOFI relationship of a_p versus chl-a but the majority of the samples have significantly higher absorption at the respective chl-a level. This “excess” particulate absorption, attributed to suspended organic sediments, is especially dominant at low chl-a and causes a_p to be up to two orders of magnitude higher than would be predicted from chl-a concentration using typical Case-1 models. In Hong Kong waters the magnitude of CDOM absorption is approximately 2-3 times higher at low chl-a and up to an order of magnitude higher at high chl-a than our CalCOFI reference data (Figure 12.4B).

Due to the high concentration of CDOM and other absorbing substances both algorithms overestimate chl-a in the turbid coastal waters of Hong Kong up to an order of magnitude. Some of the Hong Kong stations with low chl-a that were collected off the shelf break are very similar to Case-1 relationships. One dramatic difference between the East Asian data and our CalCOFI data set is the very high variance in the relationship between particle absorption and chl-a (Figure 12.4A). Soluble absorption in the region also tends to be higher than for CalCOFI (Figure 12.4B). Bias in the Asian coastal data compared to CalCOFI in the plots of reflectance ratios vs chl-a (Figure 12.2) are consistent with higher absorption that is likely due both to detrital and soluble absorption. These issues will continue to complicate remote sensing retrieval in Case-2 waters using passive reflectance in the blue-green region. This recently merged data set is being used to evaluate Case-2 algorithms in collaboration with our Asian colleagues (Kahru et al., 2002; Mitchell et al. 2002c).

Processing SeaWiFS data with SeaDAS (corresponding to global SeaWiFS re-processing v4) still results in significant underestimates of L_{wn} at 412 and 443 for some of our Case-1 water match-ups with high resolution HRPT data. Figure 12.5 shows spectral L_{wn} for SeaWiFS retrieval using SeaDAS v3 and v4 compared to our water leaving radiances computed for our freefall PRR-800 radiometer. All three stations were in Case-1 water types with moderate chl-a concentrations (0.3 – 0.8 mg chl-a m^{-3}). The offshore station between Hawaii and Japan had reasonable retrieval of spectral L_{wn} (Figure 12.5A) but the 412 nm retrieval is still sufficiently low that it would create errors in attempts to retrieve CDOM accurately.

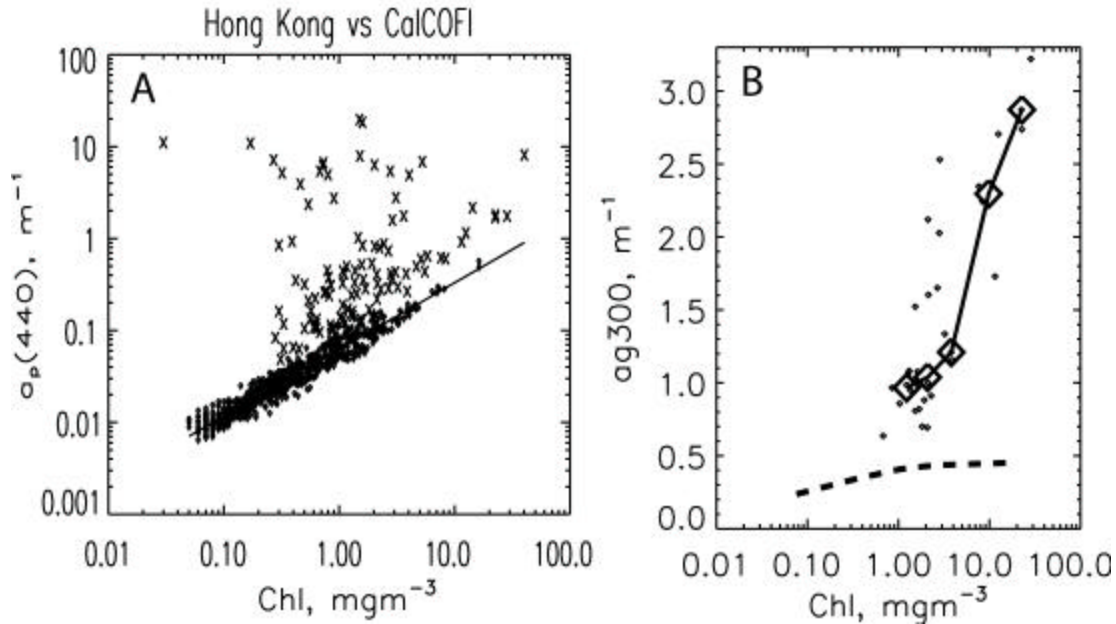


Figure 12.4: A. Absorption coefficient of particulate material at 440 nm as a function of chl-*a* for CalCOFI (filled circles, straight line for the best fit) and Hong Kong samples (×). B. Absorption coefficient of soluble material (CDOM) at 300 nm as a function of chl-*a* for CalCOFI (average relationship shown with a thick dashed line) and the Hong Kong dataset (small diamonds are individual measurements, large diamonds connected with a line represent the best fit). Both particle and soluble absorption off Hong Kong are much higher per unit chl-*a* than in Case-1 waters of CalCOFI. This increased absorption leads to the overestimates of chl-*a* using standard ocean color algorithms as shown in Figure 12.3.

The two stations closer to Asia were very close to each other and were within the Kuroshio intrusion between Japan and Korea (Figures 12.5B and 12.5C). Both stations close to the coast had severe underestimates in L_{wn} for the 412 and 443 channels and more modest underestimates at 490 nm. We believe the errors in L_{wn} retrieval between SeaWiFS and our PRR-800 *in situ* radiometer for the East Asian images are caused by errors in the aerosol models in the atmospheric correction for SeaWiFS for atmospheres that have significant terrestrial or anthropogenic aerosols. The new version of SeaDAS (corresponding to the global v4) released in summer of 2002 continues to severely under-predict L_{wn} for vast expanses of the ocean apparently due to inaccurate aerosols models. However, the chl-*a* estimates, even under the turbid absorbing aerosols for these ACE Asia stations, is surprisingly good due to the use of band-ratio empirical algorithms. Continued research on atmospheric aerosols is required to improve the accuracy of L_{wn} if we are to be able to apply multi-wavelength bio-optical retrieval algorithms that require accurate estimates of L_{wn} at 412 and 443 (e.g. Garver and Siegel, 1997; Carder et al., 1999). We collaborated with ACE Asia participants in evaluation of issues for atmospheric correction in waters of the western Pacific and marginal seas near Asia (Li et al., in press) and we will collaborate in the next year on implementing alternative atmospheric correction and *in situ* bio-optical algorithms and their validation.

12.4 FUTURE WORKS

We will continue our approach of acquiring detailed data sets at the global scale for ocean color satellite validation and algorithm development. CalCOFI will continue as our core field program and we will execute one detailed CalCOFI cruise during April 2003 with other SIMBIOS PIs and with members of the SIMBIOS Project. We are advising the CalCOFI program on concepts for a permanent optics program to be integrated into their routine CTD profiling. A close cooperation has been initiated with the IMECOCAL program off Baja California that is coordinated by scientists from CICESE in Ensenada, Mexico. We have trained a student from Peru who will deploy our optical instruments on Peru coastal cruises during 2003. The Southern Ocean and East Asian marginal seas will continue to be a high priority since it is evident that standard algorithms

for chl-a do not perform well in these regions (Mitchell and Holm-Hansen, 1991; Mitchell, 1992; Mitchell et al., 2002b; Reynolds et al., 2001; Kahru et al., 2002). Modeling efforts will continue to improve our understanding of regional bio-optical properties and their relationship to biogeochemical parameters (e.g. Stramska et al., 2000; Reynolds et al., 2001; Loisel et al., 2001). The models and data will contribute to development of advanced algorithms and parameterizations for semi-analytical inverse models for the retrieval of inherent optical properties and biogeochemical properties besides chl-a. In particular we will focus on methods to retrieve CDOM, particulate organic carbon and particle size distributions simultaneously with chl-a using our global data sets and detailed water sample analyses.

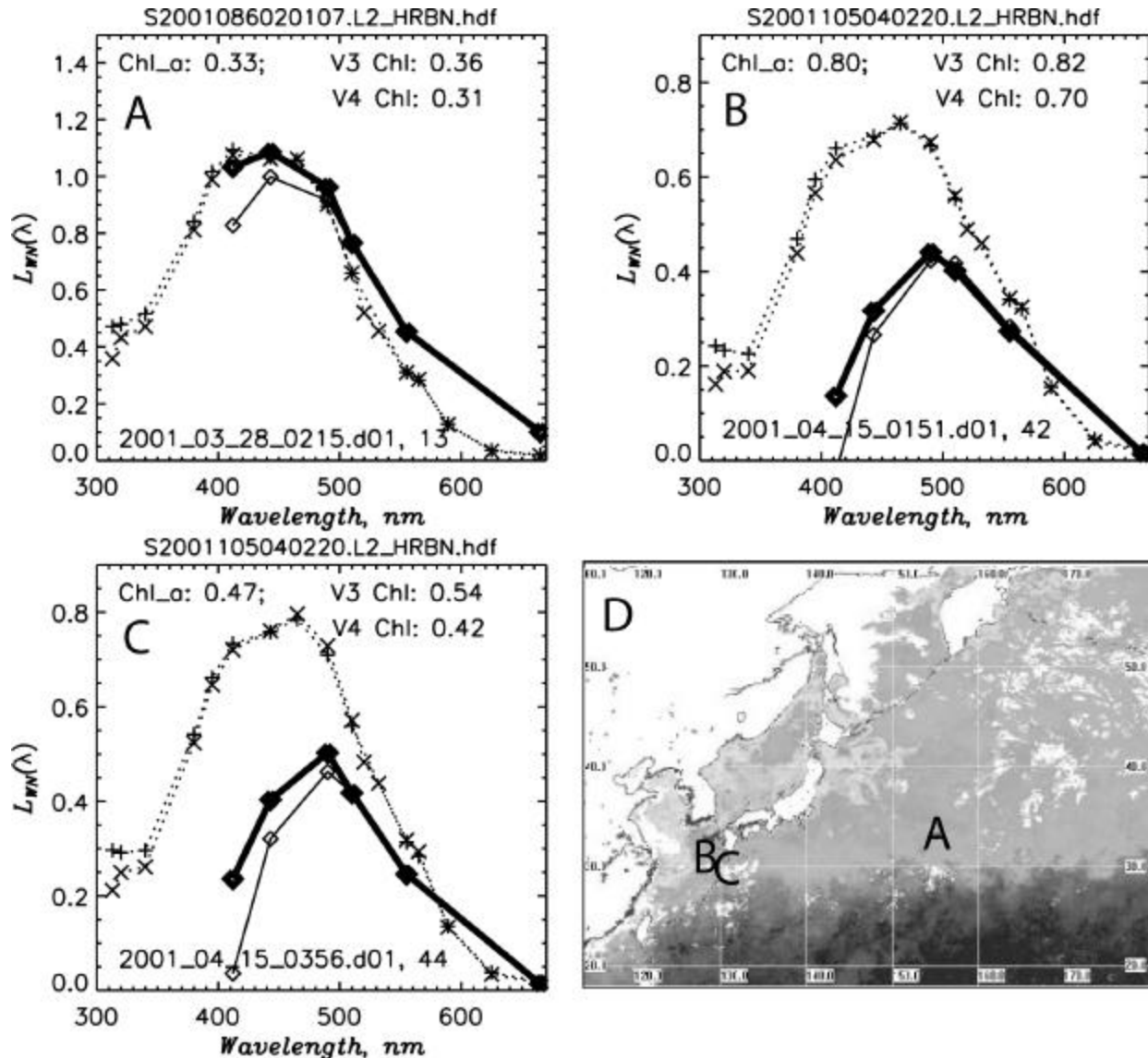


Figure 12.5: Lwn match-ups for ACE-Asia *in situ* radiometry (x) and SeaWiFS (SeaDAS 3, open diamonds connected with a solid thin line; SeaDAS 4, heavy diamonds connected with a thick solid line). The locations of the match-ups in the North Pacific (A, 32.749 N, 154.929 E), and in the Kuroshio intrusion between Japan and Korea (B, 32.420 N, 128.538 E; C, 32.523 N, 128.410 E) are shown on the composite SeaWiFS chl-a composite image for April (panel D). (Note: the SeaDAS version corresponds to the global reprocessing v3 and v4). All three match-ups had moderate chl-a concentrations and were in Case-1 waters. The chl-a determined by HPLC and the global re-processing v3 and v4 estimates are indicated on each Lwn spectral plot.

REFERENCES

- Carder, K.L., F.R. Chen, Z.P. Lee and S.K. Hawes, 1999: Semianalytic moderate-resolution imaging spectrometer algorithms for chlorophyll a and absorption with bio-optical domains based on nitrate-depletion temperatures, *Journal of Geophysical Research*, **104**(C3), 5, 403-5,421.
- Garver, S.A. and D.A. Siegel, 1997: Inherent Optical Property Inversion of Ocean Color Spectra and its Biogeochemical Interpretation: 1. Time series from the Sargasso Sea, *Journal of Geophysical Research*, **102**(C8), 18,607-18,625.
- Kahru, M. and B.G. Mitchell, 1999: Empirical chlorophyll algorithm and preliminary SeaWiFS validation for the California Current, *International Journal of Remote Sensing*, **20**(17), 3,423-3,430.
- Kahru, M. and B.G. Mitchell, 2000: Influence of the 1997-98 El Niño on the surface chlorophyll in the California Current. *Geophysical Research Letters*, **27**(18), 2,937-2,940.
- Kahru, M. and B.G. Mitchell, 2001: Seasonal and non-seasonal variability of satellite-derived chlorophyll and colored dissolved organic matter concentration in the California Current, *Journal of Geophysical Research*, **106**(C2), 2517-2529.
- Kahru, M., B.G. Mitchell, J. Wieland, J.C. Chen, N.W. Man, Y.S. Suh, M. Stramska, and D. Stramski, 2002: Evaluation of Satellite Ocean Color Algorithms for East Asian Marginal Seas, *ASLO*, Honolulu, Hawaii, February 2002.
- Kahru, M. and B.G. Mitchell, 2002: Influence of El Niño – La Niña cycle on satellite-derived primary production in the California current, *Geophysical Research Letters*, **29**(9), 10.1029/2002GL014963.
- Li, L.-P., H. Fukushima, R. Frouin, B.G. Mitchell, M. -X. He, I. Uno, T. Takamura, and S. Ohta: Influence of sub-micron absorptive aerosol on SeaWiFS-derived marine reflectance during ACE-Asia, *Journal of Geophysical Research–Atmospheres*, (in press).
- Loisel, H., D. Stramski, B.G. Mitchell, F. Fell, V. Fournier-Sicre, B. Lemasle, and M. Babin, 2001: Comparison of the ocean inherent optical properties obtained from measurements and inverse modeling, *Applied Optics*, **40**(15), 2384-2397.
- Mitchell, B.G., 1990: Algorithms for determining the absorption coefficient of aquatic particulates using the quantitative filter technique (QFT). In: Spinrad, R., ed., *Ocean Optics X*, Bellingham, Washington, *SPIE*, 137-148.
- Mitchell, B.G., 1992: Predictive bio-optical relationships for polar oceans and marginal ice zones, *Journal of Marine Systems*, **3**, 91-105.
- Mitchell, B.G. and M. Kahru, 1998: Algorithms for SeaWiFS standard products developed with the CalCOFI bio-optical data set, *Cal. Coop. Ocean. Fish. Invest. R.*, **39**, 133-147.
- Mitchell, B.G. and O. Holm-Hansen, 1991: Bio-optical properties of Antarctic Peninsula waters: Differentiation from temperate ocean models, *Deep-Sea Research I.*, **38**(8/9), 1,009-1,028.
- Mitchell B. G., M. Kahru, J. Wieland and M. Stramska, 2002a: Determination of spectral absorption coefficients of particles, dissolved material and phytoplankton for discrete water samples. In: Fargion, G.S. and J.L. Mueller, Eds. *Ocean Optics Protocols for Satellite Ocean Color Sensor Validation, NASA Technical Memorandum 2002-210004/Rev 3-Vol 2*, Chapter 15, 231-257.
- Mitchell, B.G., M. Kahru, R. Reynolds, J. Wieland, D. Stramski, C. Hewes, and O. Holm-Hansen, 2002b: Chlorophyll-a Ocean Color Algorithms for the Southern Ocean and their Influence on Satellite Estimates of Primary Production, *ASLO*, Honolulu, Hawaii.

- Mitchell, B.G., M. Kahru, J. Wieland, and H. Wang, J.C. Chen, N.W. Man, and Y.S. Suh, 2002c: Case 2 Optical relationships for East Asian marginal seas, *Ocean Optics XVI Conference*, Santa Fe, New Mexico, 2002.
- O'Reilly, J.E., S. Maritorena, B.G. Mitchell, D.A. Siegel, K.L. Carder, S.A. Garver, M. Kahru and C. McClain, 1998: Ocean color chlorophyll algorithms for SeaWiFS, *Journal of Geophysical Research*, **103**(C11), 24,937-24,953.
- O'Reilly, J.E., S. Maritorena, D.A. Siegel, M.C. O'Brien, D.A. Toole, B.G. Mitchell, M. Kahru, et al., 2000: Ocean color chlorophyll a algorithms for SeaWiFS, OC2 and OC4: Version 4. In: NASA, SeaWiFS Postlaunch Calibration and Validation Analyses.
- Reynolds, R.A., D. Stramski and B.G. Mitchell, 2001: A chlorophyll-dependent semianalytical reflectance model from derived from field measurements of absorption and back scattering coefficients within the Southern Ocean, *Journal of Geophysical Research*, **106**(C4), 7125-7138.
- Stramska, M., D. Stramski, B.G. Mitchell and C.D. Mobley, 2000: Estimation of the absorption and backscattering coefficients from in-water radiometric measurements, *Limnology and Oceanography*, **45**(3), 628-641.

Chapter 13

Variability in Ocean Color Associated with Phytoplankton and Terrigenous Matter: Time Series Measurements and Algorithm Development at the FRONT Site on the New England Continental Shelf.

John R. Morrison and Heidi M. Sosik

Woods Hole Oceanographic Institution, Woods Hole, Massachusetts

13.1 INTRODUCTION

Fronts in the coastal ocean describe areas of strong horizontal gradients in both physical and biological properties associated with tidal mixing and freshwater estuarine output (e.g. Simpson, 1981 and O'Donnell, 1993). Related gradients in optically important constituents mean that fronts can be observed from space as changes in ocean color as well as sea surface temperature (e.g., Dupouy et al., 1986). This research program is designed to determine which processes and optically important constituents must be considered to explain ocean color variations associated with coastal fronts on the New England continental shelf, in particular the National Ocean Partnership Program (NOPP) Front Resolving Observational Network with Telemetry (FRONT) site. This site is located at the mouth of Long Island sound and was selected after the analysis of 12 years of AVHRR data showed the region to be an area of strong frontal activity (Ullman and Cornillon, 1999). FRONT consists of a network of modem nodes that link bottom mounted Acoustic Doppler Current Profilers (ADCPs) and profiling arrays. At the center of the network is the Autonomous Vertically Profiling Plankton Observatory (AVPPO) (Thwaites et al. 1998). The AVPPO consists of buoyant sampling vehicle and a trawl-resistant bottom-mounted enclosure, which holds a winch, the vehicle (when not sampling), batteries, and controller. Three sampling systems are present on the vehicle, a video plankton recorder, a CTD with accessory sensors, and a suite of bio-optical sensors including Satlantic OCI-200 and OCR-200 spectral radiometers and a WetLabs ac-9 dual path absorption and attenuation meter. At preprogrammed times the vehicle is released, floats to the surface, and is then winched back into the enclosure with power and data connection maintained through the winch cable. Communication to shore is possible through a bottom cable and nearby surface telemetry buoy, equipped with a mobile modem, giving the capability for near-real time data transmission and interactive sampling control.

13.2 RESEARCH ACTIVITIES

AVPPO Deployments

Three deployments of the AVPPO were achieved since the previous end of year report, one in 2001 and two in 2002. The durations of all deployments were greater than four weeks with varying levels of technical difficulties. The final deployment of 2001 was at the FRONT site on October 4, 2001. Initially the ac-9 was non-functional and telemetry from the whole system was lost on November 5. During a maintenance cruise on November 8 the buoyant instrumentation package was successfully detached from the tethering cable and replaced by place-holding buoys. Inspection of the telemetry buoy showed the antenna to have been broken off and markings consistent with a ship strike. The antenna was replaced and communications restored. The ship strike also affected the surface radiometer which was removed for repair. Ship-board repairs to the bio-optical sensor package and other sensors on the instrument package were unsuccessful. The place-holding buoys were winched into the bottom mounted enclosure to protect the cable and the instruments returned to WHOI for repair. Replacement of a power control board restored the ac-9 data stream. The package was reattached to the tethering cable on November 13 and full system functionality restored. The whole system was recovered on December 7.

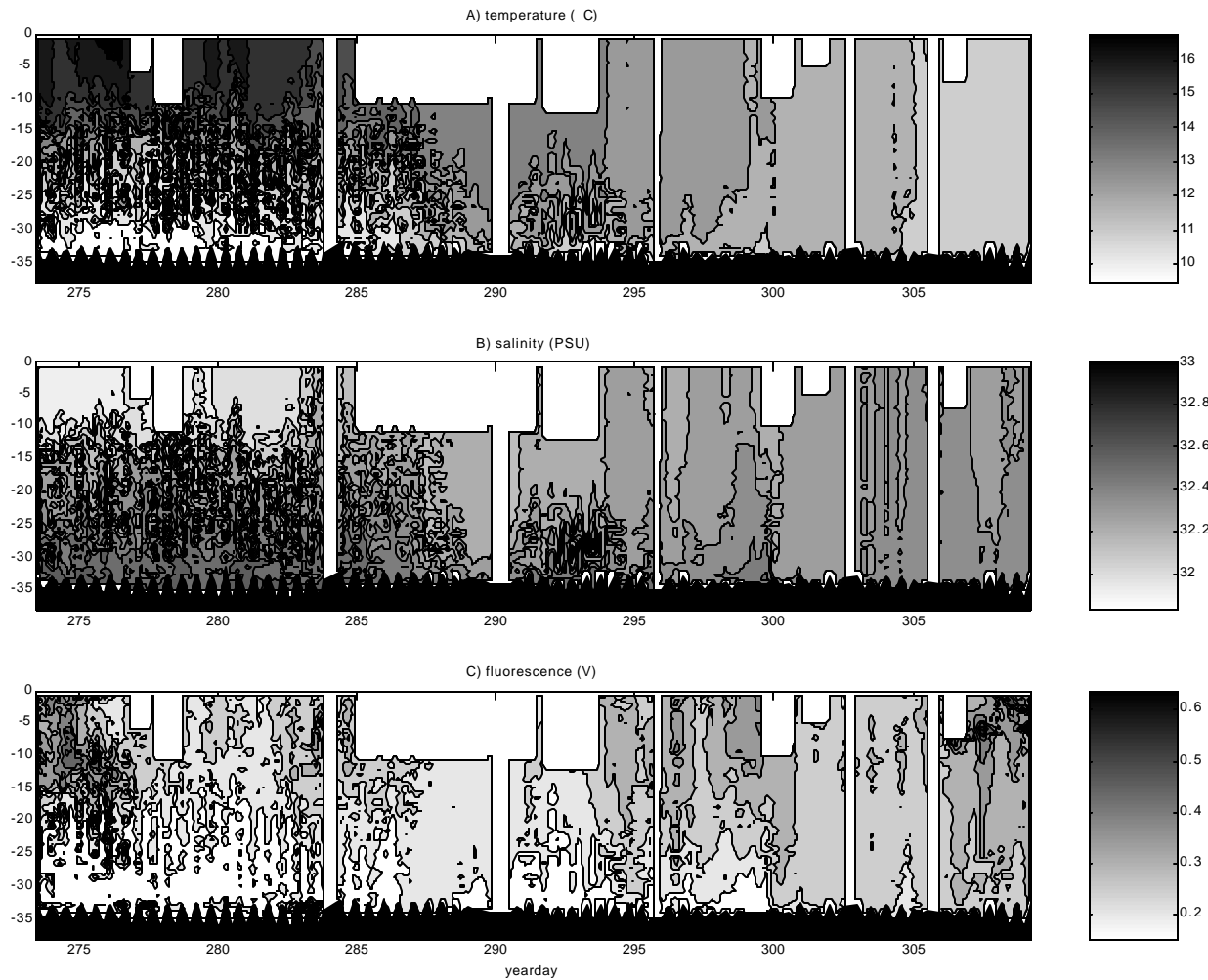


Figure 13.1: Interpolated hydrographic data and fluorescence from the 2002 Massachusetts Bay deployment. The temperature (A) and salinity (B) demonstrates the progression from strong vertical stratification with periodic internal waves to vertically more homogenous waters. Changes in the fluorescence signal (C) were indicative of variations in phytoplankton biomass.

The system was redeployed at the FRONT site on March 24 after delays due to weather and ship schedules. During deployment the AVPPO is set to continually stream data for monitoring purposes and is reset into the normal profiling mode using radio. Attempts to radio reset the mooring during two hours on station adjacent to the AVPPO and during the cruise back to Avery Point were unsuccessful. On Wednesday March 27 a radio reset was successful from the top of the lighthouse on Montauk Point, Long Island. The AVPPO started profiling. The transfer of files via ftp, which includes data from and mission and scheduling files to the mooring, failed after two activity periods. Another expedition to the Montauk Point lighthouse in an attempt to reinstate ftp file transfers successfully reset the mooring but was unsuccessful in its objective. The mooring functioned autonomously using the last mission file received from shore until April 26, 2002 and performed approximately 700 profiles to 20 m. Real time data was received from the mooring via a UDP data stream. Inspection of the system after recovery on May 29 revealed a broken winch axle to be the cause of the final system failure. A final deployment at the FRONT site was not possible due to the necessary major repairs.

The final deployment of 2002 was at a site in Massachusetts Bay close to that occupied during 2001. Deployment was on September 30 and was followed by a ten day cruise. Discrete water samples were collected for pigment analysis and absorption measurements and radiometer casts performed when near the mooring. Since the deployment data from over 490

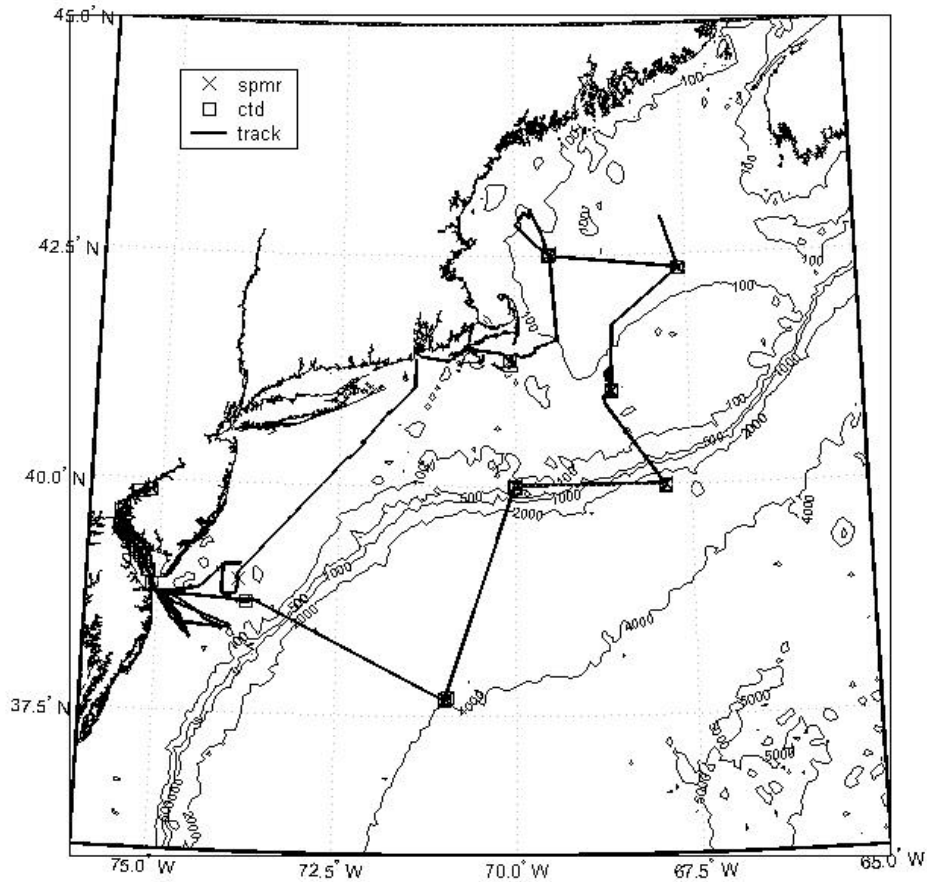


Figure 13.2: Cruise track and stations of cruise EN372.

profiles have been received. The strong stratification with periodic internal waves initially observed were replaced by a mixed water column (Figure 13.1A and 13.1B). Variations in phytoplankton abundance, as indicated by fluorometer voltage, were also observed (Figure 13.1C). Adjustment of mission and scheduling files allowed maximization of profiling frequency on cloud free days and limited the minimum depth of profiling during adverse weather conditions.

Additional Cruises.

Bio-optical data from a variety of optical water types were also collected from an additional cruise, EN372 (June 23 to July 16, 2002, Figure 13.2). The cruise entailed an extensive survey of the Delaware Estuary and measurements at 8 other stations in the North West Atlantic, some of which were occupied for two days, at which multiple radiometer and CTD casts were performed.

13.3 RESEARCH RESULTS

Much of the work during the last year has focused on determining the sources of variability of ocean color focusing on the Inherent Optical Properties measured by the ac-9. Of interest is partitioning non-water absorption, $a_{nw}(\lambda)$, into that from phytoplankton, $a_{ph}(\lambda)$, and non-algal fractions, $a_{dm}(\lambda)$, which includes both non-algal particulates and CDOM. This is achieved

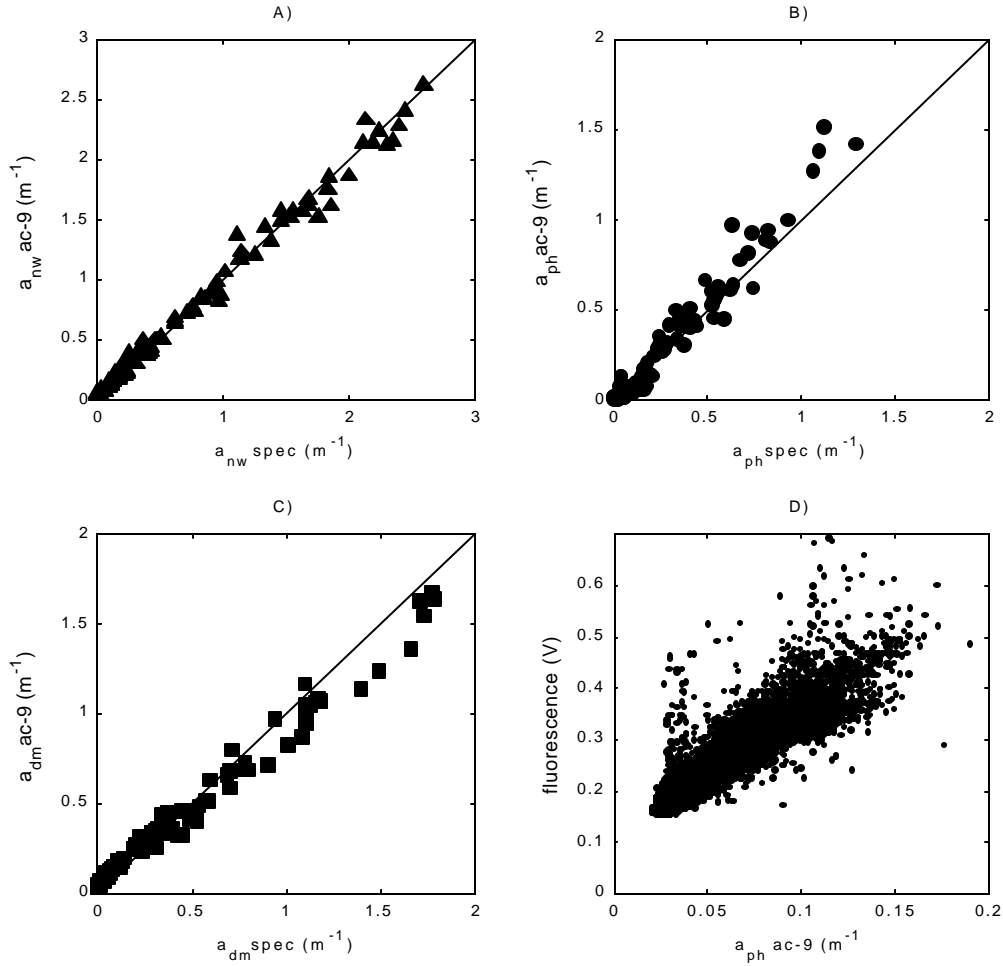


Figure 13.3: Ac-9 absorption measurements including non-water absorption, a_{nw} (A), and the partitioned phytoplankton and non-algal absorptions, a_{ph} (B) and a_{dm} (C), were highly correlated to those determined independently using a spectrophotometer (shown are measurements made at 412, 440 and 488 nm). The partitioned phytoplankton absorption measurements were also highly correlated with the fluorescence signal during the 2002 Massachusetts Bay deployment.

by assigning characteristic spectral shapes to each fraction and iteratively varying constituent concentrations to minimize the sum of square deviations between observed and predicted spectra.

$$a_{nw}(\mathbf{I}) = C \cdot a_{ph}^*(\mathbf{I}) + a_{dm}(\mathbf{I}_0) \exp[-S(\mathbf{I} - \mathbf{I}_0)] \quad (1)$$

Comparisons between partitioned ac-9 absorption measurements and independent spectrophotometric measurements confirmed the absorption decomposition approach (Figure 13.3). Variations in partitioned phytoplankton absorption during the 2002 Massachusetts Bay deployment corresponded with those observed by the fluorometer (Figure 13.3C and 13.4A). Marked variations in the non-algal matter concentrations were observed including resuspension of bottom sediments associated with bad weather between yeardays 285 and 292 (Figure 13.4B). The resuspension was also evident as increased scattering during this time (Figure 13.4C). The scattering coefficient of a constituent, like the absorption coefficient, can be represented by the product of a concentration specific coefficient and the concentration. Alternatively, the absorption of a constituent at a discrete wavelength may be considered as a proxy for concentration. The non-water scattering, $b_{nw}(\ddot{\epsilon})$ (the sum of scattering due to

phytoplankton, $b_{ph}(\lambda)$, and non-algal scattering, $b_d(\lambda)$) can then be expressed in terms of spectral absorption specific scattering coefficients for both phytoplankton, $b_{ph}^{*aph}(\lambda)$, and non-algal matter, $b_d^{*ad}(\lambda)$:

$$b_{nw}(\lambda) = b_{ph}(\lambda) + b_d(\lambda) = a_{ph}(440)b_{ph}^{*aph}(\lambda) + a_d(440)b_d^{*ad}(\lambda). \quad (2)$$

To estimate the scattering due to phytoplankton, a_{dm} was substituted for a_d in Equation 2. The specific scattering coefficients, calculated for each deployment using multiple linear regression, showed typical spectral shapes for both non-algal particle and phytoplankton scattering (Figure 13.5). For all wavelengths and all deployments greater than 80% of the variability of b_{nw} was explained by the regression.



Figure 13.4: Interpolated Inherent Optical Properties from the AVPPO ac-9 from the 2002 Massachusetts Bay deployment. A) The distribution of phytoplankton absorption is similar to that of fluorescence (Figure 1C). Resuspension of bottom sediments is apparent in non-algal absorption (B) and total scattering (C). The general increase in scattering may be indicative of fouling of the ac-9.

13.4 FUTURE WORK

With a duration of greater than five weeks and in excess of 490 profiles the final deployment of the AVPPO in 2002 has demonstrated the full potential of the system. Preliminary results suggest that it is possible to partition non-water absorption

measured by the ac-9 into that from phytoplankton and non-algal matter. Total scattering is highly correlated to the partitioned absorptions and the absorption specific scattering coefficients have shapes that are typical for the optically important constituents. Hourly profiles will allow the assessment of the variability in ocean color on timescales of importance to ocean color sensors mounted on different satellite sensors. The combination of IOP and radiometric measurements should prove useful in algorithm development.

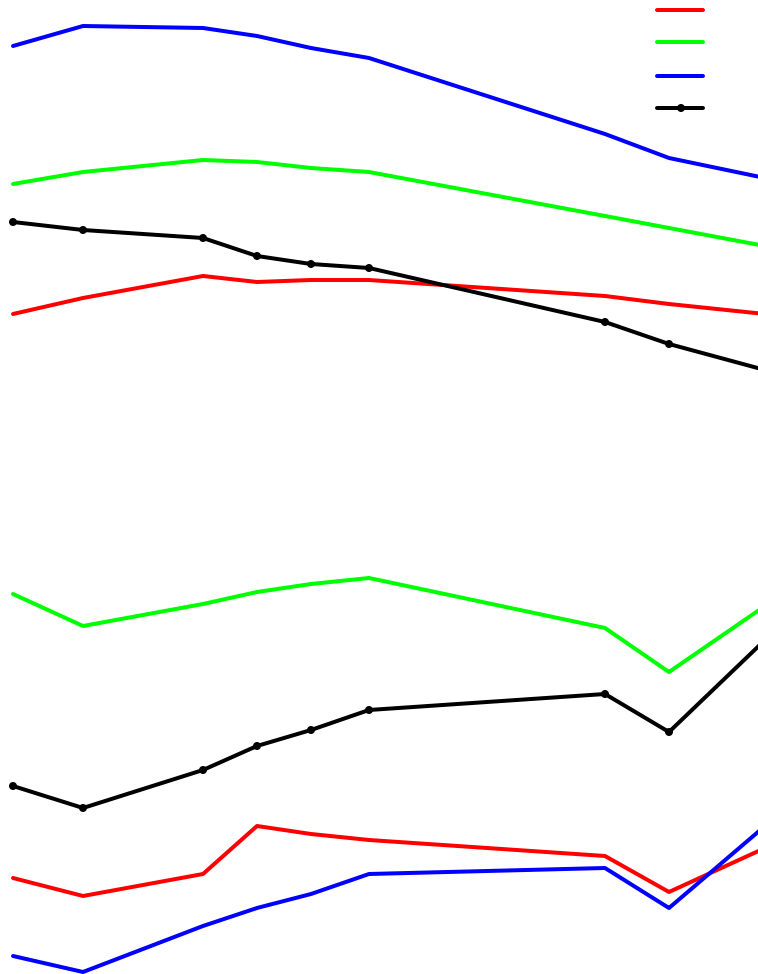


Figure 13.5: A) Absorption specific non-algal scattering, and B) absorption specific phytoplankton absorption. The absorption measurements were at 440 nm. Note the general decrease in phytoplankton scattering associated with the red and blue phytoplankton absorption peaks.

REFERENCES

- Dupouy, C., J.P. Rebert, and D. Toure, 1986: Nimbus-7 coastal zone color scanner pictures of phytoplankton growth on an upwelling front in Senegal, In: *Marine Interfaces Ecohydrodynamics*, J.C.J. Nihoul (Ed.), Elsevier Science Pub., 617-664.
- O'Donnell, J., 1993: Surface Fronts in Estuaries: A Review, *Estuaries*, **16**, 12-39.
- Simpson, J. H., 1981: The shelf-sea fronts: implications of their existence and behaviour, *Phil. Trans. R. Soc. Lon. A*, **302**, 531-546.
- Thwaites F. T., S. M. Gallager, C. S. Davis, A. M. Bradley, A. Girard and W. Paul, 1998: A winch and cable for the autonomous vertically profiling plankton observatory, *Proc. Oceans 98*.
- Ullman, D.S., and P.C. Cornillon, 1999: Satellite-derived sea surface temperature fronts on the continental shelf off the northeast U.S. coast, *J. Geophys. Res.*, **104**, 23459-23478.

Chapter 14

Ocean Optics Protocols and SIMBIOS Protocol Intercomparison Round Robin Experiments (SPIRREX).

James L. Mueller

Center for Hydro-Optics and Remote Sensing, San Diego State University, California

14.1 INTRODUCTION

The objective of research under this contract is the maintenance and annual revision of the document “Ocean Optics Protocols for Satellite Ocean Color Validation (e.g. Fargion and Mueller 2000; Mueller et al. 2002a).

14.2 RESEARCH ACTIVITIES

The research activities under the second year of this contract were devoted to the preparation of “Ocean Optics Protocols for Satellite Ocean Color Validation, Revision 4” (Mueller et al. 2002), building on Revision 3 (Mueller and Fargion 2000). The important updates, additions and revisions in the Revision 4 document are summarized in the next section.

14.3 RESEARCH RESULTS

Revision 4 to the ocean optics protocol document (Mueller et al. 2002b) comprises several significant changes compared to Revision 3 (Mueller et al. 2000a). The most obvious change is the reorganization of the document into 6 separate volumes:

- I: Introduction, Background and Conventions
- II: Instrument Specifications, Characterization and Calibration
- III: Radiometric Measurements and Data Analysis Methods
- IV: Inherent Optical Properties: Instruments, Characterization, Field Measurements and Data Analysis Protocols
- V: Biogeochemical and Bio-Optical Measurements and Data Analysis Methods
- VI: Special Topics in Ocean Optics Protocols
- VII: Appendices

The multi-volume format is intended to allow timely future protocol revisions to be made reflecting important evolution of instruments and methods in some areas, without reissuing the entire document. The content of Volumes I, II and III is carried forward from Revision 3 (Mueller et al. 2002a) and these are unlikely to require significant changes for several years. The chapters of Volume IV may require near term revisions to reflect the rapidly evolving state-of-the-art in measurements of inherent optical properties, particularly concerning instruments and methods for measuring the Volume Scattering Function of seawater. It is anticipated that in Revision 5 (2003), new chapters may be also be added to Volumes V (potential candidates include methods for measuring particle size distributions, particulate organic carbon, coccoliths concentrations, and phycobiliprotein concentrations) and VI (potential special topics include refined methods of radiometric profile analysis based on new data analysis round-robin studies, measurements using towed bio-optical arrays, and methods for measuring aerosol profiles using LIDAR).

To briefly summarize the relationship between the protocol chapters of Revision 3 and the individual volumes of Revision 4, Volume I combines chapters 1, 2 and 3 (Rev. 3) with a new chapter that includes some material from chapter 9 (Rev. 3) covering generic topics such as sampling strategy guidelines, log and record-keeping requirements, and data archival requirements (the detailed SeaBASS material from Ch. 18 and App. B of Rev. 3 has been removed from the protocols and now

appears in a separate Technical Memorandum published by the SIMBIOS Project). Volume II contains renumbered and reformatted versions of chapters 4 through 8 (Rev. 3), without significant revisions. Similarly, Volume III collects chapters 10 and 12 through 14 of Revision 3, again without significant revisions. Volume IV contains 4 new chapters on IOP measurement, calibration and analysis methods, together with chapter 15 (Rev. 3) with only minor modifications. Volume V collects chapters 16 and 17 (Rev. 3) with some minor, but important modifications to the protocols for HPLC measurements of phytoplankton pigment concentration. Volume VI collects special topics, beginning with chapter 11 (Rev. 3) on MOBY, and with new chapters included on bio-optical measurements from buoys, ocean color radiometry from aircraft, and stray light characterization of the MOBY spectrographs using LASER sources.

14.4 FUTURE WORK

In the coming year, the primary efforts will address: 1) a strengthening of the new IOP protocols (Volume IV) by soliciting review and new input from a broader community than we were able to include in the initial draft of this material, 2) data analysis round robin (DARR) experiments designed to evaluate methods, and associated uncertainties, for determining water-leaving radiance and downwelled irradiance just beneath the sea surface from radiometric profiles, and 3) any new chapters for revised versions of Volume V (biogeochemical methods such as particle size distribution, or remote sensing estimation of particulate organic carbon) and VI (special topics such as analysis methods for determining water-leaving radiance from radiometric profiles based on new DARR results, or protocols for bio-optical measurements from towed platforms). Each specific topic addressed under the third area of effort will be one for which qualified authors can be identified who are willing to contribute a chapter.

ACKNOWLEDGEMENTS

This research was supported under SIMBIOS Contract Number 00199.

REFERENCES

- Fargion, G.S. and J.L. Mueller, 2000: Ocean Optics Protocols for Satellite Ocean Color Sensor Validation, Revision 2, *NASA TM 2001-209955*, NASA Goddard Space Flight Center, Greenbelt, Maryland, 184 pp.
- Mueller, J.L., et al., 2002a: Ocean Optics Protocols for Satellite Ocean Color Sensor Validation, Revision 3, *NASA TM 2002-210004*, Mueller, J.L. and G. Fargion (Eds.), NASA Goddard Space Flight Center, Greenbelt, Maryland, 308pp.
- Mueller, J.L., et al., 2002b: Ocean Optics Protocols for Satellite Ocean Color Sensor Validation, Revision 4, *NASA TM 2002-TBD*, Mueller, J.L., G. Fargion and C.R. McClain (Eds.), NASA Goddard Space Flight Center, Greenbelt, Maryland, (in press).

Chapter 15

Bermuda Bio Optics Project

Norm Nelson

Institute for Computational Earth Science, UCSB, Santa Barbara, California

15.1 INTRODUCTION

The Bermuda BioOptics Project (BBOP) is a collaborative effort between the Institute for Computational Earth System Science (ICESS) at the University of California at Santa Barbara (UCSB) and the Bermuda Biological Station for Research (BBSR). This research program is designed to characterize light availability and utilization in the Sargasso Sea, and to provide an optical link by which biogeochemical observations may be used to evaluate bio-optical models for pigment concentration, primary production, and sinking particle fluxes from satellite-based ocean color sensors.

The BBOP time-series was initiated in 1992, and is carried out in conjunction with the U.S. JGOFS Bermuda Atlantic Time-series Study (BATS) at the Bermuda Biological Station for Research. The BATS program itself has been observing biogeochemical processes (primary productivity, particle flux and elemental cycles) in the mesotrophic waters of the Sargasso Sea since 1988. Closely affiliated with BBOP and BATS is a separate NASA-funded study of the spatial variability of biogeochemical processes in the Sargasso Sea using high-resolution AVHRR and SeaWiFS data collected at Bermuda (N. Nelson, P.I.). The collaboration between BATS and BBOP measurements has resulted in a unique data set that addresses not only the SIMBIOS goals but also the broader issues of important factors controlling the carbon cycle.

15.2 RESEARCH ACTIVITIES

BBOP personnel participate on all BATS cruises, which are conducted monthly with additional cruises during the spring bloom period, January through May. Table 1 contains a list of data products relevant to SIMBIOS. The BBOP project collects continuous profiles of apparent optical properties (AOPs) in the upper 140m and deployments are planned to optimize matchups with the BATS primary production incubations and with SeaWiFS overpasses. In 1999, a free-falling Atlantic profiling radiometer system (SPMR/SMSR s/n 028) became our primary profiling instrument. The primary optical measurements are downwelling vector irradiance and upwelling radiance, $E_d(z,t, \lambda)$ and $L_u(z,t, \lambda)$, respectively. Derived products include remote sensing reflectance ($R_{rs}(z, \lambda)$) and down- and upwelled attenuation coefficients ($K_d(z,\lambda)$, $K_u(z,\lambda)$). The sampling package also includes a second mast-mounted radiometer with wavebands matching those on the underwater instrument for measuring incident downwelling vector irradiance, $E_d(0^+,t, \lambda)$. This system was upgraded to 11 channels in 2000, and both instruments are calibrated three times annually at UCSB. The profiler also includes a WetStar fluorometer and Ocean Sensors CTD sensors. During 2002, we initiated collection of sky radiance measurements using a 5-channel Microtops handheld sun photometer.

Bottle samples for fluorometric chlorophyll-*a* and inherent optical properties (IOPs) are also collected. Chlorophyll-*a* is collected once or twice daily during each cruise. Discrete samples for determining the absorption spectra of particulates, $a_p(z, \lambda)$ and $a_t(z, \lambda)$, and CDOM ($a_g(z, \lambda)$) are collected according to Nelson *et al* (1998). Particulate absorption spectra are determined using the quantitative filter technique (Mitchell, 1990) and CDOM absorption according to Nelson *et al* (1998).

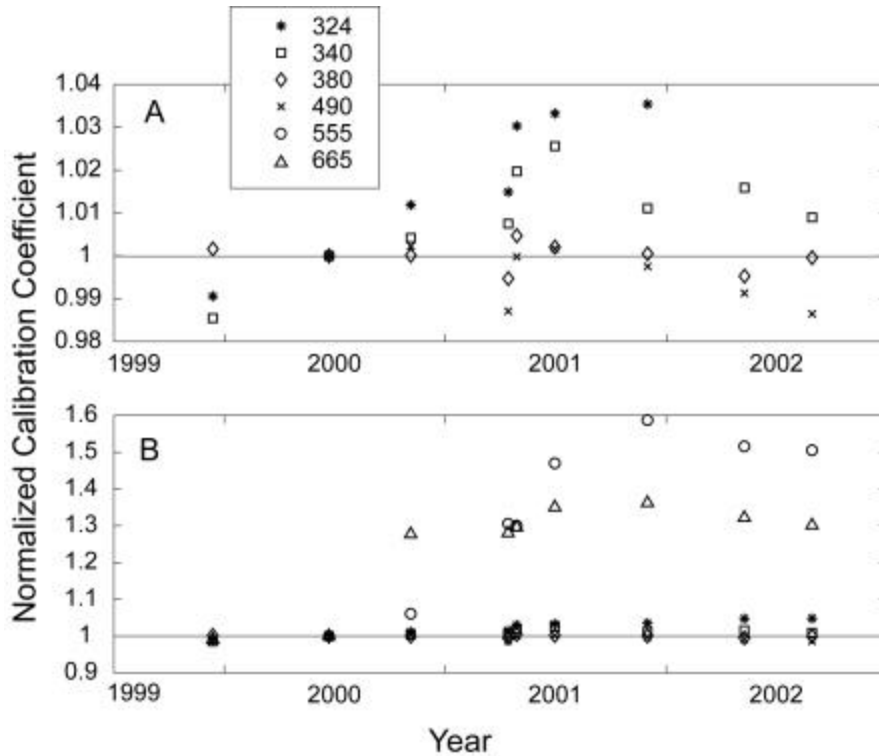


Figure 13.1. Calibration history for SPMR system sn028, Irradiance head sn058, low gain. Panel A, scaled to show the variation in the E_d380 , E_d490 , E_d555 , E_d665 channels; Panel B, same data, plus E_d325 and E_d340 , scaled for these channels.

13.3 RESEARCH RESULTS

Instrument Calibration

Careful attention to instrument behavior and calibration is crucial to assuring high quality time-series data. We have continued our efforts to determine the long-term calibration behavior of our SPMR systems using several lamps traceable to our own NIST standard. Our past experience with radiometric calibrations has shown that calibration coefficients used in the field should be averages of many calibrations using several different lamps (O'Brien *et al*, 2000). We now have more than 3 years of calibration data for SPMR-028 (2 years (8 calibrations) in its current configuration), and can assess the long-term variability of some of its channels. Figure 13.1 shows the normalized calibration coefficients for several channels on one irradiance head (SPMR system sn028, irradiance head 058). For wavelengths greater than 500nm on all sensors, there was no obvious drift during 2 years, and overall scatter was ~1% and ~2% for irradiance and radiance detectors, respectively (Fig. 13.1a). The coefficients of variation for these channels were less than 1%. The blue irradiance channels show some drift toward lower sensitivity, up to 5-8%. The drift in the blue radiance sensors was less apparent, and smaller, about 1-2%, not significantly different from variation observed in the green-red channels. The most extreme changes were noted at 325nm and 340nm in both irradiance heads: up to 50-60% for E_d325 and E_s325 , and about half that for E_d340 and E_s340 (Fig 13.1b). The drift for these wavelengths on the radiance head was noticeably smaller, 10% or less. By averaging only the 6 most recent calibrations, some CV's for the UV channels could be reduced from 15-20% to less than 10%. It appears that the sensitivity of the UV channels is still degrading. Since calibration lamp output is quite low in the UV, calibration results in this range are extremely difficult to replicate, and it is not always clear whether differences between individual calibrations are due to sensor degradation or simply to lamp variability. The growing lack of sensitivity in the UV channels may also be due to degradation of the cosine collector material (S. McLean, pers. comm.). For the most part in visible wavelengths, these instruments appear to have been stable for the last 2 years and hence, we are using long-term averages of calibration coefficients whenever

possible. Calibration certificates and plots of all sensors can be found at our website: http://www.icess.ucsb.edu/bbop/instruments/instruments_spmr.html.

One significant research result from last year was the determination of new immersion coefficients for Satlantic profiling irradiance meters, which were significantly different from the originals. Despite improvements in the coefficients we are still not completely satisfied with the values, but feel that we have about reached the limit of the existing technique. During the summer of 2002, we began testing a new water-filled chamber for determination of the cosine detector immersion coefficients. The “immersion telescope” designed by D. Menzies allows the parallel rays of the sun to be used as the light source for the experiment, removing the problem of dispersion and non-point source nature of the lamps used in the standard procedure for determining the immersion coefficient (cf. Mueller and Austin, 1995). The position of the sensor head in the chamber can be adjusted up to 80cm from the chamber’s glass window. A support stand allows the chamber’s axis to be aligned normal to the sun. Reference irradiance sensors are mounted alongside the test chamber with extension tubes to reduce contamination from sky-light. To date, measurements have been made with a 7 channel PRR instrument and a 4 channel PUV instrument. The data processing is ongoing and early results are encouraging. If satisfactory results are obtained we will repeat the procedures for our Satlantic radiometers and publish the results.

We are continuing to examine the relationships between retrieved chlorophyll-*a* from SeaWiFS imagery and *in situ* factors controlling optical properties, particularly chlorophyll-*a* and CDOM. One interesting result of this time series is that SeaWiFS consistently underestimated *in situ* chlorophyll *a* during the spring periods, with the exception of 2000 (fig. 13.2a). Spring is also the time of the largest surface CDOM concentration in this area (Nelson et al., 1998), so this and seasonal phytoplankton succession are possible factors interfering with chlorophyll concentration retrieval from SeaWiFS.

Collaborative and Project-Related Activities

We participated in two Project-sponsored HPLC round-robin activities, as a laboratory participant using the BATS HPLC facilities (Van Heukelem et al. 2002), and to collect unknown samples in the Sargasso Sea for a more recent round-robin. The BBOP calibration facility has participated in both SIMRIC experiments to date (Meister et al. 2002).

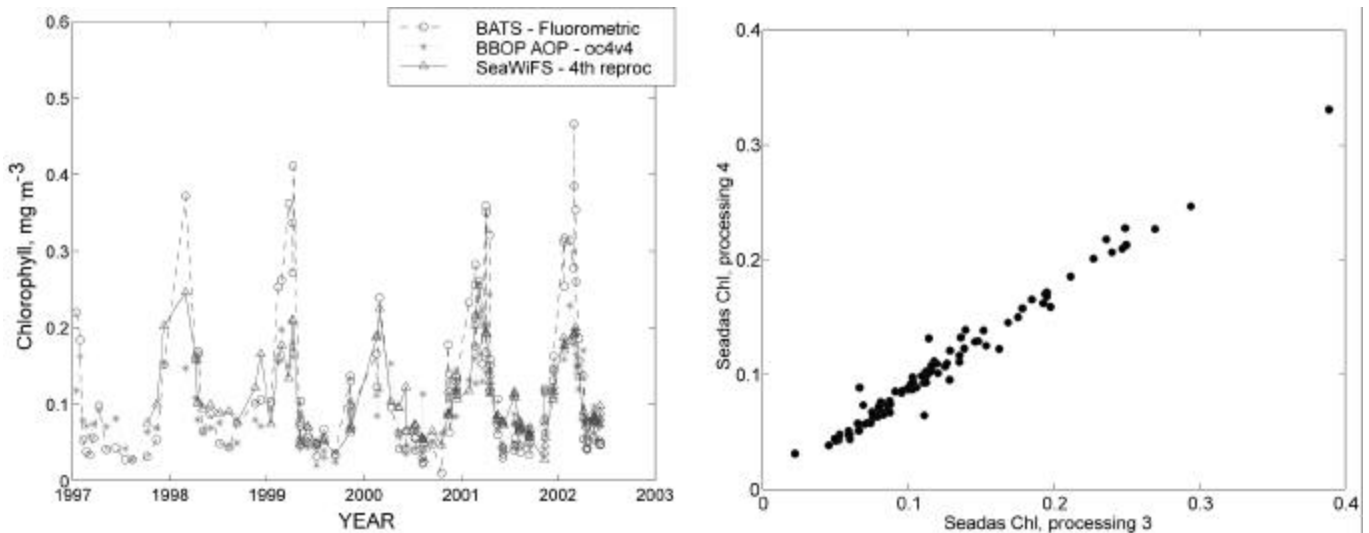


Figure 13.2: a) bottle fluorometric Chlorophyll-*a* samples compared to field radiometric data converted to Chlorophyll using OC4v4 and SeaWiFS Chlorophyll-*a* (4th processing, 8-day averages). b-d) Comparison between SeaWiFS chlorophyll-*a* values, 3rd processing and 4th processing.

REFERENCES

Meister, G., and others. The first SIMBIOS Radiometric Intercomparison (SIMRIC-1), April-September 2001. *NASA Tech. Memo, 2002-210006*, 46pp.

- Mitchell, B.G., 1990: Algorithms for determining the absorption coefficient for aquatic particles using the quantitative filter technique, *Ocean Optics X, Proceedings of S.P.I.*, **1302**, 137-142.
- Mueller, J. L. and R. W Austin. 1995: Ocean optics protocols for SeaWiFS Validation, revision 1, *NASA Tech. Memo. 104566*, Volume **25** (Hooker, S, E. Firestone and J. Acker, eds.), 67 pp.
- O'Brien, M.C., D.W Menzies, D.A. Siegel, and R.C. Smith, 2000: Long-Term Calibration History of Several Marine Environmental Radiometers (MERs), *NASA Tech. Memo*, SeaWiFS Postlaunch Calibration and Validation Analyses, Vol. **11**, Part 3, Chap. 4.
- Nelson, N.B., D.A. Siegel, and A.F. Michaels, 1998: Seasonal dynamics of colored dissolved material in the Sargasso Sea, *Deep Sea Research I*, **45**, 931-957.
- Van Heukelem, L., C.S. Thomas, and P.M. Glibert, 2002: Sources of variability in chlorophyll analysis by fluorometry and high-performance liquid chromatography in a SIMBIOS inter-calibration exercise, *NASA Tech. Memo*, 2002-211606 (G.S. Fargion and C.R. McClain, eds.).

TABLE 13.1: A PARTIAL LIST OF MEASUREMENTS MADE BY BBOP & BATS

BBOP	
Direct Measurements:	
$E_d(z, \lambda)$	Downwelling vector irradiance (325, 340, 380, 412, 443, 488, 510, 555, 565, 665 & 683 nm)
$E_d(0^+, \lambda)$	Incident irradiance (325, 340, 380, 412, 443, 488, 510, 555, 565, 665 & 683 nm)
$L_u(z, \lambda)$	Upwelling radiance (325, 340, 380, 412, 443, 488, 510, 555, 565, 665 & 683 nm)
chl-fl(z)	Chlorophyll fluorescence with a WetStar fluorometer
T(z) & S(z)	Temperature and conductivity with Ocean Sensors probes (calibrations by Satlantic)
$a_{tp}(\lambda)$	Particulate absorption spectrum by QFT
$a_d(\lambda)$	Detrital particle absorption spectrum by MeOH extraction
$a_{ys}(\lambda)$	Colored dissolved absorption spectrum
chl-a(z)	Discrete chlorophyll <i>a</i> determinations via Turner fluorometry
Primary Derived Products:	
$L_{wN}(\lambda)$	Normalized water leaving radiance (325, 340, 380, 412, 443, 488, 510, 555, 565, 665 & 683 nm)
$R_{RS}(0^-, \lambda)$	In-water remote sensing reflectance (325, 340, 380, 412, 443, 488, 510, 555, 565, 665 & 683 nm)
$K_d(z, \lambda)$	Attenuation coefficient for $E_d(z, \lambda)$ (325, 340, 380, 412, 443, 488, 510, 555, 565, 665 & 683 nm)
$K_l(z, \lambda)$	Attenuation coefficient for $L_u(z, \lambda)$ (325, 340, 380, 412, 443, 488, 510, 555, 565, 665 & 683 nm)
$a_{ph}(\lambda)$	Phytoplankton absorption spectrum ($= a_p(\lambda) - a_{det}(\lambda)$)
<PAR(z)>	Daily mean photosynthetically available radiation at depths of the <i>in situ</i> C ¹⁴ incubations
U.S. JGOFS BATS (NSF) AND RELATED BIOGEOCHEMISTRY SAMPLING PROGRAMS	
Primary Production (<i>in situ</i> ¹⁴ C incubation)	Sinking flux (sediment trap array)
Phytoplankton pigments (fluorometric & HPLC)	Nutrients (NO ₃ +NO ₂ , SiO ₄ , PO ₄)
CO ₂ system (alkalinity, TCO ₂ and pCO ₂)	Continuous atmosphere & surface pCO ₂
Dissolved oxygen (continuous & discrete)	Zooplankton biomass & grazing
POC & PON (POP infrequently)	DOC & DON (DOP infrequently)
Full water column, WOCE-standard CTD profile	Bacterial abundance and rates
Phytoplankton abundance by flow cytometry	Coccolithophore abundance
Validation spatial cruises (5 days, 4cruises/year)	Deep ocean sediment sinking rates

Chapter 16

Plumes and Blooms: Modeling the Case II Waters of the Santa Barbara Channel

D.A. Siegel, S. Maritorena and N.B. Nelson

Institute for Computational Earth System Science, University of California, Santa Barbara, California

16.1 INTRODUCTION

The goal of the Plumes and Blooms (PnB) project is to develop, validate and apply to imagery state-of-the-art ocean color algorithms for quantifying sediment *plumes* and phytoplankton *blooms* for the Case II environment of the Santa Barbara Channel. We conduct monthly to twice-monthly transect observations across the Santa Barbara Channel to develop an algorithm development and product validation data set. The PnB field program started in the summer of 1996. At each of the 7 PnB stations, a complete verification bio-geo-optical data set is collected. Included are redundant measures of apparent optical properties (remote sensing reflectance and diffuse attenuation spectra), as well as *in situ* profiles of spectral absorption, beam attenuation and backscattering coefficients. Water samples are analyzed for component *in vivo* absorption spectra, fluorometric chlorophyll, phytoplankton pigment (by the SDSU CHORS laboratory), inorganic nutrient and biogenic and lithogenic silica concentrations (Table 16.1). We are also in the process of developing quality assurance procedures for optical data sets to assess complimentary optical property determinations. Our goal is to use the PnB field data set to objectively tune semi-analytical models of ocean color for this site and apply them using available satellite imagery (SeaWiFS and MODIS). In support of this goal, we have also been addressing SeaWiFS ocean color and AVHRR SST imagery (Otero and Siegel, submitted). We also are using the PnB data set to address time/space variability of water masses in the Santa Barbara Channel and its relationship to the 1997/1998 El Niño and have been active in various outreach activities (see below).

16.2 RESEARCH ACTIVITIES

So far this year, we have conducted 12 one-day cruises since November 2001. In addition, we have participated in three 8-day cruises on the *R/V Pt. Sur* in support of the Santa Barbara Channel Long Term Ecological Research (LTER) study (sbc.lternet.edu/). In combination, we have completed 100 stations and collected nearly 200 discrete water samples. All processed data has been submitted to the SeaBASS system. We have continued conducting regular research cruises the on *Spirit of Santa Barbara* as we await the completion of the Channel Islands National Marine Sanctuary (CINMS) research vessel. The new research boat is anticipated in January 2003. We have continued our partnership with CINMS have split the cost of chartering *The Spirit*. However, budget constraints have required us to cut our cruise schedule from twice a month to once a month.

We have continued our acquisition and analysis of satellite ocean color (SeaWiFS) and thermal imagery (AVHRR) from the UCSB HRPT ground station (HUSC). The UCSB ground station is supported by SIMBIOS, NSF and NOAA/NESDIS. The PnB project has an extensive education and outreach component. At least two undergraduate students volunteer on each one day cruise and the PnB data is presently being used in the theses and dissertations of three graduate students at UCSB. Prof. Siegel made a live television presentation of the PnB program during an episode of Project Oceanography when it came to Santa Barbara (www.marine.usf.edu/pjocean/). We also participated in several CINMS outreach programs sponsored.

16.3 RESEARCH RESULTS

Academic research has gone along two major fronts; 1) the analysis of field and satellite data to assess the sources of ocean color variability (Toole and Siegel, 2001; Otero, 2002; Otero and Siegel, 2002) and the assessment of the time/space variability in the Santa Barbara Channel (Siegel et al. 2002; Shipe et al. 2002; Mertes and Warrick, 2001; Warrick et al. 2002a;

2002b). Of particular interest is our work assessing the sources and modes of ocean color variability within the Santa Barbara Channel from the six-year PnB observational record (Siegel et al. 2002; Toole and Siegel, 2001). The characterization of the substances, processes, and mechanisms that regulate coastal ocean color variability is crucial for the application of ocean color imagery to the management of marine resources. Using an empirical orthogonal function (EOF) analysis, we find that nearly two-thirds of the observed variability in remote sensing reflectance is contained in a backscattering mode. Phytoplankton absorption makes a much smaller contribution to the observed variance in the water-leaving radiance spectrum. Hence, particulate backscattering associated with suspended sediment concentrations is the dominant driver of ocean color variability for this environment. However, sediment plumes appear to play a much smaller role on biological processes. An empirical partitioning of physical, biological and chemical oceanographic parameters suggests that physical oceanographic processes (i.e., upwelling and horizontal advection) have the dominant role in determining phytoplankton pigment biomass for this region. One goal is to use these spectral EOF modes with satellite data to map out where and when blooms occur. Using EOF analysis of the space/time patterns of satellite ocean color imagery, we find a similar partitioning (Otero, 2002; Otero and Siegel, 2002). This work attempts to differentiate between the role of local (wind-driven upwelling and seasonal heating) vs. non-local (i.e., advection and ENSO) processes in regulating biological distributions in the Santa Barbara Channel (Otero and Siegel, 2002).

On a technical note, we have noticed from PnB cruises that values of specific absorption of phytoplankton at 676 nm [$a_{ph}^*(676)$] often exceed the theoretical maximum of $0.0206 \text{ m}^2 \cdot \text{mg}^{-1}$. One possible reason of this overestimate is the pathlength amplification factor (β). Our measurements to date have been corrected using the pathlength amplification factor of Mitchell (1990) which was obtained from mixed phytoplankton cultures. To assess the potential source of bias, we examined the relationship between the optical density in suspension (OD_s) and the optical density of the same sample on a GF/F filter (OD_f) of natural samples. This in effect will enable us to determine our own β factor. Two samples were processed for pathlength amplification factors spanning a range of chlorophyll concentrations (1.5 vs. 5.2 mg m^{-3}). We find similarities between our two observations and these are both a factor of 1.7 times lower than the Mitchell (1990) coefficients. We feel that this explains the large overestimate we have noted in our filter-pad absorption data sets and plan to publish these results in an upcoming SIMBIOS technical report.

16.4 FUTURE WORK

PnB has had a good year, especially considering the unplanned ship issues. We expect that the Channel Islands National Marine Sanctuary will take delivery of its new research boat in the next few months. This will greatly help our program out enabling us to use conducting wire and our CTD/rosette system (instead of hanging Niskin bottles). That said, we plan to continue our field program as we have in past years. From an analysis perspective, we plan to focus on the evaluation of the inherent optical property determinations made and their relationship with the determinations of water-leaving radiance. We also plan to tune a semi-analytical ocean color model using PnB data with the goal of assessing differences in ocean color model tunings on local and global scales. There are also several data quality issues that we still need to work out; now with the *in situ* optical instrumentation (AC-9 and Hydrosat). A new graduate student has joined our group and he plans to make this modeling the focus of his masters thesis.

REFERENCES

- Mertes, L.A.K., and J.A. Warrick, 2001: Measuring flood output from 110 coastal watersheds in California with field measurements and SeaWiFS, *Geology*, **29**, 659-662.
- Otero, M.P., and D.A. Siegel, 2002: Spatial and temporal characteristics of sediment plumes and phytoplankton blooms in the Santa Barbara Channel, *Deep-Sea Research, Part II* (submitted).
- Siegel, D.A., and others, 2001: Time-series assessment of sediment plumes and phytoplankton blooms in the Santa Barbara Channel, California, *Continental-Shelf Research*, (submitted).
- Shipe, R.F., U. Passow, M.A. Brzezinski, D.A. Siegel and A.L. Alldredge, 2001: Effects of the 1997-98 El Nino on seasonal variations in suspended and sinking particles in the Santa Barbara Basin. *Progress in Oceanography* (in press).

Warrick, J.A., L.A.K. Mertes, D.A. Siegel and C. MacKenzie, 2002a: Estimating suspended sediment concentrations from remotely sensed SeaWiFS imagery, *Remote Sensing of the Environment* (submitted).

Warrick, J.A., L.A.K. Mertes, L. Washburn, and D.A. Siegel, 2002b: A conceptual model for river plume dispersal and forcing in the Santa Barbara Channel, California, based on field and remote sensing observations, *Continental-Shelf Research* (submitted).

TABLE 16.1: PLUMES AND BLOOMS MEASUREMENTS AND DATA PRODUCTS

Direct Measurements:	
$E_d(z, \lambda)$	Downwelling vector irradiance (325, 340, 380, 412, 443, 490, 510, 555, 565, 665 & 683 nm)
$E_d(0^+, \lambda)$	Incident irradiance (325, 340, 380, 412, 443, 490, 510, 555, 565, 665, 683 & 350-1050 nm)
$L_u(z, \lambda)$	Upwelling radiance (325, 340, 380, 412, 443, 490, 510, 555, 565, 665 & 683 nm)
$a(z, \lambda)$	<i>In situ</i> absorption spectrum using WetLabs AC-9 (410,440,490,520,565,650,676 & 715 nm)
$c(z, \lambda)$	<i>In situ</i> beam attenuation spectrum (same as above)
$b_b(z, \lambda)$	<i>In situ</i> backscattering spectrum - HOBI Hydrosat (442,470,510,532, 590 & 671 nm)
T(z) & S(z)	SeaBird temperature and conductivity probes
$a_p(z_o, \lambda)$	<i>In vivo</i> particulate absorption spectrum by Mitchell (1990)
$a_{det}(z_o, \lambda)$	<i>In vivo</i> detrital particle absorption spectrum by MeOH extraction
$a_d(z_o, \lambda)$	<i>In vivo</i> colored dissolved absorption spectrum
chl-a(z_o)	Discrete chlorophyll <i>a</i> determinations by Turner fluorometry
pigs(z_o)	Discrete phytoplankton pigment sample to be run by HPLC (SDSU CHORS analysis)
nuts(z_o)	Discrete inorganic nutrient concentrations (NO ₃ , SiO ₄ , PO ₄ , NO ₂)
PSi(z_o)	Discrete particulate biogenic & lithogenic silica concentrations
$L_{sat}(x, y, \lambda)$	SeaWiFS and AVHRR imagery from the HUSC ground station
Primary Derived Products:	
$R_{RS}(0^-, \lambda)$	In-water remote sensing reflectance from profiling radiometry (see above)
$L_{wN}(\lambda)$	Normalized water leaving radiance calculated from $R_{RS}(0^+, \lambda)$ and $R_{RS}(0^-, \lambda)$
$a_{ph}(z_o, \lambda)$	<i>In vivo</i> phytoplankton absorption spectrum (= $a_p(z_o, \lambda) - a_{det}(z_o, \lambda)$)
$K_d(z, \lambda)$	Attenuation coefficient for $E_d(z, \lambda)$ from profiling radiometry (also $K_L(z, \lambda)$)
$b(z, \lambda)$	<i>In situ</i> total scattering spectrum (= $c(z, \lambda) - a(z, \lambda)$)
Chl(x, y), etc.	Processed SeaWiFS and AVHRR imagery

Chapter 17

Algorithms for Processing and Analysis of Ocean Color Satellite Data for Coastal Case 2 Waters

Richard P. Stumpf

NOAA National Ocean Service, Silver Spring, Maryland

Robert A. Arnone and Richard W. Gould, Jr.

Naval Research Laboratory (NRL), Stennis Space Center, Mississippi

Varis Ransibrahmanakul

Technology Planning and Management Corporation, Silver Spring, Maryland

Patricia A. Tester

NOAA National Ocean Service, Beaufort, North Carolina

17.1 INTRODUCTION

SeaWiFS has the ability to enhance our understanding of many oceanographic processes. However, its utility in the coastal zone has been limited by valid bio-optical algorithms and by determination of accurate water reflectances, particularly in the blue bands (412-490 nm), which have a significant impact on the effectiveness of all algorithms.

Two major factors which contribute to the errors in the atmospheric correction are: (1) water-leaving radiance in the near-infrared due to scattering from inorganic particles and (2) absorbing aerosols associated with land that cannot be incorporated into atmospheric corrections based on near-infrared (NIR) bands. Iterative techniques, which draw on coupling the atmospheric and oceanic models, offer a solution to these problems. However, they require accurate ocean bio-optical models for Case 2 waters that are robust when applied to an interactive, coupled atmosphere-ocean model.

We developed a solution to the NIR atmospheric correction procedure that NASA implemented into the latest processing of SeaWiFS data. Furthermore, we are utilizing the new products to monitor and successfully predict harmful algal blooms along the west Florida shelf and develop new products for SeaWiFS and MODIS.

In addition to algorithm development, we continue to collect data sets of bio-optical properties in turbid Case 2 waters, which are less common in the SEABASS database. These data sets will provide the basis for improving and evaluating *in situ* and atmospheric correction algorithms for coastal waters. In coastal waters with a high sediment load and/or high concentrations of colored dissolved organic matter (CDOM), standard processing algorithms typically fail (negative or erroneous retrievals of water-leaving radiance) due to invalid assumptions related to the atmospheric correction. Our efforts will focus on describing the reflectance properties at near-infrared (NIR) and blue wavelengths in coastal waters, and utilization these properties to improve the atmospheric correction. We will continue to modify and develop new coastal bio-optical algorithms, as well as, validate the algorithms and atmospheric corrections. We (NRL) have implemented MODCOLOR and MODSST into our processing software. We have also modified the MODIS processing software in cooperation with NASA and University of Miami to use the same NIR atmospheric correction SEADAS is using.

17.2. RESEARCH ACTIVITIES

We have collected *in situ* bio-optical data on twenty-one cruises. Measurements in the Northern Gulf of Mexico include absorption coefficient, beam attenuation coefficient, scattering coefficient (ac9), remote sensing reflectance (above water

method), aerosol optical thickness (Microtops), and HPLC pigments (Table 17.1). A substantial number of these stations were collected during minimum cloud cover and matched up with SeaWiFS and MODIS passes. Measurements in North Carolina waters include water samples, water profile measurements (YSI), and remote sensing reflectance. The water samples were collected to determine chlorophyll, CDOM, filter pad absorption, HPLC, total suspended solids (TSS), and nutrients. Measurements along the Gulf coast include remote sensing reflectance from 400-900 nm, spectral absorption and scattering profiles (from an ac9), water samples, and aerosol optical depth (MICROTOPS sunphotometer). The water samples were collected to determine chlorophyll, CDOM, filtered pad absorption, HPLC (through CHORS), total suspended solids (TSS), and nutrients.

Table 17.1: Summary of Data Collected

Experiment	Cruise	Date	Ac8/ctd/etc.	ASD rrs	HPLC
Cojet 3 –Northern Gulf of Mexico	Mopex	16-May-01	26	36	0
Cojet 3–Northern Gulf of Mexico	Lgssur	16-May-01	31	31	29
Cojet 3–Northern Gulf of Mexico	Ocolor	16-May-01	22	22	25
NGLI Lake Bourne Apr01	Ocolor	04/01	4	3	4
NGLI Biloxi 11Sep01	Ocolor2	09/01	8	8	8
Leo2001- East Coast –New jersey	R/V NorthStar	7/31- 8/02/01	15	28	23
Cojet 4 – Barrier Islands, Mobile Bay			17	16	33
Cojet 5 – Barrier Is., Mobile Bay	Pelican	12/3/01-12/7/01	26	25	26
Cojet 6- Barrier Is., Mobile Bay	Pelican	3/5/02-3/6/02	8	9	9
Cojet 7 – Barrier Island	Pelican	5/17/02-5/26/02	29	17	27
Cojet 7 – Barrier Island	Ocolor	5/17/02-5/26/02	24	25	25
NGLI Biloxi 19Nov01		5/01			5
ECOHAB- West Florida Shelf	ECOHAB	9/25/00-9/29/00			25
NC-04/01- North Carolina	Pamlico	4/10/01-4/11/01	8	10	14
NC-05/01 – North Carolina		5/24/01		4	4
NC 07/01 North Carolina	Pamlico	7/24/01 – 7/26/01		4	11
NC 08/01	Pamlico/NC shelf	08/1/01-8/2/01			5
NC-10/01	NC Shelf/Pamlico	10/16/01-10/19/01		8	13
NC-02/02	Pamlico	2/19/02-2/21/02		8	8
CA-03/02	Offshore San Francisco, Gulf of Farallones	3/2/02-3/4/02		7	20
NC-07/02	Pamlico	7/3/02		2	6
Totals			218	263	320

The current chlorophyll algorithm fails in high CDOM areas. We have collected simultaneous SeaWiFS, LIDAR, hyperspectral radiance, and water samples from Pamlico Sound to develop a more robust Case 2 bio-optical algorithm. Airborne LIDAR have been used to determine synoptic chlorophyll-*a* and CDOM in coastal North Carolina. Pat Tester has started a collaborative research project with Bob Swift at NASA Wallops Island. She has contracted for six more over flight windows to use LIDAR during the spring and fall from 2003 through 2005. In addition to the utility of CDOM (and organic C), CDOM signals may serve as mimics for salinity or nutrients pulses after runoff events.

17.3 RESEARCH RESULTS

NIR Atmospheric Correction Implemented To Latest SEADAS (NOAA & NRL)

We submitted the NIR atmospheric correction code and manuscript to Sean Bailey in March and September 2002, respectively. After Gene Feldman compared the products derived from many atmospheric corrections and posted them to SeaWiFS community for review, NASA implemented our NIR-correction approach into SEADAS 4.4 (released July 2002).

In addition to NASA's evaluation, we independently compared the products derived from different atmospheric corrections against measured data. The comparison shows that the proposed NIR reduced both the bias (Figure 17.1) and root-mean square error. Description and validation of our NIR correction may be found in Stumpf et al. (in press).

Calibration (NOAA)

At the AGU meeting in San Francisco, December 2001, Ransibrahmanakul and Stumpf (2001) presented a new method for validating calibration gain values in the blue bands.

Background & Problem. The current calibration of SeaWiFS involves two steps: correction for temporal changes using lunar observations and periodic vicarious calibration of the radiance based on comparison with the Marine Optical Buoy (MOBY) sites. The later has potential uncertainty of 0.5 % in the top-of-atmosphere (TOA) radiance calibration (Barnes et al. 2000), partly because each band is calibrated independently. In coastal areas, the calibration of the 412 nm band is of particular concern owing to the need to correct for absorbing aerosols in the atmosphere and the need to monitor and compensate for colored dissolved organic matter (CDOM) in the water. Calibration errors of 0.5-1% between bands in the blue (412 nm, 443 nm, 490 nm) can introduce significant errors in the retrieved water reflectance (5-10% in case 1 water, and 20-100% in case 2 water).

We proposed two methods: one involving examination of case 2 water; another, in all water types. Both methods use an inter-band relationship found in the field (and assumed to be intrinsic) to validate the spectral shape observed in satellite data. The coastal method examines spectral curvature in the blue bands. Satellite data typically shows a convex shape from 412 to 490 nm, while field data shows a concave shape. By defining coastal water spectra as those with remote sensing reflectance at 443 nm greater than remote sensing reflectance at 412 nm, we found that 90% of the 420 field coastal water spectra are concave (index < 0). In contrast, 90% of the satellite coastal water spectra are convex (index > 0).

Using the latest calibration and software, we found the calibration at 412 nm appears to be underestimated by about 1% (Figure 17.2). For validation, we computed the overall bias and root mean square error (rms) from 105 pairs of satellite and same-day cloud-free measured remote sensing reflectance in US waters. Using the adjusted calibration, the bias at 412 nm is reduced by four folds (Figure 17.3). Adding a component to the current protocol to calibrate multiple bands simultaneously may improve the total calibration.

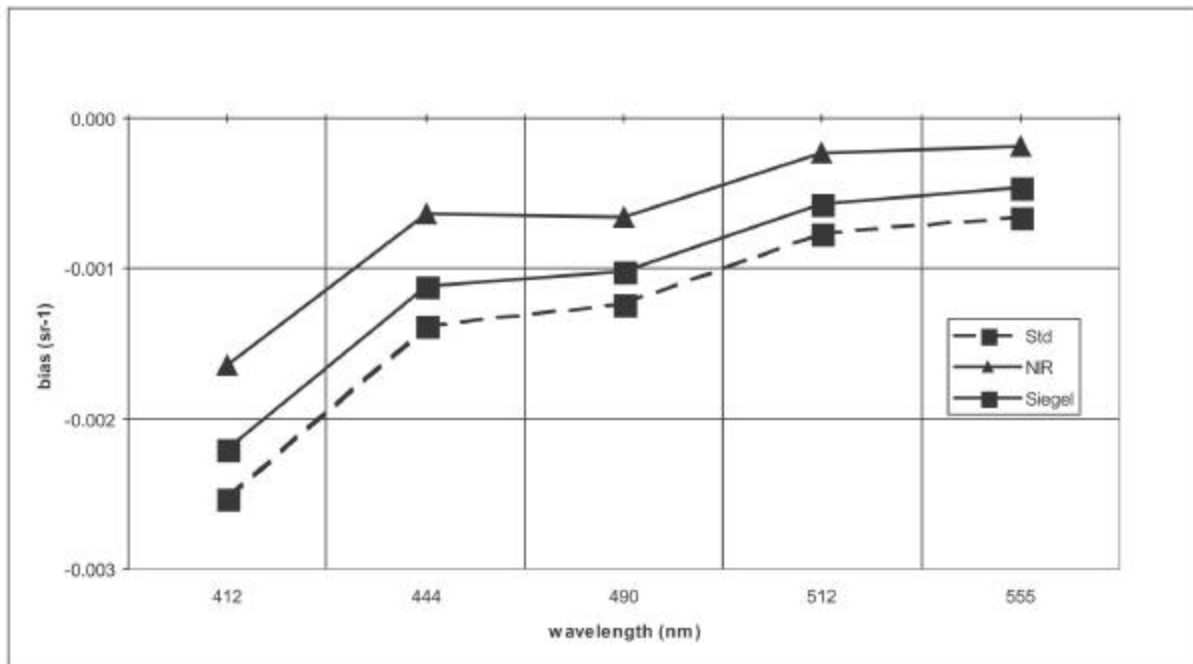


Figure 17.1: Bias of non-iterative (standard), Siegel-iteration (used in repro3), and the NIR-iteration for 105 same day matchups of satellite and field water reflectances.

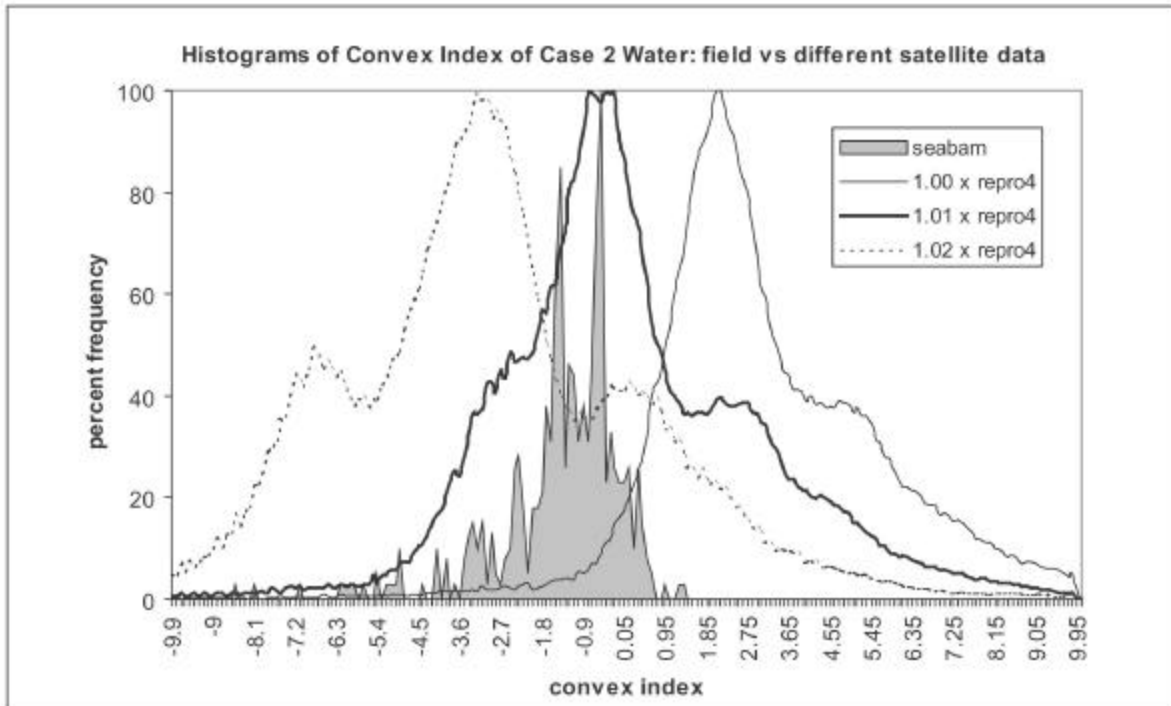


Figure 17.2: The histograms of slope index are shown. In coastal water, most the remote sensing reflectance at 412 nm is often higher than the remote sensing reflectance at 444 (due to strong CDOM absorption). However, this spectral characteristic is seldom observed in SeaWiFS data using repro4 calibration. An adjustment of 1.01 to the MOBY- based calibration of 412 nm would match the statistical distribution of spectral slopes in SeaWiFS imagery to the field data. The Convex index = $(R_{rs444} - R_{rs412}) / (444 - 412) - (R_{rs490} - R_{rs444}) / (490 - 444)$.

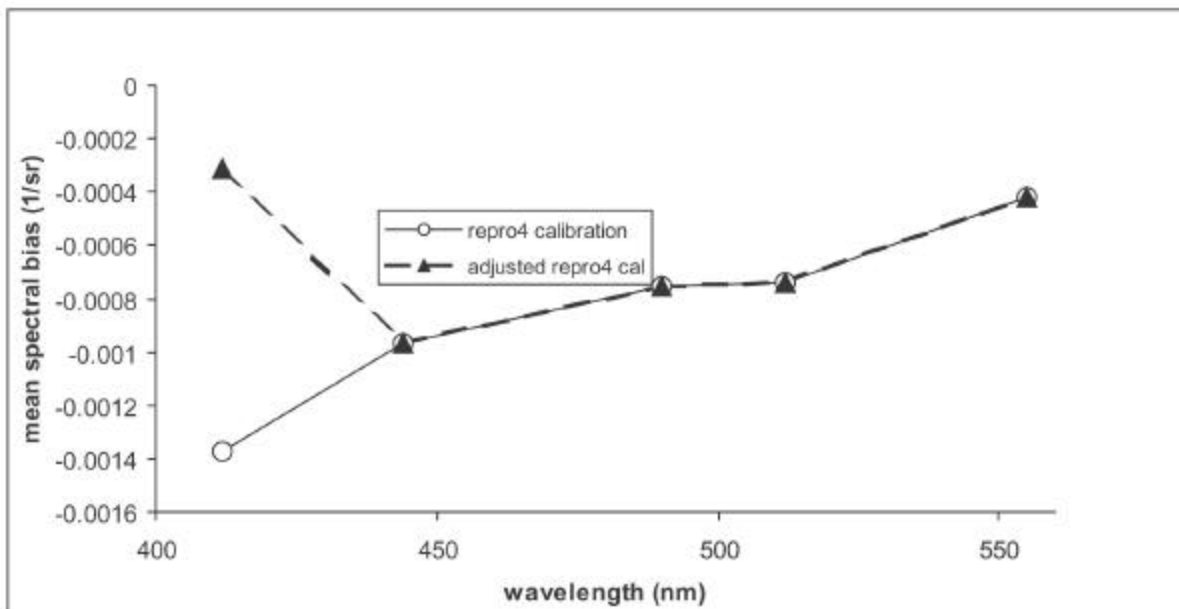


Figure 17.3: For validation, the overall bias of 105 pairs of satellite and same-day measured remote sensing reflectance in US coastal waters was examined for the existing calibration (thin) and the proposed calibration (dash). The new 412 calibration reduced most of the relative bias at 412 nm by four folds.

Remote Sensing Reflectance At 670 Nm (NOAA)

Remote sensing reflectance at 670 nm is used in the NIR correction. Inaccurate remote sensing reflectance at 670 nm would contribute errors in all bands. We have observed large patches of negative remote sensing reflectance at 670 nm near the coast in the North Atlantic. In an effort to identify the problem, we compared SeaWiFS remote sensing reflectance at 670 nm with two modeled estimates in the Sargasso Sea. This area was chosen because of its extremely low chlorophyll characteristics, therefore reducing the number of assumptions made in the models. We observed satellite remote sensing reflectance at 670 nm to be higher than both modeled estimates. This was unexpected, considering that negative remote sensing reflectance has been observed. In conclusion, adjusting the calibration at 670 nm in any direction is not a global solution, indicating that a local problem, possibly in some of the atmospheric correction models, may be producing the negative radiances at 670 nm.

Validation Of Atmospheric Correction And Chlorophyll Algorithms For Processing SeaWiFS Data (NOAA)

With at least four atmospheric corrections and chlorophyll algorithms for SeaWiFS available, a user may be interested in their performances in different water types. To facilitate this comparison, Zhong Ping Lee and Bob Arnone have started an Ocean-Color-Algorithm working Group (OCAG), where the first meeting will take place on November 17, 2002, Sata Fe, NM, prior to the Ocean Optics Conference.

We presented the results comparing atmospheric corrections and five chlorophyll algorithms in different water types at the 7th International Conference on Remote Sensing for Marine and Coastal Environments, Miami, May 2002 (Ransibrahamanukul et al., 2002). We have developed an evaluation protocol to evaluate the performance of the available atmospheric corrections (including the NOAA/NRL developmental atmospheric correction) and chlorophyll algorithms. To date, we have used 159 same-day field-satellite pairs of remote sensing reflectance spectra to determine the best atmospheric correction applicable to the entire US coastline. The five atmospheric corrections considered were developed by Gordon & Wang (1994), Siegel et al. (2000), Gould et al. (1998), Ruddick et al. (2000), and NOAA/NRL (Stumpf et al., in prep). We did not include the atmospheric correction developed by Hu et al. (2000) because it requires manual interaction and is not appropriate for automated processing.

Similarly, we have developed protocols and software for evaluating multiple chlorophyll algorithms for regional application. The analysis involves examination of spatial matches and ranking of the procedures. In both the evaluations of atmospheric correction and chlorophyll algorithms, the selection procedure was designed to determine an algorithm that works best over a range of water types and compensates for distribution biases. The process also allows comparison of the chlorophyll with unique optical properties where algorithms may fail. This occurs in Pamlico Sound, North Carolina, during flood conditions, and in Atchafalaya Bay, Louisiana, under high flow. We are examining the potential factors.

MODIS Terra Processing (NRL)

We are working with the University of Miami and NASA Goddard for processing MODIS ocean color data. We have obtained MODCOLOR and MODSST and implemented on our Linux operating system and integrated it into the Automated Processing System (APS) (Navy's satellite processing software). We have modified the MODIS software with the NIR atmospheric correction used in SeaWiFS processing and implemented coastal algorithms. The output of all the APS is an HDF file format that is directly input into SEADAS or ENVI. Our efforts in MODIS processing required that we closely coordinate efforts with the MODIS Science team and MODIS calibration Science Team. These required updated calibration, level 0 and 2 processing etc. We have worked with the programmers and scientists at University of Miami (Evans group), and Goddard (Esaisas group, and C. Lyons group). They have provided quality data and cooperative efforts which have allowed us the ability to do our research. This cooperation is strongly acknowledged.

We are generating the standard NASA products (Chlorophyll, absorption and scattering) in addition to bio-optical navy algorithms (over 50 products) in both MODIS (TERRA) and SeaWiFS. We are comparing the differences in the sensors for a 2 year period in the Gulf of Mexico by looking at weekly composites. These results are being presented at the Ocean Optics Conference in Nov 02.

We have implemented routine processing of MODIS-TERRA for selected ocean regions in the US (Gulf of Mexico, and Chesapeake Bay) and other areas. We have automated the procedure for transfer and processing of MODIS data from the "MODIS Direct Broadcasting" and the NOAA/NASA Project. We have obtained software and data from MODIS -AQUA but are not currently processing this data routinely. We expect to do this within 2 months.

Other SeaWiFS Activities

- We have developed new methods to understand terrestrial flux from coastal rivers. By unravelling the ocean color signatures into the basic in water constituents; we developed a 2 year time series of SeaWiFS optical properties. We established the covariance of this 2 year satellite time series with river discharge of the Mississippi river.
- We developed new algorithms for extending the satellite near surface chlorophyll algorithms to depth. We assimilate the mixed layer depth and surface wind stress from NCOM with the latest satellite observations and define a vertical profile. This is being performed daily and has been automated for the Gulf of Mexico.
- We developed methods to limit cloud cover by using the spatially and temporally varying time series of satellite imagery. We developed methods of compositing more recent imagery into latest pixel composite. This method has created new products for optimizing ocean color products. We are using these methods for SeaWiFS and MODIS in the Gulf of Mexico.
- We have used the data collected in SIMBIOS to validate the coastal algorithms. We have tested the algorithms used for bio-optical properties (absorption and scattering derived from SeaWiFS). We have published this in Sea Technology.
- We have organized a real time data base on our web server to provide real time access to ocean products. These include SeaWiFS and MODIS sensors. Real time access is available to test algorithm products and determine the sensitivity of the algorithms for SeaWiFS and MODIS. <http://www7333.nrlssc.navy.mil>
- We developed a relationship between absorption and salinity, to derive surface salinity maps from coastal SeaWiFS imagery.
- We developed a relationship between $b(555)$ and total suspended solids (TSS), to derive surface TSS maps from SeaWiFS.
- We linked physical processes (currents, tides, winds, wave resuspension) to optical distribution patterns in northern Gulf of Mexico.
- We developed new algorithms to estimate particulate inorganic matter (PIM) and particulate organic matter (POM) from SeaWiFS imagery.
- We developed new SeaWiFS algorithms to estimate separate CDOM and detritus absorption coefficients, rather than a single combined term. This will facilitate development of a new optical water mass classification system.
- We have improved coastal SeaWiFS optical algorithms through investigation of b_b/b and F/Q parameters.
- We have implemented a new Quasi- Analytical Algorithms (QAA) into the NRL APS processing of SeaWiFS and MODIS for coastal bio-optical algorithms. The QAA is a linearized version of the optimization algorithms which accounts for the majority of the optimization within the computation required. Products of chlorophyll, scattering and absorption from CDOM, phytoplankton and particles are currently being generated. They are available on the web. (Lee et al 2002).
- We have developed automated methods for collection and processing *in situ* ocean optics data for processing of field data. These methods have been applied to all our advanced *in situ* instrumentation. We have organized a calibration laboratory and track all our instrumentation. These include the ac9 and above water reflectance instruments and particle size instrument measurements. Additionally we have developed methods for partitioning particles into organic and inorganic fraction. These new methods are providing measurements for advanced algorithms.

17.4 FUTURE WORK

Between the two groups, NOAA and NRL, we are developing an extensive data set for coastal and case 2 waters. We are in the process of merging the information for examination of remote sensing reflectance and chlorophyll. NRL has a data set from over 21 cruises. There are now 218 vertical profiles, 263 field spectra, and 320 HPLCs. NOAA has approximately 100 same-day match-ups of remote sensing reflectance and chlorophyll from the southeast and Gulf of Mexico. We assembled a database of *in situ* optical properties to evaluate SeaWiFS-derived properties collected from 1997 to present in a variety of coastal regions (Mississippi Bight, Mississippi River, West Florida Shelf, Loop Current, North Carolina, New Jersey). The data cover a broad range of absorption ($0.4 - 15 \text{ m}^{-1}$) and scattering ($0.1 - 27 \text{ m}^{-1}$) coefficients and remote sensing reflectance. The collected data set contributes to the SEABASS database, particular its Case 2 component. In addition to data collection, our groups produced the NIR-iterative technique used by the SeaWiFS project for the fourth reprocessing (repro4). We anticipate the following cruises:

- February, 2003: North Carolina
- April, 2003: North Carolina (including NASA overflights with CDOM and pigment lidar fluorometers and hyperspectral radiometer)
- July, 2003: North Carolina
- August, 2003: Texas (linked to MERHAB cruise)
- October, 2003: North Carolina (with NASA overflights)

Additional cruises in the northern Gulf of Mexico are planned but not yet scheduled. Cruises of opportunity will continue as have occurred in the past two years.

REFERENCES

- Barnes, R.A., R.E. Eplee Jr., W.D. Robinson, G.M. Schmidt, F.S. Patt, S.W. Bailey, M. Wang, and C.R. McClain, 2000: The calibration of SeaWiFS on orbit, *Earth Observing Systems V*, William L. Barnes (eds.), *Proceedings of SPIE*, Vol. **4135**, 281-293.
- Carder, K.L., F.R. Chen, Z.P. Lee, S.K. Hawes, and D. Kamykowski, 1999: Semianalytical moderate resolution imaging spectrometer algorithms for chlorophyll a and absorption with bio-optical domains based on nitrate-depletion temperatures, *Journal of Geophysical Research*, **104**, 5403-5421.
- Fu, G., K.S. Baith, and C.R. McClain, 1998: SEADAS: The SeaWiFS Data Analysis System, *Proceedings of the 4th Pacific Ocean Remote Sensing Conference*, Qingdao, China.
- Gordon, H.R., and M. Wang, 1994: Retrieval of water leaving radiance and aerosol optical thickness over the oceans with SeaWiFS: a preliminary algorithm, *Applied Optics*, **33**, 443-452.
- Gould, R.W. Jr., R.A. Arnone, and M. Sydor, 1998: Testing a new remote sensing algorithm to estimate absorption and scattering in CASE 2 waters, *SPIE Ocean Optics XII*, Hawaii.
- Hu, C., K.L. Carder, and F.E. Muller-Karger, 2000: Atmospheric correction of SeaWiFS imagery over turbid coastal waters: a practical method, *Remote Sensing of Environment*, **74**, 195-206.
- Kahru, K., and G.B. Mitchell, 1999: Empirical chlorophyll algorithm and preliminary SeaWiFS validation for the California Current, *International Journal of Remote Sensing*, **20**, 34323-3429.
- O'Reilly, J.E., S. Maritorena, G.B. Mitchell, D.A. Siegel, K.L. Carder, S.A. Garver, M. Kahru, and C. McClain, 1998: Ocean color chlorophyll algorithms for SeaWiFS, *Journal of Geophysical Research*, **103**, 24937-24953.
- Ransibrahmanakul, V., and R.P. Stumpf, 2001: Refining SeaWiFS Vicarious Calibration Using Spectra Slopes, *American Geophysical Union*, 2001 Fall Meeting, San Francisco.
- Ransibrahmanakul, V., R.P. Stumpf, S. Ramachandran, H. Gu, R. Sinha, and K. Hughes, 2002: Evaluation of atmospheric correction and chlorophyll algorithms for processing SeaWiFS data. *Seventh International Conference on Remote Sensing for Marine and Coastal Environments*, Miami.
- Ruddick, K., F. Ovidio, and M. Rijkeboer, 2000: Atmospheric correction of SeaWiFS imagery for turbid coastal and inland waters, *Applied Optics*, **39**, 897-912.
- Siegel, D., M. Wang, S. Maritorena, and W. Robinson 2000: Atmospheric correction of satellite ocean color imagery: the black pixel assumption, *Applied Optics*, **39**, 3582-3591.
- Siegel, S., 1956: *Nonparametric statistics for the behavioral sciences*. McGraw-Hill Book Company, New York.

- Stumpf, R.P., R.A. Arnone, R.W. Gould, P. Martinolich, V. Ransibrahmanakul, P.A. Tester, R.G. Steward, A. Subramaniam, M.E. Culver, and J.R. Pennock, 2000: SeaWiFS ocean color data for US Southeast coastal waters, *Sixth International Conference on Remote Sensing for Marine and Coastal Environments*, Veridian ERIM Intl. Ann Arbor, 25-27.
- Stumpf, R.P., R.A. Arnone, R.W. Gould, Jr., P. Martinolich, V. Ransibrahmanakul, 2002: A Partially-Coupled Ocean-Atmosphere Model for Retrieval of Water-Leaving Radiance from SeaWiFS in Coastal Waters: In: Patt, F.S., and et al., 2002: Algorithm Updates for the Fourth SeaWiFS Data Reprocessing. *NASA Tech. Memo. 2002--206892*, Vol. 22, S.B. Hooker and E.R. Firestone, Eds., NASA Goddard Space Flight Center, Greenbelt, Maryland, (in press).
- Stumpf, R.P., M.E. Culver, P.A. Tester, M. Tomlinson, G.J. Kirkpatrick, B.A. Penderson, E. Truby, V. Ransibrahmanakul, M. Soracco. Monitoring *Karenia brevis* blooms in the Gulf of Mexico using satellite ocean color imagery and other data, *Harmful Algae* (in press).

Chapter 18

Varied Waters and Hazy Skies: Validation of ocean color satellite data products in under-sampled marine areas: II

Ajit Subramaniam

University of Maryland, College Park, Maryland

Edward J. Carpenter

University of Southern California, California

Douglas G. Capone

U SUNY at Stony Brook, New York

18.1 INTRODUCTION

“Airborne plumes of desert dust from North Africa are observable all year on satellite images over the Tropical Atlantic. In addition to its radiative impact, it has been suggested that this mineral dust has a substantial influence on the marine productivity. This effect is however difficult to gauge because present atmospheric correction algorithms for ocean color sensors are not capable of handling absorbing mineral dust” (Moulin *et al.* 2001). In order to validate atmospheric correction algorithms for ocean color sensor with an independent set of in-situ optical measurements and to fill in gaps in satellite data, a turnkey, stand-alone optical package consisting of Satlantic OCR-507 irradiance and radiance sensors and WETLabs ECO DFLSB fluorometers was deployed on the PIRATA mooring at 8° N, 38° W on the 9th of April, 2002 (Figure 18.1). The normalized water leaving radiance derived from the *in-situ* measurements provided by this project can be compared to those calculated from satellite measurements and will thus allow us to evaluate algorithms for absorbing mineral dust. The normalized water leaving radiance can also be used in conjunction with algorithms such as OC4 (O’Reilly *et al.* 2000) to calculate chlorophyll concentrations as well as with semi-analytical algorithms such as GS97 (Garver and Siegel, 1997) to derive colored dissolved organic matter absorption, backscatter at 555 nm etc. Independent measures of the diffuse attenuation coefficient, especially in the Amazon River plume will help in radiation budget models. In addition, other algorithms such as that used to detect *Trichodesmium* (Subramaniam *et al.*, 2001), can also be used for calculating additional parameters. The effect of dust on marine productivity especially that of diazotrophs such as *Trichodesmium* can be studied by looking at changes in biomass following a dust event. These mooring based measurements will also provide daily high resolution chlorophyll data from the tropical Atlantic even in the presence of clouds and hence will fill in missing satellite based measurements. Both SeaWiFS and MODIS have gaps in daily coverage due to change in tilt or orbit parameters and hence daily equatorial data is not available even for clear skies. The WETLabs ECO fluorometers provide an additional measure of chlorophyll concentration at the two depths to compare against the optically derived estimate as well as to estimate for depth dependent changes if any.

The Satlantic sensors are powered by a battery pack, have 128MB of local storage for all the data collected, and also have their own Argos telemetry package. The instrument suite is programmed to make measurements every 2 hours of about 30 seconds duration each day, from 8AM to 6 PM local time (1400 UTC). While all the measurements are being stored locally on the STORE-X, the very first set of the noontime measurement from each of the three radiometers is being telemetered real-time through the Argos satellite to keep track of sensor viability. Each fluorometer is powered by its own 9V batteries that provide 4000 mA hours of operation and has its own 64kB storage device that can store up to 10,910 samples.

The OCR-507 sensors are 7 channel digital spectroradiometers with bioshutters added for these long-term deployments to protect their sensors heads against biofouling or dust deposition. The wavelengths were chosen to match the mix of channels available on the MODIS and SeaWiFS sensors. The mooring has one irradiance sensor (OCR-507-ICSA s/n 0048) above the

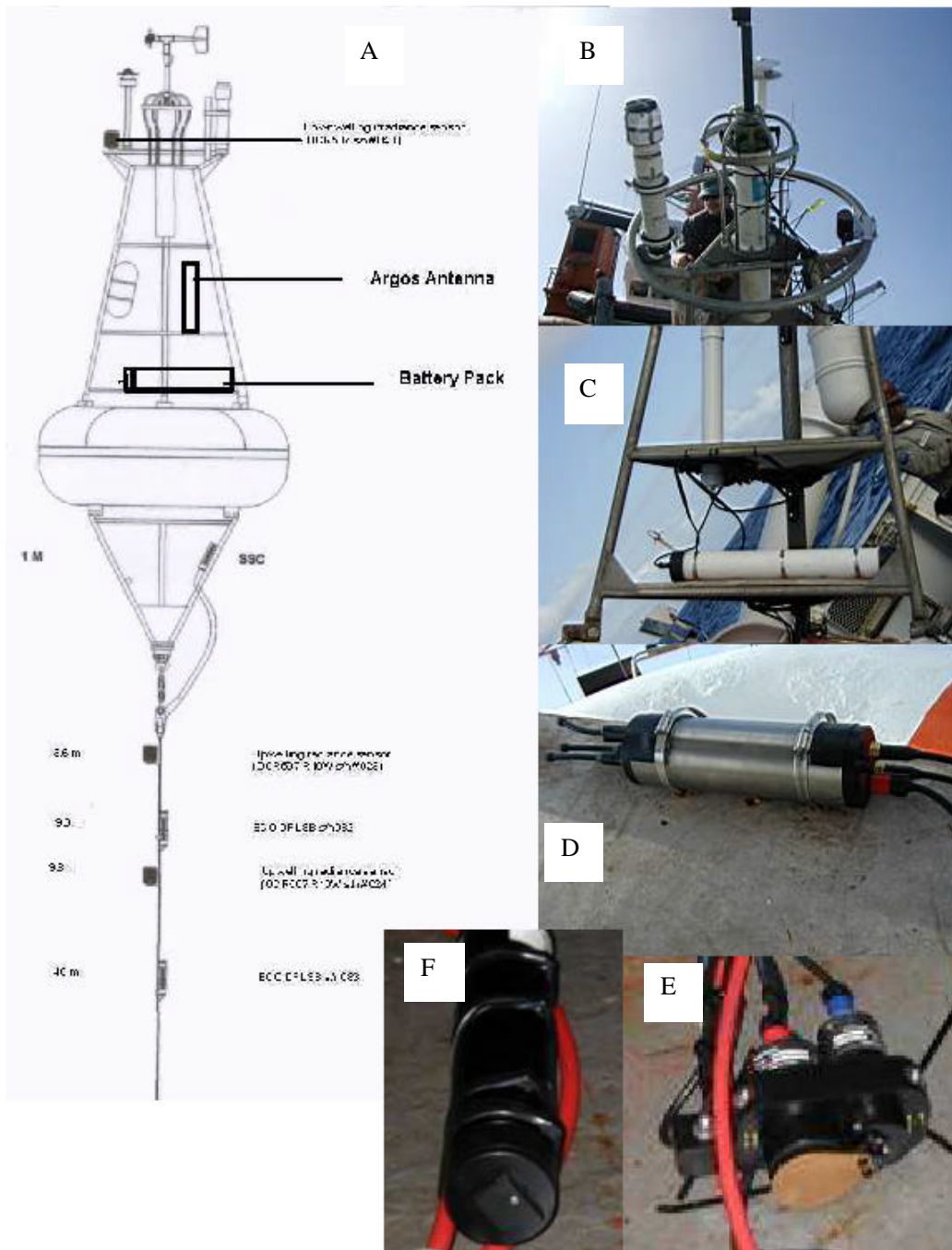


Figure 18.1: Optical sensors on the Lambda mooring (8N, 38W). A) A schematic of the TAO buoy showing the locations of the various instruments. B) The downwelling irradiance sensor is placed on the top ring of the buoy and is not under the shadow of any other instrument. C) The Argos transmitter (the vertical white tube) and the battery pack (the horizontal white tube) are connected to the STORE-X (seen in D). E) The upwelling radiance sensors are normally covered by the copper bioshutter and mounted at 3.6 m and 9.6 m below the surface. F) The fluorometers, placed 9 and 40 m below the surface, have shutters that open only when the measurements are made.

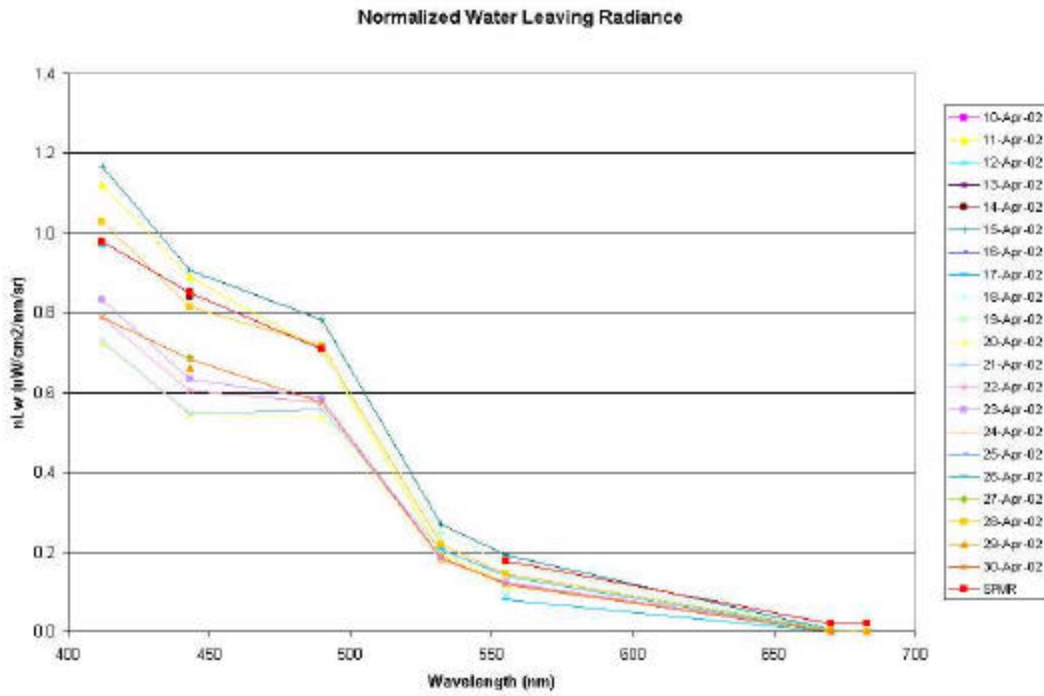


Figure 18.2: Daily Downwelling Irradiance through 30 April 2002. The first data point (9th April was made with the SMSR).

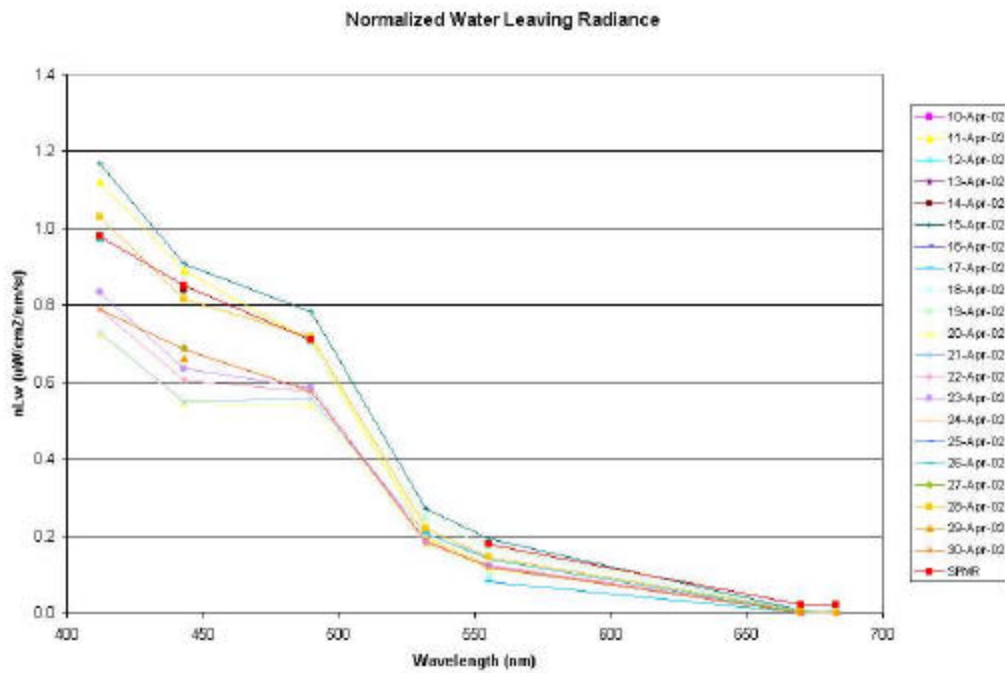


Figure 18.3: Spectra of Normalized Water Leaving Radiance through 30 April 2002. The measurement made with the SPMR on the 9th of April is also shown for comparison

surface and two radiance sensors at 3.6m and 9.6m (OCR-507-R10W s/n 0023 and OCR-507-R10W s/n 0023 respectively) below the surface. The irradiance sensor is placed on the superstructure of the buoy and measures downwelling irradiance at 412, 443, 490, 532, 555, 670 and 865 nm (10 nm FMHH). The OCR-507R (serial # 023 and 024) are radiance sensors and measure *in-situ* upwelling radiance at 412, 443, 490, 532, 555, and 683 nm. The “Bioshutters” are similar to that described by Chavez *et al.* (2000) and used very successfully in the Pacific Ocean. They consist of copper paddles attached to a shaft and a motor. The copper paddles cover the sensor when not in use, opening only when measurements are to be made. Copper is toxic at high concentrations and the plate corrodes in seawater to produce a toxic layer that is trapped between the shutter and the sensor when it is closed. The combination of this toxic layer and darkness seems to eliminate the formation of biofilms. Chavez *et al.* 2000 showed that sensors protected with these copper shutters provided acceptable data for at least five months, the length of their deployment. In contrast, unprotected sensors at the same site lasted only about two months before there was evidence of biofouling. The Bioshutter on the irradiance head should prevent build up of salt and dust on the sensor.

The WETLabs ECO DFLSB (s/n #082 and 083) fluorometers were deployed at 9m and 40m respectively and have their own version of bioshutters consisting of a copper plate and a brush that protect the sensor head against biofouling (Figure 18.3F). The fluorometers are programmed to sample every three hours, thus making 8 measurements per day.

18.2 RESEARCH ACTIVITIES

The upwelled diffuse attenuation coefficient (K_L) can be determined from the L_u sensors (OCR R 023 and 024) at 3.6m (Z_1) and 9.6m (Z_2) using:

$$K_L(I) = \frac{1}{z_2 - z_1} \ln \left[\frac{L_u(z_1, I)}{L_u(z_2, I)} \right]$$

The upwelling radiance then propagated to the surface using:

$$L_u(0^-, I) = L_u(z_2, I) \exp[K_L(I)z_2]$$

and then propagated through the water/air interface using:

$$L_w(0^+, I) = \frac{T_F}{n^2} L_u(0^-, I)$$

where T_F is the Fresnel transmittance of the water-air interface, and n is the index of refraction of seawater. Normalized water leaving radiance is calculated from this using:

$$nL_w = L_w(0^+, I) \frac{F^0(I)}{E_s(I)}$$

where F^0 is the mean extra terrestrial solar irradiance and E_s is the downwelling irradiance measured by OCR I 048.

Contemporaneous freefalling spectroradiometric cast and mooring based measurement was not permitted during the PIRATA V cruise. However, the site was sampled using a Satlantic 13 channel freefalling spectroradiometer (SPMR) with freefloating surface reference (SMSR) the day before (9 April 2002) the moored instruments went operational (10 April 2002). The SMSR measurements of above surface downwelling irradiance and the SPMR/SMSR based normalized water leaving radiance seem to be comparable to the measurements derived from the moored sensors (Figures 18.2 and 18.3). The maximum incoming short-wave radiation measured by the Eppley pyronometer on the buoy is also shown to compare variability due to clouds (Figure 18.2). A perfect one to one match is not seen between these two measurements because the Eppley measurements are the maximum values for the day rather than the measurement at noon coincident with the OCR irradiance measurements. A few data points that did not pass the quality control check have been removed from the normalized water leaving radiance plot (Figure 18.3). These data were mostly due to bad irradiance measurements by OCR023 at 3.6m. Sometimes an acquisition period could end while the program is in the midst of collecting a frame from an instrument and the system would then errantly use this partial record during the next acquisition cycle. This causes corruption of the first frame collected during that cycle but should not affect following frames. This bug was recently noted and corrected in a new version of the STOR-X software. Microtops sunphotometer Aerosol optical thickness data were acquired at 8 additional stations during this cruise.

In addition, we participated in a cruise in the Pacific Ocean from 21 September to 17 October 2002, working around the Hawaiian Islands (Figure 18.4). Twenty-one stations were sampled for IOP and AOP parameters in addition to various biological, chemical and physical parameters. The data from this cruise is still being worked up. We have participated in 4

short 1-day cruises in Massachusetts Bay in February, April, July and October. We assisted in the Akademik Ioffe cruise in December-January 2002, the details of which are covered in the report by Frouin (see chapter 6).

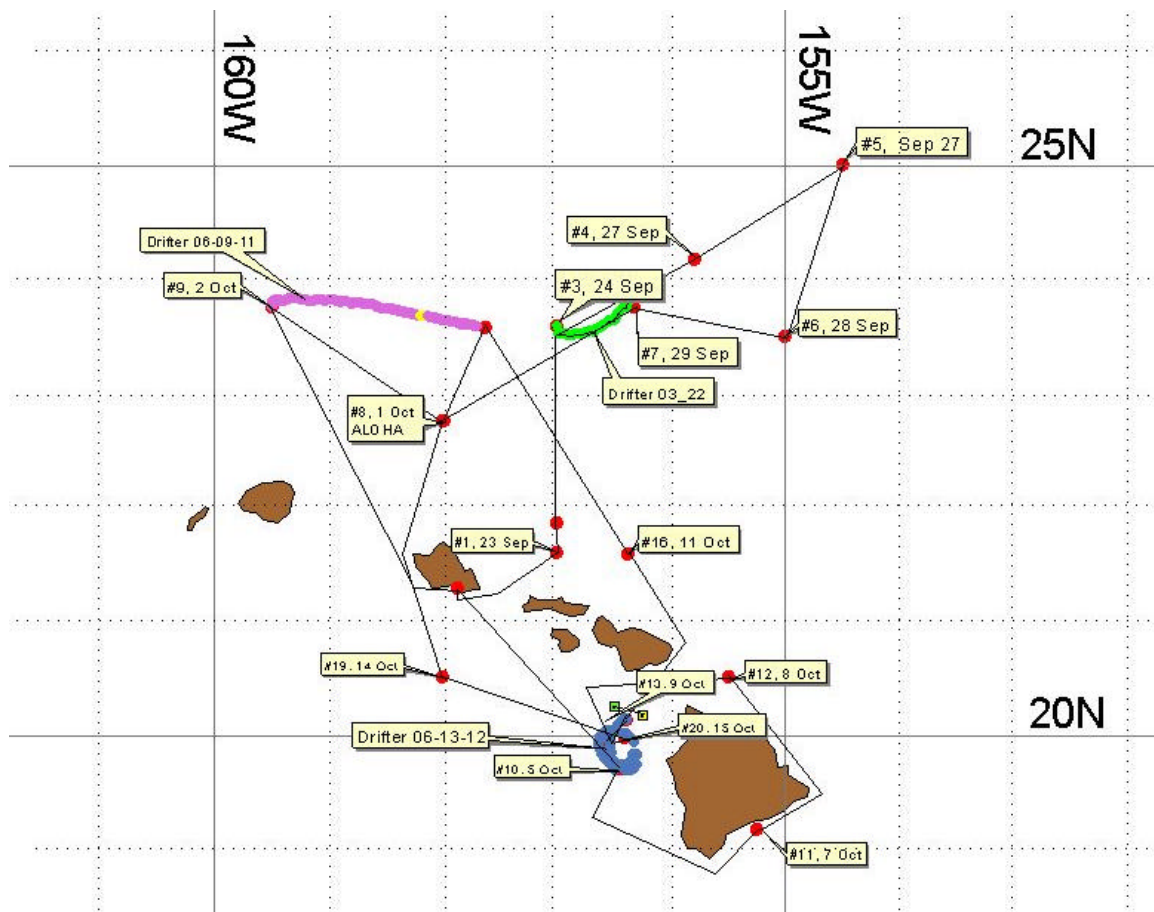


Figure 18.4: Cruise track of the SEP02PAC (MP6) cruise in September-October 2002.

REFERENCES

- Chavez, F. P., D. Wright, R. Herlien, M. Kelley, F. Shane and P. G. Strutton, 2000: A Device for Protecting Moored Spectroradiometers from Biofouling, *Journal of Atmospheric and Oceanic Technology*, **17**, 215-219.
- Garver, S. A. and D. A. Siegel, 1997: Inherent optical property inversion of ocean color spectra and its biogeochemical interpretation. 1. Time series from the Sargasso Sea, *Journal of Geophysical Research*, **102**(C8), 18,607-18,625.
- Moulin, C., H. R. Gordon, R. M. Chomko, V. F. Banzon and R. H. Evans, 2001: Atmospheric correction of ocean color imagery through thick layers of Saharan dust, *Geophysical Research Letters*, **28**(1), 5-8.
- O'Reilly, J. E., and et al. 2000: Ocean color chlorophyll a algorithms for SeaWiFS, OC2 and OC4: Version 4, SeaWiFS Postlaunch Calibration and Validation Analyses, part 3, NASA Goddard Space Flight Center, 8-22.
- Subramaniam, A., R. R. Hood, C. W. Brown, E. J. Carpenter and D. G. Capone, 2001: Detecting *Trichodesmium* Blooms in SeaWiFS Imagery, *Deep-Sea Research. Part II*, Vol. **49**, 107-121.

Chapter 19

HPLC Pigment Measurements For Algorithm Development and Validation in Support of the SIMBIOS Science Team

Charles C. Trees and Jason R. Perl

Center for Hydro-Optics and Remote Sensing, San Diego State University, California

19.1 INTRODUCTION

Remotely sensed ocean color is determined by the absorption and scattering properties of dissolved organic material and suspended particulates. In most oceanic and many coastal areas, phytoplankton and their associated suite of pigments dominate the optical signal viewed by satellite sensors. Because these pigments have distinct spectral signatures, changes in the pigment-algal assemblage result in spectral shifts in absorption and reflectance. Therefore, accurate measurements of phytoplankton pigments are essential in understanding global carbon cycles in the ocean by minimizing satellite retrieval uncertainties when mapping these properties at regional to global scales.

The focus of this program is to characterize phytoplankton pigments in the water column during NASA's Sensor Intercomparison and Merger for Biological and Interdisciplinary Oceanic Studies (SIMBIOS) Project. This research is to provide high performance liquid chromatography (HPLC) pigment analysis on samples collected by the SIMBIOS Science Team for bio-optical algorithm validation and development. This effort will provide the SIMBIOS Project with an internally consistent pigment database of the highest quality to evaluate ocean color products.

19.2 RESEARCH ACTIVITIES

In January 2002, the PI and Mr. Perl participated in the SIMBIOS Science Team Meeting. At the meeting, a comparison of HPLC results between CHORS and Horn Point Laboratories (HPL) were reported. Discussion on a second round robin was also discussed. Norm Nelson (UCSB), volunteered to collect samples from a station in Bermuda and supply replicates for Round Robin analysis. Samples were sent to CHORS as well as to HPL. Mr. Perl and Laurie Van Heukelem (HPL) organized the comparison of the Bermuda samples and additional standard samples to complete this round robin, which was run on the HPLC on June 24, 2002.

In late January, we sent the FL3000 fluorometer to Thermo Finnigan for repair. They replaced the lamp and lamp socket. In March, a new HPLC column (Alltech spherisorb column, ODS-2 5um) as well as a primary calibration of the detectors was performed.

During the June 02 HPLC run (started June 5, 2002), it was determined that a software problem between ChromoQuest and Microsoft Windows NT existed. Since it was not a hardware problem, and the data quality was not compromised, the HPLC continued to run. Mr. Perl found that restarting the computer every four days during a run kept the system from freezing, eliminating the random computer crashes seen previously.

In June 2002, CHORS received a new Digital Turner 10-AU Fluorometer for comparisons with the HPLC. Various calibrations were performed and comparisons between the CHORS analog Turner Fluorometer and the digital model were made. There is some variation between the Analog and the Digital models. This may be due to a difference in lamp type between the two machines. The digital Fluorometer contains a Turner "D" Daylight White Lamp, the analog machine contains

During data analysis of multiple sample sets in June 2002, Mr. Perl discovered that the response factor for Chlorophyll c3 (Chl_c3) was off by a factor of 10. After reviewing the archived calibration data, it was determined that DHI Denmark may have reported incorrect concentration values for the Chl_c3 standards (this error was later confirmed by Louise Schluter from DHI Denmark). Based on the calibration of March 2002, and calibrations conducted by Dr. Trees in 2001, it was decided that Chl_c3 response factors, and concentrations for the samples sets run between June 2001 and December 2001, should be

corrected. Mr. Perl sent out correction factors to the PI's to adjust their data sets, and requested that each PI re-submit the data to SeaBASS with the corrected Chl_c3 values.

The CHORS/ Horn Point Labs (HPL) Round Robin experiments continued, with a second set of samples simultaneously run at CHORS and HPL during the last week of June 2002. Samples were provided by Norm Nelson (12) and Larry Harding (12). The results were discussed during a conference call on 6 August (J. Perl, L. Van Heukelem, G. Fargion, L. Harding, and C. Trees participated in the call). The results showed that CHORS and HPL were not statistically different in carotenoid pigment concentrations. Concentrations for chlorophyll c₂ and c₃ were different, but the summation of "Total Chlorophyll c" was similar. Chlorophyll *a* (both monovinyl and divinyl *a*) concentrations determined by the two laboratories continued to differ significantly. This difference may be due to calibration and response factor differences between CHORS and HPL. Further comparisons were discussed, with CHORS scheduled to participate in SeaHarre-2 (December 2002).

In July 2002, the UV6000 Photodiode Array Detector (PDA) required lamp replacement due to lamp degradation. In addition, the light intensity was low, and the detector required servicing from Thermo Finnigan. During this quarter, Mr. Perl included multiple, primary and secondary, calibrations to verify the repairs on the detector maintained the overall system calibration. It should be noted, that the response factor for Chlorophylls *a* and *b*, did not vary throughout the PDA problems, lamp replacements, detector replacements, and re-calibrations (3 separate detector calibrations). In fact, the coefficient of variation of the Chlorophyll *a* response factor is 2.07%, with Chlorophyll *b* at 3.92% for these calibrations.

Final HPLC results have been sent out for July 02, August 02, and September 02 data sets. We are currently comparing archived Fluorometric comparisons between the Digital and Analog versions of the Turner Fluorometer. The final Fluorometric results will be submitted to the PI's once the comparison is completed.

At the time the annual report was submitted, data from the Oct 2002 run were being processed, and an additional Nov 2002 HPLC set was being run on the system. These results will be reported in FY2003.

19.3 RESEARCH RESULTS

CHORS processed 3,471 pigment samples (total delivered = 3,492 samples) sent during the second year of support. Less than 1% of the samples were not processed due to a variety of reasons, including, improperly charged shipping dewars, samples arriving thawed out, cryovials received without filters, and mislabeled samples. Any inconsistencies between the samples delivered and those listed on the PI's data logs, were noted in each final report submitted.

Overall, the calibration of the HPLC detectors has remained within an acceptable range. For calibrations from May 2001 through September 2002, the variation of Chlorophyll *a* correction factors was 4.55%, and that for Chlorophyll *b* was 4.82% .

19.4 FUTURE WORK

Laboratory intercalibration effort will continue with CHORS participating in SeaHarre-2 (December 2002). The number of samples expected to be processed in FY2003 are approximately 4,000. I have requested that the PI's ensure that filter collection, numbering and storage meticulously follow SIMBIOS protocols.

Chapter 20

Assessment, Validation, and Refinement of the Atmospheric Correction Algorithm for the Ocean Color Sensors

Menghua Wang

University of Maryland, Baltimore County, Baltimore, Maryland

20.1 INTRODUCTION

The primary focus of this proposed research is for the *atmospheric correction algorithms evaluation and development and satellite sensor calibration and characterization*. It is well known that the atmospheric correction, which removes more than 90% of sensor-measured signals contributed from atmosphere in the visible, is the key procedure in the ocean color remote sensing (Gordon and Wang, 1994). The accuracy and effectiveness of the atmospheric correction directly affect the remotely retrieved ocean bio-optical products. On the other hand, for ocean color remote sensing, in order to obtain the required accuracy in the derived water-leaving signals from satellite measurements, an on-orbit vicarious calibration of the whole system, i.e., sensor and algorithms, is necessary. In addition, it is important to address issues of (i) cross-calibration of two or more sensors and (ii) in-orbit vicarious calibration of the sensor-atmosphere system. The goal of these researches is to develop methods for meaningful comparison and possible merging of data products from multiple ocean color missions. In the past year, much efforts have been on (a) understanding and correcting the artifacts appeared in the SeaWiFS-derived ocean and atmospheric products; (b) developing an efficient method in generating the SeaWiFS aerosol lookup tables, (c) evaluating the effects of calibration error in the near-infrared (NIR) band to the atmospheric correction of the ocean color remote sensors, (d) comparing the aerosol correction algorithm using the single-scattering epsilon (the current SeaWiFS algorithm) vs. the multiple-scattering epsilon method, and (e) continuing on activities for the International Ocean-Color Coordinating Group (IOCCG) atmospheric correction working group. In this report, I will briefly present and discuss these and some other research activities.

20.2 RESEARCH ACTIVITIES

- It has been found that, at the certain solar and sensor-viewing geometry and for certain atmosphere conditions, discontinuity lines appear in the SeaWiFS retrieved atmospheric and ocean color products. Such discontinuity lines, which do not happen very often, are apparently artifacts from the atmospheric correction scheme that uses the lookup tables to process SeaWiFS data. A study has been carried out to understand these artifact effects of the SeaWiFS atmospheric correction algorithm, which result in discontinuities in the SeaWiFS-retrieved atmospheric and ocean color products at the certain solar and sensor-viewing geometry and for certain atmosphere conditions (Wang, 2002a). It was found that the artifacts of the atmospheric correction are resulted from the model across in the epsilon values of two significantly different aerosol models, i.e., the aerosol reflectance contribution at the visible can not be well characterized by the corresponding single-scattering reflectance at the two NIR bands. To correct these artifacts, a simple modification to the current atmospheric correction algorithm is proposed and tested with both the simulated and the SeaWiFS data. Results show that, with a simple modification to the algorithm in the case of the model across with two aerosol models, the discontinuities appearing in the derived ocean color and atmospheric products can be effectively removed. This modification scheme has been implemented in the SeaWiFS 4th data reprocessing in August 2002.
- An efficient method for the multiple radiative-transfer computations is developed (Wang, 2002b). The purpose of this work is for generating the aerosol lookup tables (e.g., for SeaWiFS) more efficiently. Therefore, it is easy to test for various aerosol models. The method is based on the fact that, in the radiative-transfer computation, most of the CPU time is used in the numerical integration for the Fourier components of the scattering phase function. With the new method, the lookup tables, which are usually needed to convert the spaceborne and the airborne sensor-measured signals to the desired

physical and optical quantities, can be generated efficiently. The CPU efficiency of a factor of more than 6 can be achieved using the new method in generating the SeaWiFS lookup tables. The new scheme is useful and effective for the multiple radiative-transfer computations.

- In collaboration with Prof. H. R. Gordon, a study was completed (Wang and Gordon, 2002) to evaluate the effects of calibration error in the NIR band to the ocean color remote sensors. It is shown that as long as the calibration error at NIR band less than ~10% in magnitude, the post-vicarious-calibration-corrected radiances are sufficiently accurate to retrieve useful water-leaving radiances. This is completely independent of the initial calibration error in the short-wave bands. The results immediately suggest that pre-launch calibration is necessary only to the extent required to set the sensitivity of the instrument in the desired range. Rather than trying to achieve a highly accurate pre-launch calibration, resources would be better expended on improved radiometric stability and complete characterization of the instrument.
- A study has been carried out to compare the aerosol correction algorithm using the single-scattering epsilon (the current SeaWiFS algorithm) (Gordon and Wang, 1994) vs. the multiple-scattering epsilon (Su, 2000) method. Simulations show that, when the testing aerosol is identical to one of the candidate aerosol models that are used for the atmospheric correction, the exact solutions are more likely to be obtained using the multiple-scattering epsilon method, i.e., errors in the derived normalized water-leaving radiance are nearly to zero. For aerosols that are different from the candidate aerosol models (realistic case), results show that the atmospheric correction using the single-scattering epsilon method usually performed better than those using the multiple-scattering epsilon method.
- I have been continuing on activities for the IOCCG atmospheric correction working group. The main objective of the working group is to quantify the performance of the various existing atmospheric correction algorithms used for the various ocean color missions. Therefore, the derived ocean color products from various ocean color missions can be meaningfully compared and possibly merged. During the past year, I have been working with H. R. Gordon, R. Frouin, and the POLDER team to deal with issue that two different assumptions were used in deriving the ocean color products: (a) the water-leaving radiance is uniform just *beneath* the ocean surface and (b) the water-leaving radiance is uniform just *above* the ocean surface.
- I have been closely working with the SeaWiFS and SIMBIOS projects at NASA Goddard Space Flight Center, providing helps and many discussions. For example, I have spent a lot of time in evaluating and helping the SeaWiFS 4th data reprocessing completed in August 2002. In particular, I worked with and helped Dr. Tasuku Tanaka, the SIMBIOS visiting scientist from NASDA of Japan, for the radiative transfer computations with both the Rayleigh and aerosol atmospheres for the development of the high order scattering (double and triple scattering) formula for the TOA reflectance (Tanaka and Wang, 2002).

20.3 RESEARCH RESULTS

Some results are briefly reported in here due to the length limitation for the document and also due to preliminary nature for some of on going works.

Correction Of Artifacts In The SeaWiFS Atmospheric Correction Algorithm

Since it was launched on August 1, 1997, SeaWiFS has been continuously providing global ocean color and atmospheric products (McClain et al., 1998). It has been found, however, that for some atmospheric conditions and at certain solar and sensor-viewing geometry, discontinuity lines appear in the SeaWiFS-retrieved atmospheric and ocean color products. Figure 20.1 provides examples of such cases for the SeaWiFS-derived aerosol optical thickness at 865 nm $t_a(865)$ and the normalized water-leaving radiance at 412 nm $[L_w(412)]_w$. These images were derived from the SeaWiFS data (file name S1998138130801), which were acquired on May 18, 1998 from the Bay of Biscay at location around 46°N of latitude and 9°W of longitude. Figs. 1(a) and 1(b) are SeaWiFS-derived aerosol optical thickness at 865 nm $t_a(865)$ (scaled from 0–0.3) and the normalized water-leaving radiance at 412 nm $[L_w(412)]_N$ (scaled from 0–2 mW cm⁻² μm⁻¹ sr⁻¹) using the original correction algorithm. At the scene center part of image, the solar-zenith angle is ~28°, the sensor-zenith angle is ~23°, and the relative azimuth angle varies from ~168° to 177°. Both Figs. 1(a) and 1(b) show discontinuity lines. In the discontinuity regions, values of the aerosol optical thickness are artificially higher, while the normalized water-leaving radiances $[L_w(\lambda)]_N$ are artificially lower, than those at the nearby regions. The discontinuity lines in these images are corresponding to the constant scattering angle Θ (composed with vector of the solar and sensor viewing directions) of about 172°–176°. These

discontinuity lines are obviously not real. They are artifacts resulting from imperfect performance of the SeaWiFS atmospheric correction. To remove the discontinuities, a simple modification to the current atmospheric correction algorithm is developed and tested with both simulated and real SeaWiFS data. Figs. 20.1(c) and 20.1(d) show results in which data were processed with the modified code. Results in Figs. 20.1(c) and 20.1(d) can be directly compared with those in Figs. 20.1(a) and 20.1(b).

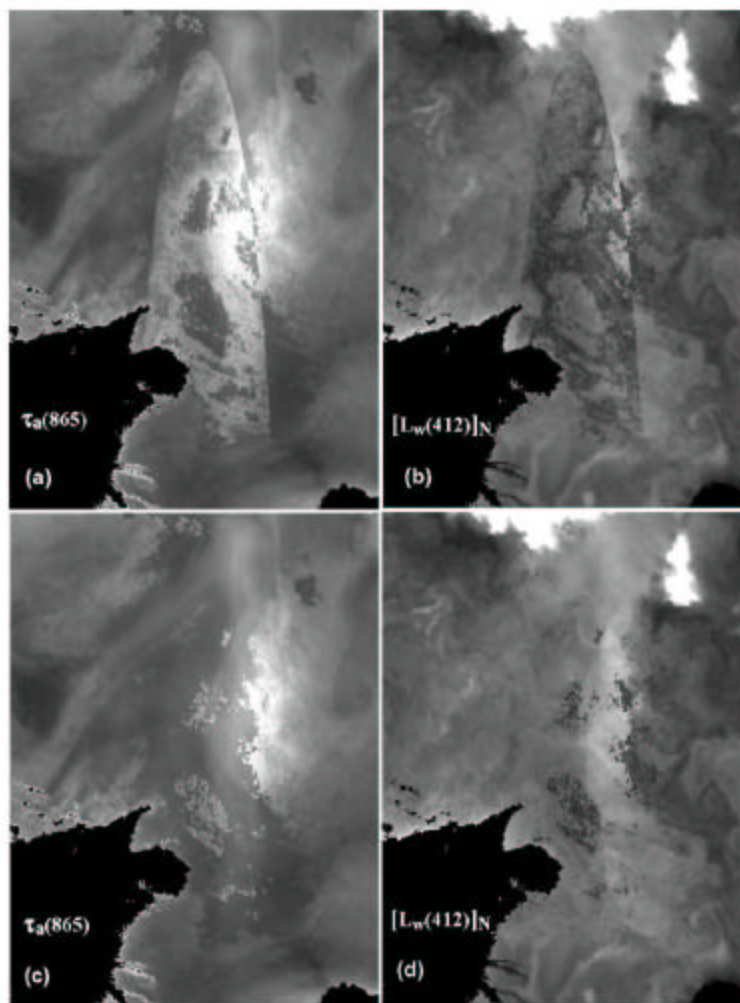


Figure 20.1. Example of the discontinuity case for (a) and (c) the aerosol optical thickness at 865 nm $\tau_a(865)$ (scaled from 0–0.3); and (b) and (d) the normalized water-leaving radiance at 412 nm $[L_w(412)]_N$ (scaled from 0–2 $\text{mW cm}^{-2} \mu\text{m}^{-1} \text{sr}^{-1}$). Results in (a) and (b) were derived with the original algorithm, while those in (c) and (d) were obtained with the modified algorithm.

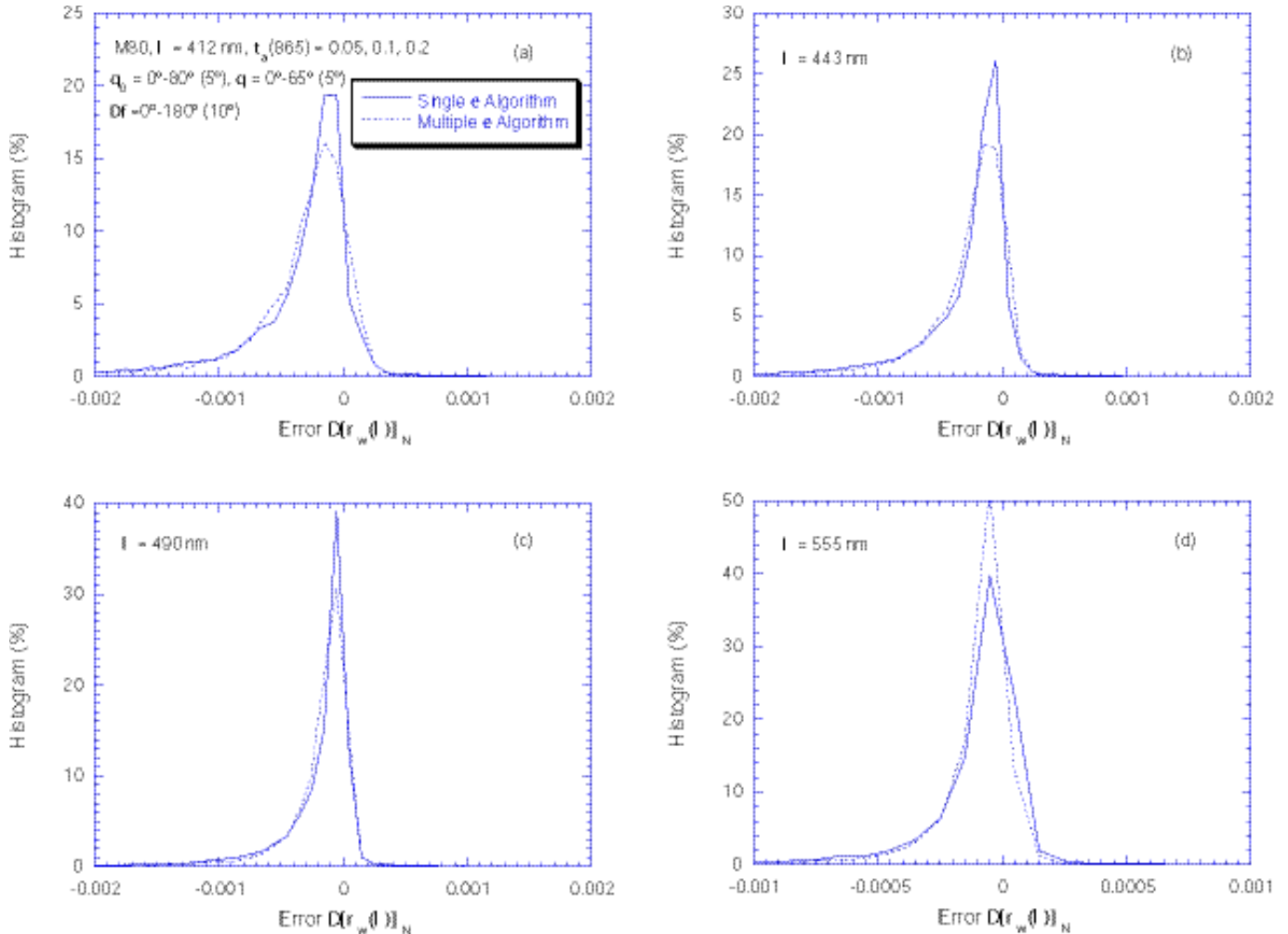


Figure 20.2. Histogram as a function of the error in the retrieved normalized water-leaving reflectance using the SSE and MSE methods for M80 aerosol with all possible solar-sensor viewing geometries and aerosol optical thicknesses of 0.05, 0.1, and 0.2 for the wavelength of (a) 412 nm; (b) 443 nm; (c) 490 nm; and (d) 555 nm.

Clearly, the discontinuities are removed with the proposed modifications to the algorithm. The modification has been implemented in the SeaWiFS 4th data reprocessing in August 2002 (Wang, 2002a).

An Efficient Method For The Lookup Table Generation

In an effort to increase efficiency in generating the lookup tables, a study has been carried out to understand the CPU time distribution in solving both the scalar and vector radiative transfer equations (Wang, 2002b). It is found that the most of the CPU time is used in the numerical computation for the Fourier component of the phase function and phase matrix for the scalar radiative transfer equation (SRTE) and the vector radiative transfer equation (VRTE) case, respectively. Therefore, a new approach in constructing and running the SRTE and VRTE codes is proposed and tested with various cases. Results show that, to generate the SeaWiFS lookup tables with SRTE code, it requires about one month CPU time (one SGI IRIX64 computer) with conventional method, while it is reduced to about five days with the new method. On the other hand, it would need about three and half years to generate the SeaWiFS lookup tables with the VRTE code using the conventional method, while it can be reduced to about 139 days with the new approach. Therefore, by using the new method, it is possible to generate the lookup

tables with including the polarization effects. This method is also useful and effective for the multiple radiative-transfer computations.

Effects Of Calibration Error At The NIR Band

A fictive vicarious calibration, in the spirit of that suggested by Gordon (Gordon, 1998), for a SeaWiFS-like sensor have been carried out using simulated data (Wang and Gordon, 2002). It is shown that when the water-leaving reflectance is precisely measured, but the atmospheric measurements have errors leading to a close, but incorrect, choice of the vicarious calibration (VC) aerosol model to predict the contribution of the aerosol component, the residual error in the calibration in the blue is small even for a $\pm 15\%$ calibration error at 865 nm. In addition, using the VC-corrected TOA reflectances, the resulting error in the Gordon and Wang (Gordon and Wang, 1994) retrieved water-leaving reflectance at 443 nm is always less than ± 0.002 , and often less than ± 0.001 , as long as the calibration error at 865 nm is less than $\sim 10\%$. These results are completely independent of the initial calibration error in spectral bands below 865 nm. This suggests that the pre-launch calibration is necessary only to the extent required to set the sensitivity of the instrument in the correct range, i.e., to achieve approximately the correct saturation radiances for each band. Therefore, it is believed that there is no reason to try to achieve highly accurate pre-launch calibration. Resources would be better expended to assure the highly desired radiometric stability, better monitoring of the stability, characterizing the instrument. These conclusions assume the presence of a permanent VC facility such as MOBY (Clark et al., 1997), and an atmospheric correction algorithm similar to that now used with SeaWiFS.

Single-Scattering Epsilon Vs. Multiple-Scattering Epsilon

A study has been carried out to compare the performance of the aerosol correction algorithm using the single-scattering-epsilon (SSE) and the multiple-scattering-epsilon (MSE) methods. The current SeaWiFS atmospheric correction algorithm uses the SSE derived from the two NIR bands and extrapolated it to the visible wavelengths. In comparing to the SSE (Gordon and Wang, 1994) which depends only on aerosol model and the solar-sensor geometry, the MSE (Su, 2000) is also dependent of the Rayleigh and aerosol optical thicknesses (in addition to the aerosol model and geometry dependents). Simulations show that, when the testing aerosols are identical to one of the aerosol models used for the lookup tables, both the SSE and MSE methods usually give comparable performances. For aerosols which are similar to but different from the lookup table aerosol models, the SSE method performed slightly better than the MSE method for retrieval of the aerosol optical properties. Figure 2 compares histogram in the error $\Delta[\rho_w(\lambda)]_N$ between using the SSE and MSE methods for almost all possible solar-sensor geometry and for the aerosol optical thickness of 0.05, 0.1, and 0.2. In Fig. 2, results include simulations for the solar-zenith angles from 0° - 80° at step of 5° , the sensor-zenith angles from 0° - 65° at step of 5° , and relative azimuth angles from 0° - 180° at step of 10° , respectively. Figs. 2(a)-2(d) show results of histogram as a function of the error in the retrieved normalized water-leaving reflectance $\Delta[\rho_w(\lambda)]_N$ for the wavelengths of 412, 443, 490, and 555 nm, respectively. Results show that both methods performed comparatively well. However, It is obvious that overall the SSE method performed better than the MSE method for the M80 aerosol model.

20.4. FUTURE WORK

Research works will be continued to evaluate the various effects on the performance of the atmospheric correction and aerosol retrieval algorithms, and for the IOCCG atmospheric correction working group activities. My main focus will be on studying and comparing the ocean color and atmospheric results from the MODIS and SeaWiFS. In addition, it is planed to study and understand aerosol model effects and possibly to include other aerosol models, e.g., dust aerosol models (Longtin et al., 1988) for the dust study. It will also be continued in studying and development of the vicarious calibration and inter-calibration techniques from the *in situ* and/or various ocean color sensors measurements. This work will be certainly helpful to development of data merging techniques from multiple ocean color missions.

REFERENCES

- Clark, D.K., H.R. Gordon, K.J. Voss, Y. Ge, W. Broenkow and C. Trees, 1997: Validation of atmospheric correction over the ocean, *J. Geophys. Res.*, **102**: 17,209-17,217.
- Gordon, H.R. 1998: In-orbit calibration strategy for ocean color sensors, *Rem. Sens. Environ.*, **63**, 265-278.
- Gordon, H.R., and M. Wang 1994: Retrieval of water-leaving radiance and aerosol optical thickness over the oceans with SeaWiFS: A preliminary algorithm, *Appl. Opt.*, **33**, 443-452.
- Longtin, D.R., E.P. Shettle, J.R. Hummel, and J.D. Pryce 1988: A Wind Dependent Desert Aerosol Model: Radiative Properties, AFGL-TR-88-0112, U.S. Air Force Geophysics Laboratory, Hanscom Air Force Base, Mass.
- McClain, C.R., M.L. Cleave, G.C. Feldman, W.W. Gregg, S.B. Hooker, and N. Kuring 1998: Science Quality SeaWiFS Data for Global Biosphere Research, *Sea Technol.*, **39**, 10-16.
- Su, W. 2000: A new epsilon function for atmospheric correction algorithm, *Geophys. Res. Letters*, **27**, 3707-3710.
- Tanaka, T., and M. Wang 2002: Solution of radiative transfer in anisotropic plane-parallel atmosphere, *J. Quant. Spectrosc. Radiat. Transfer* (submitted).
- Wang, M. 2002a: Correction of artifacts in the SeaWiFS atmospheric correction: Removing the discontinuity in the derived products, *Remote Sens. Environ.* (accepted).
- Wang, M. 2002b: An efficient method for multiple radiative transfer computations and the lookup table generation, *J. Quant. Spectrosc. Radiat. Transfer* (accepted).
- Wang, M., and H.R. Gordon 2002: Calibration of ocean color scanners: How much error is acceptable in the near-infrared, *Remote Sens. Environ.*, **82**, 497-504.

Chapter 21

Atmospheric Correction Algorithms For Japanese Satellite Ocean Programs

Hajime Fukushima, Mitsuhiro Toratani,

School of High-Technology for Human Welfare, Tokai University, Numazu, Japan

Teruyuki Nakajima

Center for Climate System Research, University of Tokyo, Tokyo, Japan

Sachio Ohta

Graduate School of Engineering, Hokkaido University, Sapporo, Japan

Wen-Zhong Chen

Earth Observation Research Center, National Space Development Agency of Japan, Tokyo, Japan

21.1. INTRODUCTION

This project has two objectives. The first one is to develop/improve our atmospheric correction algorithm focused on aerosols that are peculiar to the East Asian region and the north Pacific. We are particularly interested in Asian dust aerosol originated from the Chinese desert area and also in the anthropogenic absorptive aerosol that is often observed simultaneously with the Asian dust. The second objective is to work closely with international colleagues and the SIMBIOS project by exchanging information and opinions regarding satellite ocean color data processing algorithms, not necessarily limited to the atmospheric correction. We believe this kind of joint effort is essential in terms of securing compatibility and consistency over different satellite ocean color missions.

21.2 RESEARCH ACTIVITIES

GLI Algorithm Implementation

Toratani and Chen updated atmospheric correction code for NASDA's standard L2 product generation, implementing an iterative procedure that takes account of non-zero marine reflectance in NIR bands resulted from high pigment concentration and/or inorganic suspended particles. They are also working on code improvements such as speeding up of the data processing and refined cloud flags.

Aerosol Observation Network

Nakajima, leading Asian Atmospheric Particle Environment Change Studies (APEX) project sponsored by Japan Science and Technology Corporation (JST), coordinates international aerosol observation network and collaborations on data analysis that are essential efforts for characterization of Asian local aerosols. The description of the project, support data, and results of data analysis are posted at <http://duckbill.ccsr.u-tokyo.ac.jp/index.php>. Chemical Weather Forecast System (CFORS) that forecasts the 3D spatial distribution of each aerosol species such as mineral dust, carbonaceous, sulfate and maritime aerosols was developed and is currently operated during intensive observation periods like ACE-Asia 2001 or APEX experiments (Uno *et al.*).

ACE-Asia Ron Brown-SeaWiFS Aerosol Match-Up Data Analysis

We carried out a collaborative work with R. Frouin, B. G. Mitchell and M.-X. He, who are SIMBIOS team members, on aerosol modeling study based on the ship observations conducted aboard R/V Ron Brown on the ACE-Asia 2001 cruise in spring 2001. Observation data collected and analyzed are: aerosol optical thickness (AOT) by SIMBAD, in-water upwelling radiances, and sky-radiance by two PREDE sky-radiometers (one of which owned by the SIMBIOS Project). These data were used to define aerosol model parameters for radiative transfer simulation and derived top of atmosphere (TOA) reflectance is compared with SeaWiFS-derived contemporaneous TOA reflectance. The results (Li et al., in press) show the importance of submicron absorptive aerosol which accounts for very low or negative water-leaving radance derived from SeaWiFS data under standard atmospheric correction. The result is summarized in the following section.

IOCCG Atmospheric Correction WG Activity

We are participating in IOCCG Atmospheric Correction Working Group lead by Menghua Wang. Based on the agreed plan of the WG, we have applied the standard GLI atmospheric correction algorithm to simulated TOA radiances that were generated under various in-water/atmospheric conditions. Error analysis of the results is underway.

21.3 RESEARCH RESULTS*ACE-Asia Ron Brown-SeaWiFS Aerosol Match-Up Data Analysis*

In the ACE-Asia Intensive Observation Period in spring 2001, R/V Ron Brown made a cruise in the adjacent seas of Japan. During the cruise, R. Frouin and B. G. Mitchell made observations of aerosol optical characteristics and upwelling in-water radiance when SeaWiFS overpasses. Relatively good quality PREDE sky-radiometer data were obtained together with the contemporaneous satellite data in three stations (A1-A3) among all the stations shown in Figure 21.1. Table 21.1 summarizes the environmental conditions of the stations. SeaWiFS water-leaving radiances derived under the standard atmospheric correction gives too low or even negative values in the short wavelength region compared to the in-situ data (Figure 21.2). The new SeaWiFS version 4 calibration does not improve the situation. This suggests the presence of absorptive aerosol.

Figure 21.3 shows estimated aerosol size distribution for station A1 derived from the two PREDE sky-radiometers aboard Ron Brown. The averaged size distribution curve was used for defining size parameters of aerosol models. Assuming presence of soot aerosol in addition to oceanic and tropospheric aerosol particles, we determined the size parameter values for the three stations (Table 21.2) using an optimization technique. The parameters were further adjusted so that the TOA radiance of the radiative transfer simulation which uses the model aerosol compares well with the SeaWiFS-observed TOA radiance. The adjusted values of size parameters are also shown in Table 21.2.

Assuming these optimized “absorptive” aerosol models, we simulated the atmospheric correction applied to the SeaWiFS TOA radiances. Figure 21.4 shows the estimated water reflectances which compare very well with the in-situ measurements. Although a dust-mixed model might give a comparable result (as shown in Figure 21.4D), the study suggests that introducing soot-mixed aerosol model may suffice the atmospheric correction for Asian absorptive aerosols.

21.4 FUTURE WORK

ADEOSS-II satellite, which carries Global Imager (GLI), is supposed to be launched in mid-December, 2002. The routine operation will start in April 2003 and we will put our best efforts to initialize the calibration and the atmospheric correction for GLI observation data. In addition to the initialization effort, we will develop and test absorptive aerosol correction scheme on real GLI data. A neural network-based iterative atmospheric correction scheme, which is already implemented into the GLI standard data processing system, will also be tested and validated in collaboration with NASDA’S Cal/Val team, Joji Ishizaka and other Asian colleagues.

We will also participate in the APEX-E3 Intensive Observation (mid-March to mid-May, 2003), providing the APEX community with semi-real time SeaWiFS imageries of aerosol optical thickness, Angstrom exponent, empirical absorptive index, and water-leaving radiances for representative bands. After the observation period, aerosol match-up data which consists of ground observation data and corresponding satellite data will be analyzed in collaboration with other colleagues.

REFERENCES

Uno, I., G.R. Carmichael, D.G. Streets, Y. Tang, I.J. Yienger, S. Satake, Z. Wang, J.-H. Woo, S. Guttikunda, M. Uematsu, K. Matsumoto, H. Tanimoto, K. Yoshioka and T. Iida: Regional chemical weather forecasting using CFORS: Analysis of surface observations at Japanese island stations during the ACE-Asia Experiment (submitted).

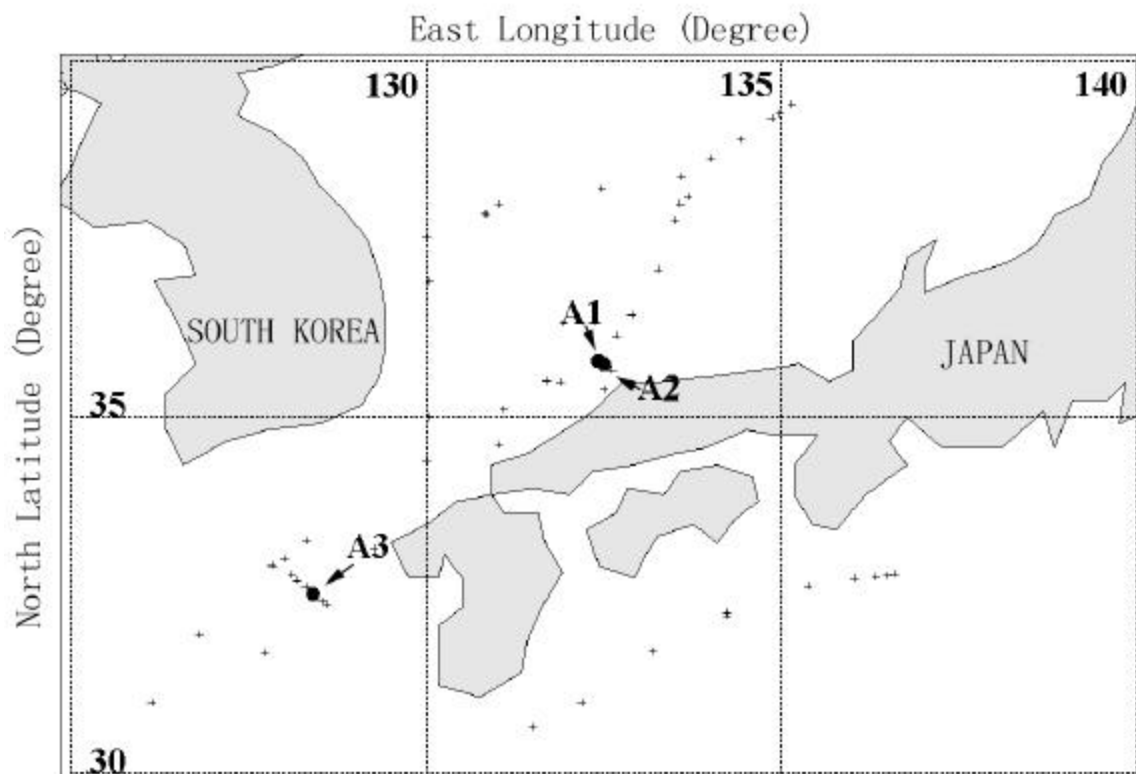


Figure 21.1: The station locations around Japan during ACE-Asia. Solid circles indicate the location of SeaWiFS match-up stations. Small plus symbols indicate the location of other water-leaving radiance and aerosol optical thickness sampling stations of R/V R. H. Brown.

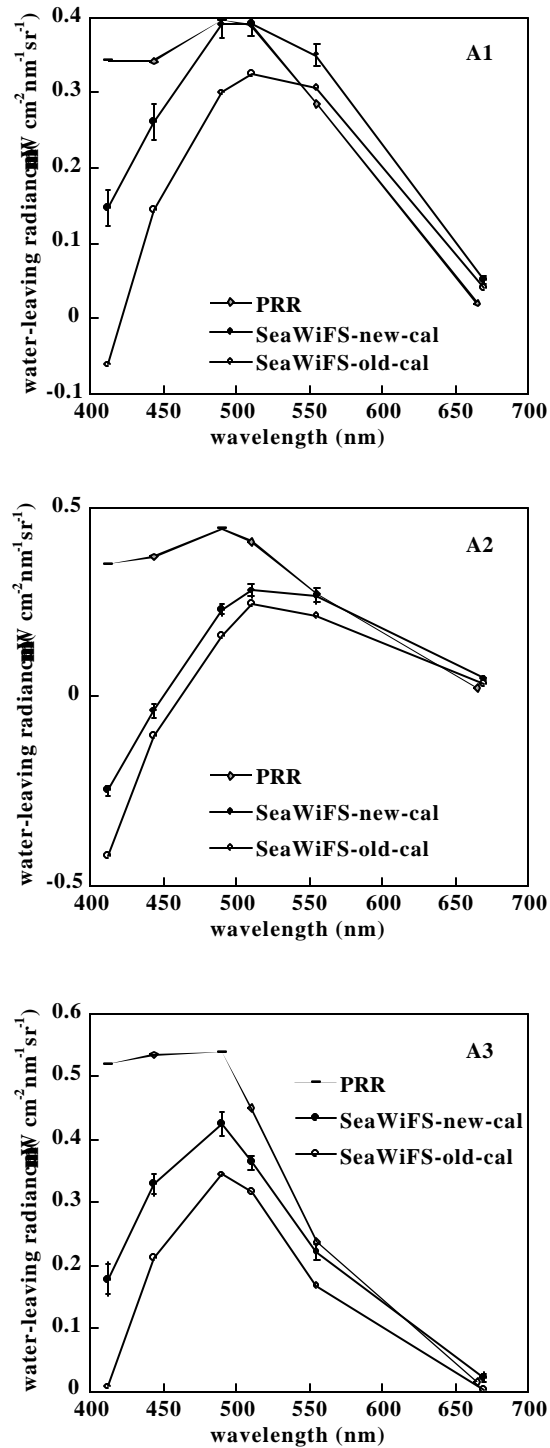


Figure 21.2: Comparison of SeaWiFS-derived L_w with *in situ* PRR measurements at the ACE-Asia match-up station. Standard SeaDAS processing is used with old and new calibration correction factors. Error bar indicates the standard deviation over 5 x 5 SeaWiFS pixels centered on the station location.

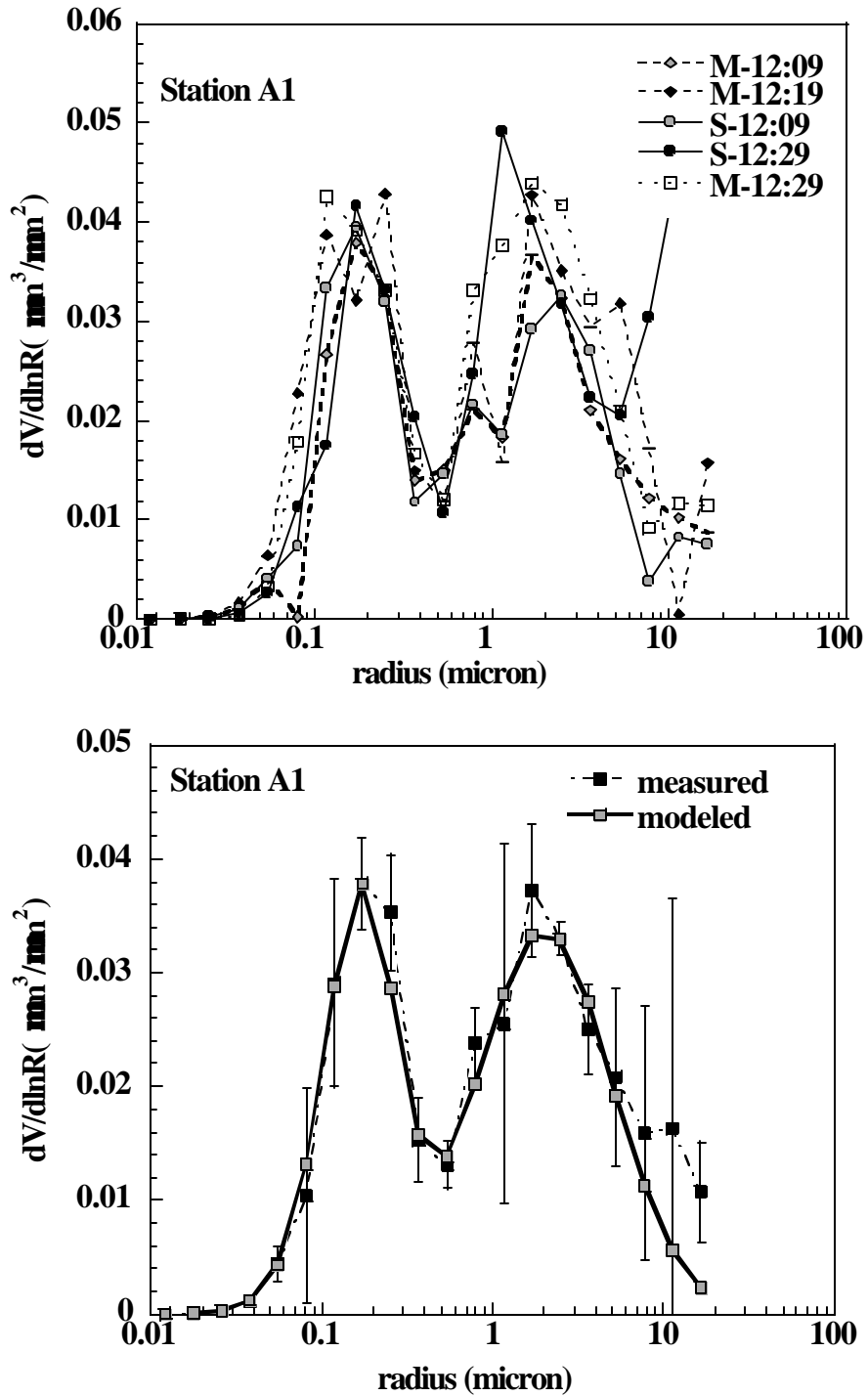


Figure 21.3: The measured and modeled size distribution for station A1. (A) Retrieved size distribution from *in situ* measurements (top figure) by two PREDE sky-radiometers (marked with M and S). (B) Comparison of modeled size distribution (bottom figure) with averaged *in situ* measurements (error bar is standard deviation).

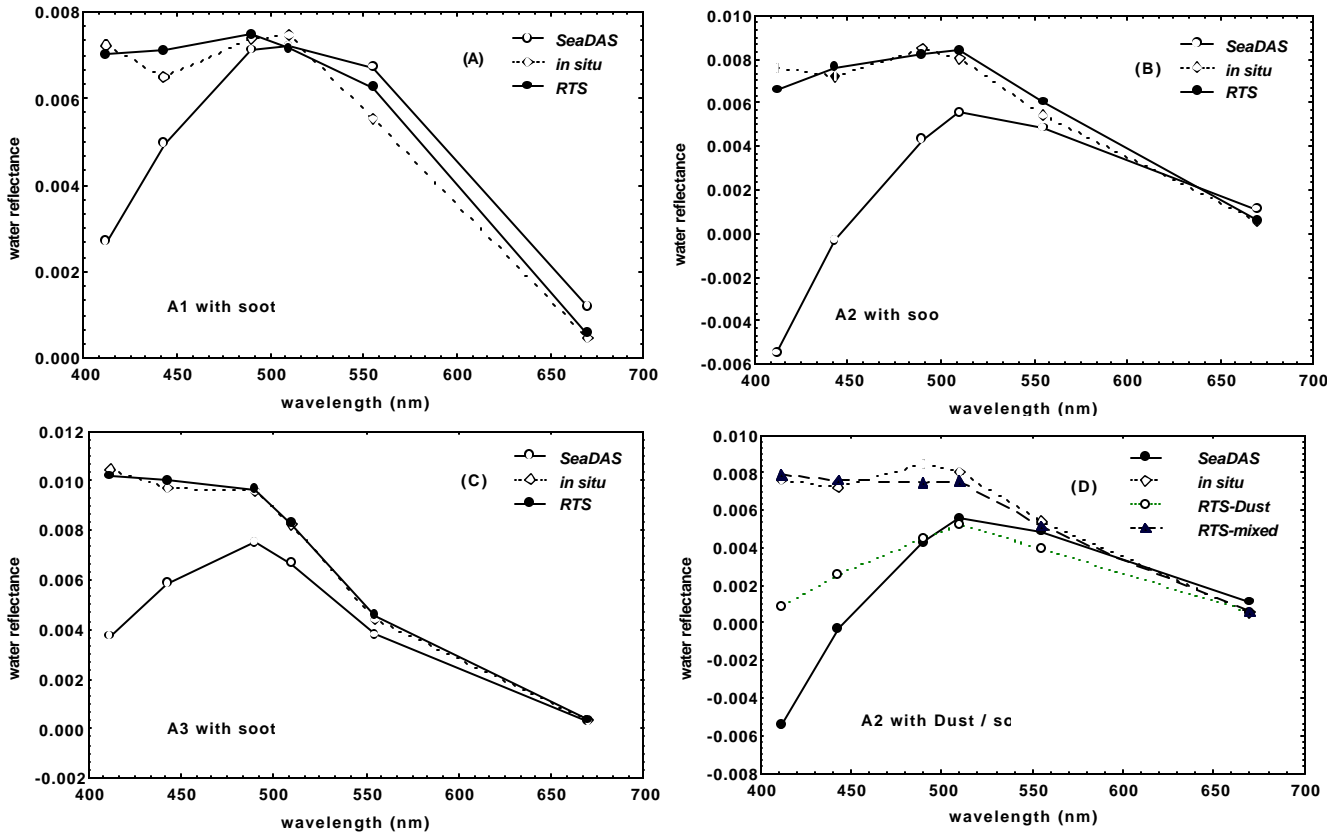


Figure 21.4: Comparison of the ρ_w derived by iterative radiative transfer simulation with SeaWiFS-derived ρ_w and *in situ* measurements. ‘RTS’ denotes values retrieved from the iterative radiative transfer simulation with the tuned aerosol model, ‘SeaDAS’ values obtained with the default atmospheric correction method, and ‘*in situ*’ the measurements by PRR800. In sub-panels A), B) and C) the tuned aerosol model includes soot-only absorptive aerosol while in sub-panel D), Asian dust (refractive index is retrieved from Chinese soil particles) is used to account for absorption instead of soot. ‘RTS-Dust’ in D) is RTS with Asian dust, and ‘RTS-mixed’ is the RTS with soot-dust mixed absorptive aerosol model.

Table 21.1: Environmental information about the selected ACE-Asia station.

Station	Date	Wind speed (m/s)	Wave-height (m)	AOT at 560nm	Chl_a (mg/l)	Air type
A1	04/07/01	3.9	1.0	0.37	1.56	Very polluted air
A2	04/13/01	8.0	1.5	0.18	1.4	Polluted air mixed with dust
A3	04/15/01	4.0	0.5	0.18	0.47	Moderately polluted air

Table 21.2: Model parameters of aerosol size distribution at the satellite match-up stations. The modeled mixture ratio is based on measurements and the tuned mixing ratio results from iterative radiative transfer simulation (see text for details).

	r_{vm}	σ_v	Model Mixture Ratio	Tuned Mixture Ratio	Assumed Species
A1					
1	0.17	1.6	0.47	0.45	Tropospheric
2	2.01	2.48	0.47	0.44	Sea-Salt
3	0.10	1.78	0.06	0.11	Soot
A2					
1	0.16	1.5	0.32	0.31	Tropospheric
2	1.23	1.5	0.63	0.55	Sea-Salt
3	0.1	1.78	0.05	0.14	Soot
A3					
1	0.12	1.57	0.38	0.275	Tropospheric
2	2.0	2.3	0.58	0.60	Sea-Salt
3	0.09	1.7	0.04	0.125	Soot

Chapter 22

Comparison Of Ocean Color Products Between OSMI And SeaWiFS: Preliminary Results

Yongseung Kim and Sungu Lee

Remote Sensing Department, Korea Aerospace Research Institute

22.1 INTRODUCTION

The ocean scanning multispectral imager (OSMI) aboard the KOREA Multi-Purpose SATellite (KOMPSAT), which was built and operated by the Korea Aerospace Research Institute (KARI), is designed to observe the global ocean color in support of biological oceanography. Since the successful launch of OSMI on Dec. 21, 1999, it has been collecting the global ocean color data in the six visible spectral bands centered at 412, 443, 555, 765, and 865 nm. KOMPSAT is on a polar orbit at an altitude of 685 km with local crossing time (ascending node) at approximately 10:50 am and the scanner has a ± 30 degree scan angle with respect to nadir. OSMI has a ground resolution of approximately 1 km with a swath width of 800 km. It has 96 CCD detectors oriented along track. The bandwidths of the first four bands are 20 nm, and those of the last two near-infrared (NIR) bands are 40 nm. The NIR bands can be used for atmospheric correction.

The primary goal of the NASA SIMBIOS project is to develop methods for the meaningful comparison and merging of data products from multiple ocean-color missions (Fargion et al., 2002). And both KARI and the SIMBIOS project team have been collaborated to achieve the OSMI cross-calibration since 2001. As a result, a cross-calibration method using SeaWiFS measurements was developed (Franz and Kim, 2001). In this study, the ocean-color products of OSMI derived from a cross-calibration will be compared to the SeaWiFS counterparts. The data processing method will be given in the next section. Then the comparative results between OSMI and SeaWiFS for 8 samples in 5 regions.

22.2 DATA PROCESSING

The processing algorithms of this study are to use the Multi-Sensor Level-1 to Level-2 (MS112) software which is freely distributed as part of SeaWiFS Data Analysis System (SeaDAS) software package. It is capable of performing atmospheric correction of top-of-atmosphere (TOA) radiances from several spaceborne ocean remote sensing spectrometers (including SeaWiFS, OCTS, MOS, POLDER, and OSMI) and deriving atmospheric and bio-optical properties using identical algorithms for each sensor (Franz, 2000).

Chlorophyll-a Algorithm

The cross calibration coefficients of OSMI based on SeaWiFS measurements were applied to produce the Level-1b. And the resultant ocean color products of OSMI are compared to the SeaWiFS counterparts. The chlorophyll-a algorithm used in the SeaWiFS and OSMI data processing is the one recommended at the SeaBAM (SeaWiFS Bio-optical Mini-workshop) workshop in 1998. This follows the experimental algorithm O`C2 that was formed on the basis of the 1,174 data sets from the observations of the oceans worldwide (O`Reilly et al., 1998).

$$\text{Chlorophyll-a} = ch1 + ch2 \times R + ch3 \times R^2 + ch4 \times R^3 \quad (1)$$

where $ch1 = -0.0929$, $ch2 = 0.2974$, $ch3 = -2.2429$, $ch4 = -0.0077$, ch is each wavelength correction coefficient, $R = \log_{10}(R_{rs}(490)/R_{rs}(555))$, and R is the reflectance ratio of 490 nm and 555 nm.

22.2 PROCEDURES

Selection of Research Areas

To represent typical oceans, we select the coast, open ocean, and complex ocean from total of 38 diagnostic sites. Each selected area is as follows: the coast is the Ligurian Sea, the open ocean is the HOT and the BATS, and the complex oceans are the Korea_SW and the Galapagos Ocean. Table 23.1 shows the detailed information related to these research areas.

Table 22.1: Information on the selected diagnostic sites

Diagnostic Sites	Date	Upper left (Lon, Lat) Upper right (Lon, Lat)		Number of pixels	
		Lower left (Lon, Lat)	Lower right (Lon, Lat)	SeaWiFS	OSMI
BATS	5 April 2002, 28 April 2001	(-65.00, 32.70) (-65.48, 31.00)	(-62.90, 32.40) (-63.43, 30.67)	19908 24538	43170 25197
Galapagos_Ocean	4 April 2001	(-92.84, 3.12) (-93.98, -1.94)	(-87.69, 2.29) (-88.79, -2.80)	77185	78905
HOT	22 May 2001	(-158.36, 23.25) (-158.60, 22.39)	(-157.43, 23.12) (-157.67, 22.26)	3788	6866
Korea_SW	20 Feb 2002	(124.61, 32.51) (124.32, 31.65)	(125.64, 32.35) (125.36, 31.49)	5808	24242
Ligurian_Sea	4 June 2001 7 July 2001 2 Sep 2001	(6.67, 43.84) (6.29, 43.00)	(7.86, 43.63) (7.46, 42.78)	6559 5870 6485	19146 5005 20392

Data Match-Up

Cloud amounts and the distribution of chlorophyll-a concentration in the images are visually examined for the selected diagnostic sites, and good Level-2 images of SeaWiFS are extracted from the SeaWiFS homepage (http://seawifs.gsfc.nasa.gov/cgi/seawifs_region_extracts.pl?TYP=ocean). The corresponding Level-1a images of OSMI are also prepared for Level-2 processing. Due to the differences in the spatial resolution between OSMI (0.85 km) and SeaWiFS (1.1 km), the number of pixels available in the sample area is different (see Table 22.1).

Level-2 Processing

To produce Level-2 data from Level-1a of OSMI, we have used the MSL12 software. Before running MSL12, we must initialize the ozone, the meteorological ancillary data file, and miscellaneous parameters. Also, the cross-calibration coefficients are utilized in this processing.

Table 22.2: Comparison of average, standard deviation and variance of OSMI and SeaWiFS in research areas.

		BATS_1 (5 Apr 2002)		BATS_2 (28 Apr 2001)		Galapagos_Ocean (4 Apr 2001)		HOT (22 May 2001)	
		OSMI	SeaWiFS	OSMI	SeaWiFS	OSMI	SeaWiFS	OSMI	SeaWiFS
[Lw(412)] _N	Avg	2.3068	1.6133	2.0335	1.7526	1.6012	0.9956	2.6770	2.4061
	S ²	0.2826	0.1509	0.3715	0.1528	0.2536	0.1586	0.2070	0.0589
	S	0.5316	0.3885	0.6095	0.3910	0.5036	0.3983	0.4550	0.2428
[Lw(443)] _N	Avg	1.9781	1.7095	1.9446	1.9028	1.5308	1.0514	2.2081	2.0278
	S ²	0.2010	0.1324	0.2354	0.0784	0.2464	0.1297	0.1360	0.0420
	S	0.4483	0.3639	0.4852	0.2801	0.4964	0.3602	0.3688	0.2049
[Lw(490)] _N	Avg	1.5098	1.3261	1.5325	1.4961	1.4507	1.0380	1.5603	1.4934
	S ²	0.0703	0.1367	0.1120	0.0342	0.1111	0.0736	0.1023	0.0245
	S	0.2652	0.3697	0.3347	0.1850	0.3333	0.2714	0.3199	0.1565
[Lw(555)] _N	Avg	0.5584	0.5352	0.5417	0.5141	0.9208	0.5984	0.5476	0.5094
	S ²	0.0366	0.0326	0.0647	0.0154	0.0413	0.0452	0.0271	0.0065
	S	0.1915	0.1808	0.2543	0.1242	0.2032	0.2126	0.1648	0.0806

		Korea_SW (20 Feb 2002)		Ligurian_1 (4 Jun 2001)		Ligurian_2 (7 Jul 2001)		Ligurian_3 (2 Sep 2001)	
		OSMI	SeaWiFS	OSMI	SeaWiFS	OSMI	SeaWiFS	OSMI	SeaWiFS
[Lw(412)] _N	Avg	3.3598	1.4575	1.4410	0.9870	0.4275	0.9810	1.0038	0.6627
	S ²	0.1884	0.0220	0.1720	0.0070	0.5655	0.0830	0.2429	0.0770
	S	0.4341	0.1483	0.4147	0.0841	0.7520	0.2882	0.4928	0.2775
[Lw(443)] _N	Avg	3.5186	2.5427	1.4390	1.2684	0.3392	1.1327	1.0821	1.0234
	S ²	0.1355	0.0200	0.1670	0.0633	0.3637	0.1391	0.1775	0.0852
	S	0.3682	0.1416	0.4087	0.2515	0.6031	0.3729	0.4214	0.2920
[Lw(490)] _N	Avg	4.4232	3.7893	1.4060	1.0241	0.2878	0.9398	0.9751	0.9681
	S ²	0.0932	0.0610	0.0845	0.0131	0.2610	0.0566	0.1010	0.0494
	S	0.3054	0.2470	0.2908	0.1147	0.5109	0.2379	0.3178	0.2224
[Lw(555)] _N	Avg	4.2817	4.2945	0.5174	0.5032	0.1326	0.4699	0.4819	0.4842
	S ²	0.1042	0.0768	0.0117	0.0020	0.0550	0.0142	0.0202	0.0139
	S	0.3228	0.2772	0.1085	0.0448	0.2345	0.1192	0.1421	0.1182

[Lw(λ)]_N, Avg, S², and S are normalized water-leaving radiance, average, variance, and standard deviation, respectively.

22.3 RESEARCH RESULTS

Water-Leaving Radiance Comparisons

Table 22.2 shows the results of statistical calculations for the retrieved water-leaving radiances at each site. Differences of averages between OSMI and SeaWiFS at each band seem to be small except for the Korea_SW site. The reason for the large difference at the Korea_SW site is not clear, and it may need the further validation study with the use of in-situ measurements. Another feature in these differences is easily discernible in Fig. 22.1. The OSMI values overestimate the water-leaving radiances compared to those of SeaWiFS except for the Ligurian_Sea. One factor causing such overestimation is that the different aerosol models were selected in the atmospheric correction since OSMI and SeaWiFS used the multi-scattering with maritime (90% rh) and the Gordon-Wang model selection and Siegel NIR iterations for their aerosol options (new), respectively. To see any differences caused with the use of the same aerosol model, we have recalculated the water-leaving radiance and chlorophyll-a concentration of OSMI for the BATS, the Korea_SW site and the Ligurian. The differences of two variables as shown in Table 23.3 are found to be reduced between OSMI and SeaWiFS.

Chlorophyll-a Comparisons

Comparisons of chlorophyll-a concentration calculated for OSMI and SeaWiFS at each site, using eq. (1), are shown in Fig. 22.2 and Fig. 22.3. The color images of SeaWiFS and OSMI columns are logarithmically scaled from 0.01 to 5 (mg/m³) and their histograms are plotted in the third column. Some differences in the distribution of chlorophyll-a concentration appear to be associated with clouds and ocean dynamics at the time of imaging. Overall, SeaWiFS estimates of chlorophyll-a concentration are shown to be larger than those of OSMI. This is summarized in Table 22.3 and well depicted in Fig. 22.2(e). The systematic underestimation by OSMI would be ascribed to its overestimation of water-leaving radiances. More prominent differences occurred at the Galapagos and Korea_SW sites (See Fig. 22.2 and Fig. 22.3) seem to be related to higher sensitivities of SeaWiFS close to the island and in the region that affected by continental sediments. However, such conjecture should be validated with in-situ measurement.

REFERENCE

Fargion, G. et al., 2002: SIMBIOS Project Data Processing and Analysis Results, SIMBIOS Project Annual Report, 8-27.

Franz, B. A. and Y. Kim, 2001: A comparative study and intercalibration between OSMI and SeaWiFS, AGU 2001 Fall Meeting, San Francisco.

Franz, B. A. 2000: MS112 Version 2.6 User's Guide.

O'Reilly, J. E., S. Maritorena, B. G. Mitchell, D. A. Siegel, K. L. Carder, S. A. Garver, M. Kahru and C. R. McClain, 1998: Ocean color chlorophyll algorithms for SeaWiFS, *J. Geophys. Res.*, **103**, 24937-24953.

Table 22.3: Results of recalculation with the same aerosol option-OSMI (new).

		BATS_2 (28 Apr 2001)			Korea_SW (20 Feb 2002)			Ligurian_2 (7 Jul 2001)		
		OSMI	OSMI (new)	SeaWiFS	OSMI	OSMI (new)	SeaWiFS	OSMI	OSMI (new)	SeaWiFS
[Lw(412)] _N	Avg	2.0335	1.9876	1.6133	3.3598	3.0106	1.4575	0.4275	1.3820	0.9810
	S ²	0.3715	0.2554	0.1509	0.1884	0.1629	0.0220	0.5655	0.1395	0.0830
	S	0.6095	0.5054	0.3885	0.4341	0.4037	0.1483	0.7520	0.3735	0.2882
[Lw(443)] _N	Avg	1.9446	2.0053	1.7095	3.5186	3.1767	2.5427	0.3392	1.0804	1.1327
	S ²	0.2354	0.2216	0.1324	0.1355	0.1239	0.0200	0.3637	0.1142	0.1391
	S	0.4852	0.4707	0.3639	0.3682	0.3520	0.1416	0.6031	0.3379	0.3729
[Lw(490)] _N	Avg	1.5325	1.5633	1.3261	4.4232	4.1844	3.7893	0.2878	0.9664	0.9398
	S ²	0.1120	0.0886	0.1367	0.0932	0.0970	0.0610	0.2610	0.0647	0.0566
	S	0.3347	0.2978	0.3697	0.3054	0.3114	0.2470	0.5109	0.2544	0.2379
[Lw(555)] _N	Avg	0.5417	0.5345	0.5352	4.2817	4.1338	4.2945	0.1326	0.5063	0.4699
	S ²	0.0647	0.0275	0.0326	0.1042	0.1029	0.0768	0.0550	0.0043	0.0142
	S	0.2543	0.1659	0.1808	0.3228	0.3208	0.2772	0.2345	0.0658	0.1192
[chl]	Avg	0.1327	0.1538	0.1776	2.0885	2.1980	3.1583	0.0524	0.1674	0.2306
	S ²	0.0031	0.0033	0.1037	0.0381	0.0469	0.0763	0.0097	0.1951	0.0119
	S	0.0564	0.0576	0.3221	0.1952	0.2167	0.2762	0.0989	0.4417	0.1092

[Lw(λ)]_N, Avg, S², and S are normalized water-leaving radiance, average, variance, and standard deviation, respectively.

Table 22.4. Comparison of chlorophyll-a of OSMI and SeaWiFS in research areas.

		Korea_SW (20 Feb 2002)		Ligurian_1 (4 Jun 2001)		Ligurian_2 (7 Jul 2001)		Ligurian_3 (2 Sep 2001)	
		OSMI	SeaWiFS	OSMI	SeaWiFS	OSMI	SeaWiFS	OSMI	SeaWiFS
[chl]	Avg	2.0885	3.1583	0.2170	0.2661	0.0524	0.2306	0.1872	0.2969
	S ²	0.0381	0.0763	0.0044	0.0475	0.0097	0.0119	0.0057	0.0108
	S	0.1952	0.2762	0.0666	0.2179	0.0989	0.1092	0.0755	0.1042
		BATS_1 (5 Apr 2002)		BATS_2 (28 Apr 2001)		Galapagos_Ocean (4 Apr 2001)		HOT (22 May 2001)	
		OSMI	SeaWiFS	OSMI	SeaWiFS	OSMI	SeaWiFS	OSMI	SeaWiFS
[chl]	Avg	0.1780	0.1763	0.1327	0.1776	0.6219	1.7524	0.1283	0.3319
	S ²	0.0096	0.1461	0.0031	0.1037	1.3193	9.9274	0.0063	0.1037
	S	0.0982	0.3822	0.0564	0.3221	1.1486	3.1507	0.0799	0.3221

Avg, S², and S are average, variance, and standard deviation, respectively.

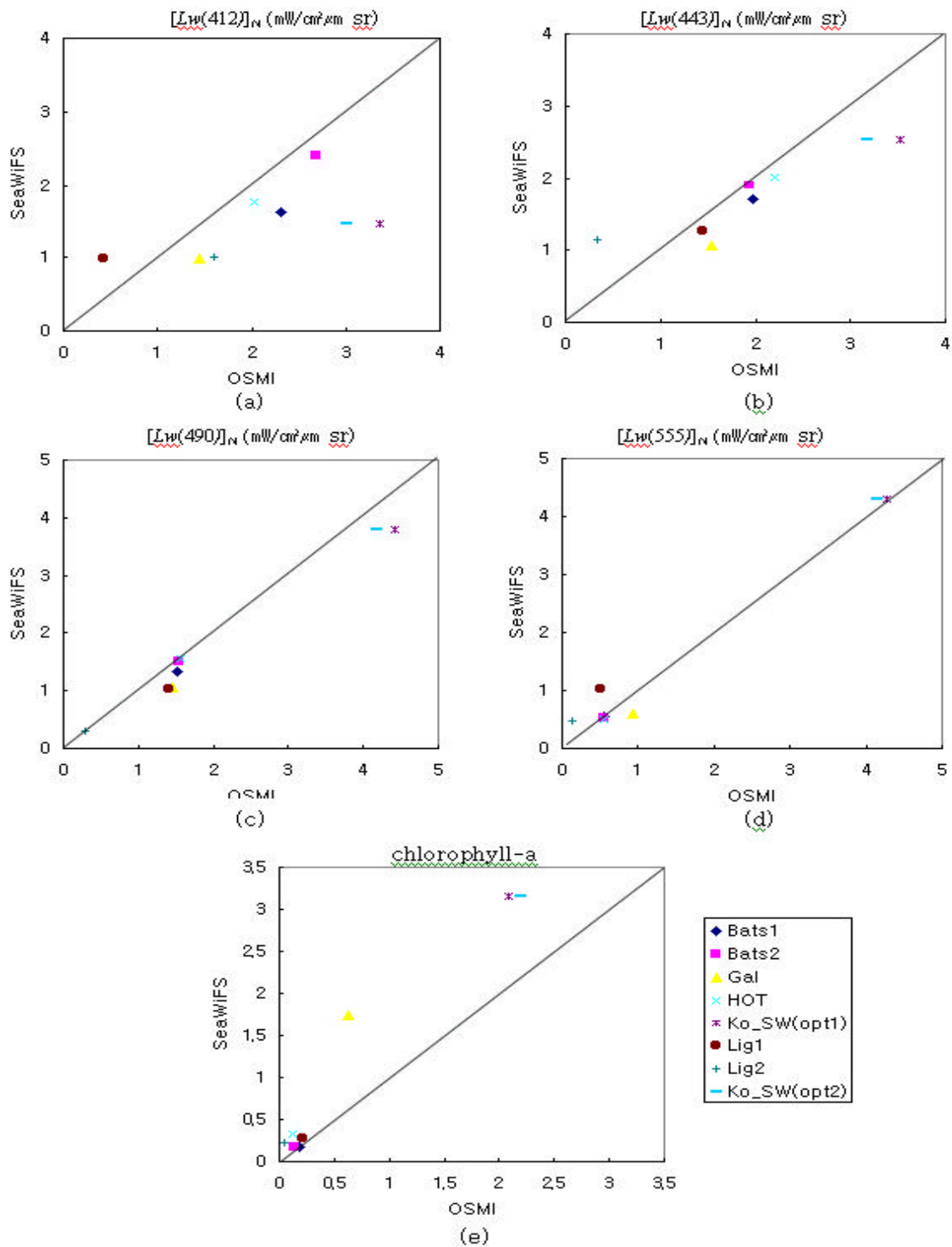


Figure 22.1: OSMI-derived normalized water-leaving radiance and chlorophyll-a compared with those of the SeaWiFS: (a) nLw 412 nm (b) nLw 443 nm (c) nLw 490 nm (d) nLw 555 nm (e) chlorophyll-a.

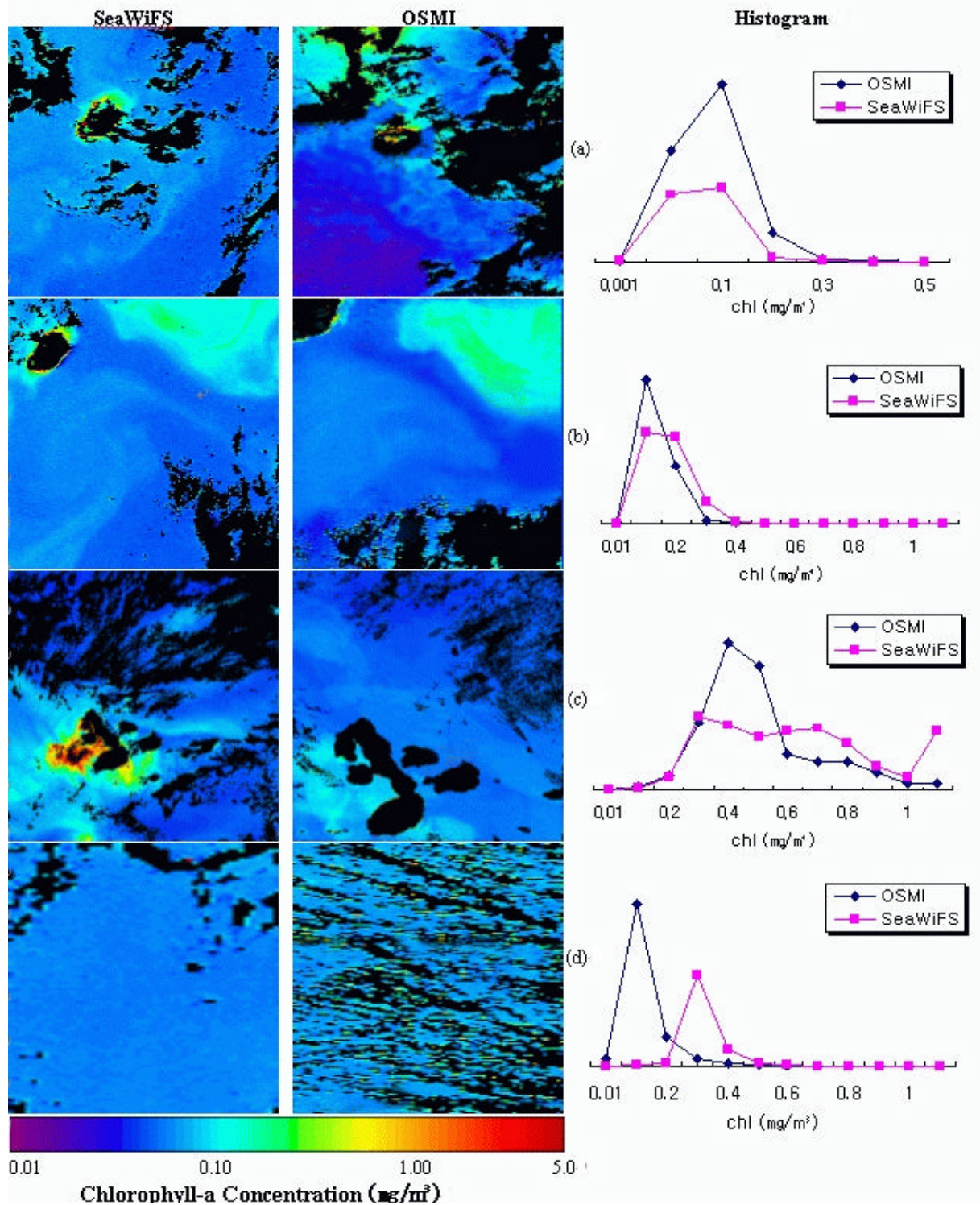


Figure 22.2. OSMI-retrieved chlorophyll-a concentration compared to those derived from SeaWiFS measurements for (a) BATS_1 (5 April 2002), (b) BATS_2 (28 April 2001), (c) Galapagos (4 April 2001), (d) HOT (22 May 2001).

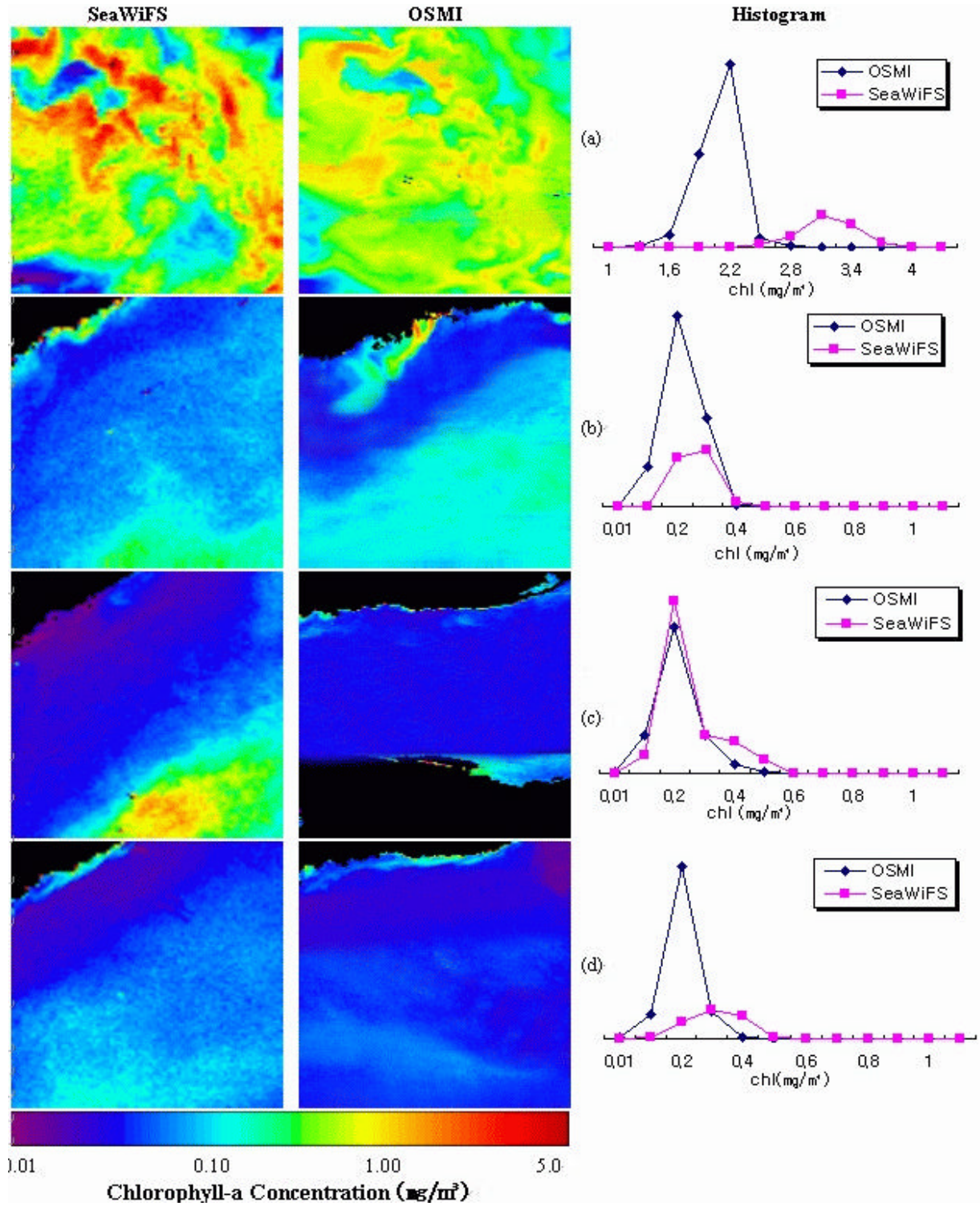


Figure 22.3: OSMI-retrieved chlorophyll-a concentration compared to those derived from SeaWiFS measurements for (a) Korea_SW (20 February 2002), (b) Ligurian_1 (4 June 2001), (c) Ligurian_2 (7 July 2001), (d) Ligurian_3 (2 September 2001)

Chapter 23

Evaluation and Improvement of the Atmospheric Correction and Bio-optical Algorithms for the Black and Barents Seas

Oleg V. Kopelevich, Vladimir I. Burenkov, Svetlana V. Ershova, Sergey V. Sheberstov,
Marina A. Evdoshenko

Ocean Optics Laboratory, P.P.Shirshov Institute of Oceanology, Moscow, Russia

23.1 INTRODUCTION

The objective of our research is evaluation, validation and improvement of the atmospheric correction and bio-optical algorithms. Our work is focused primarily on the Black and Barents Seas; since the last year we have also made joint studies with Robert Frouin (Scripps Institution of Oceanography) in the Atlantic Ocean using commercial transatlantic cruises of the Russian R/V *Akademik Ioffe* (Kopelevich et al. 2002a).

23.2 RESEARCH ACTIVITIES

Field Studies

In 2002 the ocean color collaborative US-Russia studies onboard R/V *Akademik Ioffe* have been continued (Kopelevich et al. 2002a). In January-March 2002 the studies were conducted in Antarctic during the tourist cruises from Ushuaia to Antarctica and back; 8 Mar 2002 the ship sailed for Montevideo and 15 Mar 2002 after two days of stay in Montevideo sailed for Kiel. Duration of the whole cruise was 212 days; totally 337 stations were made. The ship tracks on the both Atlantic transects are shown in Figure 23.1.

Ten October 2002 R/V *Akademik Ioffe* left Kaliningrad for the next Atlantic transect. Unlike the above described cruise where the measurements were mainly performed under way, in the new cruise they were also performed at drift stations that provided opportunity for studying vertical structure of bio-optical characteristics with a submersible transmissometer, sampling bottles and UV-PAR radiometer. The precise floating spectroradiometer was used to measure spectral water-leaving radiance and surface irradiance (Artemiev et al. 2000), the primary production was determined. The transect was ended in Montevideo on 14 Nov 2002.

Algorithm Development And Use Of SeaWiFS Data

Our previous validation studies in the Black and Barents seas have revealed great errors in chlorophyll concentration derived by the SeaDAS algorithm in the Barents Sea, and noticeable ones in the Black Sea (Burenkov et al., 1999, 2000, 2001a, Kopelevich et al. 2001). The results of the mentioned and other validation studies have been used to develop the modified algorithms providing much better agreement between *in situ* and satellite-based values of bio-optical characteristics. The mean monthly distributions of three important parameters, such as chlorophyll concentration, the particle backscattering and yellow substance absorption coefficients, have been constructed with the modified algorithms for a period of 1998-2001 and the monthly means of the above characteristics in the different regions have been calculated. The results obtained were presented in two papers submitted to Deep-Sea Research Part II (Kopelevich et al., submitted) and to Oceanology, Suppl.1 (Kopelevich et al. 2002b). The Russian version of ND-ROM with 424 color maps of the mean monthly distributions of chlorophyll concentration, the particle backscattering and yellow substance absorption coefficients from January 1998 to December 2001 has been issued (Kopelevich et al. 2002c).

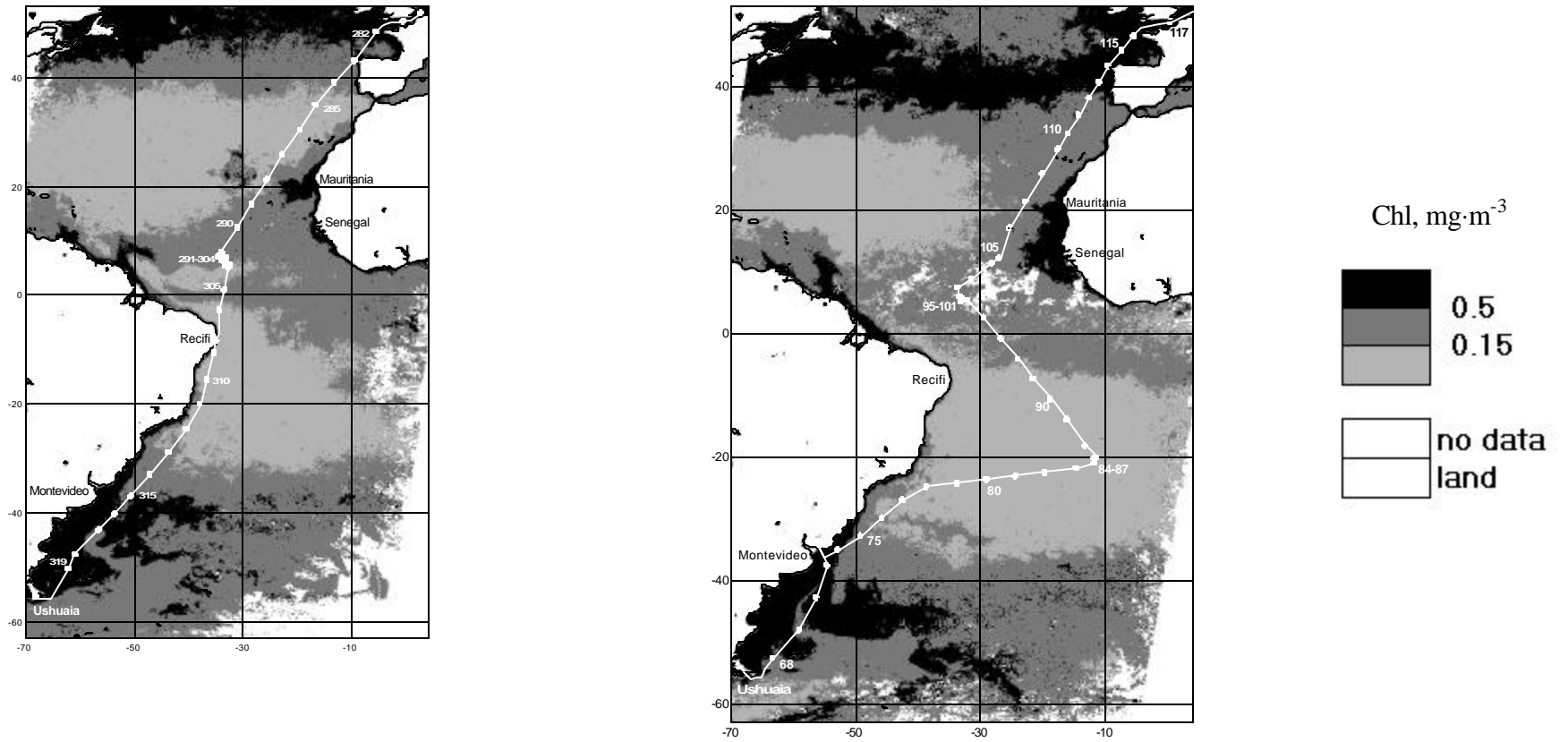


Figure 23.1: SeaWiFS monthly composites of chlorophyll conc. for the Atlantic Ocean with the Ioffe tracks in October 01 (left) and April 02 (right).

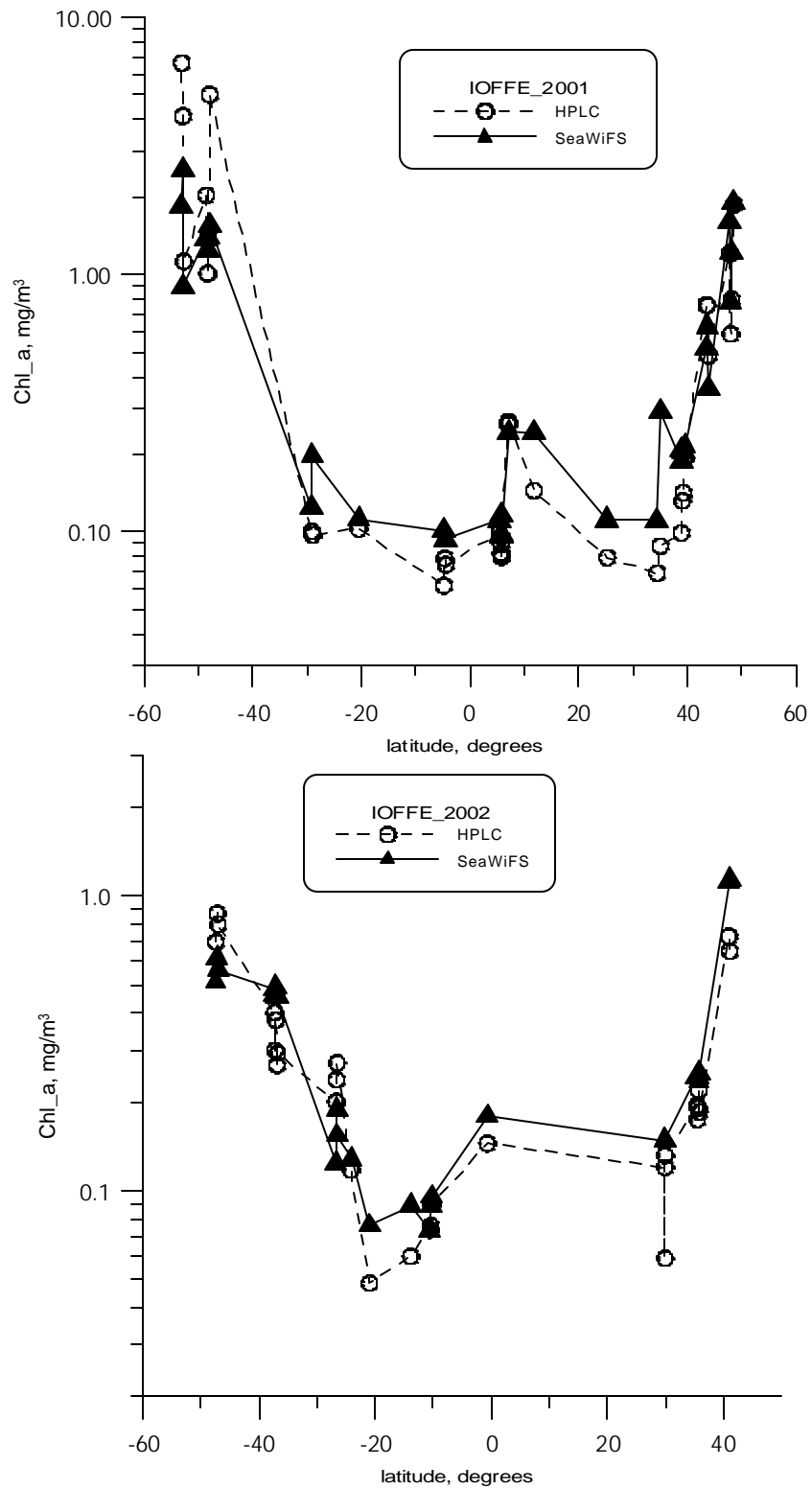


Figure 23.2: Changes of chlorophyll concentration along the Atlantic transect in October-November 2001 (upper) and March-April 2002 (lower from HPLC and SeaWiFS data).

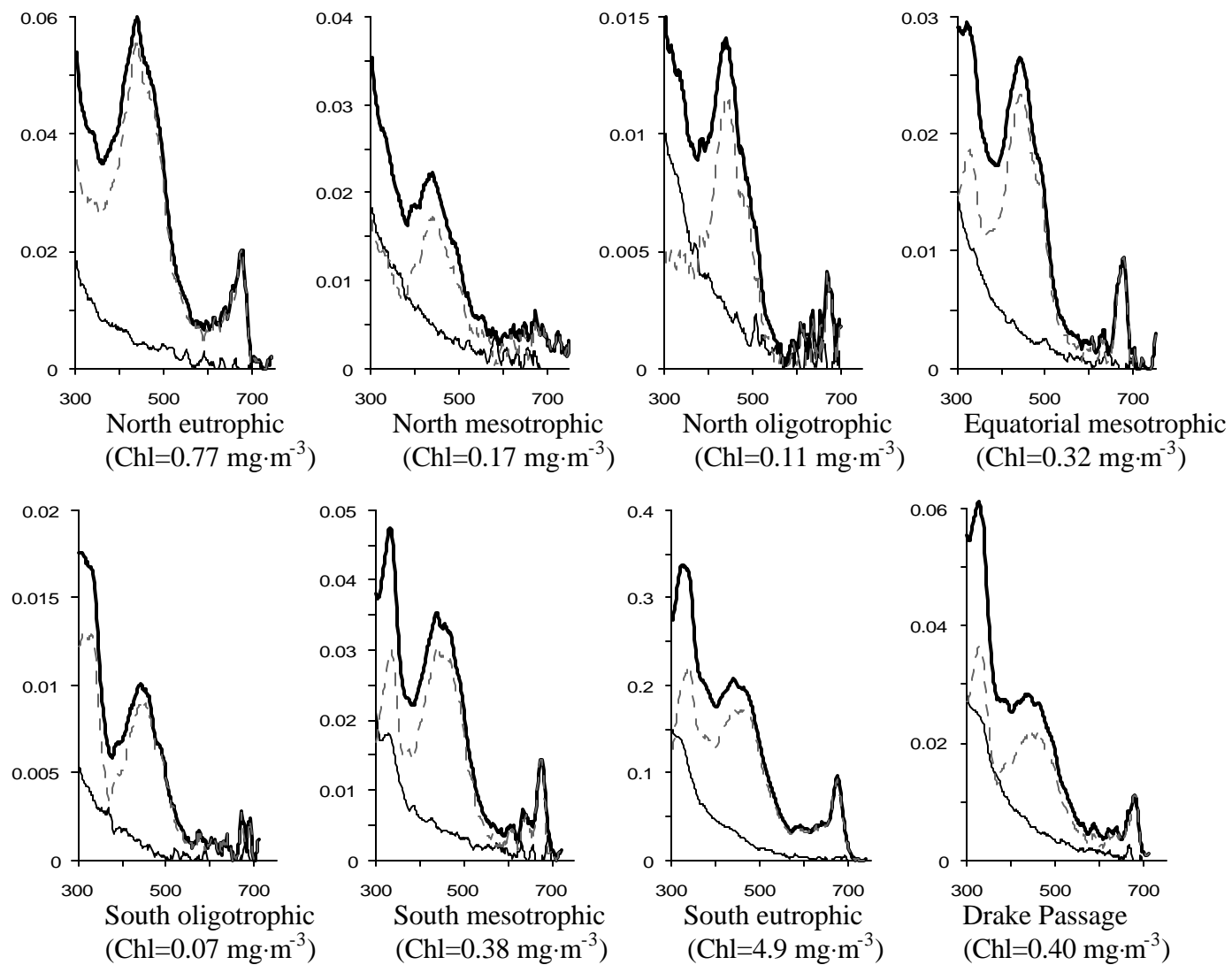


Figure 23.3: Spectra of the absorption coefficients of the particulate matter (thick line), phytoplankton pigment (dash), and detritus (thin line) in different waters in October-November 2001.

23.3 RESEARCH RESULTS

Results Of Field Studies: Atlantic Ocean

SeaWiFS monthly composites of chlorophyll concentration for the Atlantic Ocean with the Ioffe tracks in October 2001 and April 2002 are shown in Fig. 23.1. A general resemblance between the spatial distributions is observed with some distinctions in the details. The both Ioffe passages crossed the waters with diverse productivity and seven grades of chlorophyll concentration were selected based on the SeaWiFS data: eutrophic waters with chlorophyll concentration more than $0.5 \text{ mg}\cdot\text{m}^{-3}$, mesotrophic waters with chlorophyll concentration $0.15\text{-}0.5 \text{ mg}\cdot\text{m}^{-3}$, and oligotrophic waters with chlorophyll concentration less than $0.15\text{mg}\cdot\text{m}^{-3}$. As it is seen, they alternate with each other from north to south: the north eutrophic, mesotrophic and oligotrophic, then the equatorial mesotrophic, and the south oligotrophic, mesotrophic and eutrophic waters.

In the Antarctic region three zones were selected: eutrophic waters near the South America, mesotrophic-oligotrophic waters in the central part of Drake Passage, and eutrophic waters east of Antarctic Peninsula. The seasonal changes were observed: the highest chlorophyll concentration was in December, the lowest in February. In particular, the mesotrophic waters ($\text{Chl-SeaWiFS} = 0.15\text{-}0.5 \text{ mg}\cdot\text{m}^{-3}$) in the central part of Drake Passage in December became oligotrophic ($\text{Chl-SeaWiFS} < 0.15 \text{ mg}\cdot\text{m}^{-3}$) in January and February.

Figure 23.2 shows changes of chlorophyll concentration along the Atlantic transects in October-November 2001 and March-April 2002 from HPLC and SeaWiFS data (derived by the OC 4 algorithm). A good qualitative agreement is seen; some distinctions observed in the details have yet to be analyzed.

The examples of the spectral absorption coefficients of the particulate matter, phytoplankton pigment, and detritus in different waters in October-November 2001 are given in Fig. 23.3. Changes in the absolute values and form of the spectra are observed in waters of different productivity, and such features are of vital importance for development of regional bio-optical algorithms. The further joint analysis of the features of spectral absorption and phytoplankton pigment composition is needed. The mean monthly distribution of the particle backscattering coefficient b_{bp} at 555 nm derived from SeaWiFS data with the SIO/RAS algorithm (Burenkov et al. 2001b) in October 2001 and April 2002 are presented in Fig.23.4 (left images). The right images in this figure are the mean monthly distributions of the aerosol optical thickness $t_a(865)$ at 865 nm. A general resemblance is seen between the b_{bp} distributions and chlorophyll distributions in Fig. 23.1. It causes no surprise because the b_{bp} values depend on particulate matter in seawater that can originate in phytoplankton as a primary source. Not only the biogenous particles form the particle backscattering in near-surface layer but also the terrigenous ones which are brought to the ocean by rivers and winds. A general resemblance is also seen between the b_{bp} and $t_a(865)$ distributions in the central Atlantic where the area of high values of $t_a(865)$ due to transport of Sahara dust through the atmosphere in that region is observed. It is difficult to select contributions in the b_{bp} values arising from the terrigenous and biogenous particles because both $t_a(865)$ and chlorophyll concentration are high in the considered area. It is also worth keeping in mind that chlorophyll concentration can be connected with high $t_a(865)$ values because the winds bring into the ocean the mineral elements which are nutrients needed to increase primary production. Another case is observed off the Argentine coast where low values of $t_a(865)$ (less than 0.1) and high values of b_{bp} (more than 0.005 m^{-1} in October 2001) are observed. This area displayed high chlorophyll concentration, and it is evident that the primary source of particles there is phytoplankton.

The Regional Algorithms For The Barents And Black Seas

On the basis of our field data in the Barents and Black Sea regression equations were derived between chlorophyll concentration and the ratio $L_{WN}(510)/L_{WN}(555)$. For the Barents Sea the equation takes the form:

$$\text{Chl} = 0.34 [L_{WN}(510)/L_{WN}(555)]^{-1.39}. \quad (1)$$

It was calculated from our field data in August-September 1998 covering both the open regions and the Pechora Sea (n=21); a standard error of the regression equation is 0.135 mg m^{-3} . It is assumed to be valid in the whole period of study from May to September, but the errors can increase during a phytoplankton bloom in May when the relationship between the phytoplankton pigment and yellow substance absorption may be changed. For the Black Sea the regression equation takes the form:

$$\text{Chl} = 0.88 [L_{WN}(510)/L_{WN}(555)]^{-2.26}. \quad (2)$$

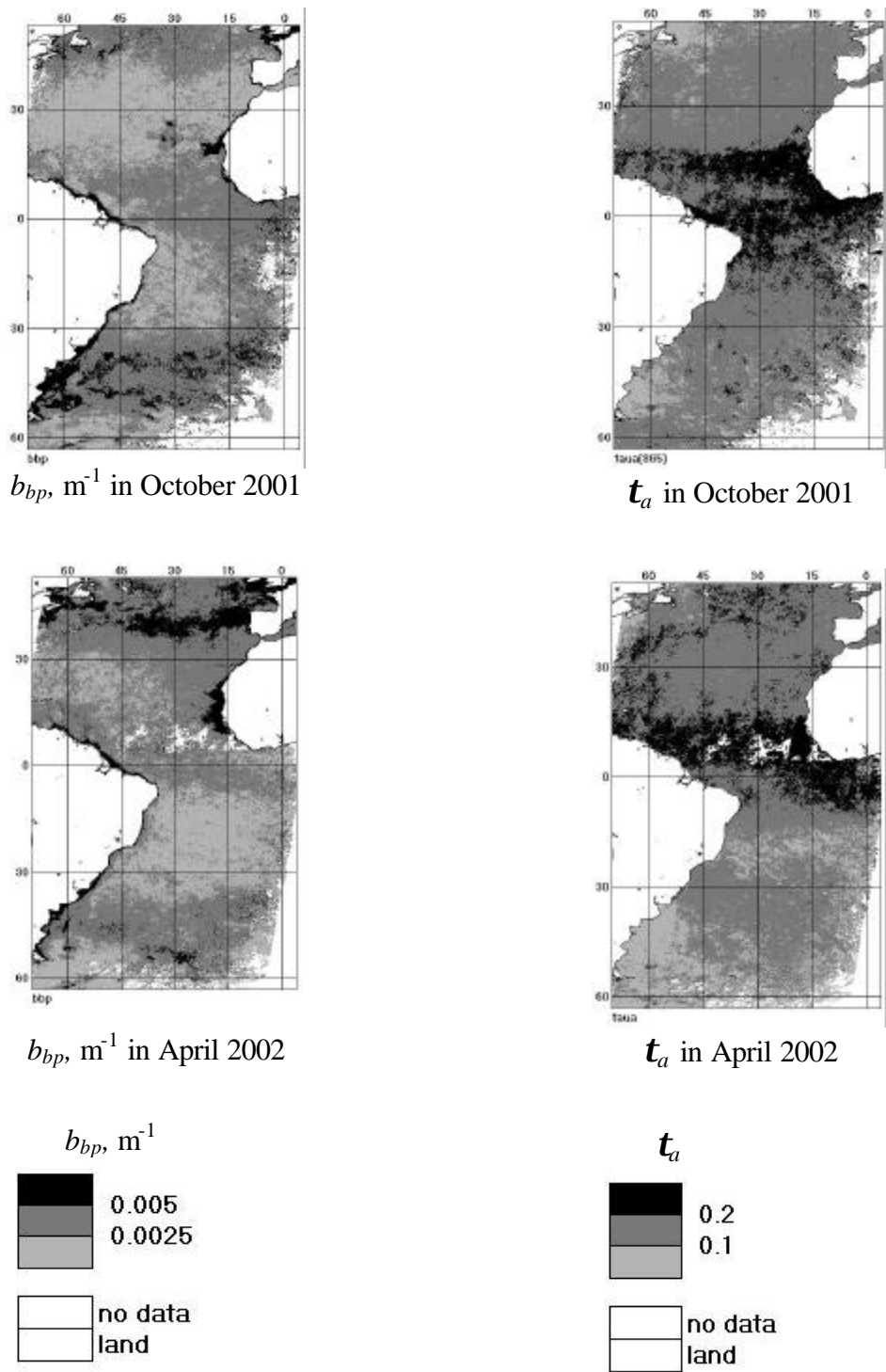


Figure 23.4: SeaWiFS monthly composites of the particle backscattering coefficients b_{bp} (left) and aerosol optical thickness τ_a (right) in October 2001 (upper) and April 2002 (lower).

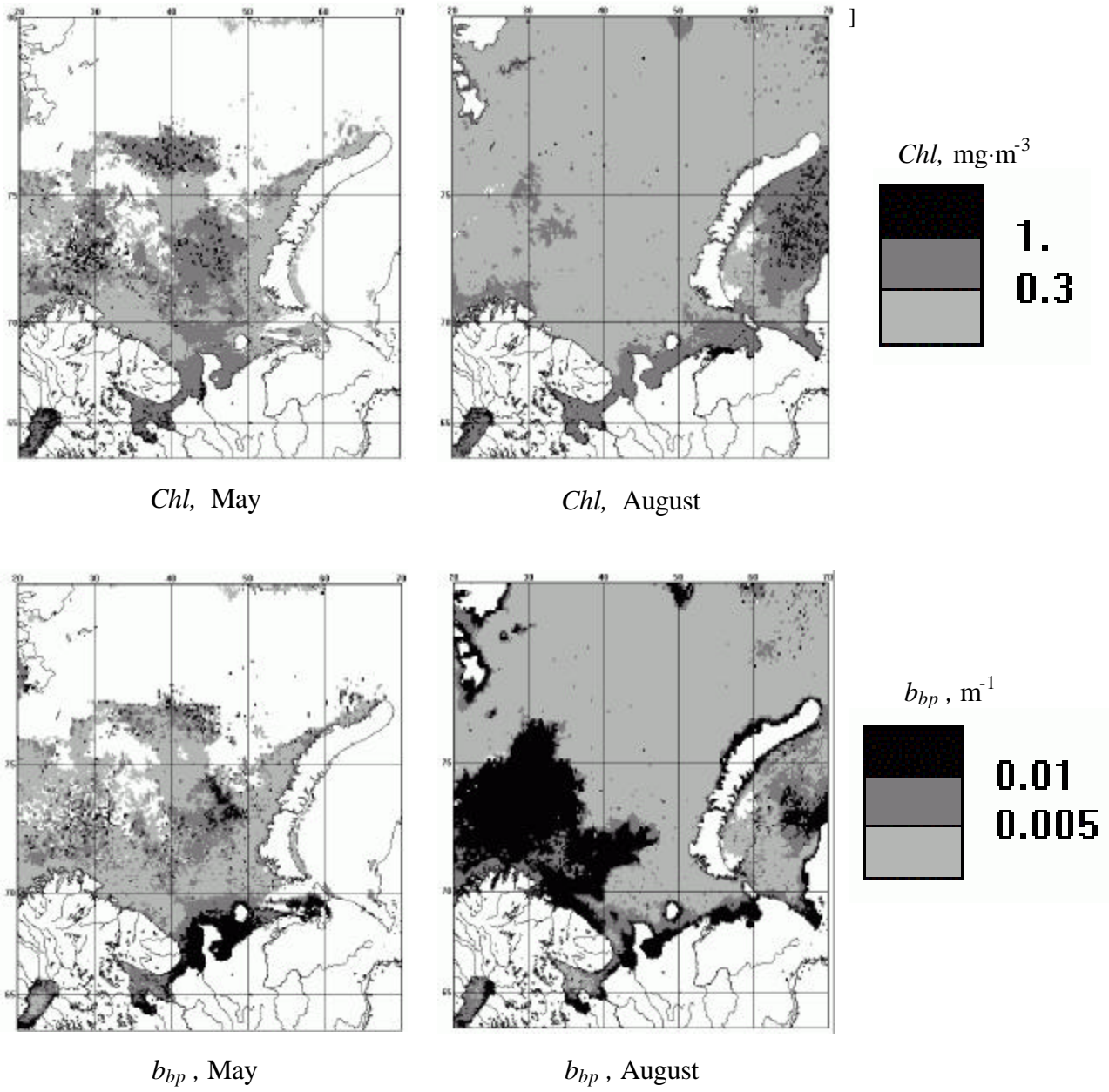


Figure 23.5: The mean monthly distributions of chlorophyll concentration and particle backscattering coefficient in the Barents Sea in May and August 2001 derived with the SIO/RAS algorithms.

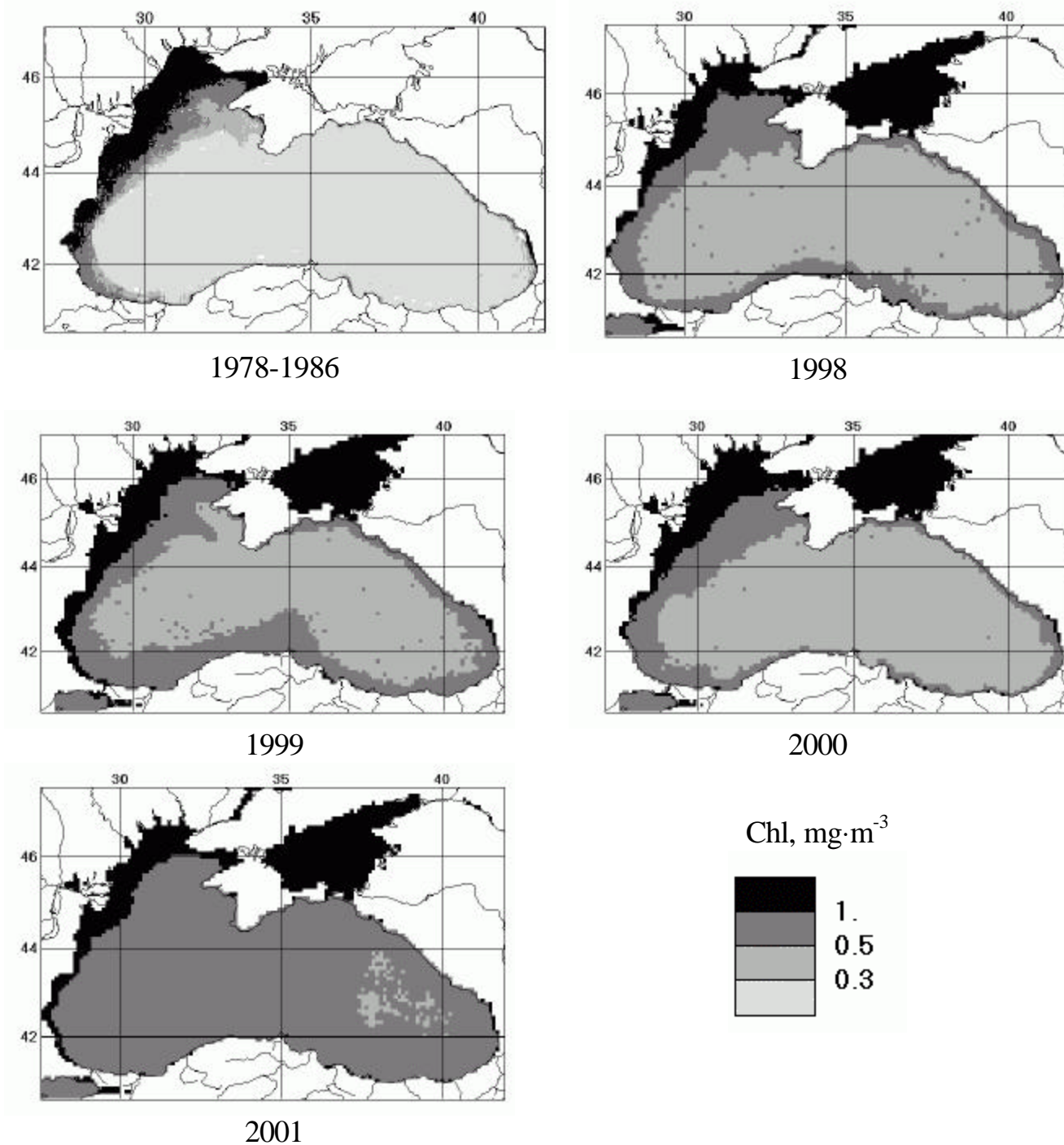


Figure 23.6: Interannual changes of the season (May-September) chlorophyll concentration in the Black Sea derived from CZCS (1978-1986) and SeaWiFS (1998-2001) data by SIO/RAS algorithms.

This equation was calculated by using our field data in the open Black Sea and the eastern part of the basin in September-October 1997 and 2000 (n=13); a standard error of the regression equation is 0.056 mg m^{-3} . Reasoning from the results of study by Kopelevich et al. (2002d), equation (2) is assumed to be valid in the open and eastern regions of the Black Sea in warm season (May-September).

Examples Of Spatial Distributions Of The Bio-Optical Characteristics

The mean monthly distributions of chlorophyll concentration and particle backscattering coefficient in the Barents Sea in May and August 2001 derived with the SIO/RAS algorithms are shown in Fig. 23.5. The relatively high values of chlorophyll concentration are observed in the northern and middle Barents in May caused by spring phytoplankton bloom. In August chlorophyll concentration in the southern region and the White Sea is higher than in the northern and middle regions. There are the enhanced values of b_{bp} in the northern and middle Barents in May connected with the spring phytoplankton bloom. The increase of b_{bp} values in the middle Barents in August is assumed to arise from the coccolithophorid bloom. Such a phenomenon has been displayed in the Barents Sea repeatedly by satellite ocean color images. The enhanced values of *Chl* and b_{bp} in the southern Barents and the White Sea are caused mainly by the river run-off. In the southern Barents both chlorophyll concentration and particle backscattering rise sharply in June that corresponds to the Pechora flood-time in May-July. The enhanced values of *Chl* and b_{bp} are held from June to September because of the Pechora discharge is high throughout summer and autumn due to frequent rain freshets.

Fig.6 shows interannual changes of the season (averaged over May-September) chlorophyll concentration in the Black Sea derived from CZCS (1978-1986) and SeaWiFS (1998-2001) data by SIO/RAS algorithms. The used algorithm for CZCS data was developed by Kopelevich et al. (2002d). CZCS data are of particular interest for the Black Sea because CZCS operated within the period when the Black Sea state was rather stable. Three periods in long-term variations of surface chlorophyll-a in the open Black Sea can be selected: the first “quiet” period from 1964 to 1986 with a mean of $0.15 \pm 0.04 \text{ mg m}^{-3}$ in May-September, the second one from 1988 to 1992 when chlorophyll concentration increased up to $0.99 \pm 0.70 \text{ mg m}^{-3}$, and the third one from 1993 to 1996 when chlorophyll concentration decreased. As seen from Fig.23.6, chlorophyll concentration in the open Black Sea was mainly $0.3\text{-}0.5 \text{ mg m}^{-3}$ in 1998-2000 but it increased significantly in 2001 (up to $0.5\text{-}1.0 \text{ mg m}^{-3}$).

23.3 FUTURE WORK

The results obtained in the previous cruise of R/V Akademik Ioffe have demonstrated that the collaborative studies using its commercial transatlantic cruises of the Russian ships are cost effective and hold much promise for collection of representative data sets for the algorithm validation. It is worth continuing such studies to collect *in situ* data for studying spatial changeability of atmospheric and oceanic characteristics in the Atlantic Ocean between 50°N and 55°S in two different seasons, validation of the processing algorithms and understanding of the regional features. It also would be important to study effects of aerosol particles blown by wind on the seawater particle backscattering and variability of absorption spectra of particulate and soluble matter, detritus and phytoplankton pigments depending on season in different bio-optical provinces. We also plan to continue validation studies in the Barents and Black seas to refine the processing algorithms there.

REFERENCES

- Artemiev, V.A., V.I.Burenkov, M.I.Vortman, A.V.Grigoriev, O.V.Kopelevich, and A.N.Khrapko, 2000: Sea-Truth Measurements of Ocean Color: A New Floating Spectroradiometer and Its Metrology. *Oceanology*, Vol.40, 139-145. Translated from *Okeanologiya*, Vol.40, 148-155.
- Burenkov, V.I., Kopelevich, O.V., Sheberstov, S.V., Ershova, S.V., Evdoshenko, M.A., 1999: Bio-optical characteristics of the Aegean Sea retrieved from satellite ocean color data. In: Malanotte-Rizzoli, P., Eremeev, V.N. (Eds), *The Eastern Mediterranean as a Laboratory Basin for the Assessment of Contrasting Ecosystems*. Kluwer Academic Publishers, Netherlands, 313-326.
- Burenkov, V.I., Kopelevich, O.V., Sheberstov, S.V., Vedernikov, V.I., 2000: Sea-truth measurements of ocean color: Validation of the SeaWiFS satellite scanner data, *Oceanology*, 40(3), 329-334 (translated from *Okeanologiya*, 40 (3), 357-362).

- Burenkov, V.I., Vedernikov, V.I., Ershova, S.V., Kopelevich, O.V., Sheberstov, S.V., 2001a: Use of data from satellite ocean color scanner SeaWiFS for assessment of bio-optical characteristics of the Barents Sea, *Oceanology* **41**(4), 461-468 (translated from *Okeanologiya* **41**(4), 485-492).
- Burenkov, V.I., Ershova, S.V., Kopelevich, O.V., Sheberstov, S.V., Shevchenko, V.P., 2001b: An estimate of the distribution of suspended matter in the Barents Sea waters on the basis of the SeaWiFS satellite ocean color scanner, *Oceanology* **41**(5), 622-628 (translated from *Okeanologiya* **41**(5), 653-659).
- Kopelevich, O.V., V.I. Burenkov, S.V. Ershova, M.A. Evdoshenko, S.V. Sheberstov, 2002a: Evaluation and Improvement of the Atmospheric Correction and Bio-optical Algorithms for the Black and Barents Seas. In: G. Fargion and Ch. McClain: SIMBIOS Project 2001 Annual Report. *NASA/TM-2002-210005*, NASA Goddard Space Flight Center, Greenbelt, Maryland, 170-175.
- Kopelevich, O.V., V.I. Burenkov, S.V. Ershova, S.V. Sheberstov, and M.A. Evdoshenko, 2002b: Variability of the Biooptical Characteristics of the Waters in the Near-Shore and Open Regions of the Russian seas from the Data of the SeaWiFS Satellite Ocean Color Scanner. *Oceanology*, Vol. **42**, Suppl.1 (in press).
- Kopelevich, O.V., V.I. Burenkov, S.V. Ershova, S.V. Sheberstov, M.A. Evdoshenko, and E.A. Lukyanova, 2002 c: Bio-optical characteristics of the Russian Seas from data of the satellite ocean color scanner SeaWiFS. *CD-ROM*. M., SIO/RAS.
- Kopelevich, O.V., S.V. Sheberstov, O. Yunev, O. Basturk, Z.Z. Finenko, S. Nikonov, V.I. Vedernikov, 2002d: Surface chlorophyll in the Black Sea over 1978-1986 derived from satellite and *in situ* data. *J. Mar. Systems*, **36**(3-4), 145-160.
- Kopelevich, O.V., V.I. Burenkov, S.V. Ershova, S.V., Sheberstov and M.A. Evdoshenko: Application of SeaWiFS data for studying variability of bio-optical characteristics in the Barents, Black and Caspian Seas. *Deep-Sea Research Part II (DSR-II)*, special issue on the application of SeaWiFS imagery for examining ocean processes (in preparation).

Chapter 24

SimbadA Calibration using a Laser Based Facility and Comparison with Previous Techniques

Nordine Souaidia, Steven W. Brown, and B. Carol Johnson

Optical Technology Division, National Institute of Standards and Technology, Gaithersburg, Maryland

24.1 INTRODUCTION

Sun photometers and sky radiometers are used to characterize the radiative properties of the atmosphere and to determine optical properties such as the aerosol optical thickness (Fargion et al. 2001). For comparison of water-leaving radiances to on-orbit sensor values in ocean-color research, the atmospheric contribution to the signal measured by the satellite must be accurately accounted for in a process termed “atmospheric correction.” The current relative standard uncertainty ($k = 1$) in the absolute radiance calibration of sky radiometers using a lamp-illuminated integrating sphere is approximately 5 % (Pietras et al. 2001). The remote sensing community requires increased confidence in the radiometric accuracy of sun photometers and radiometers used for atmospheric characterization to better model and correct for the effects of aerosols on the total radiances recorded by the satellites (Frouin et al. 2001). Reductions in the uncertainties using laboratory standards would allow for meaningful comparisons with the results from the solar-based calibration (Langley-Bouguer method) of sun photometers, resulting in independent values for the exo-atmospheric solar irradiance at the set of measurement wavelengths (Schmid et al. 1998; Wehrli 2000).

The Satellite Validation for Marine Biology and Aerosol Determination (SimbadA) radiometers are manufactured by the Laboratoire d’optique atmospherique (LOA) de Lille, France. The SimbadA is an eleven-channel filter radiometer with nominal channel center wavelengths at 350 nm, 380 nm, 410 nm, 443 nm, 490 nm, 510 nm, 565 nm, 620 nm, 670 nm, 750 nm, and 870 nm. The multi-channel filter radiometers are used to directly view the sun, resulting in determinations of aerosol optical thickness, and they are also used to measure the sky radiance, resulting in characterization of the radiative properties of the atmosphere (Fargion et al. 2001). In this study, two SimbadA radiometers operated by the National Aeronautics and Space Administration (NASA) Sensor Intercomparison and Merger for Biological and Interdisciplinary Oceanic Studies (SIMBIOS) program (serial numbers 972307 and 972309) were calibrated using a laser-based integrating sphere source (ISS), and two lamp-illuminated ISSs, as well as by cross calibration against a primary reference sun photometer. Additional measurements with the laser-based integrating sphere are planned for November 2002.

The instrument’s radiance responsivities were derived using spectral responsivities determined in this work (see below) and two lamp-illuminated ISSs of known spectral radiance: the primary calibration source at the Radiometric Calibration Facility (RCF) at the NASA Goddard Space Flight Center (GSFC), known as the Hardy source, (Pietras et al. 2001) and a lamp-illuminated ISS maintained by the National Institute of Standards and Technology (NIST) known as the NIST Portable Radiance (NPR) source (Brown and Johnson 2002). Hardy is used in the calibration of sun photometers that are part of global networks of *in situ* atmospheric characterization, and other radiometers that are employed in the validation of Earth Observing Satellite (EOS) satellite instruments. The SimbadA instruments were also calibrated for irradiance responsivity by comparison against reference sun photometers on a rooftop at GSFC (Pietras et al. 2001). The reference sun photometers are calibrated using the Langley-Bouguer technique at Mauna Loa Observatory, Hawaii (Holben et al. 1998).

The uncertainty in the spectral radiance of lamp-illuminated ISSs depends on the method used, the reference standard, and the wavelength range. The relative expanded uncertainties ($k = 2$) for Hardy are approximately 2.5 % in the visible, increasing to 6.5 % at 400 nm. For the NPR, the relative expanded uncertainties are a factor of 5 lower, approximately 1.0 % in the ultraviolet (UV), 0.5 % in the visible, and 1.5 % in the short-wave infrared (SWIR). A newly developed laser-based facility for Spectral Irradiance and Radiance Calibration using Uniform Sources (SIRCUS) at the NIST is ideally suited for both radiance

and irradiance responsivity characterizations and calibrations (Brown et al. 2000). The radiance of the laser-illuminated ISS can be determined to a relative uncertainty of approximately 0.1 % ($k = 2$).

We are interested in the spectral characterization of this type of radiometer and in the evaluation of systematic effects that affect the measurement uncertainty. SIRCUS can provide a direct, system-level, radiance or irradiance calibration, so that overall changes in the channel sensitivity (e.g. by filter degradation) are quantifiable to 10 to 100 times the sensitivity achievable using Hardy (Pietras et al. 2001). Pietras et al. (2001) identify filter degradation as a major source of error in the use of sun photometers. Using a lamp-illuminated monochromator for the spectral characterization, Schmid et al. (1998) compared the uncertainties for the Langley-Bouguer and a standard irradiance lamp method of calibration. They discussed the effects of wavelength error, finite bandpass, and spectral out-of-band, and evaluated the components for optimal conditions: solar calibrations at high altitude and the use of NIST-calibrated irradiance lamps. With SIRCUS, we are in a position to reduce the uncertainty components in the laboratory calibration method compared to that reported by (Schmid et al. 1998), because the wavelength is determined with high accuracy, the laser is monochromatic, high flux levels are possible, the entrance pupil is filled according to the conditions of solar viewing, and there is no need for a standard lamp of spectral irradiance (eliminating a measurement step and its associated uncertainty). Except for dependence on ambient temperature and pressure (which could be addressed in the future), all known uncertainty components related to the laboratory radiometer are quantified, so systematic effects can be quantified and their effect substantially reduced.

Several filter channels on both instruments were calibrated for spectral radiance responsivity on SIRCUS; additional measurements are scheduled on SIRCUS to determine the spectral irradiance responsivity of the filter channels. A description of the measurements is given, and the preliminary results from the radiance responsivity calibrations are described. Finally, a description of the irradiance responsivity comparison planned for the next year is presented.

24.2 RESEARCH ACTIVITIES

A schematic diagram of the SIRCUS facility is shown in Fig. 24.1. A number of tunable laser systems are used to generate light over a wide spectral range; this work focused on the region from 420 nm to 900 nm. The output of the laser is intensity stabilized to reduce the power fluctuations and a portion of the beam is directed to a wavemeter for wavelength determination. The main portion of the beam is coupled into an integrating sphere using an optical fiber. The effect of speckle, which produces a non-uniform radiance distribution in the exit aperture of the sphere, is reduced by placing a small length of the optical fiber in an ultrasonic bath. Averaged over the time constant of the detector, the resulting radiance distribution appears uniform. Baffles are included in the integrating sphere to improve the uniformity at the exit port. A monitor detector corrects for small fluctuations in the radiant flux during a calibration. The result is a uniform, monochromatic, Lambertian calibration source of known radiance.

Integrating sphere sources are available with overall diameters from 5 cm to 50 cm. The size of the ISS and its exit aperture are selected to match the geometric requirements of the radiometer under test—smaller exit apertures, which underfill the field-of-view of the radiometer, for irradiance characterizations and larger ones, which overfill the field-of-view of the radiometer, for radiance characterizations. For irradiance and radiance responsivity calibrations, test sensors and a reference standard detector are located on a translation stage at a known fixed distance from the sphere exit aperture. The test sensors are calibrated against the reference detector using the substitution method. A computer program controls and monitors the laser power and wavelength, moves the translation stage, and records test and reference detector signals.

The Hardy sphere is a fan-cooled fiberglass shell with a barium sulfate (BaSO_4) interior coating. The exit aperture is 25.4 cm. The sphere is equipped with 16 individually baffled, 200 W quartz-tungsten-halogen lamps. Eight 500 W power supplies control pairs of lamps in a constant current mode. During operation, the sphere output was monitored at six channels using a new Filter Radiometer Monitoring System (FRMS) (Marketon et al. 2000). Hardy was calibrated using a single-grating scanning monochromator (model OL746) operating in the irradiance mode; this configuration is known as the 746/ISIC (integrating sphere irradiance collector). A lamp standard of spectral irradiance was used to calibrate the 746/ISIC.

The NPR is a 30 cm diameter sphere, manufactured using Spectralon[®], with a 10 cm diameter aperture. It was developed by NIST in collaboration with NASA's EOS Calibration/Validation Program Office (Brown and Johnson 2002). The sphere is equipped with 4 internally baffled, 30 W lamps located at 90 degree intervals around the aperture. Two silicon photodiode monitor detectors, one fitted with an infrared filter centered at 1400 nm and the other with a photopic filter are used in the sphere. The NPR was calibrated in the NIST Facility for Automated Spectral Irradiance and Radiance Calibrations (FASCAL) (Walker et al. 1987) against primary national radiometric standards.

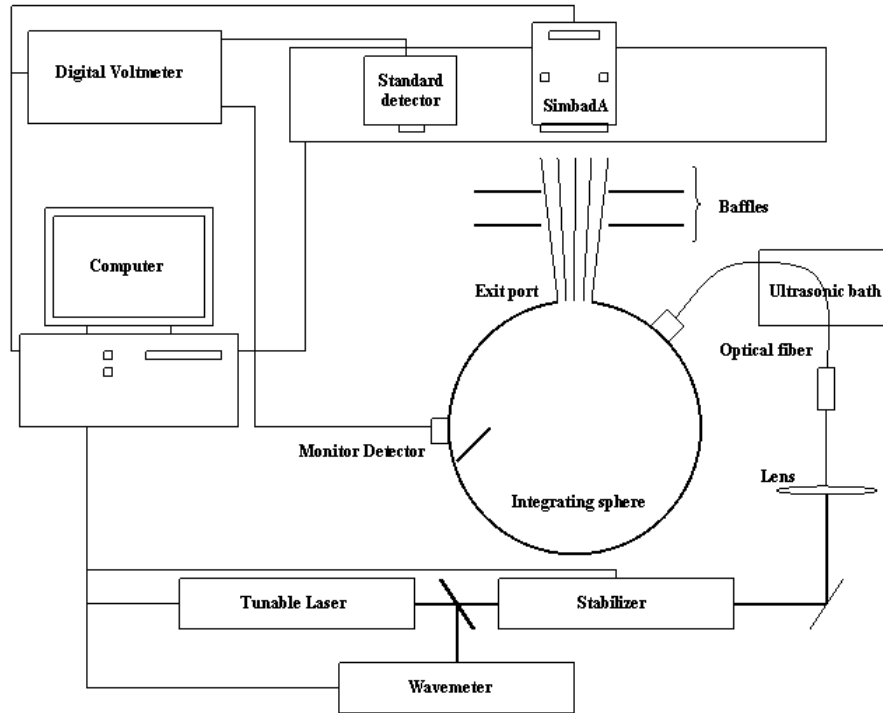


Figure 24.1: Schematic of the SIRCUS facility, illustrating the laser-illuminated integrating sphere, the standard detector, and the SimbadA.

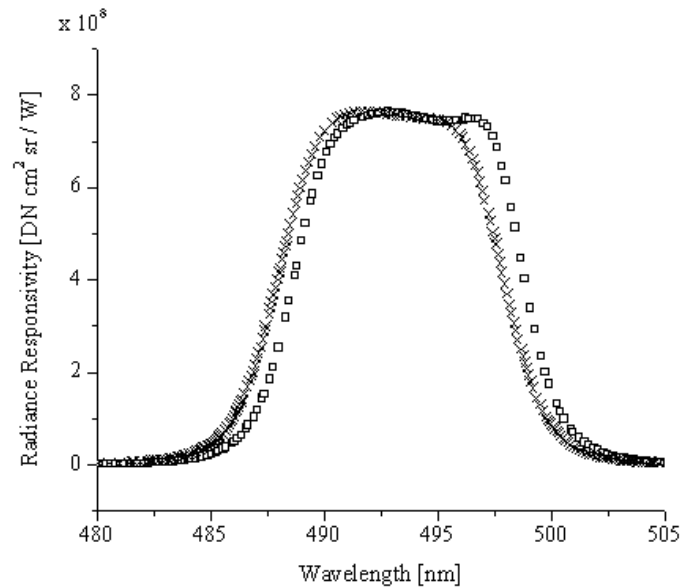


Figure 24.2: Absolute radiance responsivity data for the 490 nm channel of SimbadA S/N 972309. The square symbols are the SIRCUS values for the absolute radiance responsivity, and the cross symbols are the manufacturer values, scaled to result in the same maximum value as the SIRCUS results.

For irradiance measurements (e.g., solar-viewing), the SimbadA instruments are compared to sun photometers in a cross calibration technique on a rooftop at GSFC. The reference sun photometers, which are part of the Aerosol Robotic Network (AERONET) project are calibrated at Mauna Loa Observatory on regular intervals (Pietras et al. 2001). The cross-calibration technique, described in Holben et al. (1998), consists of near simultaneous solar observations at GSFC with the uncalibrated SimbadA instruments and the reference sun photometers. The method assumes that the ratio of the output voltages for the same channel (e.g., same spectral responsivity) for the reference and uncalibrated radiometers and a particular air mass is proportional to the ratio of the output voltage at zero air mass. If the spectral responsivities differ, a correction is made for spectral differences related to Rayleigh, ozone, and aerosol attenuation (Pietras et al. 2001). This process is sensitive to the accuracy and completeness of the spectral irradiance responsivity for each channel.

24.3 RESEARCH RESULTS

In this section, we discuss the radiance responsivity calibration comparison. The irradiance responsivity comparison will be discussed in the next section. Eight of the channels were studied in this work; no measurements were made for the 350 nm, 380 nm, and the 410 nm channels. For each channel, individual measurements, spaced in wavelength by about 0.25 nm, were used to determine the radiance responsivity in the in-band and out-of-band spectral regions. Prior to the SIRCUS measurements, the spectral out-of-band was measured using a lamp-monochromator system in the NIST Spectral Calibration Facility (SCF) (Larason et al. 1998). Preliminary results gave an out-of-band signal that was approximately 0.01 % of the maximum value.

To compare to the SIRCUS results, measurements were performed with Hardy and with the NPR source in May 2002. The SIRCUS radiance responsivities, $s(\lambda)$, were interpolated to a uniform wavelength interval, as were the sphere spectral radiance values, $L(\lambda)$, for the lamp-illuminated ISS. For each channel, the band-averaged calibration coefficient, C , follows from

$$C = \frac{v}{\int L(\lambda) s(\lambda) d\lambda} \quad (1)$$

where v is the net voltage corresponding to the Hardy or NPR measurements. For a direct assessment of the SIRCUS results, we compared the measured signal to the predicted signal (the denominator in Eq. 1). The preliminary results give an agreement of better than 0.5 % for the NPR, and between 2 % and 4 % for Hardy. For both comparisons, the difference in the measured radiance responsivity was within the combined expanded uncertainty ($k = 2$) of the measurements.

In addition to the radiance responsivity measurements, a limited characterization of the instruments was conducted during 2002. The temporal stability of the SimbadA's responsivity was evaluated on SIRCUS and with the NPR source. Measurements were made with and without a warm-up interval. The result was an observable drift of 0.5 % in the instrument's responsivity during the first hour of use. The SimbadA instruments have two gain settings, one for solar measurements and one for sky or ocean measurements. Using the NPR, the gain ratio was measured and compared to the previous value in use by the SIMBIOS program. The agreement was to within 0.5 %.

Prior to the SIRCUS measurements, the only information available to the SIMBIOS program for spectral responsivity were the transmittance data from the instrument manufacturer. The relative spectral responsivity for each channel was then modeled assuming the detector response was constant over the bandpass. SIRCUS provided the first determination of the radiance responsivity for the complete system. The SIRCUS results for the 490 nm channel are shown in Fig. 24.2. The laser-illuminated ISS overfilled the 3° field-of-view (full angle). The absolute radiance responsivity, in digital number (DN, or counts) per radiance ($\text{DN cm}^2 \text{ sr} / \text{W}$) is plotted as a function of wavelength. The previous values, from the SimbadA manufacturer, were normalized using the maximum values and are also shown in Fig. 24.2. For this channel, there is a wavelength difference, with the SIRCUS results shifted to longer wavelengths. The center wavelengths for the two approaches differ by 0.85 nm and the full-width-half-maximum (FWHM) values differ by 0.2 nm (the SIRCUS result is broader). The center wavelength was determined from the average of the values corresponding to the FWHM points. A wavelength difference of about 1 nm was also observed for the other channels measured.

As a result of the stability tests, the SIMBIOS program has changed the SimbadA measurement protocols. Previously, the instrument was turned off when not in use. Now, before any measurements are made, the instrument is warmed-up for 1 h using the power supply, and it is operated with the power supply if possible (C. Pietras, pers. comm.). Otherwise, power is supplied from the SimbadA battery.

For the first time during this comparison, the output of Hardy was monitored with the new FRMS developed by the RCF for this purpose (Marketon et al. 2000). The FRMS, which has a filter wheel for observation at discrete wavelengths, mounts to Hardy above the exit aperture. The center wavelengths of the filters are 410 nm, 440 nm, 460 nm, 640 nm, 840 nm, and 1050 nm. Correcting the Hardy radiance for sphere temporal drift using the FRMS could reduce the uncertainty in the calibration by 1 % to 2 %.

24.4 FUTURE WORK

SIRCUS will be used to determine the irradiance responsivity of the SimbadA instruments. Given the absolute exo-atmospheric solar irradiance (and there are several data sets to choose from) the SIRCUS measurements will be used to predict the top of the atmosphere signal, V_0 , and this will be compared to the value resulting from the cross calibration to the Mauna Loa sun photometers performed at GSFC. This evaluation will allow for a laboratory-based determination of the exo-atmospheric signal, and lead to an evaluation of the cross-calibration method and the input exo-atmospheric solar irradiance (Schmid et al. 1998).

The SIRCUS calibration has uncertainties an order of magnitude lower than the uncertainties from the Hardy calibration. In addition, the SIRCUS measurements provide a means of determining the band-center wavelength of each filter channel with uncertainties of 0.1 nm or less. We are currently assessing the impact of calibrations of sun photometers with reduced uncertainties on the determination of atmospheric optical properties, particularly as applied to ocean-color-remote sensing data products. Because the vendor's nominal band center wavelengths are used in the calibration, there can be several nanometer shifts in nominal and measured center wavelengths. Similar to the work by Wang for the Sea-viewing Wide Field of view Sensor (SeaWiFS) (Wang 1999), a sensitivity analysis is under way to evaluate the uncertainty in aerosol optical depth arising from this type of wavelength uncertainty.

REFERENCES

- Brown, S. W., G. P. Eppeldauer and K. R. Lykke, 2000: NIST facility for spectral irradiance and radiance calibrations with uniform sources, *Metrologia*, **37**, 579-582.
- Brown, S. W. and B. C. Johnson, 2002: A portable integrating sphere source for the Earth Observing System's calibration validation program, *International Journal of Remote Sensing* (to be published).
- Fargion, G. S., R. Barnes and C. McClain, 2001: In Situ Aerosol Optical Thickness Collected by the SIMBIOS Program (1997-2000): Protocols, and Data QC and Analysis. Greenbelt, Maryland, National Aeronautics and Space Administration.
- Frouin, R., B. Holben, M. Miller, C. Pietras, J. Porter and K. Voss, 2001: Sun and sky radiance measurements and data analysis protocols. In Situ Aerosol Optical Thickness Collected by the SIMBIOS Program (1997-2000): Protocols, and Data QC and Analysis. G. S. Fargion, R. Barnes and C. McClain. Greenbelt, Maryland, National Aeronautics and Space Administration. *NASA/TM--2001-209982*, 26-42.
- Holben, B. N., T. F. Eck, I. Slutsker, D. Tanre, J. P. Buis, A. Setzer, E. Vermote, J. A. Reagan, Y. J. Kaufman, T. Nakajima, F. Lavenu, I. Jankowiak and A. Smirnov, 1998: AERONET--A federated instrument network and data archive for aerosol characterization, *Remote Sensing of the Environment*, **66**, 1-16.
- Larason, T. C., S. S. Bruce and A. C. Parr, 1998: Spectroradiometric Detector Measurements: Part I--Ultraviolet Detectors and Part II--Visible to Near-Infrared Detectors. Gaithersburg, Maryland, U.S. Department of Commerce, Technology Administration, National Institute of Standards and Technology.
- Marketon, J., P. Abel, J. J. Butler, G. R. Smith and J. W. Cooper, 2000: A filter radiometer monitoring system for integrating sphere sources, *Proc. SPIE*, **4169**, 260-267.
- Pietras, C., M. Miller, R. Frouin, T. Eck, B. Holben and J. Marketon, 2001: Calibration of sun photometers and sky radiance sensors. In Situ Aerosol Optical Thickness Collected by the SIMBIOS Program (1997-2000): Protocols, and Data QC and

Analysis. R. B. G. S. Fargion, and C. McClain. Greenbelt, Maryland, National Aeronautics and Space Administration. *NASA/TM--2001-209982*, 11-21.

Schmid, B., P. R. Spyak, S. F. Biggar, C. Wehrli, J. Sekler, T. Ingold, C. Matzler and N. Kampfer, 1998: Evaluation of the applicability of solar and lamp radiometric calibrations of a precision Sun photometer operating between 300 and 1025 nm, *Applied Optics*, **37**, 3923-3941.

Walker, J. H., R. D. Saunders and A. T. Hattenburg, 1987: Spectral Radiance Calibrations, NBS Special Publication **250-1**. Washington, DC, U.S. Government Printing Office.

Wang, M. 1999: A sensitivity study of the SeaWiFS atmospheric correction algorithm: Effects of spectral band variations, *Remote Sensing of the Environment*, **67**, :348-359.

Wehrli, C. 2000: Calibrations of filter radiometers for determination of atmospheric optical depth, *Metrologia*, **37**, 419-422.

Yoon, H. W., C. E. Gibson and P. Y. Barnes, 2002: Realization of the National Institute of Standards and Technology detector-based spectral irradiance scale, *Applied Optics*, **41**, 5879-5890.